https://doi.org/10.15388/vu.thesis.755
https://orcid.org/0000-0003-4010-9898

VILNIUS UNIVERSITY

Agnė Petrošiūtė

Evaluation of Carbonic Anhydrase IX and CCL2-CCR2 Signaling Pathway Inhibition in Solid Tumors using *in Vitro* cellular and *in Vivo* Mouse Models

DOCTORAL DISSERTATION

Natural Sciences,
Biochemistry (N 004)

VILNIUS 2025

This dissertation was written between 2019 and 2025 (Institute of Biotechnology, Life Sciences Center, Vilnius University).

The dissertation is defended on an external basis.

Academic consultant – Prof. Dr. Daumantas Matulis (Vilnius University, Natural Sciences, Biochemistry – N 004).
Academic consultant – Dr. Jurgita Matulienė (Vilnius University, Natural Sciences, Biology – N 010)

This doctoral dissertation will be defended in a public meeting of the Dissertation Defence Panel:

Chairman – Dr. Veronika Viktorija Borutinskaitė (Vilnius University, Natural Sciences, Biochemistry – N 004).
Members:
Dr. Arvydas Kanopka (Vilnius University, Natural Sciences, Biochemistry – N 004).
Dr. Agata Mlynska (National Cancer Institute, Natural Sciences, Biology – N 010).
Dr. Vitalijus Karabanovas (National Cancer Institute, Natural Sciences, Biophysics – N011).
Dr. Seppo Parkkila (Tampere University, Finland, Natural Sciences, Biochemistry – N 004).

The dissertation shall be defended at a public meeting of the Dissertation Defence Panel at 1pm on 30 May 2025 in Room R-401 of the Life Sciences Center, Vilnius University.
Address: Saulėtekio al. 7, Room R-401, Vilnius, Lithuania.

Dissertation will be defended in English.

The text of this dissertation can be accessed at the library of Vilnius University and on the website of Vilnius University:
www.vu.lt/lt/naujienos/ivykiu-kalendorius

https://doi.org/10.15388/vu.thesis.755
https://orcid.org/0000-0003-4010-9898

VILNIAUS UNIVERSITETAS

Agnė Petrošiūtė

Karboanhidrazės IX ir CCL2-CCR2 signalinio kelio slopinimo įvertinimas standžiuosiuose navikuose naudojant *in vitro* ląstelių ir *in vivo* pelių modelius

DAKTARO DISERTACIJA

Gamtos mokslai,
Biochemija (N 004)

VILNIUS 2025

Disertacija rengta 2019–2025 metais (Biotechnologijos institutas, Gyvybės mokslų centras, Vilniaus universitetas).

Disertacija ginama eksternu.

Mokslinis konsultantas – prof. dr. Daumantas Matulis (Vilniaus universitetas, gamtos mokslai, biochemija – N 004).
Mokslinė konsultantė – dr. Jurgita Matulienė (Vilniaus universitetas, gamtos mokslai, biologija – N 010).

Gynimo taryba:
Pirmininkė – dr. Veronika Viktorija Borutinskaitė (Vilniaus universitetas, gamtos mokslai, biochemija – N 004).
Nariai:
dr. Arvydas Kanopka (Vilniaus universitetas, gamtos mokslai, biochemija – N 004),
dr. Agata Mlynska (Nacionalinis vėžio institutas, gamtos mokslai, biologija – N 010),
dr. Vitalijus Karabanovas (Nacionalinis vėžio institutas, gamtos mokslai, biofizika – N 011),
dr. Seppo Parkkila (Tamperės universitetas, Suomija, gamtos mokslai, biochemija – N 004).

Disertacija ginama viešame Gynimo tarybos posėdyje 2025 m. gegužės mėn. 30 d., 13 val., Vilnaus universiteto, Gyvybės mokslų centro R-401 auditorijoje.
Adresas: Saulėtekio al.7, R-401 auditorija, Gyvybės mokslų centras, Vilnius, Lietuva.
Disertacija bus ginama anglų kalba.

Disertaciją galima peržiūrėti Vilniaus universiteto bibliotekoje ir VU interneto svetainėje adresu: *https://www.vu.lt/naujienos/ivykiu-kalendorius*

CONTENTS

ABBREVIATIONS

3D – three-dimensional
ACKR – atypical chemokine receptor
ADMEM – advanced Dulbecco′s Modified Eagle′s Medium
ADP – adenosine diphosphate
A2AR – adenosine A2A receptor
AMP – adenosine diphosphate
AP-1 – activator protein 1
APC – antigen-presenting cells
Arg1 – arginase 1
ARNT – aryl hydrocarbon receptor nuclear translocator
AS – alternatively spliced
ATP – adenosine triphosphate
AZ19-3-2 – synthetic compound
AZ21-6 – synthetic compound
bHLH-PAS domain – basic helix-loop-helix/Per-ARNT-Sim domain
β-ME – 2-mercaptoethanol
CAs – carbonic anhydrases
CAF – cancer-associated fibroblast
CAIX – carbonic anhydrase IX
CEACAM6 – carcinoembryonic antigen-related cell adhesion molecule 6
CKR – conventional chemokine receptor
CCL – CC motif chemokine ligand
CCR – CC motif chemokine receptor
CKR – conventional chemokine receptor
CNS – central nervous system
COX4 – cytochrome c oxidase 4
CTL – cytotoxic T lymphocyte
CTLA4 – cytotoxic T-lymphocyte associated protein 4
CXCL – CXC motif chemokine ligand
CXCR – CXC motif chemokine receptor
CX_3CL – CX_3C motif chemokine ligand
CX_3CR – CX_3C motif chemokine receptor
DC – dendritic cell
DLL1– delta-like canonical Notch ligand 1
CSF-1 – colony-stimulating factor 1

CIBERSORT – cell-type identification by estimating relative subsets of RNA transcripts
DMEM – Dulbecco′s Modified Eagle′s Medium
ECM – extracellular matrix
ELISA – indirect enzyme-linked immunosorbent assay
EMAP-II – endothelial cell monocyte-activating polypeptide-II
EMT – epithelial–mesenchymal transition
ENTPD2 – ectonucleoside tri-phosphate diphosphohydrolase 2
ERK – extracellular signal-regulated kinases
epH – extracellular pH
EPO – erythropoietin
FBS – heat-inactivated fetal bovine serum
FGF – fibroblast growth factor
FIH-1 – factor inhibiting HIF-1
FFPE – formalin-fixed and paraffin-embedded
FTSA – fluorescent thermal shift assay
FOXP3 – Forkhead box P3
GBM – glioblastoma multiforme
Glut – glucose transporters
GZ22-4 – synthetic compound
HAPs – hypoxia-activated pro-drugs
HBSS – Hanks' Balanced Salt Solution
HMGB1 – high mobility group box 1 protein
HNSCC – squamous cell carcinoma of the head and neck
HIF – hypoxia-inducible factor
HRE – hypoxia response element
HCC – hepatocellular carcinoma
HUVEC – human umbilical vein endothelial cells
IEPA – imidazole-1-yl-3-ethoxycarbonylpropionic acid
ICB – immune checkpoint blockade
IFN-γ – interferon-gamma
Ig – immunoglobulin
IHC – immunohistochemistry
IL – interleukin
IL-2Rα – interleukin-2 receptor alpha chain
iNOS – inducible nitric oxide synthase

i.p. – intraperitoneally
ITC – isothermal titration calorimetry
i.v. – intravenously
i.o. – intraosseous
JHDMs – Jumanji C domain-containing histone demethylases
JNK – c-Jun N-terminal kinases
kPa – kilopascals
LDH – lactate dehydrogenase
LDHA – lactate dehydrogenase A
LDS – lithium dodecyl sulfate sample loading buffer
LZIP – leucine zipper
mDC – monocyte derived dendritic cell
MAPK – mitogen-activated protein kinase
MCT – monocarboxylate transporter
MMP – matrix metalloproteinases
MHC – major histocompatibility complex
MDSC – myeloid-derived suppressor cells
MFI – mean fluorescence intensity
NBC – sodium-dependent bicarbonate transporters
NBL – neuroblastoma
NETs – neutrophil extracellular traps
NF-κB – nuclear factor kappa B
NHE1 – Na^+/H^+ exchanger
NK – natural killer cells
NIR – near infrared
ODD – oxygen-dependent degradation domain
P13K – phosphoinositide 3-kinase
PDX – patient-derived xenograft
PD-L1 – programmed death-ligand 1
PD-1 – programmed cell death protein 1
PET – positron emission tomography
PHD2 – prolyl hydroxylase domain protein- 2
pO2 – atmospheric partial pressure of oxygen
PEG – polyethylene glycol
PBS – phosphate-buffered saline
PBMC – peripheral blood mononuclear cell

PG – proteoglycan
PHD2 – prolyl hydroxylase domain protein- 2
PDAC – pancreatic ductal adenocarcinoma
PDH – pyruvate dehydrogenase
PDK1 – pyruvate dehydrogenase kinase 1
PK/PD – pharmacokinetic/ pharmacodynamic
PMN – polymorphonuclear
PMSF – phenylmethylsulfonyl fluoride
RAGE – receptor for advanced glycation endproducts
RCC – renal cell carcinoma
RIPA – radioimmunoprecipitation assay buffer
s.c. – subcutaneously
SEMA3A – semaphorin 3A
SFA – stopped-flow assay of inhibition of enzymatic activity
STAT5 – signal transducer and activator of transcription 5
TME – tumor microenvironment
TAD – transactivation domain
TAM – tumor-associated macrophages
TAN – tumor-associated neutrophil
TBST – 1X Tris-Buffered Saline, 0.1% Tween® 20 detergent
TCGA – The Cancer Genome Atlas
TGF-β – transforming growth factor- beta
TIL – tumor-infiltrating lymphocyte
TLR – toll-like receptor
TME – tumor microenvironment
TNF-α – Tumor Necrosis Factor-alpha
Treg – regulatory T cells
TW- transwell
VEGF – vascular endothelial growth factor
VEGFR – vascular endothelial growth factor receptor
WB – western blot
XCL – XC chemokine ligand
XCR – XC chemokine receptor

INTRODUCTION

Despite advances made in the treatment of childhood malignancies, cancer remains one of the leading causes of death in children worldwide. Solid tumors encompass almost half of the cancer cases [1]. The survival of pediatric patients presenting with advanced-stage or relapsed solid tumors remains poor, even with novel treatment approaches, including immunotherapy [1]. Therefore, a better understanding of the biology of pediatric cancers and a search for novel therapies are needed. Pediatric solid tumors are different from adult solid tumors, as they have a very low tumor mutational burden/ fewer driver mutations and therefore have low immunogenicity [2]. Pediatric tumors have lower tumor-infiltrating lymphocyte (TIL) numbers and low expression of immune checkpoint molecules: programmed cell death protein 1 (PD-1), programmed death-ligand 1 (PD-L1), and PD-L2. These tumors have abundant myeloid-derived suppressor cells (MDSCs), tumor-associated macrophages (TAMs), cancer-associated fibroblasts (CAFs), and regulatory T cells (Tregs), which create an immunosuppressive niche [2]. However, adult and pediatric tumors share a common feature, which is tumor-associated hypoxia, and it is associated with tumor aggressiveness and progression.

Tumor hypoxia correlates with poor prognosis as well as resistance to conventional treatment [3]. Hypoxia drives immunosuppressive metabolites, which help create an immunosuppressive tumor microenvironment (TME) [4, 5]. Reduced oxygen in tumors stimulates changes in cellular processes that are orchestrated by the transcription factor Hypoxia–Inducible Factor (HIF). Proteins encoded by HIF-regulated genes are activated during tumor hypoxia and become active players in tumor progression. Metabolic shifts during hypoxia result in the accumulation of acidic metabolic products. To avoid prolonged intracellular acidosis, cells turn on pH regulatory machinery. Eliminating intracellular acidosis occurs through the export of lactate and protons from the cell and the import of bicarbonate ions [6]. This leads to pericellular acidosis in TME, which is associated with chemo/radio-resistance, suppressed immune responses, and induced inflammation, angiogenesis, invasion, and tumor cell dedifferentiation [6]. Hypoxia-driven immune suppression affects the function of all immune cell types: from inhibition of monocyte-derived dendritic cell (DC) activation to maturation [7] and M2 polarization of TAMs, to the suppressed T cell function [8] and recruitment of the Tregs [9]. Hypoxia also increases PD-L1 expression on tumor cells, leading to resistance to cytotoxic T lymphocyte (CTL)-mediated

lysis [10]. Such pronounced effects of hypoxia on tumor immune responses call for a better understanding of hypoxia effects on tumor-associated chemokine secretion and a search for potential targets of hypoxic TME that could synergize with various immunotherapies.

Carbonic anhydrase IX (**CAIX**) is a hypoxia-induced enzyme with an active site facing extracellular space. It can efficiently convert carbon dioxide to bicarbonate ions and protons. It is one of 15 human isoforms of the α carbonic anhydrase family that are known to regulate ion transport and pH homeostasis in the human body. CAIX maintains physiological pH in cancer cells, promoting their survival and progression [11]. This in turn leads to pericellular acidosis that becomes characteristic of such TME. Increased CAIX protein expression has been associated with worse prognosis in a variety of pediatric cancers, including brain tumors [12-14] and solid tumors outside the central nervous system (CNS) such as osteosarcoma [15] and neuroblastoma (NBL) [16]. CAIX protein expression is generally associated with a worse prognosis/increased aggressiveness in tumors [17, 18]. Tumor acidosis suppresses tumor immune responses and ensures treatment resistance [11, 19]. Therefore, CAIX inhibition may alter TME acidity and allow immunotherapy to work. Currently, the demonstration of the efficacy of CAIX inhibition paired with immune checkpoint blockade (ICB) is limited and is shown exclusively in the murine melanoma model [20]. In general, CAIX-targeted therapy development into translational clinical trials has been complicated. Although a small molecular inhibitor of CAIX enzyme SLC-0111 completed a phase 1 clinical trial in 2016, no further progress has been published [21]. There is a need to develop novel, more effective CAIX enzyme inhibitors. High homology amino acid sequence between CA isozymes makes development of specific CAIX isoform-selective inhibitors challenging [22]. My colleagues at the Institute of Biotechnology, Life Sciences Center, Vilnius University have developed benzene sulfonamides-based high-affinity and selectivity small molecule inhibitor of CAIX enzyme VD11-4-2 that showed promising *in vitro* activity [23-26]. It was further modified into inhibitor AZ19-3-2, a synthetic compound containing two VD11-4-2 head groups attached via a 12-mer polyethylene glycol (PEG) linker chain. It exhibits the best balance of affinity and selectivity toward the CAIX enzyme with the picomolar binding constant. My work presents experiments with this inhibitor.

In addition, the notion that CAIX protein is avidly expressed in solid tumors has made it an attractive objective for radionuclide diagnostics

platform creation. The development of CAIX-based radiopharmaceuticals remains a hot topic in cancer diagnostics and treatment [27]. My colleagues at the Institute of Biotechnology, Life Sciences Center Vilnius University have synthesized sulfonamide-based CAIX enzyme-recognizing compounds and tagged them to near-infrared (NIR) probe [28]. I tested the efficacy of such synthetic compounds AZ21-6 and GZ22-4 *in vivo* in a mouse model.

There is potential for using CAIX enzyme inhibitors as TME modifying agents in combination with immunotherapy. One approach could be to combine CAIX inhibition with a prominent tumor chemokine-chemokine receptor axis inhibition. **The chemokine (C-C motif) ligand 2 (CCL2) and its receptor, CC motif chemokine receptor 2 (CCR2) signaling axis** are one of the major chemokine signaling pathways that are indispensable in all stages of cancer progression, as are active in tumor hypoxia, neoangiogenesis, recruitment of immunosuppressing cells, and metastasis [29, 30]. Apart from cancer cells, the CCR2 receptor is also expressed in a plethora of cells such as monocytes/macrophages as well as Tregs, $CD4^+$, $CD8^+$ T cells, endothelial cells, and fibroblasts [31]. Therefore, it can serve as a crosstalk between cancer and immune cells. CCR2 protein affects homing of various T cell subsets to the tumor [31]. Although the CCR2 receptor can bind to other ligands, such as CCL8, CCL12, and others, CCL2 chemokine has by far the highest binding affinity [30]. CCL2 chemokine is one of the strongest chemoattractants involved in macrophage recruitment to the tumor bed [32]. Its regulation and role during tumor hypoxia are not well understood. The promoter of the *CCL2* gene contains hypoxia response elements (HRE) and so the expression of CCL2 can be induced by HIF-1. However, the regulation of expression of this chemokine in hypoxia is complex and depends on the cellular type and context. Although chronic hypoxia has been reported to decrease CCL2 chemokine levels in monocytes/ macrophages and some cancer cell lines, cyclic hypoxia (more characteristic for tumors) has been shown to increase the secretion of CCL2 chemokine and upregulate CCR2 receptors in macrophages [33, 34]. It has been shown that hypoxic tumor-derived CCL2 chemokine drives the accumulation of granulocytic $CD11b^+/Ly6C^{med}/Ly6G^+$ myeloid cells in murine mammary tumors, which helps to create the premetastatic niche. In turn, CCL2 chemokine neutralization in such a medium decreases metastatic tumor burden [35]. Targeting the CCL2-CCR2 axis as a treatment option for patients with cancer is in various stages of development [31]. Phase I/II clinical trials with CCR2 receptor antagonists or antibodies targeting the CCL2-CCR2 axis thus far resulted in poor responses or toxicities [36] [37]. However, the development

of novel CCL2-CCR2 axis inhibitors is evolving with new potential drug candidates reported [30]. For our work, we selected to use a small organic molecule RS504393 (spiropiperidine), which is a selective antagonist of the CCR2 receptor and has shown promising pre-clinical efficacy [38].

In summary, despite progress in the treatment of pediatric tumors, patients with advanced or relapsed malignancies face poor outcomes. Tumor hypoxia and acidity create a hostile tumor microenvironment that ensures tumor progression and resistance to treatment. To develop more effective combination therapies against pediatric cancers, we need a greater knowledge of the cellular interplay between cancer cells and the tumor microenvironment. Such knowledge could lay the groundwork for novel cancer therapies' development that target tumor hypoxia and the tumor chemokine networks.

The goal of this study

To investigate whether the inhibition of hypoxia-associated proteins such as the CAIX enzyme and/ or CCL2-CCR2 chemokine signaling axis is efficacious in selected pre-clinical pediatric solid tumor models and whether novel CAIX enzyme-recognizing NIR probes can effectively recognize CAIX protein-expressing tumors *in vivo.*

Objectives:

1. To characterize CAIX enzyme inhibition effects in the human neuroblastoma SK-N-AS cell-based model and human osteosarcoma 143B cell-based model *in vitro* and *in vivo* as monotherapy and in combination.
2. To characterize the effects of CAIX enzyme inhibition on the immune cell-human neuroblastoma SK-N-AS cell interaction *in vitro*.
3. To characterize the effects of CCL2-CCR2 chemokine signaling axis inhibition on the immune cell-human osteosarcoma 143B cell interaction *in vitro*.
4. To characterize CCL2-CCR2 chemokine signaling axis inhibition effects *in vivo* in the orthotopically implanted human 143B cell-based osteosarcoma xenograft mouse model.
5. To assess the feasibility of novel CAIX enzyme recognizing-NIR probe-tagged compounds AZ21-6 and GZ22-4 for CAIX enzyme recognition in the murine tumors *in vivo.*

6. Develop a cancer cell-healthy donor peripheral blood mononuclear cell (PBMC) co-culture method to study cancer cell-immune cell interaction.

Scientific novelty

Our work highlights the compensatory mechanisms involved when the CAIX protein or CCL2-CCR2 chemokine signaling axis is inhibited in the tumor. We show that hypoxic conditions alter the expression of different cellular markers and impair CCR2 antagonist effects in the experimental osteosarcoma model. In addition, this work underscores the multifaceted role of CAIX in tumor-stroma communication. This is the first study attempting a combination of CAIX enzyme and CCR2 receptor inhibition in the NBL xenograft model. This study reveals adaptive resistance in TME when the CAIX enzyme and CCR2 receptors are inhibited. Lastly, we tested the CAIX-specific specific-NIR probes in mice bearing cervical cancer xenograft tumors. This work lays the groundwork for novel cancer therapies that target tumor hypoxia together with the tumor chemokine networks and for CAIX enzyme recognition-based cancer diagnostics.

Defending statements

1. CAIX enzyme inhibition as single-agent therapy has limited efficacy in human osteosarcoma 143B cell-based mouse tumor model.
2. CAIX enzyme inhibition is effective when combined with a CCR2 receptor antagonist in the human neuroblastoma SK-N-AS cell-based xenograft mouse model.
3. CAIX inhibition decreases chemokines CCL2 and CXC motif chemokine ligand 8 (CXCL8) secretion in healthy donor PBMCs and SK-N-AS co-culture model.
4. CCL2-CCR2 chemokine signaling axis inhibition in osteosarcoma 143B cells has a divergent response in surface protein expression and secretion under hypoxia compared to normoxia.
5. CAIX enzyme recognizing-NIR probe-tagged compounds AZ21-6 and GZ22-4 are feasible for CAIX enzyme recognition in murine tumors *in vivo.*

The dissertation contains four main parts. The first part describes the *in vivo* study of the CAIX enzyme inhibition in the human osteosarcoma 143B cell-based model. The second part is devoted to studies of CCL2-CCR2 axis inhibition in the human osteosarcoma 143B cell-based model. The third part describes studies of CAIX inhibition in the human neuroblastoma SK-N-AS cell-based model. The last part discusses the creation of a CAIX enzyme-recognition-based *in vivo* imaging platform.

1. LITERATURE OVERVIEW

1.1. Physiological and Pathological Hypoxia

Oxygen is essential to sustain the life and physiology of eucaryotes. It assures aerobic respiration and adenosine triphosphate (ATP) generation in mitochondria [39]. "Normoxia" is usually recognized as oxygen levels noted in tissue culture flasks, which corresponds to about 20–21 % oxygen (160 mmHg) [40]. However, describing normoxia this way does not reflect the actual physiological scenario in a human body as almost any cell in the human body experiences lower atmospheric partial pressure of oxygen (pO_2) [40]. The pO_2 in arterial and venous blood is ~100 mmHg (~14 % O_2) and 40 mmHg (~6 % O_2), respectively. Oxygen concentration varies in different tissues [41]. Following inhalation of oxygen, red blood cells absorb oxygen, resulting in a maximal pO_2 tension in the pulmonary vasculature of 13 kilopascals (kPa) (~98 mm Hg). As oxygen is delivered to tissue, venous blood pO_2 is lowered to 5.3 kPa (~40 mm Hg). Within interstitial spaces of the tissue, the average pO_2 is only 2.7–5.3 kPa (~20–40 mm Hg) with intracellular oxygen tensions ranging from 1.3 to 2.7 kPa (~10–20 mm Hg). Physiological hypoxia has been observed in a range of tissues, including the retina, the medulla of the kidney, the epidermis of the skin, the thymus, bone marrow, and some areas within the spleen. Furthermore, the lumen of the gastrointestinal tract is mostly anoxic [39] **(Fig. 1).**

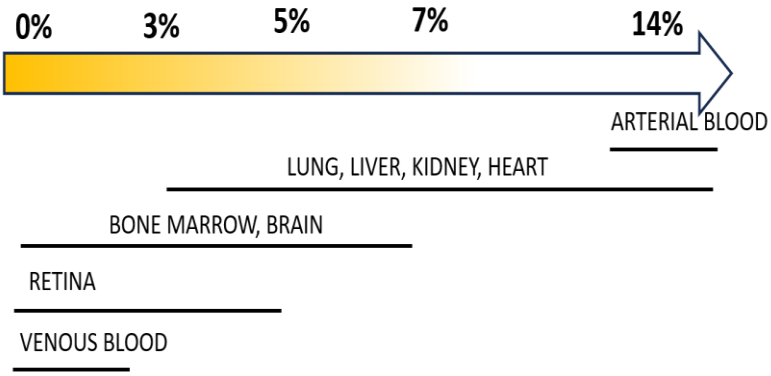

Figure 1. **Micro-environmental O_2 found in tissues *in situ*.** Adapted from Stamati et al J. Tissue Eng, 2011 [42].

Pathological hypoxia is defined as $pO_2 \leq$ ~1 kPa (≤~7–10 mm Hg or ~1 % O_2) [40]. It is at this level of pO_2 that the most responses to hypoxia occur [43].

Certain pathological conditions are associated with decreased O_2 levels due to increased demand or diminished supply, such as inflammation, high altitude, stroke, etc. Cancer is one of them. As the tumor grows, oxygen demand increases, but supply is diminished due to tumor pressure and distorted vasculature [44] (**Fig.2.**).

Based on duration, hypoxia can be acute (ranging from fractions of a second to minutes) or chronic (hours to days), or cyclic (intermittent) (oxygen concentrations alternate between low and baseline levels) [40, 45]. Chronic hypoxia induces delayed but durable responses that cause changes in mRNA and protein expression. Cyclic hypoxia is more characteristic of a malignant tumor and the greater fluctuations of oxygen are noted in the larger tumors [33]. In addition, much higher expression of pro-inflammatory genes is noted in cancer cells in cyclic hypoxia than in chronic [33]. Studies also show that cyclic hypoxia is associated with higher expression (stability and activity) of HIF-1α in cancer cells and compared to chronic hypoxia [45].

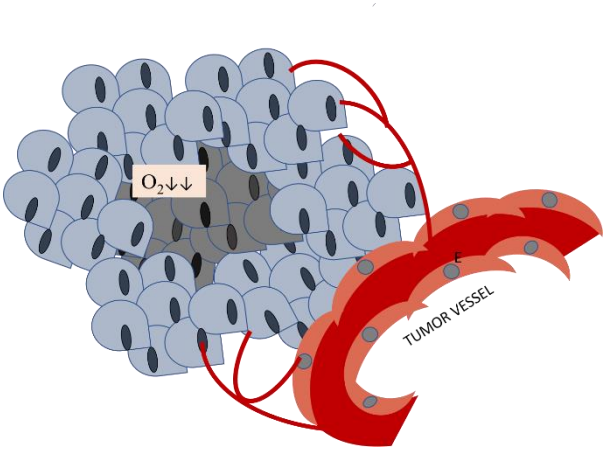

Figure 2. Scheme depicting tumor O_2 demand and delivery changes as tumor size increases.

1.2. HIF-1 is the master hypoxia response regulator

HIF-1 is a transcription factor and the key regulator of the hypoxia response [46]. HIF-1 protein was discovered in 1991 while studying the erythropoietin (*EPO*) gene [47]. Cis-acting DNA sequences (5′–RCGTG-3′) were discovered in the 3′-flanking region of this gene that were essential for the transcriptional activation of the *EPO* gene in response to hypoxia. They were named hypoxia

response elements (HRE) [47, 48]. Such transcriptional activation of many regulatory genes is initiated through the binding of a specific protein later identified as HIF-1[48]. All endogenous HREs are structurally complex, with a conserved core HIF-binding site (HBS) with a G/ACGTG consensus sequence [49].

Most oxygen-responsive genes hold HREs that bind HIF, leading to adaptive responses. HIF leads to the metabolic reprogramming of cells. Three members of HIF are identified today: HIF-1α, HIF-2α, and HIF-3α. They all consist of a heterodimeric structure, belong to the basic helix-loop-helix/Per-ARNT-Sim (bHLH-PAS) family of transcription factors, composed of an O_2-sensitive α subunit and an O_2-insensitive β subunit (HIF-1β), which is O_2-insensitive and is also called recognized as aryl hydrocarbon receptor nuclear translocator (ARNT) [46].

HIF-1α consists of 826 amino acids and HIF-1β of 789 amino acids. The first half of the subunits contain PAS and HLH domains, which are important for heterodimerization between HIF-1α and HIF-1β [45, 46]. The regions responsible for the binding to the HRE of the target are located upstream of the N-terminal of the HLH domain of both HIF-1α and HIF-1β subunits. The second half of the subunits of HIF-1α consists of two transactivation domains (TADs) (N-terminal N-TAD and C-terminal C-TAD, which control transactivation of the target gene through the recruitment of coactivators CBP/p300) and the inhibitory domain (ID), which suppresses transcription during normoxia [46]. Lastly, the oxygen-dependent degradation domain (ODD) is located upstream of N-TAD and is responsible for the hydroxylation of the two proline residues and the acetylation of lysine resulting in proteasomal degradation. HIF-1β subunit contains C-TAD but does not have ODD and the N-TAD domains. This results in functional differences between HIF-1α and HIF-1β subunits: HIF-1α is active in transcription and its function is oxygen dependent, whereas HIF-1β is active under aerobic and hypoxic conditions [46].

Although HIF-2α is structurally like HIF-1α (48 % sequence similarity) and can heterodimerize with HIF-1β and bind with HREs, it has a different pattern of tissue distributions [46, 48]. While HIF-1α is ubiquitously expressed in the body, HIF-2α expression is in specific tissues: embryonic cells and adult vascular endothelial cells, lungs, placenta, and heart [46]. HIF-2α is important during embryogenesis and is active in EPO and iron metabolism [46]. HIF-3α shows about half of amino acids sequence identity in the bHLH-PAS domain with HIF-1α and HIF-1β, and 61% in the ODD domain with HIF-1α. It does not have the C-TAD domain and therefore does not have intrinsic

transactivation activity. It contains a leucine zipper (LZIP) domain, which plays a role in protein interactions. It can also heterodimerize with HIF-1β [46]. HIF-3α isoforms can inhibit HIF-1 transcriptional activity as *HIF3* gene expression is induced by HIF-1 in hypoxic cells during prolonged hypoxia. This may be a negative feedback mechanism to attenuate HIF-1 activity.

The regulation of HIF-1α and HIF-2α depends on protein stability and accumulation through post-translational modifications [50]. The canonical oxygen-dependent regulation involves the von Hippel-Lindau tumor suppressor protein (pVHL) pathway. Under physiological pO_2, HIF-1α and HIF-2α are maintained at low levels due to constant ubiquitination-dependent degradation via interactions with pVHL. Firstly, HIF-1α and HIF-2α proline hydroxylation is catalyzed by prolyl hydroxylase domain proteins PHDs (PHD1, 2, and 3). PHD enzymes require the presence of O_2, ferrous iron (Fe (II)), and ascorbate as cofactors for their activity. pVHL, a recognition component of an E3 ubiquitin-ligase complex, recognizes and binds hydroxylated HIF-1α and HIF-2α at proline residues (Pro402 and Pro564 in HIF-1α and Pro405 and Pro531 in HIF-2α), assembling the protein complex for degradation via the ubiquitin-proteasomal pathway [50]. Alternatively, HIF-1α hydroxylation can occur by the hydroxylase called factor inhibiting HIF-1 (FIH-1). It inhibits the interaction between HIF-1α and transcription coactivators CBP/p300 [46].

Under hypoxic conditions, PHD activity is suppressed, which decreases HIF-1α and HIF-2α proline hydroxylation and degradation, resulting in HIF-1α and HIF-2α protein accumulation. The stabilized HIF-1α and HIF-2α subunit translocates into the nucleus, dimerize with HIF-1β, and bind to HREs, leading to the transactivation of hypoxia-responsive genes [50]. Regulation of HIF-1α protein is depicted in **Fig. 3.**

It is important to note that HIFs can also be regulated by non-canonical oxygen-independent pathways. For instance, growth factors via receptor tyrosine kinase activity can upregulate phosphoinositide 3-kinases (PI3K) and the mitogen-activated protein kinase (MAPK) signaling pathways that, in turn, can upregulate HIF-1α protein translation [50]. Also, cytokines, such as IL-1β, can increase HIF-1α binding to DNA under normoxic conditions based on studies with hepatocellular carcinoma HepG2 cells [51].

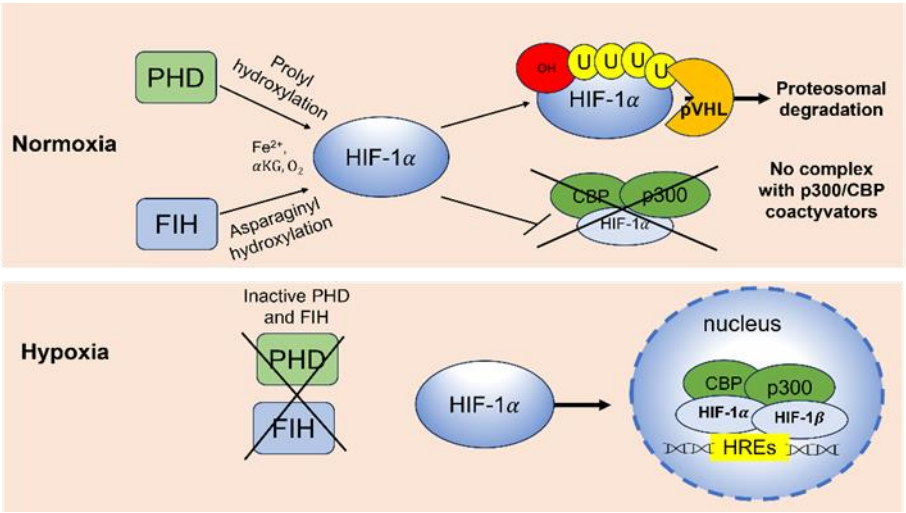

Figure 3. Canonical oxygen-dependent regulation of HIF-1α. Under normoxia (upper panel), HIF-1α is hydroxylated by PHDs and FIH, which allows the formation of pVHL/E3 ubiquitin-ligase complex and recognition and binding of hydroxylated HIF-1α at proline residues, resulting in proteasomal degradation. Under hypoxia (lower panel), the lack of oxygen limits PHD and FIH activities, leading to the accumulation of HIF-1α. After translocating to the nucleus, HIF-1α forms a heterodimer with HIF-1β. The heterodimer then binds to HRE and recruits co-activators such as CBP/p300 to the promoter region of target genes and regulate transcription. Adopted from V. Infantino et al Int J Mol Sci, 2021 [46] and Shi, Y. et al Cell Mol Life Sci, 2025 [50].

Adaptation mechanisms of the tumor cells to hypoxia include HIF-1α-mediated upregulation of glucose transporters (Glut-1 and Glut-3) and enzymes of glycolysis. Conversion of pyruvate to lactic acid is facilitated by the induction of lactate dehydrogenase (LDH). HIF-1α also induces pyruvate dehydrogenase kinase-1 (PDK-1), which inhibits the conversion of pyruvate into acetyl-CoA by pyruvate dehydrogenase (PDH), thus preventing entry of pyruvate into the TCA cycle. Switching on the cytochrome c oxidase 4 (COX4) subunits ensures optimal efficiency of mitochondrial respiration in hypoxia. These changes, in turn, cause the **Warburg effect**: aerobic glycolysis, production of lactic acid, and increased LDH activity [52]. All these processes lead to excess acidic metabolic products, including lactic acid, protons, and carbon dioxide, which threaten cancer cells' survival. Therefore, to maintain pH homeostasis, tumor cells upregulate various regulatory

mechanisms, such as the CAIX enzyme, monocarboxylate transporter-4 (MCT4), and the Na^+/H^+ exchanger (NHE1) [53] **(Fig. 4).**

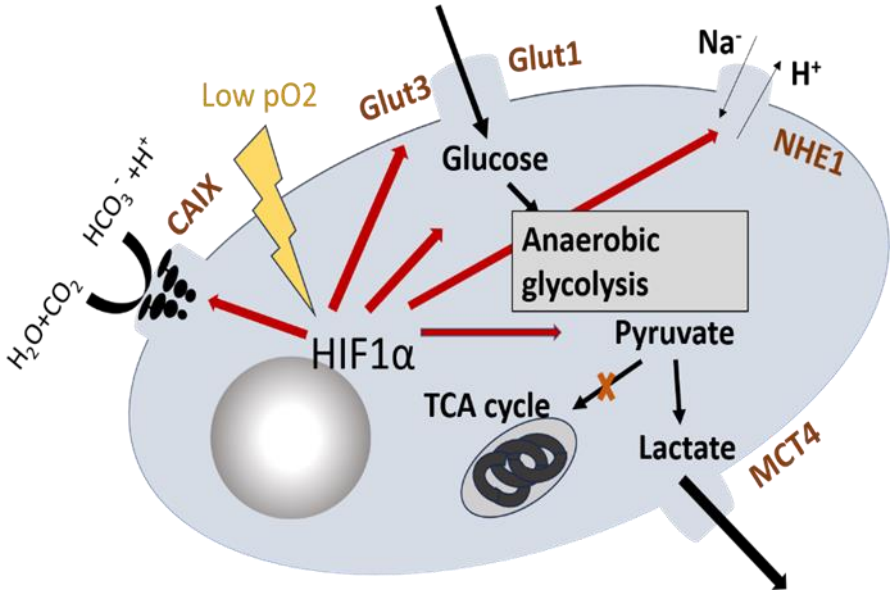

Figure 4. HIF-1α controls metabolic and pH-regulating pathways. Adapted from Weidemann et al 2008 [53].

Ultimately, reduced oxygen availability stimulates a shift to glycolytic metabolism, a slowdown in cell proliferation, diminished cell adhesion, increased migration and invasiveness, increased angiogenesis, and other energy-saving and metastasis-enabling alterations in cancers [3].

1.3. Tumor hypoxia and immune escape/ invasion

TME is a heterogeneous structure where tumor cells actively engage with stroma cells, composed of extracellular matrix (ECM), fibroblasts, endothelial cells, and immune cells. It is a dynamic milieu, where secreted bioactive molecules and interplay between cells can result in anti-tumorigenic or pro-tumorigenic tumors **(Fig. 5)** [54]. There are two main research areas for studying TME: one with a focus on physicochemical characteristics (hypoxia, acidosis) and another with a focus on the components of the TME and cellular interactions via chemokine networks [55]. Further in my work, I will review each of these research areas.

1.3.1. Impact of hypoxia on tumor immune cells and their interactions via chemokine networks

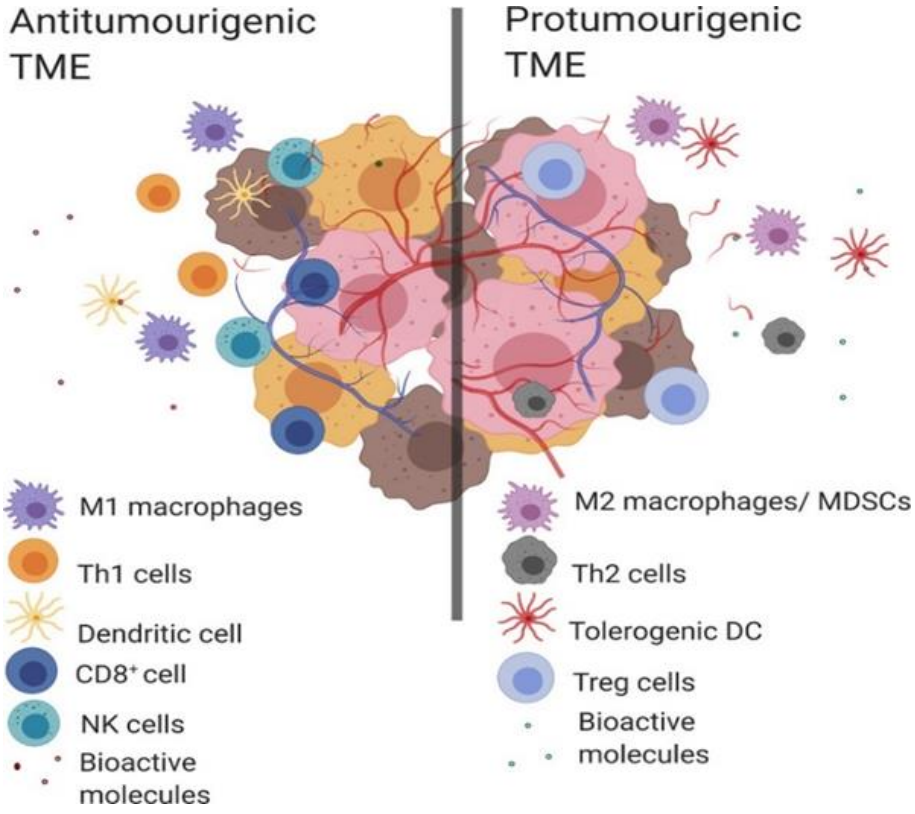

Figure 5. Anti-tumorigenic and pro-tumorigenic TME components. Left- anti-tumorigenic TME: M1 macrophages, Th1 cells, DCs, CD8+ cells, NK cells and bioactive molecules (antitumorigenic cytokines (IL-2, IL-12, IFN-γ), growth factor (GM-CSF), chemokines (CXCL9, CXCL10). Right- pro-tumorigenic TME: M2 macrophages, tolerogenic DCs, MDSCs, Th2 cells, Treg cells and bioactive molecules (protumorigenic cytokines (IL-4, IL-6, IL-10, transforming growth factor-β (TGF-β), interferon-γ (IFN-γ), angiogenic factors (VEGF), growth factors (GM-CSF, EGF, fibroblast growth factor (FGF) and chemokines (CCL2)). The image was obtained from (Hourani et al., 2021) [54].

Tumor hypoxia affects all the TME immune cell components (T cells, monocytes/macrophages, NK cells, DCs and others). B. Chen et al 2020 published the Cancer Genome Atlas (TCGA) analysis study for HIF-1α

expression in 10 types of cancers and its correlation with immune and stromal signatures. HIF-1α expression correlated with worse patient outcomes. It correlated with increased tumor suppressive signatures, including PD-L1 expression [56]. R.A Khouzam et al in 2020 performed immune cell analysis in hepatocellular carcinoma (HCC) and glioblastoma multiforme (GBM) patient samples using cell-type identification by estimating relative subsets of RNA transcripts (CIBERSORT). This analytical tool is based on a gene expression matrix of 547 genes to identify 22 immune cell types in TME. Differential immune responses were noted in hypoxia-high versus hypoxia-low tumors. The hypoxia high-risk groups showed immunosuppressive phenotype, including Treg and M0 M2 macrophages, whereas hypoxia low-risk tumors showed immune-activating cell populations, such as NK cells, CD8+ T cells, and M1 macrophages. In addition, immune checkpoint signals and immunosuppressive cytokines were noted in hypoxia-high GBM tumors [57]. In addition, the chemokine network, which is important in all stages of tumor development, is altered under hypoxia [33].

Next, I will review the effects of tumor hypoxia on specific chemokines (with emphasis on the CCL2-CCR2 and CXCL8-CXCR1/2 chemokine signaling axis) and various immune cell subsets in tumors.

1.3.1.1. Chemokine network alterations in tumor hypoxia

1.3.1.1.1. Overview of chemokines

The chemokines are a vast family of small (60–100 amino acids), secreted proteins that signal via the cell surface G protein-coupled heptahelical chemokine receptors [58], whose main function is to regulate cell trafficking. Although the first chemokine was identified in 1977, now we know more than 50 human chemokines and 20 chemokine receptors [59]. By stimulating the migration of various blood cells, chemokines play a central role in the development and homeostasis of the immune system as well as inflammatory responses. Chemokines not only stimulate chemotactic cell migration but also activate other types of cellular responses, such as cell arrest or adhesion [58].

Chemokines are defined by their primary amino acid sequence and the arrangement of the cysteine residues within the protein. Disulfide bonds form and maintain the structure of the chemokine monomer, which consists of a central three-stranded β-sheet, an overlying C-terminal α-helix, and a short unstructured N terminus that plays a critical role in receptor activation [58].

Chemokines are split into four subfamilies based on the variation of the two cysteine residues closest to the N terminus: CC (cysteines are directly set side by side), CXC (single variable amino acid between two cysteines), CX_3C (three amino acids between these two cysteines), and XC (there is a lack of first and the third cysteines of the motif) [58].

Chemokine receptors, heptahelical surface molecules that bind to chemokines, are divided into conventional chemokine receptors (cCKRs) and atypical chemokine receptors (ACKRs) [58]. Once a chemokine is tethered to a cCKR, conformational changes are induced, which translate into complex intracellular signals that activate downstream pathways such as β-arrestins, JAK-STAT pathways, and others [58]. There are currently 18 cCKRs known, which are named according to the predominant chemokine they bind (i.e., CC, CXC, CX_3C, or XC), followed by the letter R (receptor), and then a number reflecting the order of their discovery [58]. Receptor specificity is complex, as many chemokines bind to multiple cCKRs, and some cCKRs have many ligands. There are also variations in the affinity of certain chemokines toward the receptors. Some cCKRs can also be activated by nonchemokine ligands. For instance, high mobility group box 1 protein (HMGB1) is a key CXC motif chemokine receptor 4 (CXCR4) ligand [58]. Atypical chemokine receptors are structurally related to cCKRs but do not couple to the signal transduction pathways activated by cCKRs [58].

The chemokine network is complex and diverse and therefore exert multifaceted roles in the cells and cell-cell interactions **(Fig. 6).** The function of chemokines and their receptors encompasses not only chemokine-driven cell migration, which guides immunological development, homeostasis, and surveillance, but it also plays a key role in innate and adaptive responses, inflammation, and tissue repair [58]. Therefore, chemokines and their receptors are crucial factors in tumor evolution.

1.3.1.1.2. Chemokines and tumor hypoxia

Chemokines are an important component of the TME and various cell interactions in the tumor niche. They can act via the autocrine loop of the tumor cells and the paracrine loop between the tumor and the stroma cells: TAMs, CAFs, tumor-associated neutrophils (TANs), endothelial cells, and others [60]. Depending on the context and exerted functions, chemokines can be pro-tumorigenic or anti-tumorigenic [61, 62]. Chemokines can attract various cells to the tumor niche, such as anti-cancer properties bearing TILs

and natural killer (NK) cells or pro-tumorigenic monocytes that become TAMs.

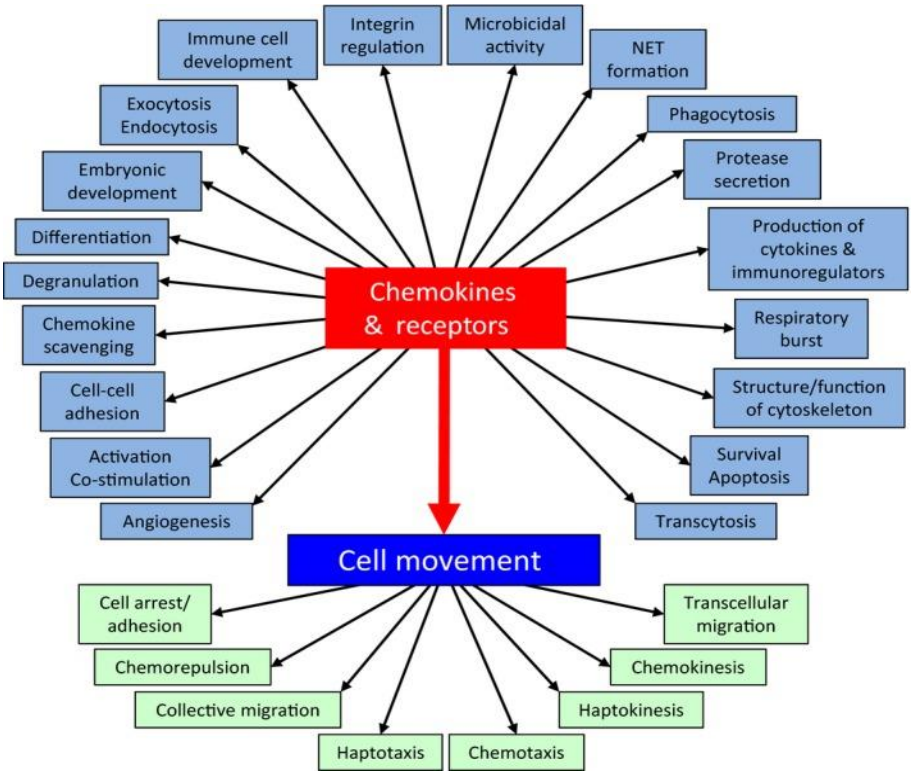

Figure 6. Functions of chemokines and their receptors. The image was obtained from (Hughes et al., 2018) [58].

The chemokine network mediates various processes in tumor development, such as progression, immune evasion, epithelial-mesenchymal transition (EMT), and metastasis [61, 62].

The data on how hypoxia in TME alters chemokine profile is limited and mainly is based on *in vitro* tests on different cell lines, which show the direct effect of hypoxia on certain neoplastic processes [33]. *In vitro* tests show that chemokine upregulation in hypoxia depends on the cell line and the context (whether hypoxia is chronic or cyclic) [33, 63]. Next, I will focus on the role of the CCL2-CCR2 and CXCL8-CXCR1/2 chemokine axis in the TME and hypoxia as they are most relevant to my work.

1.3.1.1.3. CCL2-CCR2 axis and tumor hypoxia

CCL2 was the first discovered human CC chemokine with its gene mapped on chromosome 17 (chr.17, *q11.2*). It is composed of 76 amino acids and is 13 kDa in size [59].

CCL2 chemokine is secreted by a variety of cells in response to oxidative stress, cytokines, or growth factors [59]. CCL2 binds to its receptor CCR2. There are two alternatively spliced forms of CCR2: CCR2A (expressed by mononuclear cells and vascular smooth muscle cells) and CCR2B (expressed by monocytes and activated NK cells) [59]. Structurally, the N-terminal tail at the end of the CCL2 protein determines CCR2 receptor binding affinity. CCL2 can also bind to CCR4 receptors and ACKRs. CCL2 can regulate the infiltration and migration of various cells monocytes/ macrophages, T cells, and NK cells, playing critical roles in the immune response. CCL2 acts as a potent factor in the polarization of Th0 cells toward an immunosuppressive Th2 phenotype [59]. Due to its role in the recruitment of monocytes, CCL2 is important in the pathogenesis of many diseases, such as atherosclerosis, inflammatory bowel disease, and cancer [62].

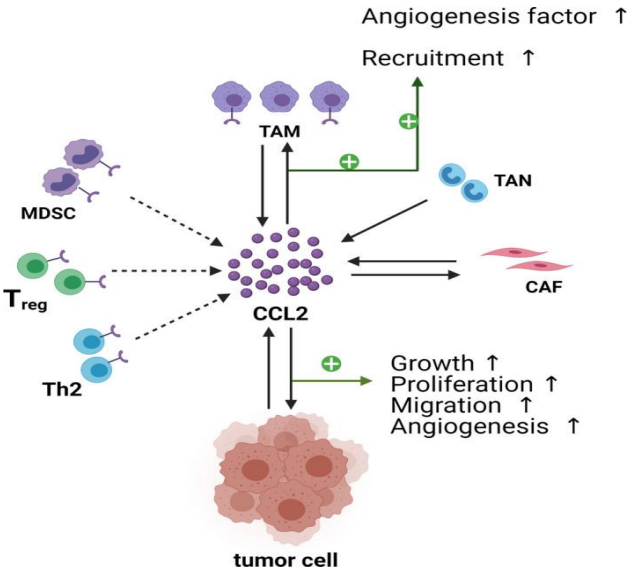

Figure 7. CCL2 can recruit various immunosuppressive cells to the TME and weaken the anti-tumor immune response. In addition to tumor cells, other cells TAMs, TANs and CAFs can secrete CCL2 (Korbecki J. et al, 2020) [30].

CCL2 chemokine can be produced by the tumor cells as well as MDSC, MSC, TAMs, TANs, and CAFs (Fig.7) [30]. CCL2 is associated with a worse

prognosis in a variety of tumors. The CCL2-CCR2 signaling axis is indispensable in all the stages of tumorigenesis, from initiation to progression and metastasis [30]. It helps recruit TAMs and MDSCs into the tumor niche and polarizes macrophages to the M2 phenotype [62]. It also recruits Treg and Th17 cells into the tumors, creating an immunosuppressive niche. In tumor cells, it increases proliferation and stemness, causing apoptosis and drug resistance. By acting via endothelial cells, it contributes to angiogenesis. In addition, it supports EMT transition and metastasis formation [62].

Studies show the variation of CCL2 secretion in response to chronic hypoxia. Chronic hypoxia decreases the expression of CCL2 chemokine in glioma, uveal melanoma cells, human umbilical vein endothelial cells (HUVEC), and macrophages. On the other hand, chronic hypoxia increases CCL2 protein in breast cancer, cervical cancer, multiple myeloma, endothelial cells, and others [33]. These differences in CCL2 protein expression in response to chronic hypoxia can be explained by the regulation of CCL2 chemokine production. The promoter of the *CCL2* gene contains HRE [33]. At the same time, chronic hypoxia decreases the activity of oxygen-dependent enzymes, such as Jumanji C domain-containing histone demethylases (JHDMs), which leads to the methylation of the histones in the promoter and enhancer regions of the *CCL2* gene. This methylation leads to a decrease in CCL2 protein expression. During cyclic hypoxia, the level of CCL2 chemokine increases in alveolar macrophages, THP-1 monocytes, endothelial cells, and melanoma cells. This effect is likely driven by the induction of nuclear factor kappa B (NF-κB) [33, 34].

The CCR2 gene contains the HRE sequence. Chronic hypoxia increases CCR2 expression in mDCs generated from primary human monocytes [64]. However, the M2 polarized macrophages derived from THP-1 monocytes did not increase CCR2 expression under chronic hypoxia, but the addition of HMGB1, a nuclear chromatin-associated protein that works as a damage-associated molecular pattern molecule, reduced CCR2 expression [65]. CCR2 mRNA expression was downregulated in mouse L929 fibroblast cells [66] and human monocytes with an impaired response to CCL2 stimulation [67].

During cyclic hypoxia, both mRNA and protein expression levels of CCR2 were significantly increased in THP-1, and it was dependent on NF-*κ*B activation and upregulation of the receptor for advanced glycation endproducts (RAGE) [68].

Data on how the tumor CCL2-CCR2 axis is affected by hypoxia *in vivo* is limited. It has been shown that hypoxic tumor-derived CCL2 chemokine drives the accumulation of granulocytic $CD11b^{+}/Ly6C^{med}/Ly6G^{+}$ myeloid

cells in murine mammary tumors, which helps to create the premetastatic niche. In turn, CCL2 chemokine neutralization in such a medium decreases metastatic tumor burden [35].

1.3.1.1.4. CCL2-CCR2 axis inhibition in cancer

Despite improved knowledge of the role of the CCL2-CCR2 axis in cancer, we still lack an understanding of the effects of CCL2-CCR2 axis inhibition in the hypoxic environment in solid tumors. Such comprehension is especially pertinent today as CCL2-CCR2 axis inhibitors fail to show efficacy in clinical trials. Targeting the CCL2-CCR2 axis as a treatment option is in various stages of development. A few CCR2 receptor antagonists have been tested in clinical trials. Sadly, PF-04136309, a small molecule targeting the CCR2 chemokine receptor, when used in combination with Nab-paclitaxel plus Gemcitabine, had a concerning safety profile [36]. Three Phase I/II clinical trials with BMS-813160, a CCR2 and CCR5 receptor dual antagonist, in various combinations, have recently been completed (NCT03767582, NCT03496662, NCT03184870), but no data have been reported. One Phase I/II trial assessing the tolerability and efficacy of BMS-813160 with Nivolumab and Gemcitabine and Nab-paclitaxel in pancreatic ductal adenocarcinoma (PDAC) is active (NCT03496662). Similar issues are seen with the development of antibodies targeting the CCL2-CCR2 axis. Carlumab, a human immunoglobulin G1κ (IgG1κ) monoclonal antibody with high affinity and specificity for human CCL2, was well-tolerated in a Phase II clinical study but did not show antitumor activity as a single agent in metastatic castration-resistant prostate cancer [37]. A phase I study using Plozalizumab, a highly specific humanized monoclonal antibody that interacts with CCR2 and inhibits CCL2 binding, was terminated (NCT02723006). Redundancy of the target, poor drug-like properties, insufficient drug level, and many other factors could all contribute to the failed clinical trials with small molecules targeting chemokine receptors [31]. However, the development of novel CCL2-CCR2 axis inhibitors is evolving with new potential drug candidates reported, including RS504393 [30] that needs to be further explored [30] [38]. There is also a need for a better understanding of how heterogeneous TME alters the response to such inhibitors.

1.3.1.1.5. CXCL8-CXCR1/2 axis and tumor hypoxia

Initially discovered as a chemotactic agent for neutrophils, CXCL8 is a peptide with 72 amino acids and has a critical N-terminal motif of Glu-Leu-Arg that can be secreted by a variety of cells in the tumor, such as CAFs, endothelial cells, DCs, monocytes, macrophages, and cancer cells [55]. CXCL8 chemokine signals through two G-protein-coupled cell-surface receptors: CXCR1 and CXCR2 [55]. In addition to CXCL8, CXCR1 can interact with CXCL6 chemokine and CXCR2 can interact with CXCL1, CXCL2, CXCL3, CXCL5, CXCL6, CXCL7 chemokines [55].

The CXCL8-CXCR1/2 signaling axis is vital for tumor progression. It helps recruit granulocytes and MDSCs to the site of the TME and promotes angiogenesis, cancer cell proliferation, and immune resistance [55] [69] [70]. The CXCL8-CXCR1/2 axis is implicated in neutrophil extracellular traps (NETs) formation. These are extracellular web-like structures composed of DNA-histone complexes and proteins released by activated neutrophils. These structures are implicated in tumor progression and metastasis [71]. CXCL8 chemokine secretion by the pancreatic cancer cells mediates CXCR2+CD68+ macrophage trafficking to the TME and contributes to cancer progression and PD-1 blockade resistance in the murine pancreatic cancer cell model [72]. IFN-γ cytokine decreased the secretion of CXCL8 chemokine in pancreatic cancer cells and inhibited TAM migration to enhance anti-PD1 efficacy [72]. CXCL8 secreted by TAMs promoted pancreatic cancer, HCC, prostate, and thyroid cancer cell proliferation and invasion [55]. Mesenchymal stem cell-derived CXCL8 promoted osteosarcoma pulmonary metastasis through CXCR1/Akt signaling in mice [73]. *CXCR1* gene knockdown improves the sensitivity of human osteosarcoma cells to cisplatin, both *in vivo* and *in vitro* [74].

CXCL8 regulation under hypoxia has not been well studied. CXCL8 upregulation depends on whether hypoxia is cyclic or chronic and the research model studied. For example, chronic hypoxia does not alter CXCL8 expression in breast cancer, lung adenocarcinoma, or uveal melanoma cells, but is increased in GBM cells [63]. Regulation of CXCL8 protein expression under chronic hypoxia is also complex. In GBM cells, CXCL8 mRNA expression in chronic hypoxia is activator protein 1 (AP-1) but not NF-κB dependent [63]. In contrast, in some bladder cancer lines, CXCL8 protein expression was associated with the activation of NF-κB but not AP-1[63]. In rhabdomyosarcoma cells, CXCL8 protein expression was regulated by AP-1 together with NF-κB and was not affected by HIF-1α. In HCC cells, an increase in the expression of CXCL8 in chronic hypoxia was dependent on the activation of HIF-1 and the effect of this transcription factor on NF-κB.

Similarly, the result of chronic hypoxia on CXCR1 and CXCR2 receptor expression in cancer cells depends on the research model. Expression of CXCR1 and CXCR2 receptors in cervical carcinoma cells and prostate cancer cells increases via HIF-1 and NF-κB activation, whereas CXCR2 expression in gastric cancer cells decreases.

CXCL8 chemokine secretion in cancer cells under cyclic hypoxia varies based on the research model. In prostate cancer cells, both cyclic and chronic hypoxia induce a similar increase in the expression of CXCL8 mRNA, but in SK-OV-3 ovarian adenocarcinoma cells, only cyclic hypoxia increases the expression of CXCL8 mRNA [75]. Interestingly, cyclic hypoxia increases the expression of CXCL8 on neutrophils and the receptor of this chemokine, CXCR2, which reduces the spontaneous apoptosis of these cells and likely impacts TAN retention in TME under hypoxia.

Chronic hypoxia in primary human macrophages upregulates CXCL8, and it is HIF-1α and HIF-2α-dependent [76]. During cyclic hypoxia, human THP-1 macrophages, either unpolarized (M0) or polarized into M1 or M2 phenotype, have increased expression of this chemokine. Such expression can be abolished in M0 macrophages with a c-Jun N-terminal kinase (JNK) inhibitor [77]. More research is needed to assess CXCL8 regulation in actual hypoxic TME.

Plasma CXCL8 chemokine level could serve as a prognostic biomarker in solid tumors, as patients with various solid tumors have elevated circulating CXCL8 chemokine levels, which are associated with increased monocyte and neutrophil infiltration, as well as worse outcomes and reduced effectiveness of ICB [78, 79]. CXCL8-CXCR1/2 axis inhibition in combination with immunotherapy may be a promising strategy. Sadly, recently published data on the use of CXCR2 antagonist Navarixin in combination with Pembrolizumab in adults with previously treated advanced or metastatic castration-resistant prostate cancer, microsatellite-stable colorectal cancer, or non-small-cell lung cancer did not show efficacy [80]. Nevertheless, the development of novel agents targeting the CXCL8 chemokine is ongoing, and several clinical trials are yet to be completed.

1.3.1.2. Changes in the tumor immune cells under tumor hypoxia

1.3.1.2.1. Cytotoxic T lymphocytes

While T-cells can function under mild to moderate hypoxia conditions, the acidic pH of tumors suppresses T-cell activation, proliferation, and cytotoxicity [81]. Interleukin-2 (IL-2)-driven T-cell proliferation stalls out at pH 6.7. Extracellular pH in hypoxic tumors can be as low as pH 5.8–6.5. In addition, lactic acid itself can block T-cell proliferation and effector functions [81]. Calcinotto et al in 2012 described how acidic TME causes TIL anergy in melanoma by suppressing IL-2 cytokine and interleukin-2 receptor alpha chain (IL-2Rα) expression, diminishing signal transducer and activator of transcription 5 (STAT5) and extracellular signal-regulated kinases (ERK) activation, and decreasing CD3 and ζ-chain expression. Such cell anergy could be reversed after pH was restored, but after some time [82].

Hypoxia triggers the release of adenosine precursor molecules, mainly ATP and adenosine diphosphate (ADP), into the extracellular space through channel-mediated transport or leakage due to non-specific membrane damage [83]. In turn, the accelerated consumption of extracellular ATP and ADP by hypoxia-sensitive, membrane-associated CD39 and CD73 ectonucleotidases leads to the accumulation of end-product adenosine [84, 85]. CD4+ and CD8+ T cells express adenosine receptors (A2AR). Therefore, an abundance of adenosine in the tumor milieu decreases the proliferation and synthesis of IL-2, Tumor Necrosis Factor-alpha (TNF-α), interferon-gamma (IFN-γ), perforin, and FAS ligand by immune cells [86]. Reactive nitrogen species cause nitration of the T-cell receptor and of CD8+, disabling recognition of the major histocompatibility complex (MHC) - antigen complexes and T-cell activation. Intratumoral nitration of the CCL2 chemokine reduces access of TILs to the inner core of tumor tissues [87].

Hypoxia also affects co-stimulatory/inhibitory molecule expression on T cells. HIF-1α increased costimulatory molecule CD137 (41-BB) expression on activated T cells in culture. In addition, the CD137 receptor is upregulated in murine tumors where TILs are experiencing hypoxia, as indicated by 18F-MISO positron emission tomography (PET). Treatment with anti-CD137 monoclonal antibody diminished murine tumor growth [88].

Cancer cells employ MHC I receptor downregulation to avoid immunosurveillance and killing [89]. Hypoxia decreases MHC I expression on murine sarcoma tumor cells *in vivo* and in three-dimensional (3D) cultures

[89]. In breast carcinoma patient tumor samples, CAIX-expressing hypoxic areas correlated with decreased CD8+ T cell infiltration [90].

1.3.1.2.2. Regulatory T cells

The forkhead box P3 *(FOXP3)* gene, a regulator of the development and function of Treg cells, has many predicted HREs. Hypoxia upregulates the Foxp3 gene in primary mouse CD4+ T cells and human Jurkat cells. Hypoxia increased the functional activity of murine Tregs [91] [92]. Facciabene et al in 2011 showed that hypoxic intraperitoneal ovarian cancer cell line ID8 tumors recruit CD4+CD25+Foxp3+ Tregs cells, which dampen effector T cell function and promote angiogenesis [9].

1.3.1.2.3. Tumor-associated macrophages and myeloid-derived suppressor cells

Myeloid cells are known to play an important role in suppressing adaptive immunity. The two main groups of suppressive myeloid cells in TME are TAMs and MDSCs [93]. TAMs can develop from both tissue-resident and circulating monocyte populations [94]. MDSCs are myeloid cells in the immature state capable of suppressing T cell activity. MDSCs can be further subdivided into 1) polymorphonuclear (PMN)-MDSCs, which express $CD11b^{+}CD14^{-}CD15^{+}$ (in mice- $CD11b^{+}Lys6C^{lo}Ly6G^{+}$) surface proteins and 2) monocytic (M)-MDSCs, which express $CD11b^{+}CD14^{+}HLA\text{-}DR^{low/-}$ $CD15^{-}$ (in mice $CD11b^{+}Ly6C^{hi}Ly6G^{-}$) surface proteins. TAMs are distinguished from MDSCs by the presence of certain mature macrophage markers that MDSCs lack, such as F4/80, CD68, and CD163, and low or absent S100A9 expression [95]. MDSCs under the influence of certain toll-like receptors (TLR) and cytokine signaling can also differentiate into TAMs [96].

Chemotactic signals from the growing tumors recruit circulating monocytes, where they differentiate into TAMs. The major chemokines that drive such recruitment include CCL2 and CCL5. Blocking of the CCL2-CCR2 axis results in a significant decrease in TAMs [94]. Other chemokines involved in monocyte recruitment are CCL3, CCL4, CCL8, and CCL22 [54]. Cytokines involved in monocyte transition to TAMs are colony-stimulating factors-1 (CSF-1), VEGF, and IL-4 [97] [98].

Once monocytes reach the tumor bed and become TAMs, they are polarized into type M1 or M2 [99]. M1 macrophages are strong effector cells, capable

of killing target cells and secreting proinflammatory cytokines. M2 macrophages promote angiogenesis and tissue remodeling, secrete anti-inflammatory cytokines, and are pro-tumoral. TAMs are predominantly M2-like with marked immunosuppressive properties [96] [99] **(Fig. 8).**

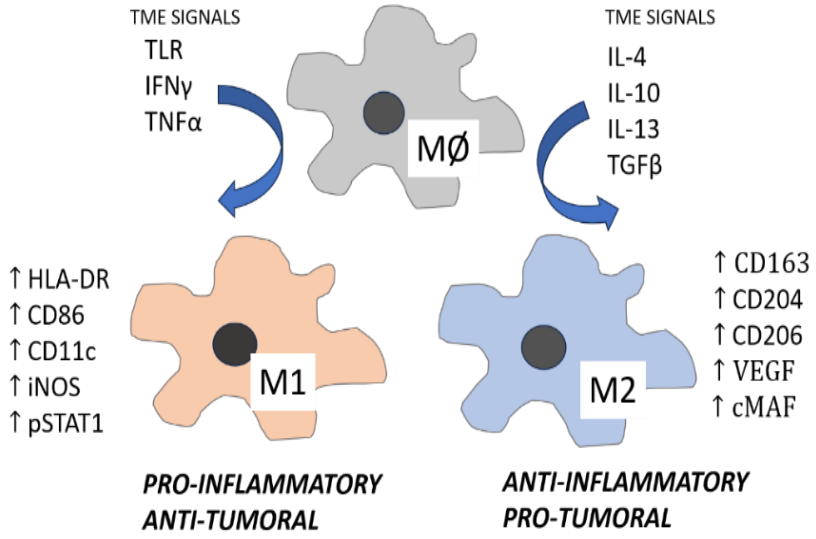

Figure 8. Macrophage polarization. Adapted from S.D. Jayasingam et al *Front. Oncol.*, 2020 [99].

Both TAMs and MDSCs employ various mechanisms to suppress T-cell immunity. They can upregulate PD-1 and cytotoxic T-lymphocyte-associated protein 4 (CTLA-4), which causes leukocyte apoptosis and anergy. They deprive the local environment of nutrients necessary for T-cell activation and function and generate nitric oxide and reactive nitrogen species by nitric oxide synthase (iNOS) expression, which induces T-cell exhaustion. These mechanisms decrease the effective killing of the tumor by T-cells and attract tumor-supporting Tregs [100].

VEGF-A, semaphorin 3A (SEMA3A), and endothelial cell monocyte-activating polypeptide-II (EMAP-II) mediate TAM recruitment to the hypoxic TME [101]. Recent evidence shows that large numbers of TAMs are attracted to and retained in avascular and necrotic tumor areas [102]. At these sites, TAMs appear to undergo marked phenotypic changes with activation of hypoxia-inducible transcription factors, dramatically upregulating the expression of many genes encoding mitogenic, proangiogenic, and premetastatic cytokines and enzymes [102]. Under hypoxic conditions,

murine and human TAMs display defective NFκB, which impairs the production of IL-12 and TNF-α, needed for antitumor immune responses [102]. In addition, tumor-derived lactate (Warburg effect) can induce M2 phenotype-related genes, promote the expression of Arg-1, and stabilize HIF-1α [103]. Hypoxia via HIF-1α induces CD47 receptor expression in cancer cells, promoting escape from phagocytosis by macrophages [104]. This way, TAMs in hypoxic tumor areas promote immunosuppression, angiogenesis, and metastasis.

Like TAMs, MDSCs preferably infiltrate hypoxic regions of the tumor. In the experimental HCC tumor model, hypoxia prevented MDSC maturation at the tumor site by inducing ectonucleoside triphosphate diphosphohydrolase 2 (ENTPD2) enzyme in cancer cells to generate a 5′-adenosine monophosphate (AMP)-rich microenvironment [105]. In addition, MDSCs increase PD-L1 protein expression under hypoxia. Furthermore, the immune suppressive function of MDSCs, isolated from the spleens of mice bearing B16-F10 tumors, was enhanced under hypoxia and was abrogated after blocking PD-L1 [106].

1.3.1.2.4. Dendritic cells and natural killer cells

DCs are antigen-presenting cells (APCs) that help regulate innate and adaptive immune responses. Interestingly, hypoxia increases the response to proinflammatory stimuli in murine DCs and improves their function [107]. Monocyte-derived dendritic cells (mDCs) are also impacted by a hypoxic environment. Recent studies show distinct gene expression profiles of mDCs under chronic hypoxic conditions, where genes involved in glycolytic metabolism, glucose transport, and coding for chemokines attracting neutrophils and activated/memory T lymphocytes are upregulated. Other genes affected were ones that code for endothelial cell survival, proliferation, adhesion, and chemotaxis (osteopontin, VEGF, etc) [108]. Interestingly, under hypoxic conditions, sCAIX may sample the microenvironment and generate an immune response against extracellular antigens and therefore can be applied for a vaccine strategy [109].

Hypoxia, in addition to its by-product lactate, inhibits NK cells' cytotoxic activity [110, 111].

1.3.2. Tumor acidosis

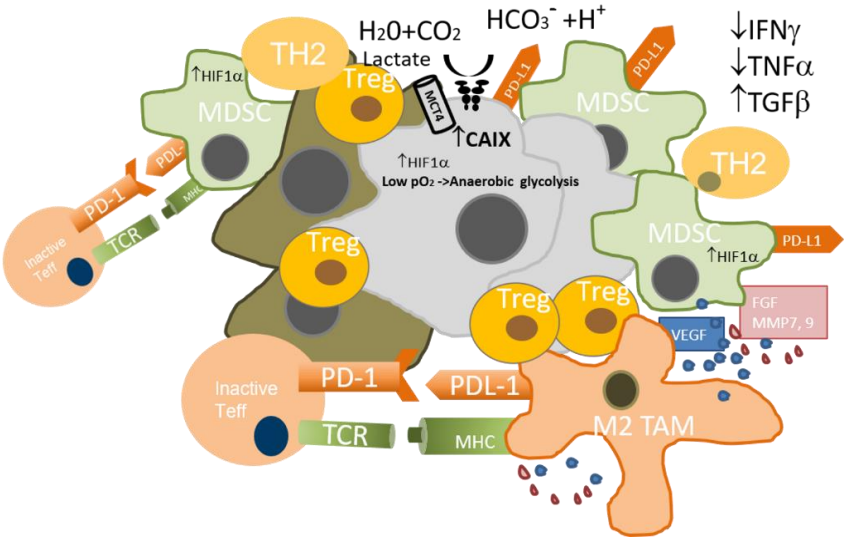

Figure 9. Low pH effects on TME and the adaptive immune response. Tumor hypoxia leads to the upregulation of HIF-1α and the shift of tumor metabolism to anaerobic glycolysis. Resultant intracellular acidosis is aborted by CAIX, which hydrates CO_2 to produce bicarbonate and protons. This leads to pericellular acidosis that is detrimental to anti-tumor immune responses. It polarizes TAMs to M2 phenotype, increases survival of MDSCs, which secrete VEGF, matrix metalloproteinases (MMPs) (pro-angiogenic), and upregulates PD-L1. Low pH causes anergy of CD8+ T cells and stimulates the progression of CD4+ T cells into the TH2 phenotype (tumor-promoting) as opposed to TH1. TH2 cells secrete TGF-β (not IFN-γ or TNF-α).

Warburg effect in growing tumors results in an acidic extracellular pH (pH 6.5- 6.9), compared to physiological conditions (pH 7.2-7.4) [112]. H+ ions accumulate in the tumor-stroma interface, promoting tissue remodeling by ECM degradation, activation of angiogenesis, and inhibition of immune response [113, 114]. Such adaptations allow tumor cells to grow and invade. Restoring pH with various treatments aborts tumor invasion [112]. The acidic microenvironment created in the tumor vicinity by glycolytic activity can cause upregulated expression of HIF-1α protein and VEGF cytokine, both of which can contribute not only to increased angiogenesis but also to decreased antigen presentation and the expansion of the population of

immunosuppressive MDSCs [115]. IFN-γ can be denatured at low pH, which diverts T cells toward the protumor TH2 phenotype, as well as prevents the activation of tumoricidal M1 macrophages [115]. As both cancer and immune cells are heavily dependent on the glycolytic pathway for active proliferation, they compete for glucose. It is a disadvantage of T cells as they cannot survive without an adequate glucose supply. On the contrary, tumor cells can enter quiescence for an extended period [116]. That way, tumor cells can endure while T cells are not able to expand in the hostile environment [115] **(Fig. 9).**

Acidic TME induces an anergy in CD8+ T cells as it decreases cytolytic activity, downregulates CD25 protein and TCR receptor, and decreases cytokine production [19]. The acidic TME does not affect CD4+ T cells as they rely on fatty acid oxidation [19]. Low pH via NF-κB transcription factor increases iNOS levels in macrophages. Exposure to lactic acid generated by tumor cells induces VEGF cytokine and macrophage polarization towards the M2 phenotype. The lactic-acid-stimulated bone-marrow-derived macrophages' co-injection with tumor cell implantation in mice resulted in significantly larger tumors than the co-injection with control macrophages [103]. Extracellular acidosis upregulates arginase 1 (Arg1) enzyme and CD206+ protein on TAMs and helps inhibit T cell activation and proliferation [19].

1.3.2.1. Targeting tumor hypoxia and acidosis

The pronounced effects of hypoxia on tumor immune responses call for a search for agents that could alter hypoxic TME and, in turn, synergize with various immunotherapies.

1.3.2.1.1. Ways to tackle tumor hypoxia

Re-oxygenation of tumor hypoxia zones could be the most direct strategy to relieve negative hypoxic effects on immune cells. Pre-clinical studies with syngeneic tumor models showed that respiratory hyperoxia could decrease intratumoral hypoxia and enhance effector T cell infiltration, reduce Tregs, and induce pro-inflammatory cytokines [117, 118]. However, such an approach in a clinical setting is not feasible.

Metformin, an antidiabetic drug, inhibits mitochondrial complex I, reducing tumor oxidative metabolism and alleviating tumor hypoxia. In turn, treatment

with metformin in combination with anti-PD-1 blockade showed complete tumor regression in pre-clinical studies [119].

Similarly, the anti-malarial drug Atovaquone inhibits oxidative phosphorylation of complex III of the mitochondrial electron transport chain and reduces oxygen consumption rates in numerous cancer cell lines. Administration of Atovaquone directly alleviates hypoxia in preclinical xenograft models [120]. Patients with NSCLC who received Atovaquone were noted to have increased tumor oxygenation that impeded hypoxic gene expression [121].

Hypoxia-activated pro-drugs (HAPs) are DNA damage or kinase inhibitors designed to be selectively activated under hypoxic conditions. They target and kill hypoxic tumor cells that are traditionally resistant to conventional therapies. To date, a limited number of HAPs have been evaluated in clinical trials, including Porfiromycin, Banoxantrone, Tirapazamine, Evofosfamide, PR-104, and Tarloxotinib. Of these, Evofosfamide is being tested in combination with ICB in clinical trials (NCT03098160), but the status of this clinical trial is unclear [122].

Targeting HIF has recently transitioned into clinical trials. A novel HIF-2 allosteric inhibitor, Belzutifan (MK-6482, PT2977), is currently being evaluated in a Phase 3 trial in advanced renal cell carcinoma (RCC) (NCT04195750) and VHL-associated RCC (Phase 2) (NCT03401788). A dose-escalation/expansion trial in advanced solid tumors is now underway (Phase I/II) (NCT02974738). One study is evaluating Belzutifan in combination with Cabozantinib in advanced clear cell RCC (NCT03634540). In addition, data from the phase II clinical trial of the HIF-2α inhibitor PT2385 were just reported, showing limited activity [123]. Whether HIF-2 inhibitors can be advantageously combined with immunotherapies remains to be determined. Pre-clinical studies show the effectiveness of HIF-1α inhibition with DC vaccines in breast cancer models [124].

As hypoxia triggers a robust pro-angiogenic switch, targeting VEGF and vascular endothelial growth factor receptor (VEGFR), angiopoietin-2 or CXCL8 in combination with HIF inhibition is another attractive option.

1.3.2.1.2. Targeting tumor acidosis

The most direct approach to diminish tumor acidosis is by using buffers. In pre-clinical murine models using buffers such as bicarbonate, imidazole-1-yl-3-ethoxycarbonylpropionic acid (IEPA) to improve acidosis showed positive results [125] [126]. A buffer therapy approach failed clinically in

three clinical trials (NCT1350583, NCT01198821, NCT1846429) due to poor patient compliance and grade 2 gastrointestinal toxicity [19].

Another approach to targeting tumor acidosis is via enzyme inhibition. Ureases are urea-degrading enzymes that convert urea into more toxic ammonia and lead to a local pH rise from the generated ammonia. Carcinoembryonic antigen-related cell adhesion molecule 6 (CEACAM6)-targeted Jack bean urease (L-DOS47) has begun to be used in preclinical tumor models and clinical trials to modify the TME [127]. Research in targeting lactate metabolism, by inhibiting lactate dehydrogenase A (LDHA) has also gained speed [19].

Ion transport, which permits cancer cell survival, inhibition may impede acidosis. As a catalyzer of reversible hydration of CO_2 to bicarbonate and protons at the extracellular surface, CAIX controls intracellular and extracellular acid-base balance to maintain the survival of cancer cells and is the key regulator of extracellular acidity. Therefore, inhibition of the catalytic activity of CAIX to modulate acidity in TME has become a pursuit of many researchers.

1.4. CAIX as a target in cancer therapeutics

1.4.1. CAIX in cancer

CAIX is a hypoxia-induced enzyme that belongs to hypoxia niche modulatory proteins. CAIX is α carbonic anhydrase, a zinc metalloenzyme that catalyzes the reversible hydration of carbon dioxide to bicarbonate ions and protons in a cell, maintaining acid-base balance[11].

CA9 gene is located on the p12–p13 region of chromosome 9 [128]. The basis of the unique properties of *CA9* gene expression is the organization of its promoter. The TACGTG HBS, located immediately upstream of the transcription start, is the central regulatory element in the *CA9* promoter, and HIF-1 complex binding to the *CA9* HRE is a prerequisite for further transcription[49]. The remaining *cis*-acting elements in the *CA9 gene* are subordinated to HRE and play significantly lesser roles [128]. Epigenetic silencing via methylation of the *CA9* promoter has been described and represents a resistant mechanism during CAIX-directed therapies [49]. Other mechanisms can regulate CAIX expression: inactive VHL increases CA IX expression via active HIF-1α, and p53 activation leads to CA IX down-regulation. Also, oncogenic PI-3K and ERK pathways can regulate CA IX expression by targeting *cis*-acting elements of the CA IX promoter [128].

In addition, *CA9* gene expression can involve alternative splicing [129] as the alternatively spliced (AS) variant of *CA9* mRNA was demonstrated in tumors, normal tissues, and under normoxia. The human AS mRNA lacks exons 8–9 and codes for a truncated CA IX protein [129]. Such a variant of CAIX can be present in normoxic cells. In the absence of full-length CA IX, it can produce false-positive results in studies designed to assess hypoxia [129].

CA IX forms a homodimer in the crystal structure and is a multidomain protein. It consists of an extracellular part with an active site and a proteoglycan (PG) domain, which can open or close the active site of the enzyme, a transmembrane segment, and a cytosolic tail [128] **(Fig.10).**

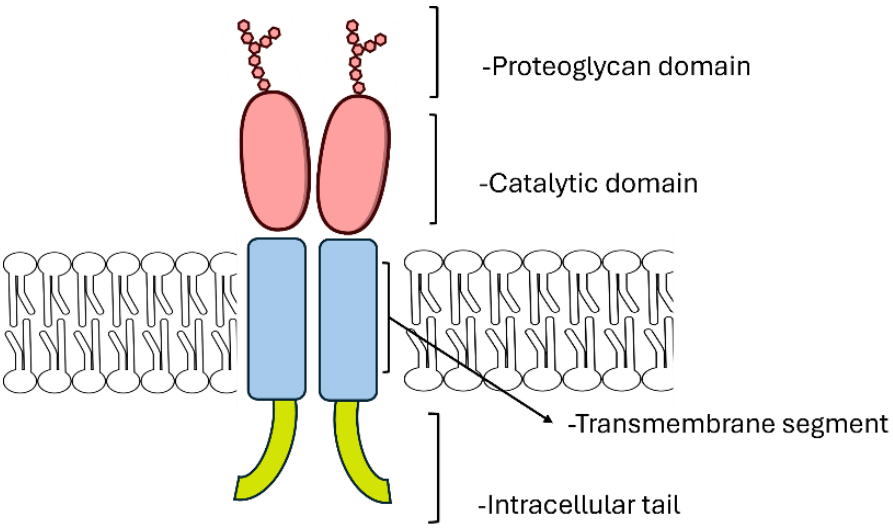

Figure 10. Depiction of the CAIX dimer with its four distinct parts: the proteoglycan domain, catalytic domain, transmembrane segment, and the intracellular tail. Certain objects in the image were obtained from NIH Bioart.

The CAIX enzyme's catalytic domain faces the extracellular space. Like other catalytically active CA isoforms, it contains a zinc ion at the bottom of an active site cleft, which is essential for the catalysis and binding of inhibitors. It is coordinated by three His residues (His94, His96, His119) and a water molecule/hydroxide ion, which is nucleophilically activated upon binding to the metal ion and efficiently transforms CO_2 into bicarbonate [128]. It is important to note that among the 12 catalytically active human CAs, the active site amino acid residues are rather conserved. By CO_2 hydration CAIX enzyme contributes to pH regulation across the plasma membrane, facilitating

CO_2 diffusion and proton mobility. It exerts its action in partnership with other acid extruders and bicarbonate importers such as sodium-dependent bicarbonate transporters NBCe1 and NBCn1, lactate and proton-exporting MCT1 and MCT4, NHE1, and others. It has been shown that CAIX can form a transport metabolon with MCT1 and MCT4 [130]. In addition, CA IX can also behave as an adhesion molecule. Its PG domain helps form focal adhesion contacts during cell attachment and spreading on solid supports. It can also disrupt intercellular adhesion contacts, disengaging E-cadherin from the cytoskeletal base through the competitive binding to beta-catenin [11].

By helping maintain physiological pH in cancer cells, the CAIX enzyme promotes tumor cell survival and progression. In addition, CAIX enzymatic activity leads to pericellular acidosis in TME. As discussed previously, tumor acidosis is associated with chemo/radio-resistance, suppressed immune responses, and angiogenesis [6]. In addition, CAIX also drives cancer cell migration, invasion, and epithelial-mesenchymal transition by both catalytic and non-catalytic mechanisms [130-132]. Patients with high CAIX-expressing tumors have a higher risk of disease progression and development of metastases, independent of tumor type or site [14]. Increased CAIX expression has been associated with worse prognosis in a group of devastating pediatric cancers[14]: brain tumors [12, 13] and solid tumors outside the CNS, such as bone and soft tissue sarcomas [15], NBL [16, 17] and others.

A recently published study of patients with recurrent/metastatic squamous cell carcinoma of the head and neck (HNSCC), who received anti-PD-1 therapy, showed that lower tumor hypoxia, defined by lower CAIX staining in patients' tissues, was associated with significantly improved disease control rate, progression-free survival, and overall survival. Lower tumor hypoxia was associated with increased efficacy of anti-PD-1 therapy in these patients [133].

1.4.2. CAIX as a target for cancer treatment

CAIX, as a hypoxia-induced enzyme, is an attractive target for cancer hypoxia niche modulation. This protein is overexpressed in a variety of solid tumors but has restricted expression in normal human tissues. Strong expression of CAIX protein is seen in the basolateral surface of proliferating crypt enterocytes of the duodenum, jejunum, and ileal mucosa [134]. In addition, weak and diffuse CAIX protein expression is noted in the epithelia of male efferent ducts and occasional foci in the pancreatic acini [134].

To date, several small-molecule CAIX inhibitors have been designed, but none have shown efficacy in clinical settings, likely due to limited drug-like properties**.** The design of small-molecule inhibitors is based on sulfonamides and their isosteres, such as sulfamates and sulfamides [128]. They act through coordination to the zinc ion within the active site of the enzyme. The prototype of such derivatives is acetazolamide, which is not selective for the CAIX enzyme and, therefore, was further modified to achieve better selectivity towards the CAIX enzyme. Second and third-generation agents include benzolamide and SLC-0111. But despite multiple research papers on the activity of various small-molecule CAIX inhibitors *in vitro* (and less so *in vivo)*, the clinical trials are sparse and do not show promising results. Most studies use a non-specific CAIX inhibitor, acetazolamide, with limited efficacy. Ongoing studies in lung cancer (NCT03467360) and GBM (NCT03011671) still await the results.

Small-molecule compound SLC-0111 entered phase 1 clinical trial in 2014. No dose-limiting toxicities were reported up to 1000 mg/ day/ dose, other than discontinuation of the drug by some patients due to the taste and texture of the compound [21]. A multi-center, open-label Phase 1b study of SLC-0111 (oral) in combination with gemcitabine in CAIX-positive patients with metastatic PDAC was recently terminated (NCT03450018).

Limited results of CAIX inhibitors in the clinic can be attributed to gaps in understanding how CAIX functions and how inhibitors exert their actions on CAIX. In addition, CAIX upregulation is a dynamic process with flexible compensatory mechanisms taking place when it is inhibited. Lastly, there is a high homology in amino acid sequences between CA isozymes, which makes the design and development of CA isoform-selective inhibitors challenging. The sequence identity of the CA catalytic domain is more than 30 % [135]. The active sites of CA isoforms are conical in shape and differ only by a few amino acids. The top of the binding site is variable, and the most conserved residues are found deep in the active site and close to the zinc ion [136]. Therefore, most inhibitors used in the clinic today lack selectivity towards the targeted CA isozymes [22].

Our laboratory has developed and patented a series of lead small-molecule CAIX inhibitory compounds, benzenesulfonamide derivatives, with VD11-4-2 being the leading one [23] [26]. We further modified the leading VD11-4-2 compound into doubly headed AZ19-3-2 (https://patents.google.com/patent/WO2022118277A1/en). AZ19-3-2 is a highly selective inhibitor of CAIX. The binding of AZ19-3-2 to various CAs was tested by fluorescent thermal shift assay (FTSA), isothermal titration

calorimetry (ITC), and confirmed by stopped-flow assay of inhibition of enzymatic activity (SFA). These studies showed exceptional sensitivity and specificity toward CAIX enzyme with a picomolar binding constant. This dissertation is based on studies with this novel CAIX inhibitor.

1.4.3. CAIX as a target for radiotherapy and diagnostics

As it was discussed previously, hypoxia is a predictor of worse outcomes and treatment resistance in a variety of solid cancers. Therefore, the characterization and detection of hypoxic regions within solid tumor masses is an important task. Therefore, a molecular imaging application that targets selective proteins that serve as markers for tumor hypoxia is needed. Such imaging could help decide which patients will benefit from anti-hypoxia therapy and help detect and follow the response of disseminated metastatic disease to systemic and targeted therapies [137]. As increased CAIX expression has been noted in a variety of cancers, the development of CAIX recognition-based theranostic radiopharmaceuticals is of value [27]. Numerous CAIX-targeted radionuclide therapy agents are in various phases of clinical trials [27]. The most suitable design approach for CAIX-targeting theranostic compounds involves the formation of a conjugate between an effective CAIX inhibitor and a metal chelator, tethered to a suitable linker [27]. Several CAIX-targeting agents (monoclonal antibodies, antibody fragments, peptides, and small molecules) conjugated to ^{89}Zr, ^{18}F, ^{124}I, or ^{111}In have been suggested for PET/CT or SPECT/CT [27]. Many clinical trials (NCT05018442, NCT03849118, NCT04897763, NCT05046665, NCT04758780, NCT00884520, etc) have been initiated to evaluate the diagnostic value of these radio-conjugates, including ^{89}Zr-labeled Girentuximab (monoclonal antibody) and ^{18}F-VM4-037 (small molecule), for the detection of urothelial, clear cell renal cell, and other cancers.

The ideal radiotracer must have high sensitivity and high specificity for CAIX-positive metastases. As myelotoxicity was observed in most patients treated with radioimmunoconjugate, small molecules remain a more promising approach [138]. While most studies with small-molecule conjugates are preclinical, few tracers have been tested in clinical trials with mixed results. For instance, ^{18}F-VM4-037, a small-molecule radiotracer developed on the sulfonamide pharmacophore, a derivative of the CA ligand ethoxzolamide, failed to localize ccRCC tumors as it had a high background in the kidney and liver [139]. Recently, a ^{99m}Tc labeled acetazolamide

derivative, ^{99m}Tc-PHC-102, showed encouraging results in the pilot study using a SPECT/CT scanner, identifying substantial tumor and metastasis uptake. Gallbladder and stomach uptake was noted [140]. A pilot study of ^{68}Ga-NY104, again based on an acetazolamide core, connected to a hydrophilic spacer, and a chelator NOTA, in 3 patients with ccRCC showed excellent tumor uptake and tumor-to-background. However, significant uptake in the stomach and kidneys was noted [141]. The off-target uptake of these compounds could be related to the non-specific CA binding.

Therefore, the first step in developing such theranostic pairs should involve designing and synthesizing specific CAIX enzyme-recognizing compounds. Our laboratory has designed and synthesized promising CAIX enzyme-targeting compounds and tagged them to the NIR probe (CAIX enzyme specific-NIR probe) as the first step in assessing the specificity and biodistribution of these candidate probes for further development. Next, we investigated the targeting abilities of the new CAIX enzyme specific-NIR probes *in vitro.* My work encompassed the study of such compounds' ability to recognize CAIX enzyme in tumors *in vivo* in a proper xenograft platform.

In summary, tumor hypoxia and associated acidosis are linked to worse cancer outcomes as they permit tumor progression, invasion, metastasis, and immunosuppression. Mechanisms of immune suppression and ways to overcome it are still not understood. Hypoxia and acidosis polarize macrophages toward a tumor-promoting phenotype, block tumor killing by the effector T cells, and attract immunosuppressive Treg cells. Therefore, scavenging for pathways that could abort tumor hypoxia and acidosis is needed. CAIX enzyme is one of the key regulators of tumor acidity in TME. It is an attractive target for immunomodulation as well as diagnostics. The CCL2-CCR2 chemokine signaling axis is indispensable in the immunosuppressive microenvironment and is another attractive target to explore. This work encompasses studies of these pathways in selected solid tumor models.

2. MATERIALS AND METHODS

2.1. Materials

75cm tissue culture flasks (#90076, TPP Techno Plastic Products AG)
12 well tissue culture plates (#92412, TPP Techno Plastic Products AG)
6 well tissue culture plates (#92406, TPP Techno Plastic Products AG)
96-well tissue culture plates (#92196, TPP Techno Plastic Products AG)
96-well cell culture plates, F-bottom (#655976, Greiner)
Nunc™ Polycarbonate Cell Culture Inserts in 12-well Plates, 0.4 µm pore size (#140652, Thermo Scientific)
Dulbecco′s Modified Eagle′s Medium (DMEM) (# 61965-026, gibco)
Advanced DMEM (ADMEM) (#12491-015, gibco)
Fetal bovine serum (FBS) (#12491-015, gibco)
Penicillin/streptomycin (#15140122) 100 units/mL
Tryple Express (#12604-021, gibco)
Phosphate Buffered Saline (PBS) (#20012019, gibco)
Hanks' Balanced Salt Solution (HBSS) (#SH30588.01, Cytiva)
Dymethylsulfoxid (DMSO) (#472324632, Roth)
Kolliphor HS 15 (#42966, SIGMA)
CCR2 antagonist RS504393 (#2517, TOCRIS)
Avastin (100mg/5ml solution, Roche)
AZ19-3-2 synthetic compound
GZ22-4 synthetic compound
AZ21-6 synthetic compound
Cytotoxicity Detection Kit (LDH) (#11644793001, Roche)
CyQUANT ™ XTT Cell Viability (# X12223, Invitrogen)
anti-hCD3 AF488 (#300320, BioLegend)
anti-h/mCD11b FITC (#101206, BioLegend)
anti-hCD86 AF488 (#53-0869-42, Invitrogen)
anti-hCD274 APC (#17-5983-42, Invitrogen)
anti-hCD8 PE/Cy7 (#344712, BioLegend)
anti-hCAIX AF488 (#FAB2188G, R&D)
anti-hCD45 PE/Cy7 (#304016, BioLegend)
anti-hVEGFR PE/Cy7 (# 393008, BioLegend)
anti-hPD1 PE (#621608, BioLegend)
anti-hCCR2 PE (#357206, BioLegend)
anti-hCD4 APC (#51-0049-42, eBioscience)
anti-hCD206 APC (#17-2069-42, Invitrogen)

anti-hF4/80 APC (#123116, BioLegend)
anti-hCD44 APC (#559942, BD Pharmingen
anti-hCXCR1 FITC (#11-1819-42,eBioscience)
anti-hCXCR2 PerCP-eFluor710 (#44-1829-42, Invitrogen)
TruStainFcX anti-human (#422302, BioLegend)
TruStainFcX anti-mouse (#101320, BioLegend)
anti-mCD206 APC (#141708, BioLegend)
anti-mCD86 PE (#105008, BioLegend)
anti-mPD-L1 PE (#155404, BioLegend)
anti-mCCR2 PE (#150610, BioLegend).
7aad stain (#00-6993-50, eBioscience)
Partec CyFlow® Space cytometer.
mouse IgG1κ PerCP-eFluor710 (#46-4714-82, Invitrogen)
mouse IgG2aκ AF488 (#400233, Biolegend)
mat IgG2bκ FITC (#400606, BioLegend)
ratIgG2aκ APC (#400512, BioLegend)
mouse IgG2bκ AF488 (#53-4732-80, Invitrogen)
mouse IgG1κ APC (#17-4714-82, Invitrogen)
mouse IgG1κ Pe/Cy7 (#25-4714-80, Invitrogen)
mouse IgG2a AF488 (#IC003G, R&D)
mIgG2bκ PE (#17-4732-81, eBioscience)
mIgG2aκ PE (#98190, BioLegend)
mIgG2bκ APC (#555745, BD Pharmingen)
anti-hCAIX M75 antibody (#00414, Abs Ab)
anti-mouse IgG HRP antibody (HAF007, R&D)
β-actin antibody (#MA5-15739, ThermoFisher)
Collagenase D (#1108885, Roche)
DNAse (#52779120, Roche)
70 μm strainer (#CLS431751, Corning)
Ammonium-chloride-potassium (ACK) lysing buffer (#A1049201, Gibco)
Flow cytometry staining (FACS) buffer (1xPBS, 0.5%FBS, 2.5mM EDTA (#AM9260G, Thermo Fisher Scientific)
Radioimmunoprecipitation assay buffer (RIPA) (#89900, ThermoFisher)
Phosphatase inhibitor cocktail ((#78428, Thermo Scientific™)
Halt Protease Inhibitor Cocktail (#78425, Thermo Scientific™)
Phenylmethylsulfonyl fluoride (PMSF) Protease Inhibitor (#36978, Thermo Scientific™)
4X lithium dodecyl sulfate sample loading buffer (LDS) (#NP0007, Invitrogen)

2-mercaptoethanol (β-ME) (#1610710, BioRad)
Bolt 4-12% Bis-Tris Plus gels (#NW0412, Thermo Scientific™)
0.2 µm nitrocellulose membranes (#LC2000, Thermo Scientific™).
2% milk-TBST (1X Tris-Buffered Saline, 0.1% Tween® 20 detergent)
Tween-20 (#13474259, Fisher Scientific)
Novex ECL Chemiluminescent Substrate Reagent Kit (#WP20005, Invitrogen).
NanoShuttle™ (#B22073BP, Greiner)
Holding drive (#655837, Greiner)
Ficoll-Paque™ PREMIUM (#17-5442-02, GE Healthcare).
Human IL-6 uncoated ELISA kit (#88-7066, Invitrogen)
Human IL-10 uncoated ELISA kit (#88-7106, Invitrogen)
Human TNF-α uncoated ELISA kit (#88-7346, Invitrogen)
Human MCP-1/ CCL2 uncoated ELISA kit (#88-7399, Invitrogen)
Human IL-8 uncoated ELISA kit (#88-8086 Invitrogen)
Human IFN gamma ELISA Development Kit (TMB) #900-T27, PeproTech)
Human IL-4 ELISA Development Kit (TMB) ((#900-T14, PeproTech)
Human VEGF DuoSet ELISA (#DY293B-05, R&D Systems)
3,3',5,5'-tetramethylbenzidine (TMB) substrate solution
3.6% H_2SO_4
SouthernBiotech™ Mycoplasma Detection Kit
Alliance™ Q9 Imager system.
UVIBAND MAX analysis software system
Mettler Toledo SevenCompact™ pH meter S210 (#15360161, Fisher Scientific)
Partec CyFlow® Space cytometer.
Life Technologies EVOS FL Auto Imaging System
Multiscan GO microplate spectrophotometer.

2.2. Methods

2.2.1. Cell culture

SK-N-AS, a MYCN non-amplified, human NBL cell line was originally purchased from ATCC and provided by Prof. A.Y. Huang, Case Western Reserve University, USA. SK-N-BE, be2c, SH-SY5Y, LA1-55n lines were kindly provided by Prof. Kanopka and Dr. E. Kriukiene, Vilnius University. 143B cell line was purchased from ATCC. The HeLa cell line was kindly provided by Prof. Kanopka. The HeLaCAIX^{KO} line was developed by Dr. J. Matuliene, as published [28]. Cell lines were mycoplasma negative, as confirmed using the SouthernBiotech™ Mycoplasma Detection Kit.

All lines were cultured in DMEM supplemented with 10% heat-inactivated FBS, 100 units/mL penicillin, and 100 mg/mL streptomycin. Cells were grown in a humidified incubator with 21 % O_2 and 5 % CO_2 at 37 °C. Hypoxic conditions, when needed, were achieved in the hypoxic chamber (MACS VA500 microaerophilic workstation, Don Whitley Scientific, UK) with 1 % O_2, 5 % CO_2, and 94 % N_2. Depending on experiments, cells grew in hypoxia from 48 hours to 11 days.

2.2.2. Animal care

For the *in vivo* animal study, female Nude mice (CR ATH HO Code 24106216), 5-6 weeks old, were obtained from Charles River Laboratories. Animals were housed and handled in the Department of Animal Models Animal Facility at Life Sciences Center, Vilnius University, Lithuania. Animals were housed in an Allentown 48 Cage NexGen Mouse IVC Cage & Rack System with individual ventilation, sterilized cages, and bedding. 5 mice were housed per cage using a 12-h light-dark cycle, at 21–23 °C and 40–60 % humidity. Animals were fed with a sterilized irradiated breeding/maintenance diet for transgenic mice (#1414, Altromin) and sterilized water *ad libitum.* Animals dedicated to imaging experiments were fed an irradiated chlorophyll-deficient diet (#C1086194, Altromin). All experimental procedures conformed to Directive 2010/63/EU requirements and were approved by the Lithuanian State Food and Veterinary Service (Approval No G2-233, 2023-01-18, No G2-194, 2021-11-09). Mice were observed every weekday and weighed once weekly.

2.2.3. Human neuroblastoma xenograft mouse model experiment

Before injection into animals, mycoplasma-free SK-N-AS cells in the exponential growth phase were harvested, washed, and resuspended in PBS. 10-12 weeks female Nude mice (25 g) were inoculated subcutaneously (s.c) into the right flank with 5×10^6 SK-N-AS cells resuspended in 100 µL of PBS. Once tumors reached the average size of 35 mm^3, mice were randomized to ensure equal tumor size distribution per group (n=7 per group). The 7 mice per group were used based on published guidelines (54). Treatment with AZ19-3-2 compound at 10 mg/ kg/ dose intraperitoneally (i.p.) daily was initiated on the day of randomization. This dose was chosen based on preliminary pharmacokinetic/ pharmacodynamic (PK/PD) studies. CCR2 antagonist RS504393 at a 2 mg/ kg/ dose i.p. daily was started on the 5th day post-randomization to allow saturation of AZ19-3-2 compound with resultant reduced pericellular tumor acidity. Such a dose of RS504393 was derived from research publications [142]. The drug administration scheme is depicted in **Fig.11.**

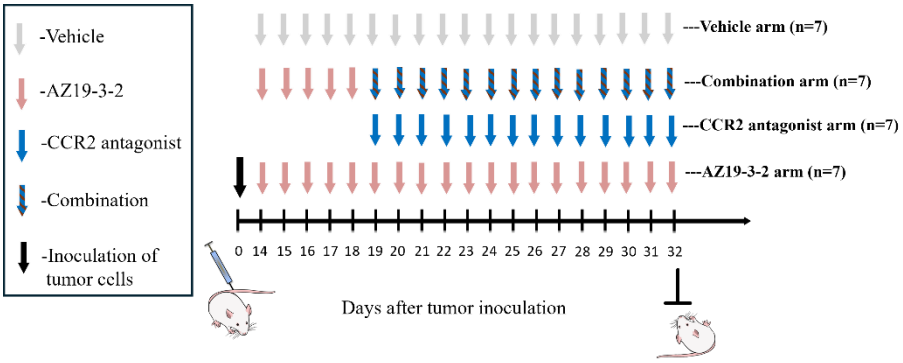

Figure 11. Drug administration and timing scheme. Mice images obtained from NIH BioArt.

Tumor volume was monitored serially every other day using a digital caliper and calculated using the formula: volume = (D*$d^{2*}\pi$)/6, where D represents the largest diameter and d the smaller diameter (55, 56). All mice were sacrificed once a single tumor reached 1500 mm^3 volume. Animals were euthanized with a flow of 8.0 L/ min of medical CO_2 gas (Elme Messer Lit, Vilnius, Lithuania) followed by cervical dislocation. Harvested tumors were weighed and analyzed using flow cytometry as described in the flow cytometry section of the methods.

2.2.4. Human osteosarcoma xenograft mouse model experiments

Before injection into animals, mycoplasma-free 143B cells in the exponential growth phase were harvested, washed, and resuspended in PBS. 8-12 weeks old female Nude mice were inoculated intraosseous (i.o.) under isoflurane anesthesia with 0.5×10^6 143B cells resuspended in 20 µL of PBS into the right tibia. Once tumors reached palpable size, on the 16th day post-tumor inoculation, mice were randomized based on tumor size and treated with CCR2 antagonist RS504393 at a dose of 2 mg/ kg/ dose i.p. daily or vehicle control. 10 mice per group were used based on published guidelines [143]. The drug administration scheme is depicted in **Fig.12.**

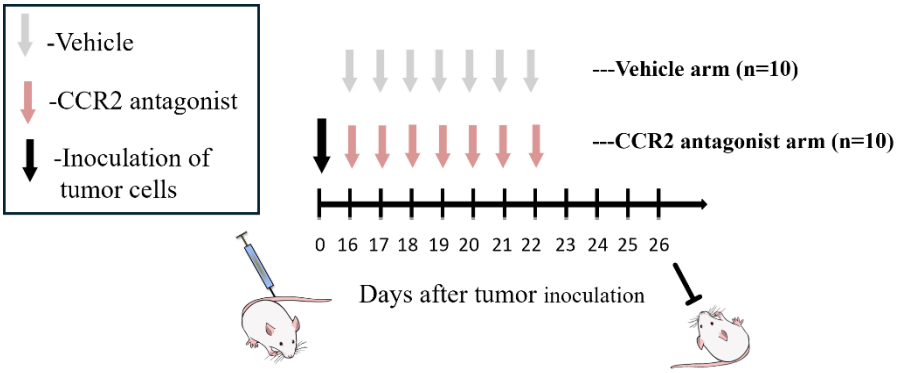

Figure 12. Drug administration and timing scheme. Mice images obtained from NIH BioArt.

For the experiments utilizing Avastin, treatment of mice was initiated on day 12 post-143B cell i.o. injection. AZ19-3-2 compound 10 mg/ kg/ dose i.p. was administered daily, and Avastin was administered at 10 mg/ kg/ dose i.p. twice weekly. Such a dose of Avastin was chosen based on available published data [144]. The drug administration scheme is depicted in **Fig.13.**

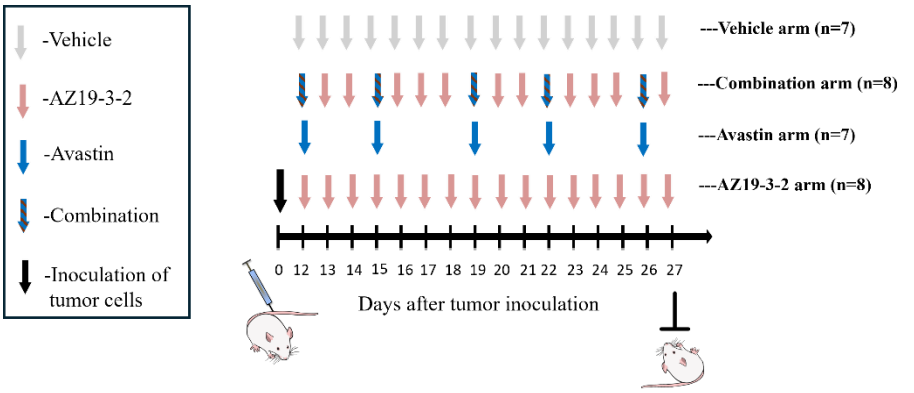

Figure 13. Drug administration and timing scheme. Mice images obtained from NIH BioArt.

Tumor size was calculated as follows: volume = (D*d^2*π)/6, where D is the longer measurement and d is the shorter one (55, 56). All mice were sacrificed once a single mouse reached a tumor volume of 1500 mm^3. At the end of the experiment, animals were euthanized with a flow of 8.0 L/ min of medical CO_2 gas (Elme Messer Lit, Vilnius, Lithuania) followed by cervical dislocation.

2.2.5. Human cervical cancer xenograft mouse model visualization experiment

Before injection into animals, mycoplasma-free cells in the exponential growth phase were harvested, washed, and resuspended in PBS. 8-12 weeks old female Nude mice were inoculated s.c. with $3×10^6$ $HeLaCAIX^{WT}$ cells in 100 µL of PBS into the right flank of the mice, and the same number of $HeLaCAIX^{KO}$ cells were injected into the left flank of the same mouse. Once tumors reached a suitable size for imaging, GZ22-4 or AZ21-6 compounds were injected intravenously (i.v.) at a dose of 2 mg/ kg/ dose once. Mice were imaged every 24 hours post-injection using isoflurane anesthesia with the Alliance™ Q9 Imager system. Images were quantified using the UVIBAND MAX analysis software system. At the end of the experiment, animals were euthanized with a flow of 8.0 L/ min of medical CO_2 gas (Elme Messer Lit, Vilnius, Lithuania) followed by cervical dislocation.

2.2.6. LDH and XTT assays

Approximately 6250 SK-N-AS cells per 100 µL of DMEM medium were seeded in a sterile 96-well tissue culture plate. After 24 hours of incubation in 1 % O_2, we removed the supernatant and titrated the CAIX inhibitor AZ19-3-2 at doses 0.01, 0.05, 0.1, 0.5, 1, 2, 4, and 6 µM in the ADMEM (final volume 200 µL per well) in triplicate for each condition. The cells were then incubated in 1 % O_2 for 48 hours. Subsequently, LDX and XTT assays were performed according to the manufacturer's protocol using the Cytotoxicity Detection Kit and CyQUANT ™ XTT Cell Viability Assay kit. The untreated cells/ control OD was used as a reference value and set as 100 %. The treatment value was calculated as % of the control. Data encompasses 3 separate experiments.

2.2.7. Extracellular pH measurements

For extracellular pH measurements, 0.15×10^6 SK-N-AS or 0.075×10^6 143B cells were resuspended in 1 ml of DMEM per well and were seeded into 12-well plates. CAIX inhibitor AZ19-3-2 at doses of 0.05 and 0.2 µM was added, as well as a vehicle control. Cells were incubated for 48 hours under normoxia and hypoxia. The pH measurements were taken using a Mettler Toledo SevenCompact™ pH meter S210. Data encompasses 9 repeats per condition.

2.2.8. Flow cytometry

PBMCs, SK-N-AS, and 143B cells were collected by detaching with TrypLE solution for 5 min, followed by the addition of DMEM supplemented with 10 % FBS and 1 % penicillin/streptomycin. After washing collected cells, the cell surface receptors FcγRIII (CD16) and FcγRII (CD32) were blocked with Fc block (anti-human CD16/32) solution (1:100). Cells were stained with the following anti-human antibodies (1:100): anti-hCD3 AF488, anti-h/mCD11b FITC, anti-hCD86 AF488, anti-hCD274, anti-hCD8 PE/Cy7, anti-hCAIX AF488, anti-hCD45 PE/Cy7, anti-hCD80 PE/Cy7, anti-hVEGFR PE/Cy7, anti-hPD1 PE, anti-hCCR2 PE, anti-hCD4 AF647, anti-hCD206, and anti-hF4/80 APC with corresponding isotypes. The 7aad stain was used to discern live cells from the dead. Live cells were analyzed by flow cytometry using Partec CyFlow® Space cytometer.

Flow cytometry on tumors harvested from mice. Tumors were dissected from mice and placed into a separate 100 mm Petri dish on ice, quickly minced with scalpels into fragments. Collagenase D 1mg/ ml and DNAse 0.05 mg/ ml

were added into 2 ml HBSS and incubated at 37 °C for 15 min. Digested tumors were passed through a 70 μm strainer. Cells were centrifuged and lysed with 2 ml of ACK lysing buffer for 1 minute to deplete red blood cells. The reaction was quenched with HBSS, followed by centrifugation and washing with FACS buffer, and the cells were then subjected to flow cytometry analysis. TruStainFcX was used for non-specific receptor blockade. To analyze tumor fraction in human cell xenografts, anti-hCD274 APC, anti-hCA9 AF488, anti-hVEGFR PE/Cy7, anti-hCCR2 PE, and anti-hCD44 APC with corresponding isotype controls were used. Anti-mouse antibodies were utilized to analyze the immune fraction in xenograft tumors. Additionally, non-specific receptor blockade was employed. TruStainFcX anti-mouse was used. Antibodies used were anti-mCD206 APC, anti-mCD86 PE, anti-mPD-L1 PE, and anti-mCCR2 PE with corresponding isotype controls. The 7aad stain was used to discern live cells from dead. Cells were analyzed by flow cytometry using Partec CyFlow® Space cytometer.

Data were analyzed using FlowJo. Isotype controls were used to depict the threshold of positive cells. In all cases, the percentage of positive cells in the isotype controls was calculated from all live cells. The percentage of live tumor cells was calculated and used for further analysis. In the case of stroma cells, live $CD11b^+$ cells were selected for analysis. The percentage of $F4/80^+$, $CCR2^+$, $CD206^+$, and $CD86^+$ was calculated of $CD11b^+$ cell population.

2.2.9. Immunohistochemistry

Immunohistochemistry (IHC) of 143B, SK-N-AS, and HeLa tumors was performed at the National Pathology Center, Vilnius, Lithuania. Formalin-fixed and paraffin-embedded (FFPE) slides cut at 3 microns were subjected to H&E and IHC staining with BenchMark Ultra VENTANA. In brief, before initial deparaffinization, sections were steamed at 60 °C for 24 min, then antigen retrieval with CC1 for 64 min at 95 °C. The slides were incubated with the CCR2 antibody (Roche clone SN707, 1:400) or CAIX antibody (Cell Marque clone EP161; 1:50). Tissues were exposed to Dab chromogen for 8 min and then counterstained with hematoxylin, dehydrated, and mounted. A universal DAB detection kit (# 92760-500, Roche) was used for visualization.

2.2.10. Western Blot

After 72 hr incubation under hypoxia or normoxia, neuroblastoma SK-N-AS and osteosarcoma 143B cells were harvested, washed with PBS twice, and resuspended in RIPA containing protease and phosphatase inhibitors

(ThermoFisher Halt™ Phosphatase inhibitor cocktail, Halt Protease Inhibitor Cocktail, and PMSF) for 30 min on ice and centrifuged at 16000×g for 15 min at 4 °C. Total protein lysate was quantified by the Bradford method (53). Lysate was boiled for 10 min at 95 °C in 4×LDS containing β-ME, then separated using Bolt 4-12 % Bis-Tris Plus gels and transferred onto 0.2 µm nitrocellulose membranes. Subsequently, the membrane was blocked using 2 % milk-TBST for 1 hour and incubated overnight at 4 °C with the primary antibody anti-hCAIX in 2 % milk-TBST. β-actin was used as a protein loading control. Membranes were then washed three times for 5 min in TBST and incubated for 2 hours at room temperature with a 1:1000 dilution of corresponding secondary antibodies. After incubation with a secondary antibody, membranes were washed an additional three times and incubated using Novex ECL Chemiluminescent Substrate Reagent Kit substrate. Bands were visualized using the Alliance Q9 Advanced (UVITEC) system.

2.2.11. Three-dimensional neuroblastoma cell SK-N-AS spheroid culture experiment

Approximately 0.2×10^6 SK-N-AS cells per 2 mL DMEM medium were seeded per well into 6-well plates. The next day, NanoShuttle™ 70 µL was added into each well. After 24 hours of incubation, cells were seeded into 96-well cell culture plates, F-bottom (400 cells per well in 150 µL tumor cell medium). Cells were kept on the 96-well holding drive for 30 min. Plates were transferred into the incubators with 1 % O_2 versus 21 % O_2 conditions. Once spheroids were formed, after 48 hrs incubation, AZ 19-3-2 compound 200 nM (n=10 (hypoxia), n=7 (normoxia)) and vehicle control (n=10) were added into the corresponding wells. Spheroids were imaged daily starting the first day of the addition of drugs using a Life Technologies EVOS FL Auto Imaging System at 4X magnification. Compounds with the medium were changed regularly every 48 hours. Images were analyzed using ImageJ software.

2.2.12. Cancer cell – PBMC assay

The healthy donor PBMC co-culture method better reflects *in vivo* cell behaviors and has emerged as an important method with various applications in cancer research [145, 146]. Our model did not allow direct cell-to-cell contact and was focused on paracrine signaling and response to soluble signaling factors [146]. We chose the co-culture study model as it involves

the cultivation of different types of cells in the same conditions and allows the exploration of dynamic interactions between cancer-immune cells [147].

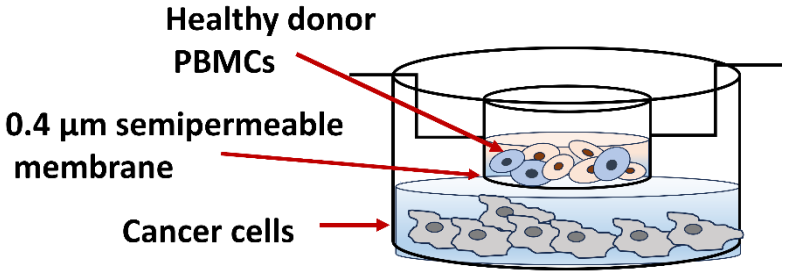

Figure 14. Scheme of cancer cell - PBMC co- culture assay using transwell.

Fig. 14 depicts the transwell assay setup. We used Thermo Scientific, Nunc™ Polycarbonate Cell Culture Inserts in 12-well Plates, 0.4 µm pore size for the experiments with neuroblastoma SK-N-AS cells. First, 0.15×10^6 SK-N-AS cells were seeded in 2 mL of ADMEM per well and incubated in 1 % O_2. After 24 hours, 0.2 µM AZ19-3-2 or vehicle control was added, and cells were incubated in 1 % O_2 for an additional 24 hours. Subsequently, healthy donor blood was collected in compliance with the bioethics protocol approved by the Vilnius Regional Committee of Biomedical Research (2020 03 31 Nr.2020/3-1209-694) (6 donors). PBMCs were isolated using Ficoll-Paque™ PREMIUM according to the manufacturer's protocol. Once isolated, PBMCs were counted and seeded at 1×10^6 per well with ADMEM + 5 % FBS and placed in hypoxia. After 48-hour incubation in 1 % O_2, supernatants were collected from the top or bottom chambers, centrifuged, and prepared for indirect enzyme-linked immunosorbent assay (ELISA) analysis. PBMC from the top chamber and SK-N-AS cells from the bottom chamber were harvested for flow cytometry analysis. Data encompasses 6 different experiments.

For co-culture experiments with 143B cells, Thermo Scientific, Nunc™ Polycarbonate Cell Culture Inserts in Multi-Well Plates, 0.4 µm pore size, 12-well, were used. First, 0.15×10^6 osteosarcoma 143B cells per well were seeded and left for 24 hours in 1 % O_2 in ADMEM with 3 % FBS. Vehicle or RS504393 at 0.5 µM concentration was added, and cells were incubated in 21 % and 1 % O_2. After 24 hours, healthy donor blood was collected in compliance with the bioethics protocol approved by the Vilnius Regional Committee of Biomedical Research (2020 03 31 Nr.2020/3-1209-694) (3 donors). PBMCs were isolated using Ficoll-PaqueTM PREMIUM according to the manufacturer's protocol. Once isolated, PBMCs were counted and

seeded at 1×10^6 per well with advanced DMEM + 5 % FBS. After 48-hour incubation in 1 % or 21 % O_2, supernatants were collected from the top or bottom chambers and centrifuged at 300×g for 5 min. Supernatants were collected and centrifuged again at 1000×g for 5 min and prepared for ELISA analysis. PBMC from the top chamber and 143B cells from the bottom chamber were harvested for flow cytometry analysis.

Data were analyzed using FlowJo. Isotype controls were used to depict the threshold of positive cells. The percentage of live SK-N-AS or 143B cells was calculated and used for further analysis. In the case of PBMCs, live $CD45^+$ cells were selected for the study. T cell markers CD4, CD8, or PD-1 were calculated in the $CD3^+$ population as a fraction of positive cells. The percentage of cells expressing $PD\text{-}L1^+$, $CCR2^+$, $CD86^+$, $CD206^+$, and $CD86^+CD206^+$ receptors was calculated from the $CD11b^+$ cell population. For experiments with SK-N-AS cells, to avoid data variation among blood donors, immune cell data were normalized. The percentage of positive cells of each set of markers ($PD\text{-}L1^+$, $CCR2^+$, $CD86^+$, $CD206^+$, and $CD86^+CD206^+$) was divided by the average value of positive cells of all treatments per donor. Normalized data were presented as a relative % of positive cells of certain markers in the graphs.

2.2.13. Quantitation of cytokines and chemokines in cell culture supernatants

For quantification of cytokines and chemokines in cell culture supernatants, the following ELISA kits were used: IL-6, IL-10, TNF-α, CCL2, CXCL8, IFN-γ, IL-4, and VEGF. ELISA kits are based on the sandwich immunoassay technique. Supernatants were diluted up to 1:200. All procedures were performed according to manufacturers' protocols. In the last step, 3,3',5,5'-TMB substrate solution was added to each well. The plates were monitored for 15 min for color development, the reaction in wells was stopped with 3.6 % H_2SO_4 solution, and the wells were read at 450 nm with reference wavelength at 620 nm using a Multiscan GO microplate spectrophotometer. A standard curve was generated from the cytokine standard, and the cytokine concentration in the samples was calculated. Data encompasses 6 experiments.

2.2.14. Statistical analysis

Data were analyzed using Graph Pad Prism software (version 10.0.2) and presented as bar graphs with individual data points of at least five independent

experiments. Data graphs are presented using Matplotlib 3.9.0. Independent experiments referred to as *n* means the number of independent cell culture preparations or animals. Kolmogorov–Smirnov normality test was carried out to test if the values come from a Gaussian distribution. Statistical comparisons between treatment groups and controls were performed using two-way ANOVA or one-way ANOVA in conjunction with a Tukey multiple comparison test. For differences between treated and non-treated cohorts, a paired Student's t-test was applied. In other cases, a Kruskal–Wallis test with Dunn's post hoc test was used for non-parametric data. P values < 0.05 were considered significant and were shown ($^{*}p < 0.05$; $^{**}p < 0.01$, $^{***}p < 0.001$, $^{****}p < 0.0001$).

3. RESULTS

CAIX enzyme, being one of the key regulators of tumor acidity in hypoxic TME, is an attractive target for immunomodulation and cancer diagnostics. We therefore investigated the efficacy of CAIX inhibition in the osteosarcoma cell line 143B model and the neuroblastoma SK-N-AS cell line model. We also assessed the feasibility of the CAIX protein recognition-based imaging platform for the *in vivo* testing of fluorescent CAIX-enzyme-recognizing compounds.

As the CCL2-CCR2 axis is indispensable in tumor progression, we also investigated the role and the efficacy of CCR2-CCL2 axis inhibition in the osteosarcoma cell line 143B model as well as the neuroblastoma SK-N-AS cell line model. We hypothesized that by targeting both tumor hypoxia (CAIX enzyme inhibition) and the CCL2-CCR2 chemokine axis, which is indispensable in immunosuppressive tumor niche creation, we would achieve a better anti-tumor efficacy.

3.1. Efficacy of CAIX inhibition in human osteosarcoma 143B cell-based model

Osteosarcoma is an aggressive bone cancer [148]. CAIX is expressed in osteosarcoma and is associated with worse outcomes [15, 149]. CAIX inhibition may be an attractive strategy for this type of cancer treatment [149]. Here we went on to test the efficacy of CAIX blockade in the 143B cell line xenograft [150]. It is an attractive model to study metastatic disease [151]. We used our novel CAIX inhibitor AZ19-3-2, which contains two VD11-4-2 head groups attached via a 12-mer PEG linker chain. Among the available synthesized CAIX inhibitors in our laboratory, it exhibits the best balance of affinity and selectivity toward the CAIX enzyme with a picomolar binding constant.

3.1.1. 143B cells have increased CAIX expression

We performed western blot (WB) analysis and flow cytometry analysis to assess CAIX protein expression in the 143B cell line. We see a degree of CAIX protein upregulation in normoxia with an increase in hypoxia **(Fig. 15A, B).**

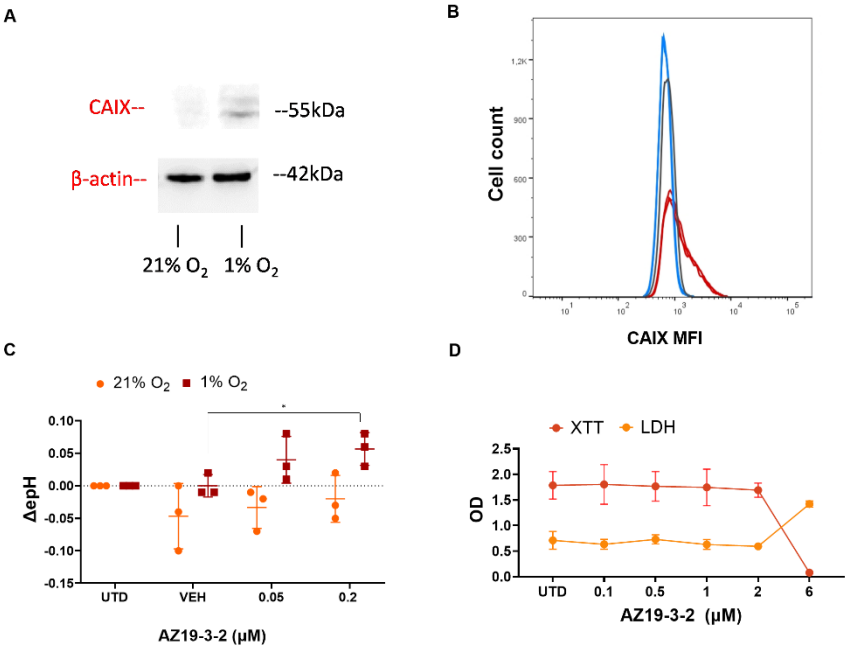

Figure 15. CAIX protein expression pattern of 143B cells and CAIX inhibitor AZ19-3-2 induced phenotypic outcomes. A) WB analysis depicting CAIX protein upregulation in 1 % O_2 compared to 21 % O_2. B) Flow cytometry analysis shows an increase in CAIX protein expression on 143B cells in 1 % O2 (red lines) compared to 21 % O2 (blue line); black line-isotype control. C) epH changes in 143B cell supernatants in normoxia and hypoxia with or without the addition of AZ19-3-2 in comparison to untreated cells (UTD) and vehicle control (VEH). D) XTT (red circles) and LDH (orange circles) measurements on 143B cells exposed to AZ19-3-2 treatment for 72 hr under hypoxia.

CAIX enzyme, via CO_2 hydration, contributes to pH regulation across the plasma membrane, facilitating CO_2 diffusion and proton mobility, and in turn helps maintain physiological pH in cancer cells with resultant pericellular acidosis [130]. Therefore, we assessed whether CAIX protein inhibition alters pericellular pH in osteosarcoma 143B cells. *In vitro*, AZ19-3-2 caused extracellular pH (epH) changes at a dose of 200 nM (Fig. 8C) as compared to untreated (UTD) and vehicle (VEH) controls. These epH changes were evident in hypoxia, but not in normoxia. Data shows that the AZ19-3-2 compound is fairly non-toxic. XTT and LDH profiles on 143B cells **(Fig. 15D)** show significant toxic effects on cells only at a dose of 2 μM and higher.

3.1.2. CAIX inhibition is ineffective in orthotopically implanted human osteosarcoma 143B cell-based xenograft mouse model

Next, we investigated the effects of CAIX protein inhibition in orthotopically implanted human 143B cell-based osteosarcoma xenograft mice model *in vivo*. As CAIX enzyme inhibition as monotherapy did not show efficacy in this model, we attempted a combination approach. We chose the VEGFR blockade for potential synergy using the VEGF-A-targeting monoclonal antibody Bevacizumab (Avastin) [152]. The VEGF-VEGFR cytokine axis is implicated in tumor neo-angiogenesis and is active in osteosarcoma patients [153]. McIntyre et al have shown that CAIX knockdown in cancer cells, together with Bevacizumab treatment, reduced xenograft growth rate in the colon adenocarcinoma cell line HT29 and glioblastoma cell line U87 [154]. In addition, the nonspecific CA inhibitor Acetazolamide enhanced Bevacizumab treatment in HT29 xenografts [154]. However, data on the efficacy of specific CAIX inhibition in conjunction with Bevacizumab in osteosarcoma is lacking.

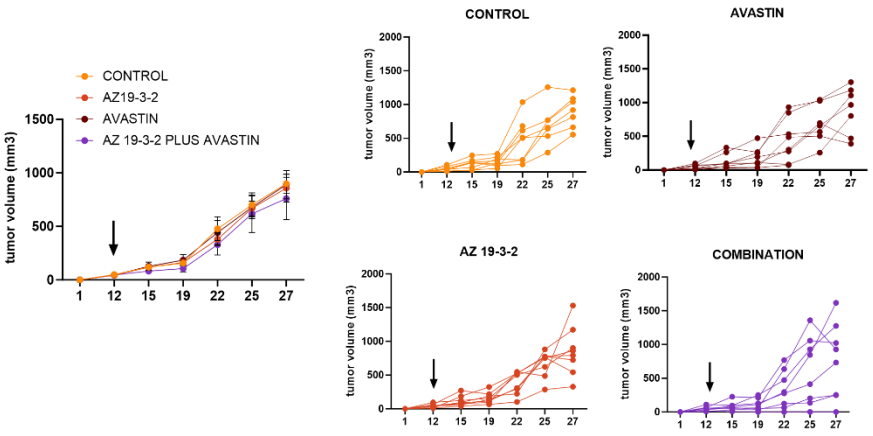

Figure 16. AZ19-3-2 compound as a single agent or in combination with Avastin failed to slow the growth of orthotopically implanted human 143b cell-based osteosarcoma xenograft tumors *in vivo*. The left graph shows tumor volume changes over time in mice treated with: AZ19-3-2 compound (red line and circles), Avastin (brown line and circles), combination (purple line and circles), or control (orange line and circles). Corresponding tumor-growth kinetics for individual animals in each group are shown on the right.

6-12 weeks old Nude mice from Charles River Laboratories were injected i.o. with 0.5×10^6 143B cells into the tibia under anesthesia. Once tumors were palpable, mice were randomized based on tumor size, and treatment was initiated on day 12 post-cell injection. AZ19-3-2 compound 10 mg/ kg/ dose i.p. was administered daily. Avastin was administered at 10 mg/ kg/ dose i.p. twice weekly. Mice were sacrificed on day 27 of the experiment as tumors reached 1500 mm^3 in size. 2 mice were sacrificed earlier due to ill appearance. Only a minimal decrease in tumor size in the combination group was noted **(Fig. 16)**.

Tumors from the sacrificed mice were harvested and subjected to flow cytometry analysis. Flow cytometry analysis of tumor cells revealed that 13.8 % of tumor cells express CAIX protein with an increase in the percentage of CAIX protein-expressing cells in AZ19-3-2 treatment group **(Fig. 17B).** Interestingly, there is an increase in CCR2 receptor percent expression in the tumors from mice that received AZ19-3-2 compound compared to the vehicle control (7.5±1.3 % in vehicle group and 14.6±0.1 % in AZ19-3-2 treated group) (**Fig. 17 A, B).** No difference was noted in the PD-L1 protein or VEGFR receptor expressions among the groups **(Fig. 17 A, B)**.

We also harvested *ex vivo* tumor cells back into the tissue culture. Once cells grew back, we subjected them to 1 % O_2 and analyzed CAIX protein expression. There was 23 % increase in CAIX expression based on mean fluorescence intensity (MFI) hypoxia/normoxia ratio in outgrown cells compared to the original cultured cells (1.2±0.1 in the original cell culture and 1.4±0.2 in the outgrown cells from tumor) (**Fig. 17C)**. The reason for such an increase in CAIX protein needs to be further investigated.

In summary, combining the CAIX enzyme inhibition with Avastin was unsuccessful. The reasons for such treatment inefficiency are not clear, likely it is related to resistance to treatment via upregulation of alternative angiogenic/ hypoxia signaling pathways [152]. As we saw CCR2 receptor upregulation on tumors from mice treated with the AZ19-3-2 compound, we elected to explore the role of the CCL2-CCR2 axis in the 143B osteosarcoma model.

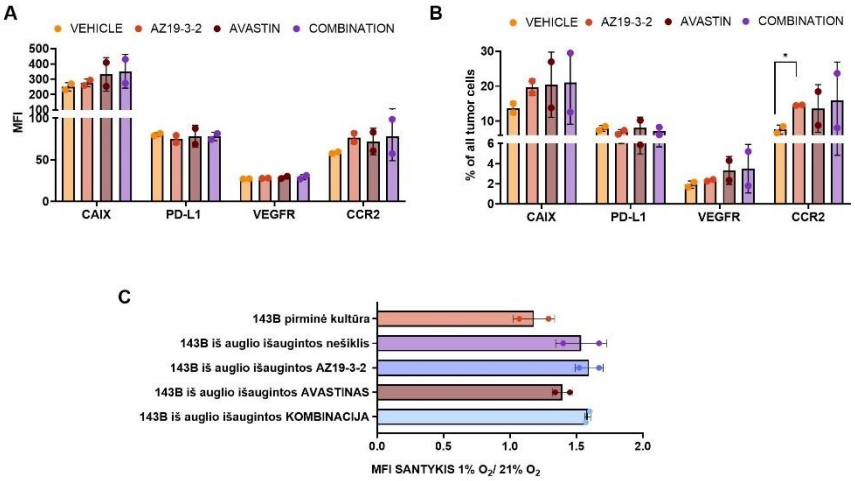

Figure 17. Changes in surface protein expression of osteosarcoma 143B xenograft tumors harvested from mice after treatment with AZ19-3-2, Avastin, a combination of both, or vehicle control. A) CAIX, PD-L1, VEGFR, and CCR2 protein surface expression MFI by flow cytometry on harvested tumors. B) CAIX, PD-L1, VEGFR, CCR2 protein percent surface expression on tumor cells harvested tumors. C) CAIX upregulation ration (1 % O_2/ 21 % O_2) in outgrown tumor cells from AZ19-3-2 treated tumors (blue bar) versus vehicle control (purple bar) versus original 143B (orange bar) cell line. Avastin group- brown bar, combination-light blue bar.

3.2. Hypoxia alters CCR2 antagonist efficacy in human osteosarcoma 143B cells

Here, we aimed to study the differential effects of CCL2-CCR2 axis inhibition in hypoxia compared to normoxia in the pre-clinical metastatic osteosarcoma human cell line 143B model [150]. We studied interaction mechanisms between osteosarcoma cells and immune cells in hypoxia versus normoxia and compensatory mechanisms involved when the CCR2 receptor was inhibited. We used two approaches – an *in vitro* co-culture of 143B cells with PBMCs and the *in vivo* mouse osteosarcoma xenograft model. As discussed in the methods section, the healthy donor PBMC co-culture method better reflects *in vivo* cell behaviors and is an important method for studying cell-cell paracrine interactions [145, 146].

For CCL2-CCR2 axis inhibition we selected a small organic molecule RS504393. It is a selective antagonist of the CCR2 receptor, that does not induce chemotaxis and does not stimulate post-receptor signaling [38]. This

compound blocks the CCR2 receptor by occupying a binding site for CCL2 without affecting CXCR1, CCR1, or CCR3 [38]. RS504393 has shown pre-clinical activity when used in combination with ICB in solid tumors [142].

3.2.1. CCL2-CCR2 axis is active in human osteosarcoma 143B cell-based model

143B cells secrete minimal CCL2 in cell culture under normoxia and hypoxia. Although there was a 40 % decrease in secreted CCL2 protein level under hypoxia when compared to normoxia, it was not statistically significant (136±6 pg in 21 % O_2 and 81±18 pg in 1 % O_2) **(Fig. 18A).** We then went on to test whether the addition of IFN-γ, a key cytokine in tumor immune niche modulation [155], can alter CCL2 secretion by 143B cells. We saw a significant 5-8-fold increase in CCL2 secretion in 143B cells under normoxia and hypoxia **(Fig. 18A).** This data points to the importance of the cytokine context in which cancer cells grow and how it can alter chemokine production by cancer cells. This observation needs to be further explored.

CCR2 expression on 143B cells is not as robust *in vitro.* However, CCR2 receptor expression on CD11b+ cells increased 1.4-fold in hypoxia compared to normoxia (from 0.7 % in normoxia to 1±0.03 % in hypoxia) and increased by another 1.6-fold when CD11b+ cells encountered secretants from 143B cells in a transwell system (1±0.03 % hypoxia/ mono-layer to 1.7±0.2% hypoxia/ transwell) **(Fig. 18B).** Notably, CCR2 expression of CD11b+ cells from a transwell was more pronounced under hypoxia. Chronic hypoxia can affect CCR2 receptor expression in monocytes/macrophages differently depending on the context [33]. Cyclic hypoxia, in general, upregulates CCR2 receptors in macrophages [156] [33]. In our experiments, CCR2 expression on CD11b+ cells aligns with cyclic hypoxia findings. In addition, we detect CCR2 expression in osteosarcoma 143B cell-based xenograft tumors *ex vivo* by IHC staining **(Fig. 18C).**

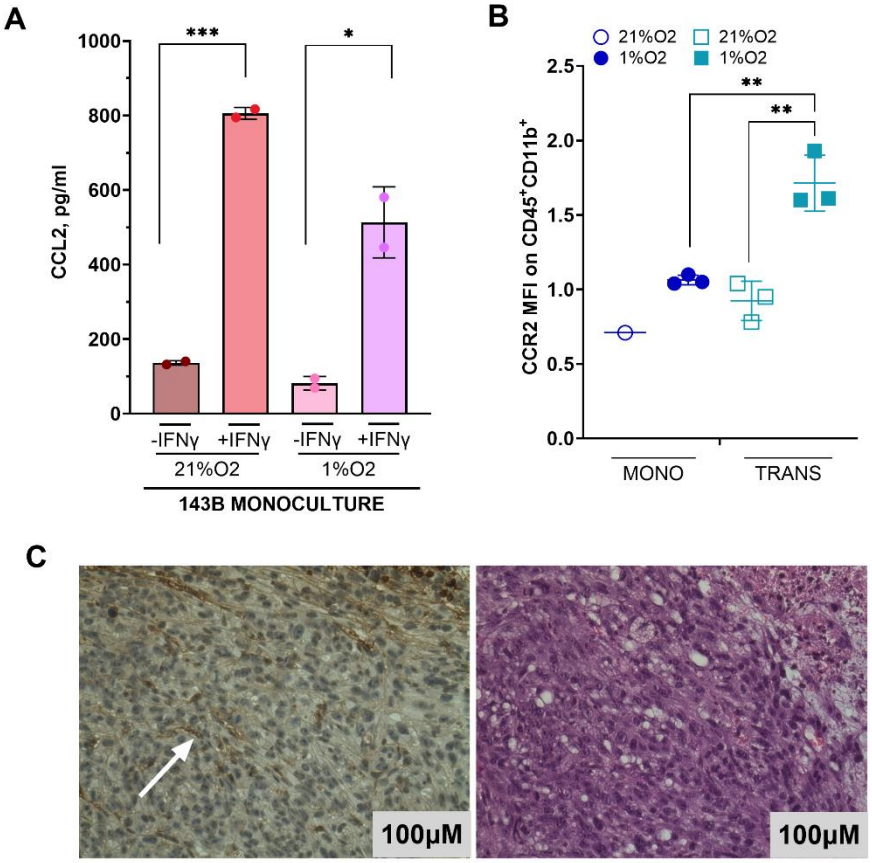

Figure 18. 143B cell phenotype in mono-culture and co-culture with immune cells. A) ELISA analysis for differences in CCL2 secretion of 143B cells grown in normoxia or hypoxia, without/with (+/-) IFN-γ (n=2 per experimental group). B) CCR2 receptor expression differences by MFI on CD11b cells when PBMC are grown in mono-culture (blue circles) and in transwell (teal squares) in normoxia (empty shapes) or hypoxia (filled shapes) (n=3 per experimental group). C) CCR2 receptor expression (left) and H&E stain (right) on 143B tumors by IHC; scale bars – 100 μm. *P < 0.05; **P < 0.01, ***P < 0.001, significance was determined using the Student's t-test.

3.2.2. Co-culture with PBMCs alters 143B cells' phenotype

As we saw that the crosstalk of 143B cells with immune cells can upregulate CCR2 receptor on CD11b cells under hypoxia, we went on to test the effects of co-culture and different oxygen tensions on osteosarcoma 143B cells. We assessed surface expression changes of CAIX, PD-L1, and

CD44 proteins. We studied CD44 protein expression as it is a surface glycoprotein, involved in cell adhesion, and is considered a cancer stem cell marker [157]. Although hypoxia increased CAIX protein percent expression in 143B cells in mono-culture from 1.5±0.2 % in normoxia to 3.1±0.2 % in hypoxia, it was significantly increased in co-culture with PBMCs under hypoxia (11.2±3.5 %) **(Fig. 19A, B).** PD-L1 protein percent expression decreased in 143B cells from the one seen in cells grown in mono-culture under normoxia (35.7±4 %) to the one seen on cells grown in hypoxia in mono-culture (25±0.5 %) and in the transwell, regardless of oxygen conditions (26.9±1.1 % in normoxia and 26±0.6 % in hypoxia) **(Fig 19A, B).** Similarly, CD44 protein mean fluorescence on 143B cells decreased from 2.9±0.9 seen in cells grown inmono-layer under normoxia to 2.2±0.3 in mono-layer cells under hypoxia and in transwell regardless of oxygen conditions (2.5±0.5 in 21 % O_2 and 1.2±0.2 in 1 % O_2) **(Fig. 19A).** In normoxia, percent of 143B cells with VEGFR receptor expression increased from 0.5±0.2 % in mono-culture to 1.6±0.3 % in transwell. However, under hypoxia, the percentage of 143B cells with VEGFR receptor expression decreased from 0.9±0.2 % in mono-layer to 0.5±0.2 % in transwell **(Fig. 19B).**

We elected to study the expression of CXCL8, VEGF, and CCL2 secretion in osteosarcoma cells, as they have all been implicated in osteosarcoma metastasis formation [158-160]. An ELISA analysis of the cell supernatants revealed that 143B cells secreted very low amounts of CCL2 chemokine under normoxia or hypoxia. However, CCL2 chemokine was notable in PBMCs supernatants **(Fig. 19C).** Total CCL2 chemokine secretion was most prominent in the transwell system under normoxia (1018±180 pg) but decreased significantly under hypoxia (160±65 pg) **(Fig. 19C).** We found that VEGF cytokine secretion was prominent in 143B cells, but not in PBMCs **(Fig. 19C)** and it did not change when cells were grown in co-culture. Next, we assessed changes in CXCL8 chemokine secretion. CXCL8 chemokine can be pro-tumorigenic as it promotes the trafficking of neutrophils and MDSCs into the TME [70] and is important in osteosarcoma progression [161]. In our experiment, CXCL8 chemokine was primarily secreted by PBMCs (6070±665 pg in 21 % O_2 and 27212±1950 pg in 1 % O_2) and increased further when cells were grown in a transwell system, more so in hypoxia (11720±12861 pg in 21 % O_2 and 12500±9985 pg in 1 % O_2) **(Fig. 19C).**

Lastly, we performed a multiple-variables analysis of surface protein expression changes in hypoxia. We uncovered changes in total CCL2

chemokine secretion and expression of PD-L1, CD44, and CAIX proteins on 143B **(Fig. 19D)** in the co-culture compared to mono-culture of 143B cells.

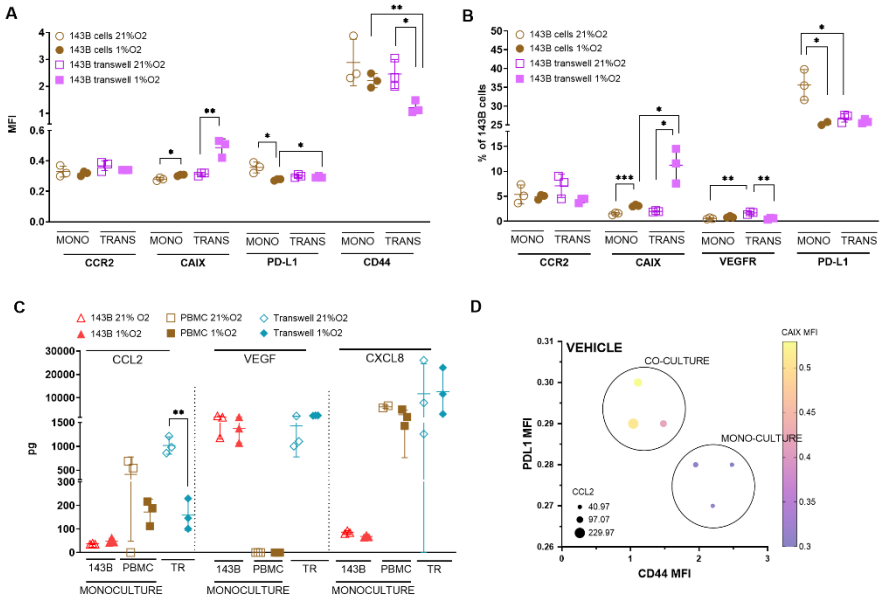

Figure 19. 143B cell phenotype in mono-culture and co-culture with immune cells. A) Changes of surface protein expression MFI of the following markers: CCR2, CAIX, VEGFR, and PD-L1 when 143B cells were gown in mono-culture (brown circles), or they were exposed to PBMC cells in a transwell assay (co-culture, purple squares) under normoxia (empty shapes) or hypoxia (filled shapes). B) Changes in percentage of surface protein expression of these markers: CCR2, CAIX, VEGFR, PD-L1, and CD44, when 143B cells were grown in mono-culture (brown circles) or when they were exposed to PBMC cells in a transwell assay (purple squares), either under normoxia (empty shapes) or hypoxia (filled shapes). C) Secretion of CCL2, VEGF, and CXCL8 by 143B cells (pink triangles) or PBMC (red squares) in mono-culture, in transwell (teal rhombi) under normoxia (empty shapes) or hypoxia (filled shapes). D) Multiple variables analysis for PD-L1, CCL2, CD44, and CAIX expression in hypoxia, comparing transwell co-culture phenotype with mono-culture. *P < 0.05; **P < 0.01, ***P < 0.001; significance was determined using the Student's t-test, n=3 per experimental group.

Our data confirms that co-culture methods reveal more physiologically relevant biological effects on cancer cells compared to mono-culture. We see

significant changes in surface protein expression and chemokine production by cancer cells when they are exposed to paracrine factors secreted from PBMCs compared to mono-culture.

3.2.3. CCR2 inhibition alters 143B cell surface protein expression pattern in co-culture with PBMCs

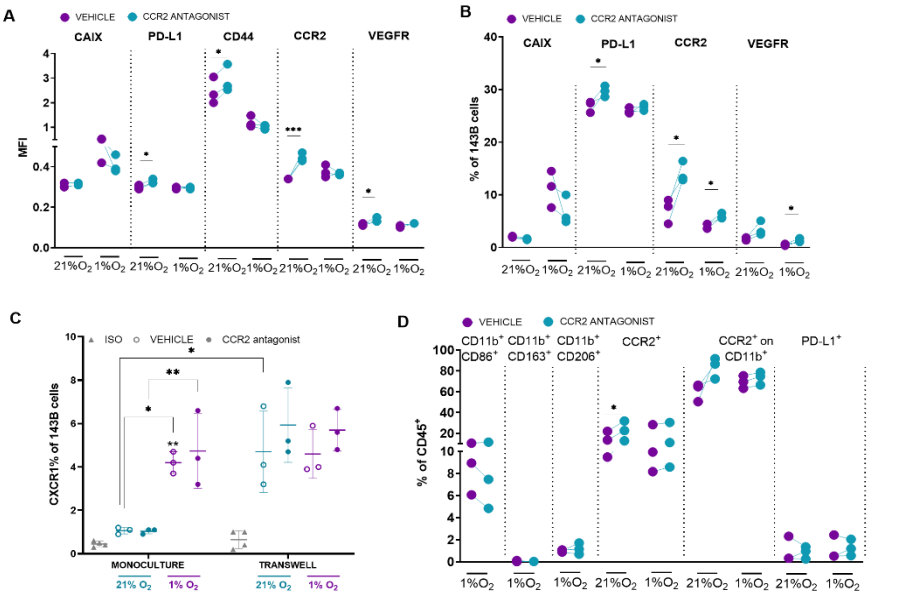

Figure 20. Changes in expression of tumor cell markers upon CCR2 inhibition in hypoxia and normoxia. Changes in CAIX, PD-L1, CD44, CCR2, and VEGFR protein surface expression on 143B cells by MFI (A) and by percentage of live cells (B) in the co-culture when cells were pre-treated or not with 500 nM of CCR2 antagonist under hypoxic or normoxic conditions, (C) CXCR1 surface expression by percentage on live 143B cells in mono-culture and co-culture when cells were pre-treated or not with 500 nM of CCR2 antagonist under hypoxic or normoxic conditions. (D) Changes in CD11b+CD86+, CD11b+CD163+, CD11b+CD206+, CCR2+, CD11b+CCR2+, and PD-L1+ percentage of CD45+ cells by flow cytometry on PBMCs in their co-culture with 143B cells pre-treated or not with CCR2 antagonist under hypoxic or normoxic conditions. * $P < 0.05$; ** $P < 0.01$, *** $P < 0.001$; significance was determined using the Student's t-test, n=3 per experimental group.

Comparing surface protein expression on osteosarcoma 143B cells in their co-culture with PBMCs under normoxia and hypoxia conditions, we observed

that CCR2 inhibition increased MFI of CD44 protein (from 2.5±0 in vehicle control group to 2.9±0.5 after CCR2 antagonist) and PD-L1 protein (from 0.3±0.01 in vehicle group to 0.32±0.01 in CCR2 antagonist group) expression on 143B cells in normoxia and increased VEGFR receptor expression in both, normoxia (from 1.6±0.3 % to 3.5±1.3 % after CCR2 antagonist) and hypoxia (from 0.5±0.2 % to 1.3±0.4 % after CCR2 antagonist) **(Fig. 20A, B).** When measuring the percentage of cells expressing CAIX protein, there was a notable trend of decreased CAIX protein expression in hypoxia after adding the CCR2 antagonist (from 11.2±3.5 % in the vehicle group to 6.8±2.8 % after CCR2 antagonist addition) **(Fig. 20A).**

CXCR1 and CXCR2 are cognate receptors for CXCL8 chemokine [162]. Therefore, we analyzed changes in CXCR1 and CXCR2 receptors in 143B cells and PBMCs. CXCR2 receptor was not detected (data not shown). CXCR1 receptor percent expression on 143B cells in mono-culture increased significantly in hypoxia compared to normoxia (from 1±0.2 % in normoxia to 4.2±0.5 % in hypoxia) **(Fig. 20C)**. Interestingly, CXCR1 percent expression in transwell under normoxia (4.7±1.9 %) reached a similar level to that of mono-culture under hypoxia (4.2±0.5 %) **(Fig. 20C).** This can be explained by a prominent CXCL8 secretion by PBMCs that in turn can affect tumor cell receptor expression. CCR2 receptor inhibition did not significantly affect CXCR1 expression **(Fig. 20C).**

We also determined changes in CD11b+CD86+, CD11b+CD163+, CD11b+CD206+, CCR2+, CD11b+CCR2+, and PD-L1+ cell percentage of CD45+ cells by flow cytometry on PBMCs that were co-cultured with 143B +/- CCR2 antagonist under hypoxic or normoxic conditions. No significant changes were noted except for a CCR2+ increase on CD11b when a CCR2 antagonist was added under normoxia (from 60.5±8.7 % in the vehicle group to 83.5±10 % in the CCR2 antagonist group) **(Fig. 20D)**. It is likely a compensatory effect.

Next, we investigated cytokine secretion changes after the addition of a CCR2 antagonist. A decrease in CXCL8 protein secretion by PBMCs in mono-culture (more so under normoxic conditions) was noted (from 6070±665 pg in the vehicle group to 3599±323 pg in the CCR2 antagonist group in normoxia). However, CXCL8 chemokine secretion was not altered in transwell **(Fig. 21A).** CCR2 antagonist decreased VEGF chemokine secretion in the transwell under hypoxic conditions (from 2336±74 pg in vehicle group to 1533±84 pg in CCR2 antagonist group) **(Fig. 21B),** but not in 143B cells in mono-culture. CCR2 receptor inhibition increased CCL2 protein secretion in PBMC mono-culture as well as transwell under both

hypoxia and normoxia (in the transwell. under normoxia. it was 1018±180 pg in the vehicle group and 2337±440 pg in CCR2 antagonist group, and, under hypoxia, it went from 159±65 pg in the vehicle group to 863±181 pg in the CCR2 antagonist group) **(Fig. 21C).**

Figure 21. **Changes in cytokine/chemokine secretion pattern upon CCR2 inhibition.** Differences in secretion of CXCL8 (A), CCL2 (B) and VEGF (C)

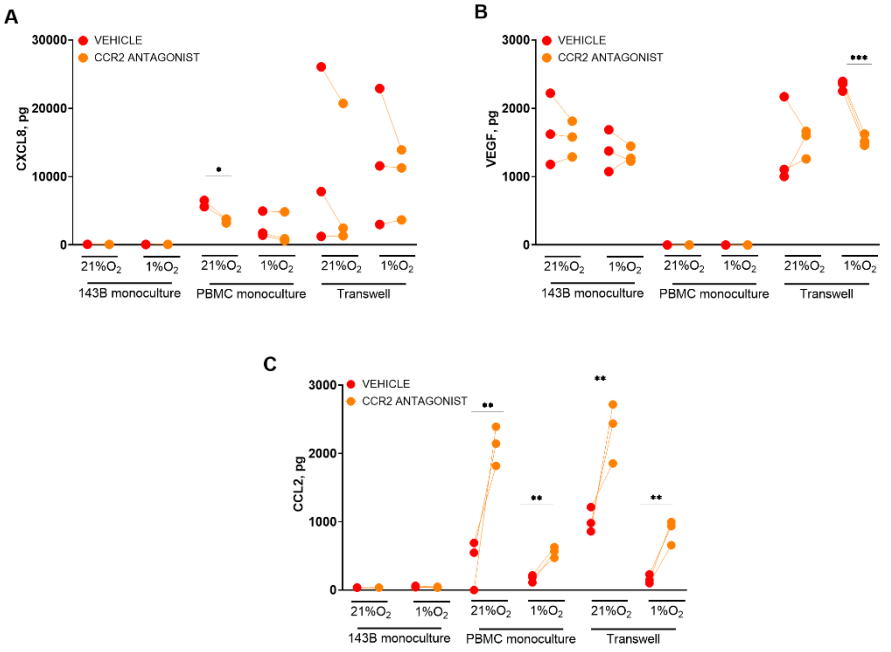

proteins by ELISA when osteosarcoma 143B cells were pre-treated or not with 500 nM of CCR2 antagonist. The difference is shown as a sum of cytokine secretion levels from untreated (vehicle, red squares) to treated conditions (orange squares) in osteosarcoma 143B cells or PBMC mono-culture and transwell under hypoxic or normoxic conditions.

Our data show that CCR2 receptor antagonist effects in hypoxia are only seen in the VEGF-VEGFR axis, where we see VEGFR upregulation on osteosarcoma 143B cells, but diminished VEGF secretion in a transwell. It is apparent that CCR2 receptor antagonist effects were mainly evident in normoxia (such as increased PD-L1 and CD44 protein surface expression on osteosarcoma 143B cells) and decreased CXCL8 chemokine secretion in the transwell. The PD-L1 protein upregulation with CCR2 antagonist treatment is very interesting, as recent publications suggest that the treatment with CCR2 receptor antagonist enhances tumor response to ICB [142].

3.2.4. CCR2 receptor antagonist efficacy in mice with orthotopically implanted human 143B cell-based osteosarcoma tumors

To assess osteosarcoma 143B tumor growth *in vivo* under CCR2 inhibition, 143B cells were inoculated i.o. into the right tibia of Nude mice. Once tumors reached palpable size, we randomized them into two treatment groups (n = 10 per group). We started treating tumors with the CCR2 receptor antagonist RS504393 at a dose of 2 mg/ kg/ dose i.p. daily from the day of randomization. Treatment did not induce differences in tumor growth **(Fig. 22A).** Lack of response to CCR2 antagonist *in vivo* can be linked to tumor hypoxia. Hypoxia is a prominent feature in 143B tumors [163]. In agreement with that, 143B tumors from our experiment had pronounced expression of hypoxia-induced CAIX protein detected by flow cytometry **(Fig. 22C)** [164].

We also performed flow cytometry analysis on tumor cells and some immune cells, mainly murine monocytes/macrophages (since these xenografts were grown in Nude mice with impaired T cells). It showed no changes in CCR2 or PD-L1 protein surface expression in tumor cells from mice that received CCR2 antagonists **(Fig. 22B).** In contrast, the VEGFR receptor signal decreased significantly under CCR2 receptor inhibition compared to vehicle controls **(Fig. 22B).** Interestingly, we observed two tumor cell populations having different expressions of CD44**:** $CD44^{low}$ and $CD44^{high}$ **(Fig. 22B, D).** The ratio of these populations changed after treatment with the CCR2 antagonist. CCR2 inhibition equalized the percentages of cells in each population by increasing the number of $CD44^{high}$ cells (percentage of $CD44^{low}$ cells decreased from 57±14 % in vehicle group to 52.9±16.6 % in CCR2 antagonist group, and percentage of $CD44^{high}$ cells increased from 40±14 % in vehicle group to 47±16 % in CCR2 antagonist group) **(Fig. 22B, D).** When surveying the monocytes/macrophage cell population, we observed an increased percentage of infiltrating $CD11b^{+}CD86^{+}$ cells into the tumor (from 4.6±1.6 % in vehicle group to 8.3±4.7 % in CCR2 antagonist group) **(Fig. 22E).** However, we did not detect the change in a fraction of $CD11b^{+}CCR2^{+}$ cells **(Fig. 22E).**

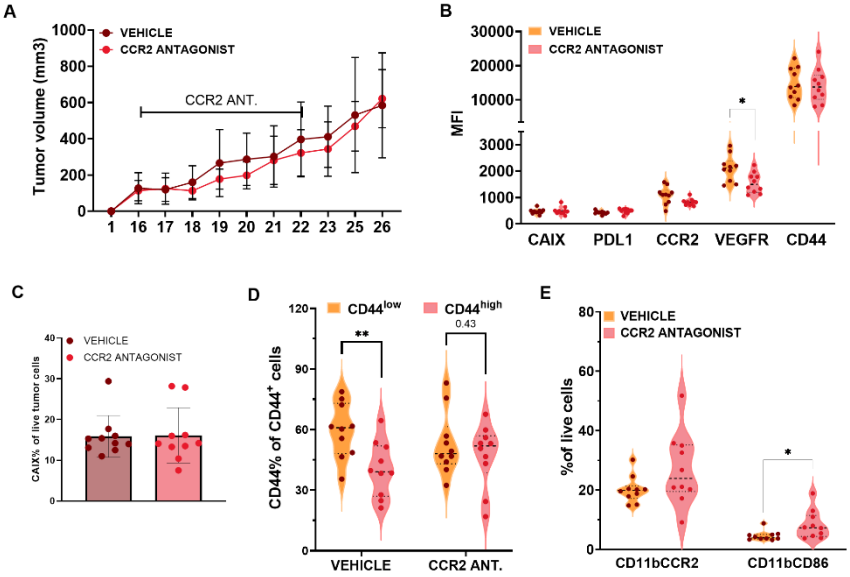

Figure 22. ***In vivo*** **treatment with CCR2 antagonist did not affect tumor growth or metastasis, but altered surface receptor expression on tumor cells and infiltrating monocytes/macrophages.** A) 143B tumor growth dynamics in Nude mice when they were administered with CCR2 antagonist (red circles) versus vehicle controls (brown circles). Data shown as Means +SD, n=10 per experimental group). B) Dot and violin plots depicting MFI of CAIX, PD-L1, CCR2, VEGFR, and CD44 surface protein staining on tumor cells from mice treated with vehicle control (pink with red circles) or CCR2 antagonist (yellow with brown circles). Each data point represents a separate tumor sample from mice. C) Percentage of CAIX+ cells in tumors from mice treated with vehicle versus CCR2 antagonist by flow cytometry. D) Differences of CD44 protein expression on tumor cells: population having low expression of CD44 ($CD44^{low}$) and population having high expression of CD44 ($CD44^{high}$). E) CD11bCCR2 and CD11bCD86 surface expression differences in monocytes/macrophages from tumors of mice treated with CCR2 antagonist (yellow with brown circles) versus controls (pink with red circles). Each data point represents a separate tumor sample from mice, n=10 per experimental group. * P < .05; ** P < 0.01, *** P < 0.001, significance was determined using the Student's t test.

These results reveal CCR2 receptor antagonists' effects on VEGF- VEGFR cytokine axis, as we see 1.35-fold downregulation of the VEGFR receptor

MFI. Interestingly, in tumors harvested from mice treated with CCR2 antagonist, we observed two populations of cells having either low or high expression of CD44 protein. CCR2 antagonist shifted the cells from $CD44^{low}$ to $CD44^{high,}$ in this way increasing overall CD44 protein expression. This is likely an unwanted effect of treatment as the CD44 protein expression in osteosarcoma cells is linked to proliferation and invasion [165, 166].

3.2.5. Proteome array of selected cancer-related targets of 143B cells

The lack of response to CCR2 antagonist treatment *in vivo* prompted us to go back to co-culture experiments. We analyzed cancer-related protein changes in osteosarcoma143B cell-PBMC co-culture assay under the different oxygen environments when cancer cells were exposed to CCR2 antagonist or vehicle control. We performed a proteome array analysis of these cells using the Human XL Oncology Array Kit. First, we assessed changes in osteosarcoma 143B cells harvested from transwells versus from monoculture. We observed a global increase in the majority of tested cancer-related proteins in co-culture compared to monoculture **(Fig. 23A).** More importantly, treatment of osteosarcoma 143B cells with CCR2 antagonist in co-culture revealed differential upregulation of various proteins. For instance, expression of receptor tyrosine kinase AXL, implicated in osteosarcoma metastasis, increased under CCR2 inhibition in normoxia, but decreased in hypoxia **(Fig. 23B).** In addition, similar to co-culture experiment results, we see a decrease in VEGF protein expression after CCR2 antagonist treatment on osteosarcoma 143B cells in hypoxia, but not in normoxia **(Fig. 23B).** Also, proteins associated with drug resistance, such as delta like canonical Notch ligand 1 (DLL1) were upregulated in 143B cells when they were exposed to CCR2 antagonist in co-culture under hypoxia but not normoxia (**Fig. 23B).**

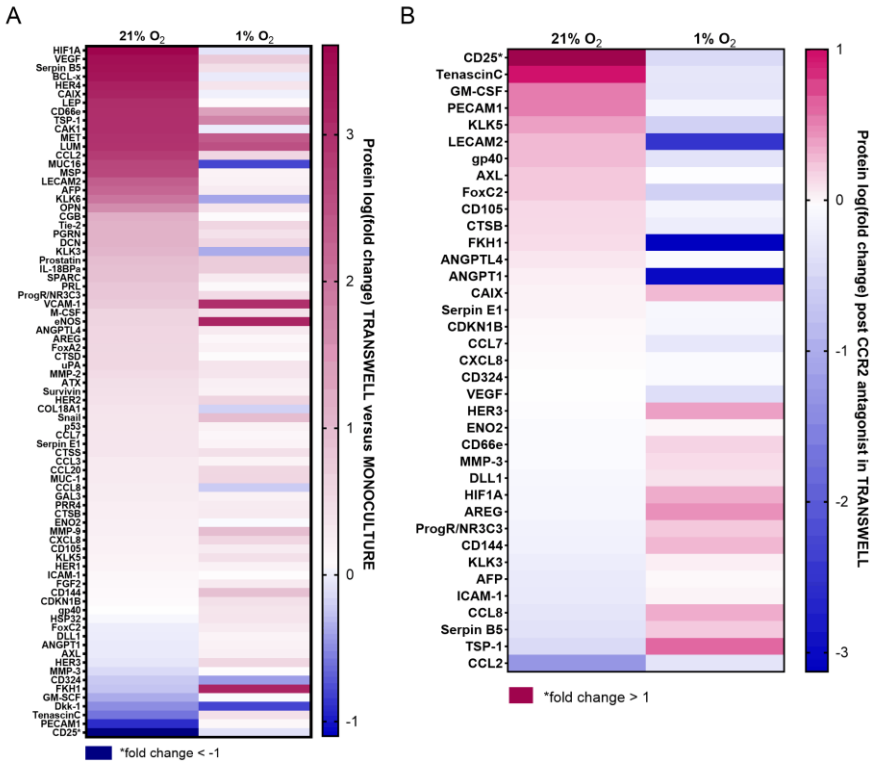

Figure 23. Selected human cancer-related protein analysis on 143B cells comparing mono-culture to co-culture and CCR2 antagonist response in 143B cells from co-culture in hypoxia versus normoxia. (A) Protein array depicting differential protein expression fold changes of transwell compared to mono-culture in hypoxia versus normoxia. (B) Protein array depicting different fold changes in protein expression of CCR2 treated versus vehicle control cells from co-culture in hypoxia versus normoxia.

These findings confirm that the healthy donor PBMC co-culture method with cancer cells better reflects *in vivo* cell behaviors than cell mono-culture experiments [145, 146]. We see an upregulation of most tested cancer-related proteins in co-culture as compared to monoculture. In addition, we see the opposite effect of CCR2 receptor antagonists on the same proteins on 143B cells in co-culture in normoxia as compared to hypoxia. Investigation of differential cellular responses to drugs under normoxia and hypoxia is gaining more interest [167]. But no such studies have been performed using our osteosarcoma research model using the 143B cell line with CCR2 receptor

antagonists. These results will hopefully stimulate more research in osteosarcoma treatment responses.

3.3. The efficacy of CAIX inhibition in neuroblastoma SK-N-AS cell-based model.

NBL is the most common extracranial solid tumor in childhood, accounting for 12-15 % of childhood cancer-related deaths [168]. Primary NBLs arise from neural crest cells of the sympathetic nervous system. Clinical disease evolution is heterogeneous, from spontaneous resolution to deadly disseminated disease. Treatment also varies from observation, surgery for low-risk patients, surgery plus chemotherapy for intermediate-risk diseases, to multimodality treatments for devastating high-risk diseases. In turn, survival depends on the NBL risk status, where low-intermediate risk patients have an 85-80% cure rate, and high-risk patients have – 50 % [169].

Hypoxia is an important factor in NBL progression [170, 171]. Hypoxia in NBL is associated with tumor reprogramming, induced de-differentiation, increased metastatic potential, resistance to chemotherapy, and poor prognosis [172] [173] [174]. Therefore, the development of alternative anti-cancer agents targeting hypoxia-associated signals is important.

CAIX is expressed at significantly higher levels in NBLs from patients with adverse features (such as MYCN amplification) [16, 17]. However, to this date, evidence of single-agent CAIX inhibition efficacy in NBL is lacking.

Targeting CAIX alone is complicated by the plasticity in compensatory mechanisms when CAIX is blocked and therefore is not enough to achieve therapeutic efficacy [11]. Therefore, combination strategies tailoring plastic CAIX compensatory mechanisms could result in robust tumor responses. We identified three predominant chemokines of interest that NBL secretes: CXCL8, VEGF, and CCL2 [175, 176]. The increased expression of CXCL8 in NBL patients [177] correlates with poor cancer prognosis and metastasis [70, 178]. The CCL2 expression is pronounced in MYCN non-amplified NBLs [175, 179]. Recent evidence points to a possible combinatory approach of either CXCL8 or CCR2 inhibition with ICB in various cancers [142] [180]. These findings prompted us to investigate whether CAIX inhibition alters the secretion profile of CXCL8 and CCL2 chemokines in NBL cells and whether CAIX enzyme inhibition with CCR2 inhibition is feasible in this disease model. As in 143B studies for CCL2-CCR2 axis inhibition, we used the small organic molecule RS504393. For the immunomodulatory effects of

CAIX inhibition investigation, we employed PBMC and SK-N-AS co-culture as described in the methods section and 143B studies.

3.3.1. CAIX protein is highly expressed in human neuroblastoma SK-N-AS cells

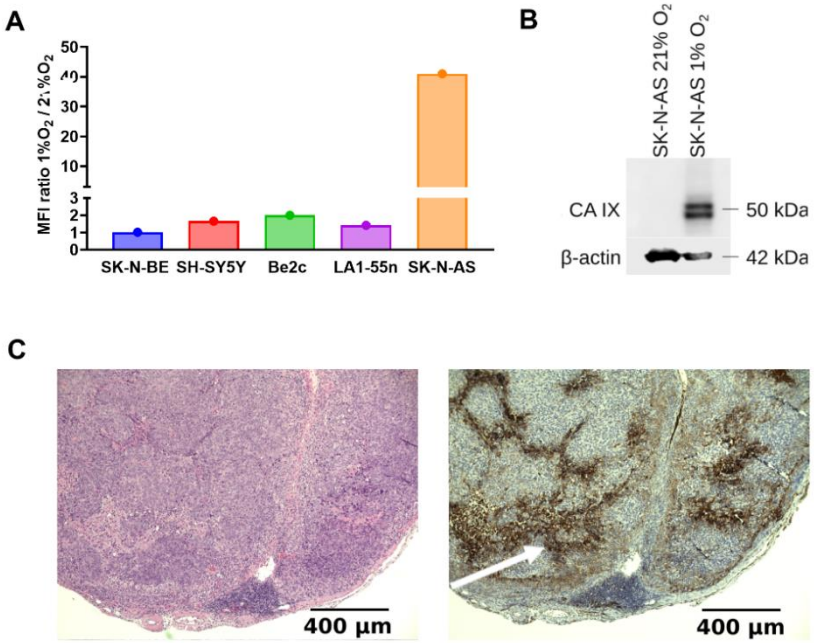

Figure 24. CAIX protein expression in human neuroblastoma SK-N-AS cells. A) CAIX expression in various human NBL cell lines (SK-N-BE, SH-SY5Y, Be2C, LA1-55n, SK-N-AS) by calculating MFI ratio in 1 % O_2 / 21 % O_2 conditions. B) WB analysis of CAIX expression in SK-N-AS cell line in normoxia compared to hypoxia. C) IHC staining of the SK-N-AS xenograft tumor's section (left image- H&E staining, right image- CAIX staining); scale bars – 400 µm. The white arrow shows positive CAIX antibody staining (brown).

We have tested a handful of human NBL cell lines (SK-N-BE, Be2C, SH-SY5Y, LA1-55n, SK-N-AS) for CAIX protein upregulation in hypoxia by performing flow cytometry analysis. Neuroblastoma SK-N-AS cell line had by far the strongest CAIX expression in hypoxic conditions when assessing MFI ratio of CAIX protein expression intensity from cells in hypoxia compared to normoxia **(Fig. 24A).** WB analysis confirmed avid CAIX protein expression in hypoxia as compared to normoxia **(Fig. 24B).** In addition, we

validated CAIX protein expression by performing immunohistology staining on SK-N-AS tumors grown in Nude mice **(Fig. 24C).** All results confirmed that neuroblastoma SK-N-AS cell-based tumor model is attractive for CAIX enzyme inhibition testing.

3.3.2. *In vitro* effects of AZ19-3-2 compound in the neuroblastoma SK-N-AS cells

Toxicity studies revealed that the AZ19-3-2 compound is non-toxic on SK-N-AS cells, as XTT and LDH results show meaningful changes in values only at high, non-selective doses of this compound (starting at 2 μM) **(Fig. 25A).** We then assessed whether CAIX protein inhibition alters pericellular pH in neuroblastoma SK-N-AS cells. We performed a series of epH measurements with various doses of AZ19-3-2 and assessed epH changes. AZ19-3-2 compound showed diminished acidification at a dose of 200 nM only in hypoxic conditions **(Fig. 25B).**

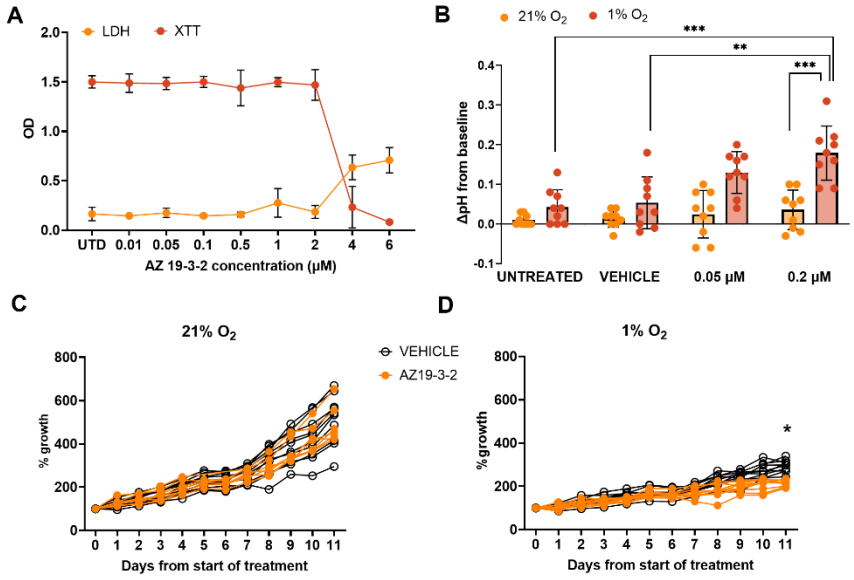

Figure 25. CAIX-inhibitor induced phenotypic outcomes in neuroblastoma SK-N-AS cell line. A) XTT (red circles) and LDH (orange circles) results of 72hr exposure of SK-N-AS line in 1 % O_2 after AZ19-3-2 treatment with various doses of the compound. B) epH measurements of SK-N-AS medium in normoxia and hypoxia 96 hrs post AZ19-3-2 treatment with 50 and 200 nM doses of the compound. Comparisons were made between

21 % O_2 (orange circles) condition and 1 % O_2 (red circles). C) SK-N-AS spheroid growth (relative size) over time in normoxia when subjected to AZ19-3-2 (n=7) or vehicle control (n=10). D) SK-N-AS spheroid growth (relative size) over time in hypoxia when subjected to AZ19-3-2, or vehicle control (n=10 per group).

The *in vitro* efficacy of the AZ19-3-2 compound was also studied in the 3D neuroblastoma SK-N-AS cell spheroid culture model. 3D culture methods reveal more physiologically relevant biological effects on cells as compared to mono-culture [89]. We chose to grow 3D spheroids in normoxia and hypoxia, as studies show that only 16% of cells of 3D spheroids grown in "normoxic" 21 % O_2 conditions experience hypoxia [89]. Actual oxygenation in tumors is significantly lower, ranging from 0.3 % to 4.2 % O_2, with most falling below 2 % [40]. Gomes et al performed 3D spheroid growth analysis under non-physiological 21 % and physiological 5 % O_2 conditions [181]. They found that in the 3D spheroids, cells at the spheroid surface proliferate well both at 5 % and 21 % oxygen concentrations, but 3D spheroid growth was strongly inhibited when oxygen concentration was reduced to 5 %, compared with spheroids cultured at 21 % oxygen. Lower environmental oxygen concentration resulted in a faster decrease of the oxygen available within the spheroid, leading to cell cycle arrest, whereas the 21 % external oxygen concentration resulted in higher oxygen partial pressure deeper in the spheroid, allowing cells to sustain proliferation [181]. With these uncertainties in mind, we elected to perform 3D spheroid growth experiments in both 21% and 1 % O_2 conditions. 48 hours after seeding, formed spheroids were treated with 200 nM AZ19-3-2 or vehicle control for 11 days. We noted that spheroid growth under hypoxia was diminished by half compared to normoxia (294±28 % in the vehicle group in hypoxia and 512±114 % in the vehicle group in normoxia on day 11 measurements) (**Fig. 25C, D)**. As depicted in **Fig. 25D and Fig. 26,** we observed a significant decrease in spheroid percent growth in hypoxia when spheroids were treated with AZ19-3-2 compared to vehicle controls (294±28 % in the vehicle group and 215±14 % in the AZ19-3-2 treated group). Importantly, such an effect was not detected when spheroids were grown under normoxia (512±114 % in vehicle group and 487±86 % in AZ19-3-2 treated group) **(Fig. 25C).** This could be related to elevated oxygen tensions deeper in 3D spheroids with resultant lower CAIX expression. However, we did not test CAIX protein expression differences in spheroids under both conditions. It would be optimal to perform such

experiments in around 5 % O_2 conditions that more closely resemble oxygenation levels in the actual tumor tissues.

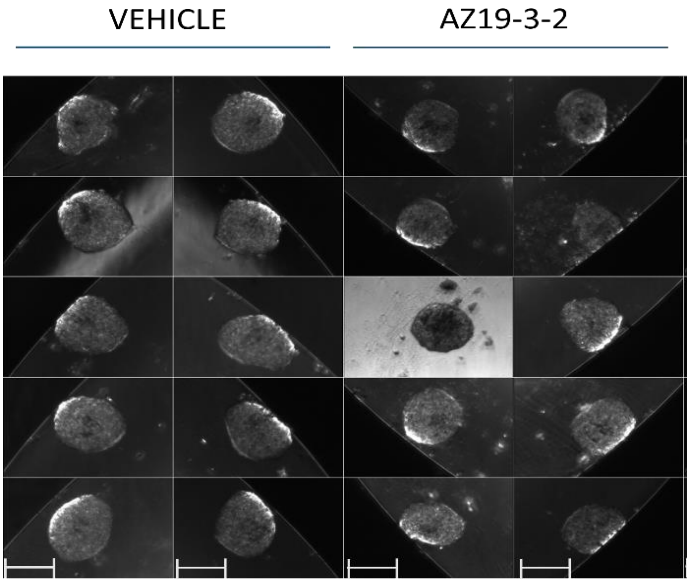

Figure 26. Optical images of SK-N-AS spheroids under hypoxia on the last day of imaging. The first two columns show vehicle control, the second and third rows show- AZ19-3-2 treatment. The scale bar is 200 μm.

3.3.3. AZ19-3-2 compound attenuates CCL2 and CXCL8 chemokine secretion

We interrogated changes in SK-N-AS cell- PBMC crosstalk under hypoxia and how CAIX enzyme inhibition alters them. We applied the transwell co-culture assay as described in the studies with the osteosarcoma 143B cell line and in the methods section. We discovered that the percentage of cells with CAIX and PD-L1 protein surface expression significantly increased in tumor cells exposed to supernatants from PBMCs (percent of CAIX protein expressing cells increased from 44±12 % in mono-culture to 85±5 % in transwell and percent of PD-L1 protein expressing cells increased from 5±3 % to 36±6 %) (**(Fig. 27A).** It is likely related to additional stimuli from PBMCs that promote the expression of these markers and likely reflect real-life TME changes. The CCR2 receptor expression on the SK-N-AS cells from the transwell co-culture had a minimal increase **(Fig. 27A).**

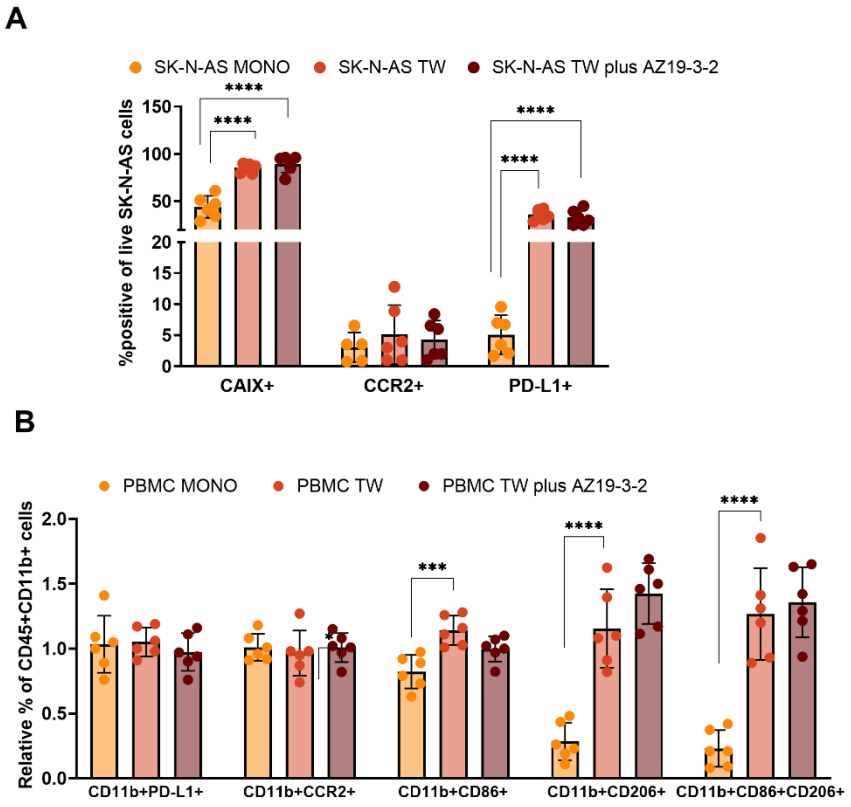

Figure 27. Changes in expression of surface markers after SK-N-AS cell supernatant exposure to PBMC cells in a co-culture assay. A) Change of CAIX, CCR2, and PD-L1 expression on cancer cells. Orange–cancer cells without PBMCs, red–cancer cells exposed to PBMCs, brown–cancer cells exposed to PBMCs and 200 nM AZ19-3-2 (n=6 per group). B) Surface expression of PD-L1, CCR2, CD86, CD206, and $CD86^{+}CD206^{+}$ on CD11b population of PBMCs in the co-culture in the presence (red bars) or absence (dark blue bars) of 200 nM AZ19-3-2. The expression is represented as a relative fraction of $CD11b^{+}$ cells. Control is the PBMCs monolayer depicted in light blue bars (n=6 per group). In graphs A and B statistics were determined using ANOVA (Tukey's multiple comparison). * $p < 0.05$; ** $p < 0.01$, *** $p < 0.001$, **** $p < 0.0001$.

In contrast, when assessing PBMC surface expression changes, we observed no differences in the surface expression of CD4, CD8, or PD-1 on T-cells. Furthermore, there were no changes in CCR2 or PD-L1 protein

expression on CD11b cells **(Fig. 27B).** Percent surface expression of co-stimulatory molecules CD86 and CD206 on CD11b cells compared to cells not exposed to the SK-N-AS cell line increased significantly (CD86% increased from 0.8±0.1 % to 1.1±0.1 % and CD206% from 0.3±0.1 % to 1.2±0.3 %) **(Fig. 27B).** When CAIX enzyme was inhibited on SK-N-AS cells, CD86 percent protein surface expression on CD11b cells trended downward from 1.1±0.1 % to 1±0.1 %, whereas CD206 protein percent surface expression trended upward from 1.2±0.3 % to 1.4±0.2 %) **(Fig. 27B).**

Next, we investigated changes in the cytokine/chemokine secretion profile by PBMCs and SK-N-AS in transwells. The cytokine values were below the assay detection limit in various pro- and anti-inflammatory cytokines (such as TNF-α, IL-6, IFN-γ, IL-4, IL-10, TGF-β). However, the secretion of VEGF, CCL2, and CXCL8 proteins showed significant variations. First, we noted a significant increase in VEGF, CCL2, and CXCL8 chemokine secretion when cells were exposed to each other's solutions in a transwell system compared to immune or cancer cell monolayers **(Fig. 28A, B, C, D).** The addition of CAIX inhibitor AZ19-3-2 significantly increased VEGF cytokine secretion in PBMCs (from undetectable to 187±57 pg) but not in transwell (from 2469±1345 pg to 2165±1500 pg). AZ19-3-2 compound significantly attenuated CCL2 (from 1525±1014 pg to 831±372 pg) and CXCL8 (from 52487±30315 pg to 28966±15457 pg) chemokine secretion in transwells but not in mono-layers **(Fig. 28B, C).**

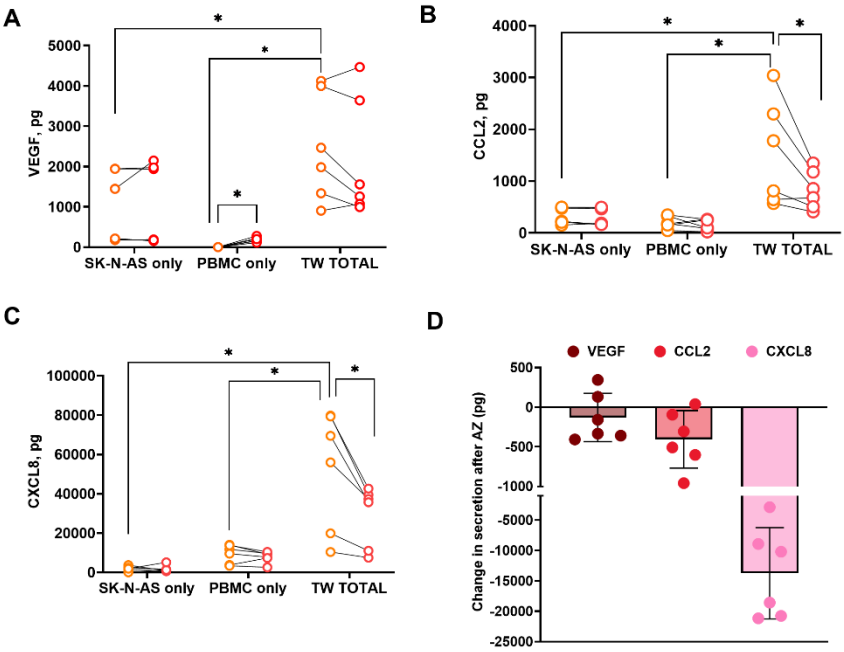

Figure 28. Changes in chemokine/cytokine secretion in neuroblastoma SK-N-AS cell -PBMC cell transwell (TW) assay. Secretion of A) VEGF, B) CCL2, and C) CXCL8 in SK-N-AS cell monolayer, PBMC monolayer, and TW when cells are exposed to AZ19-3-2 (red circles) or vehicle control (orange circles) (n=6 per group). D) Differences in VEGF, CCL2, and CXCL8 chemokine/cytokine levels in TWs when SK-N-AS were pre-treated or not with 200 nM of AZ 19-3-2. The difference is shown as a change in total cytokine secretion levels from untreated to treated conditions (NETO values, n=6 per group). Data are presented as the mean ± SD. Significance was determined using Kruskal-Wallis multiple comparison tests for differences between monolayer and TW values, and for differences between treated and non-treated cohorts, a paired Student's t-test was applied. * $p < 0.05$; ** $p < 0.01$, *** $p < 0.001$.

These results show that cancer cell exposure to immune cells under hypoxia reshapes cell surface expression with a significant increase in CAIX and PD-L1 protein expression in cancer cells. CAIX enzyme inhibition interfered with VEGF cytokine secretion on PBMCs and with CCL2 (2.10-fold) and CXCL8 (1.8-fold) chemokine secretion in a transwell. Whether these changes are a result of the direct CAIX inhibition effect or indirect effects mediated by one or more variables needs to be determined.

3.3.4. Treatment efficacy of AZ19-3-2 compound in combination with CCR2 receptor antagonist in neuroblastoma SK-N-AS cell-based xenograft mouse model

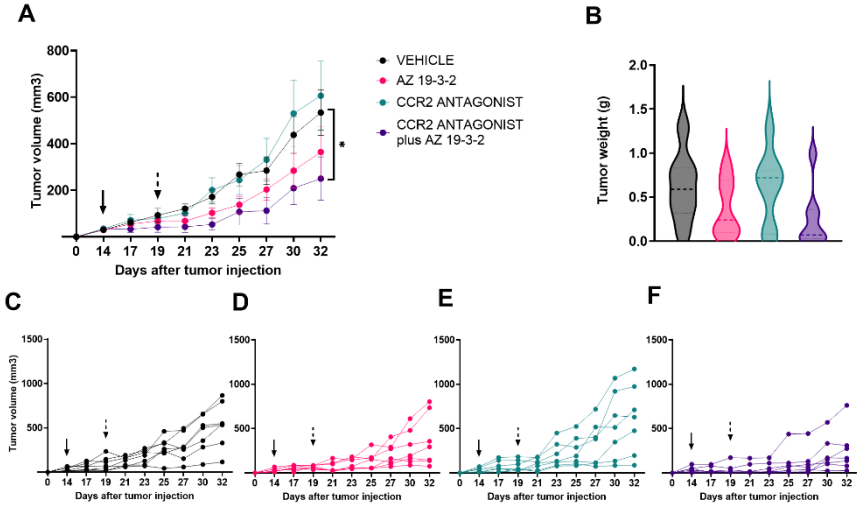

Figure 29. AZ19-3-2 in combination with CCR2 antagonist diminishes growth of subcutaneously implanted SK-N-AS tumors. A) Tumor-growth kinetics of subcutaneously implanted SKNAS tumors, that were subjected to AZ19-3-3 treatment (pink circles), CCR2 antagonist (green circles), combination (purple circles) or control (black circles). B) Final tumor weights of the sacrificed animals at the end of experiment AZ19-3-3 treatment (pink columns), CCR2 antagonist (green columns), combination (purple column) or control (black column). C) Tumor-growth kinetics for individual animals in each group. Each data point represents a separate tumor sample from mice (n=7 per group). Significance was determined using ANOVA (Tukey's) multiple comparison test. * $p < 0.05$; ** $p < 0.01$, *** $p< 0.001$.

After establishing compound activity *in vitro*, we tested AZ19-3-2 efficacy as a possible anti-cancer compound *in vivo*. SK-N-AS cells were inoculated s.c. into the right flank of Nude mice. Once tumors reached palpable size (mean volume 32 mm^3), we randomized them into four treatment groups (n = 7 per group). We started treating tumors with the compound AZ19-3-2 at a dose of 10 mg/ kg/ dose i.p. daily on the day of randomization. We initiated the administration of the CCR2 antagonist five days later at a dose of

2 mg/ kg/ dose i.p. daily to allow saturation of AZ19-3-2 compound in the tumors with resultant reduced pericellular tumor acidity. Tumor growth was the slowest in the group of mice that received combination treatment (mean tumor volume at the end of the experiment was 533±258 mm^3 in the vehicle group and 250±247 mm^3 in the combination group) **(Fig. 29A, C, D, E, F)**. Although statistically significant differences in tumor weights between vehicle control and combination treatment were not detected (mean tumor weight at the end of the experiment was 0.6±0.4 g in the vehicle group and 0.3±0.3 g in the combination group) **(Fig. 29B)**.

Although no synergy between CCR2 antagonist and CAIX inhibitor was observed, results show the feasibility of combining CAIX enzyme inhibition with CCR2-CCR2 axis inhibition. Further studies are needed to assess whether changing the timing of CCR2 antagonist administration could improve results. Translating this approach to a different tumor system would also be beneficial.

3.3.5. Treatment-associated changes in subcutaneously implanted human SK-N-AS neuroblastoma xenografts

We performed flow cytometry analysis on harvested neuroblastoma SK-N-AS tumors from mice. We analyzed tumor cells and a limited number of immune cells, mainly murine monocytes/macrophages (Nude mice have impaired T cells). Although we did not observe significant alterations in tumor or stroma cell surface expression of analyzed markers in tumors from mice treated with AZ19-3-2, treatment with CCR2 antagonist showed more pronounced CCR2 percent expression in tumors (6±3.6 % in the vehicle group, 16±8 % in the CCR2 antagonist group and 20±6 % in the combination group) **(Fig. 30A).** We think it is a compensatory effect. In addition, the VEGFR receptor-expressing cell population was significantly higher in tumors from mice treated with the combination compared to other groups (0.9±0.2 % in the vehicle group and 6.9±5.2 % in the combination group) **(Fig. 30A).** VEGFR is another potent hypoxia signal that could be activated as a compensatory mechanism when CCR2 and CAIX proteins are inhibited.

In addition, CAIX protein percent expression significantly increased in the group of mice treated with the combination (23.7±7 % in the vehicle group and 52±11 % in the combination group) **(Fig. 30A)**. The percent surface expression of stem cell marker CD44 decreased (although not significantly) in tumors treated with a combination of AZ19-3-2 compound and CCR2

antagonist (21.6±4.2 % in the vehicle group and 16.3±3.2 % in the combination group) **(Fig. 30A)**.

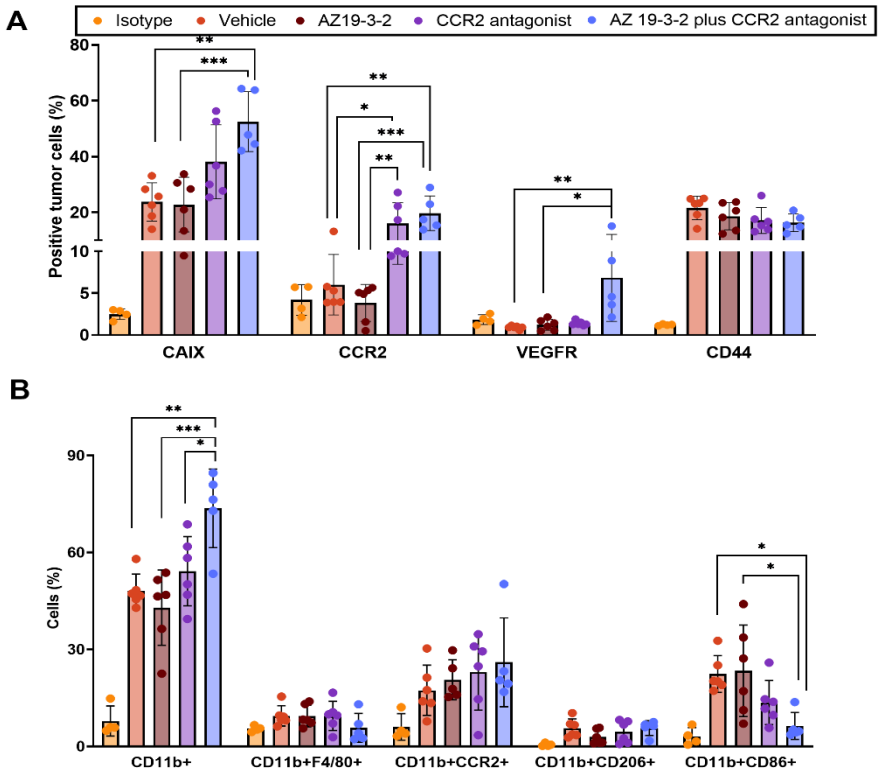

Figure 30. Flow cytometry analysis of harvested neuroblastoma SK-N-AS tumors. A) Flow cytometry analysis of the percentage of CAIX$^+$, CCR2$^+$, CD44$^+$, VEGFR$^+$ cells in the tumor fraction cell population. AZ19-3-2 treatment (brown columns), CCR2 antagonist (purple columns), combination (blue column), or control (red column). Isotype control is depicted in orange columns. B) Flow cytometry analysis of the percentage of CD11b$^+$, CD11b$^+$ F4/80$^+$, CD11b$^+$ CCR2$^+$, CD11b$^+$ CD206$^+$, and CD11b$^+$CD86$^+$ cells in the stroma cells of the tumor of the mice. Each data point represents a separate tumor sample from mice, n=7 per group. Significance was determined using the Student's *t*-test.

When assessing murine stroma cells for CCR2 surface expression, we noticed similar sharp increase effects in mice treated with CCR2 antagonist or a combination. The percentage of CD11b$^+$F4/80$^+$ cells decreased in mice treated with the combination of AZ19-3-2 and CCR2 (5.5±0.8 % in the vehicle group to 9.4±4.5 % in the combination group) **(Fig. 30B)**. However, no difference was noted in CD11b$^+$CCR2$^+$, CD11b$^+$CD206$^+$, or CD11b$^+$PD-L1$^+$

cell populations. The percentage of $CD11b^+CD86^+$ cells significantly decreased in tumors treated with AZ19-3-2 and CCR2 (3±2.7 % in the vehicle group to 9.4±4.5 % in the combination group) **(Fig. 30B)**. Interestingly, combination treatment significantly increased the percentage of monocyte/macrophage cells ($CD11b^+$ population) in tumors (from 7.8±4.6 % in the vehicle group to 54±10.7 % in the combination group) **(Fig. 30B)**.

All these surface protein changes on tumor and monocyte/macrophage cell populations potentially point to evasive mechanisms involved when mice receive combination treatment, such as VEGFR protein upregulation and a decrease in $CD11b^+CD86^+$ cell population.

3.4. Creation of an imaging platform for CAIX enzyme recognizing compounds

The development of theranostic radiopharmaceuticals remains an important trend in cancer diagnostics and treatment [182]. Numerous targeted radionuclide therapy agents are currently undergoing various phases of clinical trials [183]. CAIX-recognizing, small molecule-based, radiotracer conjugates developed to date are non-specific, such as acetazolamide. That causes off-target binding, such as the uptake in the stomach, kidneys, or liver [141]. Better, more specific, and sensitive radiotracer small molecules are needed. My colleagues at the Department of Biothermodynamics and Drug Design, Institute of Biotechnology, Life Sciences Center, Vilnius University, have designed and synthesized several CAIX enzyme-recognizing compounds and tagged them to the NIR probe. They also performed *in vitro* work that helped choose the best candidate compounds for further testing. My work encompassed the study of selected CAIX enzyme specific-NIR probe-tagged compounds' ability to recognize CAIX enzyme in live tumors in a suitable mouse xenograft platform.

3.4.1. Human HeLa cell-based cervical cancer xenograft mice models feasibility assessment for the imaging

Our laboratory has developed a HeLacr$CAIX^{KO}$ cell line ($HeLaCAIX^{KO}$). The efficiency of the decrease in CAIX protein expression was confirmed by flow cytometry and WB studies **(Fig. 31A, B).** In addition, IHC staining of HeLa tumors shows negative CAIX staining **(Fig. 31C).** We then injected human cervical cancer $HeLaCAIX^{WT}$ cells and $HeLaCAIX^{KO}$ cells s.c. into opposite flanks of the same Nude mice. Such an approach allowed us to

compare compound distribution in CAIX enzyme non-expressing and CAIX enzyme-expressing tumors in real-time in the same mouse.

3.4.2. Imaging of mice bearing HeLa tumors with novel CAIX enzyme specific-NIR probe compounds

To analyze fluorescent compound uptake, the two best candidate compounds were chosen: AZ21-6 and GZ22-4. They had the best solubility properties and the best *in vitro* binding to cells. Although both are CAIX enzyme-recognizing compounds tagged to NIR probes, their light absorption spectrum differs. Absorption of GZ22-4 is ≈770-780 nm, whereas AZ21-6 ≈650-750 nm. Therefore, images were obtained using different fluorescence filters: C780F850 for GZ22-4 compound distribution studies and C690F760 for AZ21-6 compound distribution studies. Compounds were injected i.v. into the tail vein of the mouse, and images were obtained every 24 hours. We saw differential uptakes of the compounds in HeLaCAIX^{WT} tumors compared to HeLaCAIX^{KO} tumors **(Fig. 32A, B and Fig. 33A, B).**

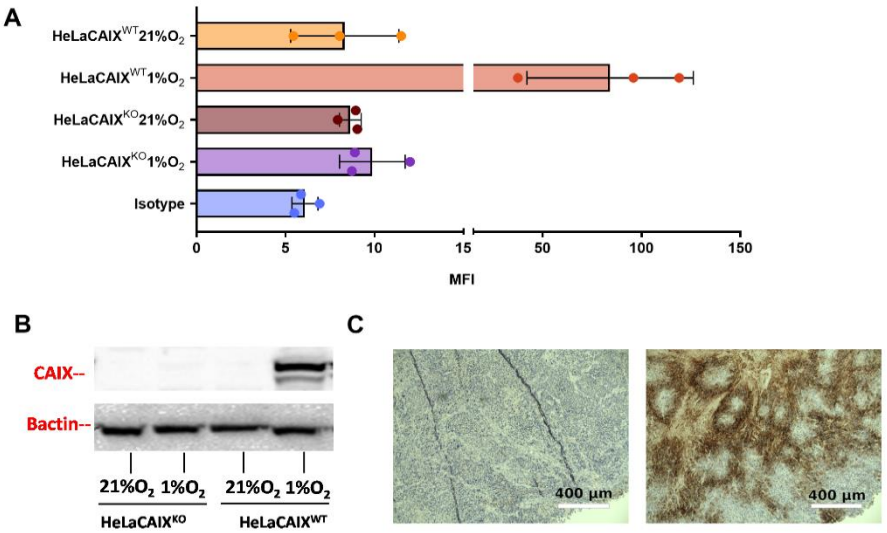

Figure 31. CAIX expression pattern in HeLaCAIX^{WT} versus Hela CAIX^{KO} cells. A) CAIX MFI by flow cytometry analysis in HeLaCAIX^{WT} versus Hela CAIX^{KO} lines. B) CAIX protein expression in 21 % O_2 versus 1 % O_2 by WB in HeLaCAIX^{WT} versus HelaCAIX^{KO} lines. C) IHC of HeLaCAIX^{WT} versus HelaCAIX^{KO} lines xenograft tumor sections reveal absent CAIX staining in HelaCAIX^{KO} tumor (left) compared to the section of HeLaCAIX^{WT} (right) tumor. Scale bars, 400 µm.

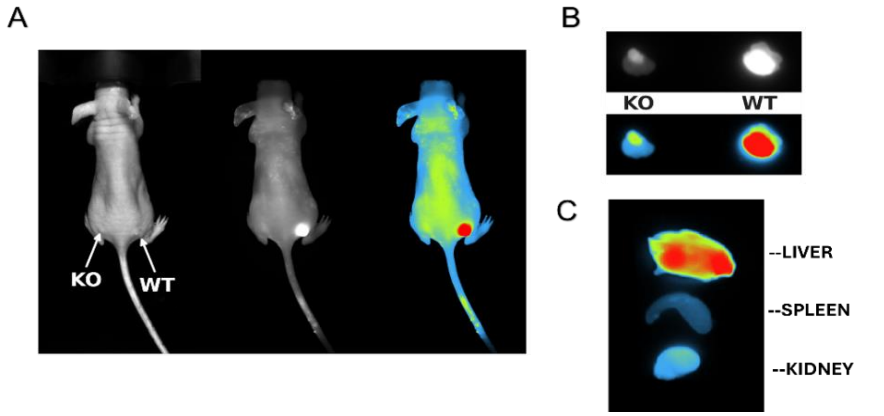

Figure 32. **GZ22-4 compound uptake in Nude mice.** A) GZ22-4 compound uptake in Nude mice bearing HeLaCAIX^{WT} tumor (left flank) compared to HeLaCAIX^{KO} tumors (right flank) 3 days after compound injection. Three images are shown of a single mouse with three imaging techniques: left-raw brightfield image, middle-grey scale fluorescence image, right-multicolor fluorescence image. B) Uptake intensity in HeLaCAIX^{WT} compared to HeLaCAIX^{KO} tumor *ex vivo.* C) Uptake intensity of harvested organs *ex vivo.* Images obtained 3 days after compound injection i.v.

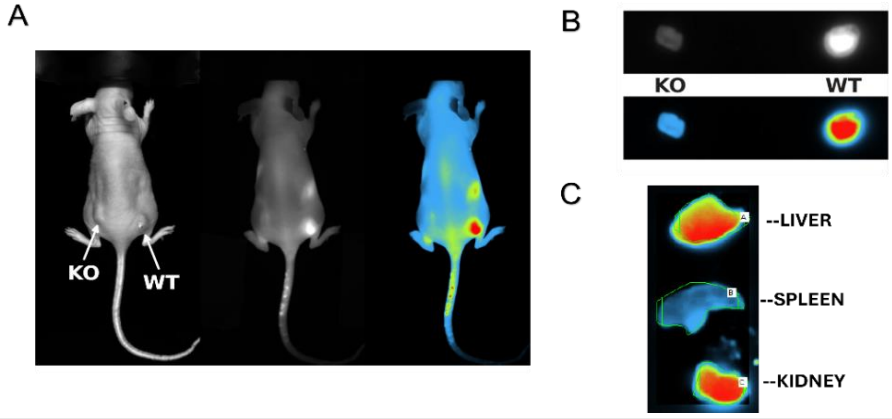

Figure 33. **AZ21-6 compound uptake in Nude mice.** A) AZ21-6 compound uptake in Nude mice bearing HeLaCAIX^{WT} tumor (left flank) compared to HeLaCAIX^{KO} tumors (right flank) 7 days after compound injection. Three images are shown of a single mouse with three imaging techniques: left-raw brightfield image, middle-grey scale fluorescence image, right-multicolor fluorescence image. B) Uptake intensity in HeLa CAIX^{WT} compared to HeLaCAIX^{KO} tumor *ex vivo.* C) Uptake intensity of harvested organs *ex vivo.* Images obtained 7 days after compound injection i.v.

Although CAIX enzyme specific-NIR probes showed great selectivity toward HeLaCAIX^{WT} tumors as compared to HeLaCAIX^{KO} ones, the excretion pattern of these compounds raised certain concerns. We noted the prolonged accumulation of both compounds in the liver **(Fig. 29C, 30C).** In addition, AZ21-6 compound was still detectable in the kidney **(Fig. 30C)** 7 days after the compound injection. Further improvements in the design of these compounds are needed to avoid prolonged off-target organ accumulation.

3. DISCUSSION

Despite novel immunotherapy approaches, a significant number of pediatric patients with solid tumors still fail to respond to treatment. Osteosarcoma and NBL are no exception. Tumor hypoxia is a driving force behind tumor progression and resistance to the treatment. CAIX protein is one of the prominent hypoxia markers across a variety of tumors. For decades, attempts have been made to develop selective CAIX inhibitors without much success. Similarly, although avidly expressed in the majority of solid tumors, single-agent CCL2-CCR2 axis inhibition does not seem to be enough to treat cancer effectively [31]. Such treatment failures can be attributed to plasticity in hypoxia responses and an active interplay in hypoxia signals. Tumors develop evasive resistance during treatment, where alternative pathways are activated to sustain tumor growth when the primary target remains inhibited. For instance, during anti-angiogenic therapies tumors emerge with alternative pro-angiogenic signaling pathways such as FGF that help employ the pericytes to cover vasculature and augment metastasis [184].

In the 143B osteosarcoma xenograft model studies, single-agent CAIX inhibition was ineffective. In tumors from mice that received CAIX inhibitor, we saw CCR2 protein upregulation as a possible evasive mechanism at play. An attempt to combine CAIX inhibition with Avastin in this model was not successful. Adaptive resistance mechanisms when CAIX protein is inhibited are less studied, but upregulation of other CAs, such as CAXII, likely take place [185]. For instance, when the *CA9* gene is knocked down in LS174Tr colon carcinoma cells, partial compensation by up-regulation of CA XII *in vitro* and *in vivo* was observed, suggesting cross-talk between CAs [186]. The mechanism of this specific cross-talk between the CAs remains unclear. Another reason for treatment failures can be linked to difficulties in developing specific inhibitors. Most inhibitors used clinically lack selectivity towards targeted CA isozymes, as there is a high homology of amino acid sequence between isozymes, which makes the design and development of CA inhibitors challenging [22]. The sequence identity of the CAs catalytic domain is more than 30 % [135].

NBL cell line SK-N-AS has more avid CAIX protein expression under hypoxia compared to osteosarcoma 143B line. **Therefore, we explored CAIX enzyme inhibition in this model as well.** We used a cancer cell-PBMC co-culture model to understand the effects of CAIX inhibition in tumor cell-immune cell crosstalk. We uncovered an interplay between PBMCs and cancer cells, where the presence of PBMCs exaggerated hypoxia responses

with increased CAIX, CCR2, PD-L1 protein surface expression on cancer cells, and increased VEGF, CXCL8, and CCL2 chemokine secretion. Mechanisms are not clear but are likely via various secretory signals. The addition of CAIX inhibition to co-culture resulted in decreased CXCL8 and CCL2 chemokine secretion. CXCL8 chemokine is extensively explored due to its relation to poor cancer prognosis and metastasis [187-191]. It can act as an independent predictive marker in patients receiving ICB. Therefore, CXCL8 blockade has been tested in conjunction with ICB in pre-clinical models [178] or with other therapies [162]. Therefore, the link between CAIX and CXCL8 signaling would be important to pursue further.

Our work also highlights the importance of choosing the right *in vitro* platform in investigating complex biological interactions. The co-culture method revealed exaggerated upregulation of CAIX protein compared to the mono-culture method, suggesting other, not yet identified factors involved in CAIX protein expression regulation.

The combination of CAIX enzyme inhibition with CCR2 receptor inhibition in the SK-N-AS xenograft model showed moderately slower tumor growth in the combination group. We detected a downregulation trend of CD44 protein surface expression in tumors from mice treated with a combination. Likely, it's a treatment effect and not adaptive resistance. CD44 protein belongs to a heterogeneous group of surface glycoproteins, involved in cell-cell and cell-matrix interactions. In NBLs, its expression and functional activity are more pronounced in MYCN non-amplified tumors/cell lines [192]. CD44+ NBL xenografts have pronounced metastatic patterns [193] and $CD44^{high}$ NBL cells sorted from cell lines, mouse xenografts, or patient-derived xenografts (PDXs) have increased proliferative and self-renewal capacity [194]. Therefore, lower CD44 protein expression on tumor cells is likely beneficial. Analysis of murine CD11b+ expressing cells in tumors showed a significant decrease in CD86+ surface protein expression on CD11b of tumors from mice treated with the combination compared to other groups. CD86 protein is one of the type I transmembrane proteins, a ligand for CD28 that is associated with T cell activation of the immune system [195]. It is a costimulatory molecule that $CD11b^{+}$ cells express as a response to pro-inflammatory signals [196]. As CD11b+CD86+ cells are important in activating adaptive immune responses, a decrease in CD86+ cells could be an unwanted tumor escape mechanism resulting from treatment pressure.

We also attempted to elucidate CCR2-CCL2 axis-driven mechanisms of 143B osteosarcoma cell lines in different oxygen microenvironments. First, we interrogated the effect of the CCR2 receptor antagonist on the ability

of 143B cells to secrete chemokines CXCL8, CCL2, and VEGF. All these pro-angiogenic and pro-inflammatory chemokines are angiogenic and implicated in cancer metastasis [197] [198]. CXCL8 chemokine and VEGF cytokine were shown to be increased in the blood serum of patients with osteosarcoma [161]. We investigated cytokine secretion differences in the co-culture model when 143B cells were exposed to PBMC-secreted molecules to 143B mono-culture. In mono-cultures, PBMCs secreted more CXCL8 protein than 143B cells, and this difference was more notable in normoxia than in hypoxia. Conversely, there was an increase in CXCL8 chemokine secretion in both oxygen conditions in the co-culture. Interestingly, the CCR2 antagonist effectively decreased CXCL8 chemokine secretion by PBMCs, but only in normoxia.

CCL2 chemokine secretion was also more pronounced in PBMCs but not in 143B cells. Although the CCL2 protein level increased in the transwell co-culture under normoxia, it decreased significantly in hypoxia. The mechanism of such downregulation of CCL2 protein secretion in hypoxia is unclear. Treatment with CCR2 receptor antagonist dramatically increased CCL2 chemokine production across experimental conditions. We believe this is a compensatory effect of the CCR2 receptor blockade, preventing CCL2 binding.

The VEGF-VEGFR cytokine axis is implicated in tumor neo-angiogenesis and represents a prognostic marker in osteosarcoma patients [153]. Notably, the VEGF cytokine secretion pattern was different from that of chemokines CCL2 and CXCL8, as this cytokine was produced mainly by 143B cells and not PBMCs in mono-cultures. In the co-culture, we noticed that VEGF cytokine secretion was more pronounced in hypoxia than in normoxia. CCR2 antagonist was more effective in decreasing VEGF protein secretion in hypoxia, with increased VEGFR protein expression on 143B cells in the co-culture.

We also noted differential changes in the expression of PD-L1, CD44, CAIX, and CCR2 proteins on the surface of 143B cells in the transwell co-culture model compared to the cell monolayer. The CD44 protein is linked to worse survival in osteosarcoma patients [199] as it promotes osteosarcoma cell migration and proliferation. CD44 positively correlates with PD-L1 in osteosarcoma [200] [166]. In agreement with this notion, we observed that 143B cells have high expression of both markers, PD-L1 and CD44, and hypoxia decreases expression of both. Interestingly, the addition of a CCR2 antagonist increased PD-L1 and CD44 protein expression in normoxia but failed to do so in hypoxia. CAIX protein expression increased on the surface

of 143B cells in hypoxia, and even more so in their co-culture with PBMCs. CCR2 antagonist caused a decrease in CAIX protein expression, although not significant. The possible mechanism of the link between the CCR2-CCL2 axis and CAIX protein needs to be further explored. Although CCR2 protein expression slightly decreased on 143B cells in hypoxia, there was a significant increase in CCR2 protein surface expression in $CD45^{+}CD11b^{+}$ cells. Our data aligns with the notion that cyclic hypoxia can upregulate CCR2 receptors in macrophages [156] [33], but chronic hypoxia can induce various CCR2 receptor expression changes in monocytes/macrophages depending on the context [33] [65]. The CCR2 antagonist increased CCR2 protein surface expression on 143B cells in transwell across different oxygen conditions, and this was likely a compensatory effect.

In agreement with these observations, the treatment of mice bearing osteosarcoma 143B cells-based tumors with CCR2 antagonist *in vivo* did not slow tumor progression. It is likely due to decreased oxygen tensions in the tumor that alter treatment response, as we saw in the co-culture model. Flow cytometry analysis of harvested osteosarcoma tumors from mice showed alterations in tumor CD44, VEGFR, and PD-L1 protein expression as well as CD86 protein surface expression on monocytes/macrophages in the CCR2 antagonist treatment group compared to vehicle controls. CCR2 receptor inhibition increased the fraction of $VEGFR^{+}$ and $PD\text{-}L1^{+}$ tumor cells, which might indicate an evasive mechanism when an alternative pro-angiogenic, immunosuppressive pathway is activated. Interestingly, we observed two populations having either low or high expression of the CD44 protein. CCR2 antagonist shifted the cells from $CD44^{low}$ to $CD44^{high}$ in this way increasing overall CD44 protein expression. This is likely an unwanted effect as CD44 protein expression is linked to worse survival in osteosarcoma patients [199]. In tumor stroma analysis, we noted an increase in $CD11b^{+}CD86^{+}$ cells after CCR2 inhibition. TAMs that express $CD86^{+}$ can exert both pro-tumorigenic and anti-tumorigenic functions depending on their activation state [201]. Therefore, an increase in the number of subsets of these cells could potentially be a desired effect of CCR2 inhibition-related treatment.

We also performed a more in-depth proteome analysis of cancer-related targets in 143B tumor cells grown in co-culture with PBMC and when they are subjected to CCR2 antagonist in hypoxia versus normoxia. Proteome analysis revealed differential expression patterns in tumor cells. Hypoxia-related proteins such as CAIX and HIF-1α further increased with CCR2 antagonist administration in hypoxia. VEGF cytokine secretion decreased in 143B cells from the hypoxic co-culture when a CCR2 antagonist was added,

and we observed the same trend in the mice tumors' VEGFR protein expression. Also, protein associated with drug resistance, such as DLL1was upregulated in osteosarcoma 143B cells from the co-culture treated with a CCR2 antagonist under hypoxia but not under normoxia. These hypoxia-driven mechanisms are likely responsible for poor response to CCR2 treatment and need to be addressed in future therapy designs.

Lastly, we investigated the feasibility of tumor CAIX detection *in vivo* in the cervical cancer HeLa xenograft mouse model. We have chosen the most promising CAIX enzyme-recognizing compounds and tagged them to the NIR probes as the first step in assessing the specificity and biodistribution of these candidate probes for further development. We saw differential uptakes of the CAIX enzyme-specific NIR probe compounds in HeLaCAIX^{WT} tumors as compared to HeLaCAIX^{KO} tumors in mice *in vivo*. Based on the images, the GZ22-4 compound is more specific toward CAIX and has a faster clearance when compared to other compounds (based on *ex vivo* mouse organ images showing no fluorescence in the kidney compared to the AZ22-4 compound). However, the persistence of the fluorescence uptake in the liver raises concerns and the need to improve the design of these compounds to avoid prolonged liver accumulation. These findings will serve as a platform for future CAIX-based cancer imaging technology development.

CONCLUSIONS

Despite recent breakthroughs in cancer treatment, such as immunotherapy, targeted therapies, and cellular therapies, the survival of pediatric patients presenting with advanced-stage or relapsed solid tumors remains poor [1]. Tumors employ a variety of compensatory mechanisms to evade tumor killing. Tumor hypoxia and associated peritumoral acidosis significantly contribute to cancer progression and treatment resistance. CAIX, a hypoxia-induced enzyme, helps cancer cells overcome intracellular acidosis and survive. The CCL2-CCR2 axis is activated in hypoxic TME and helps sustain immunosuppression. Both have become attractive targets in cancer therapy development.

Our work highlights the compensatory mechanisms involved when CAIX or CCL2-CCR2 axis is inhibited in pediatric cancer solid tumor models, such as neuroblastoma and osteosarcoma, the role of hypoxia in tumor editing, and the potential for attenuating both signals, CAIX and CCL2-CCR2, that are indispensable in helping tumor cells survive.

Chemical compounds possessing high affinity (approximately 30 pM Kd) and significant (approx. >100x) selectivity for CAIX over remaining catalytically active CA isozymes were designed, synthesized, and evaluated in our laboratory (Department of Biothermodynamics and Drug Design). My work encompassed the biological evaluation of the AZ19-3-2 inhibitor, demonstrating compound suitability and limitations for cancer therapy and diagnostics. AZ19-3-2 compound successfully reduced NBL SK-N-AS cell spheroid growth under hypoxia, but not under normoxia. This compound also reduced tumor growth in mice NBL xenograft model when it was used in combination with a CCR2 antagonist.

In addition, selected CAIX enzyme-recognizing-NIR probe-tagged compounds GZ22-4 and AZ21-6 were injected into mice bearing tumors; they accumulated in the $CAIX^{WT}$ tumors, but not in $CAIX^{KO}$ tumors. These results demonstrate the compound's potential suitability for future CAIX-expressing cancer diagnostics.

Additionally, we show that hypoxic conditions alter the expression of different cellular markers and impair CCR2 antagonist effects in the experimental 143B osteosarcoma model. This investigation suggests potential strategies to overcome such resistance by using dual targeting with CCR2 inhibition, such as inhibiting CAIX, VEGFR, or CD44 expression or activity.

Importantly, we show the advantages of using tumor cells and the PBMC co-culture model over mono-cultures in better reflecting the actual *in-situ* phenotype of the tumor cells.

All these findings can serve as a foundation for future hypoxic tumor niche recognition-based therapy and diagnostics development.

Conclusions:

1. CAIX enzyme inhibition with the AZ19-3-2 compound as a monotherapy or in combination with Avastin was ineffective in an osteosarcoma 143B xenograft model.
2. *In vitro*, CAIX enzyme inhibition with 200 nM of the AZ19-3-2 compound reduced neuroblastoma SK-N-AS spheroid growth 1.38-fold under hypoxia but not normoxia.
3. Combination of CAIX enzyme inhibition using AZ19-3-2 compound with CCR2 receptor antagonist diminished mean tumor growth *in vivo* by half in the neuroblastoma SK-N-AS model.
4. CAIX enzyme inhibition using 200 nM of AZ19-3-2 compound decreased CXCL8 by 1.8-fold and CCL2 chemokine secretion by 2.19-fold in PBMCs in PBMC-SK-N-AS co-culture assay using a transwell model.
5. CCR2 antagonist was not effective in the experimental osteosarcoma 143B mouse model.
6. CAIX enzyme recognizing-NIR probe-tagged compounds AZ21-6 and GZ22-4 selectively recognized and differentiated $CAIX^{WT}$ tumors from $CAIX^{KO}$ tumors in mice.
7. Under hypoxia, co-culture of osteosarcoma 143B cells or neuroblastoma SK-N-AS cells with human PBMCs increased CAIX protein surface percent expression by 3.6-fold on 143B cells and 1.9-fold on SK-N-AS cells compared to cell monolayers.

Future directions will include 1) different therapy combination approaches that address hypoxic TME and 2) CAIX protein-based diagnostics development.

REFERENCES

1. Sherif, S., et al., *The immune landscape of solid pediatric tumors.* J Exp Clin Cancer Res, 2022. **41**(1): p. 199.
2. Belgiovine, C., et al., *Pediatric Solid Cancers: Dissecting the Tumor Microenvironment to Improve the Results of Clinical Immunotherapy*. Int J Mol Sci, 2024. **25**(6).
3. McDonald, P.C., S.C. Chafe, and S. Dedhar, *Overcoming Hypoxia-Mediated Tumor Progression: Combinatorial Approaches Targeting pH Regulation, Angiogenesis and Immune Dysfunction.* Front Cell Dev Biol, 2016. **4**: p. 27.
4. Barsoum, I.B., et al., *A mechanism of hypoxia-mediated escape from adaptive immunity in cancer cells.* Cancer Res, 2014. **74**(3): p. 665-74.
5. Noman, M.Z., et al., *Hypoxia: a key player in antitumor immune response. A Review in the Theme: Cellular Responses to Hypoxia.* Am J Physiol Cell Physiol, 2015. **309**(9): p. C569-79.
6. Sedlakova, O., et al., *Carbonic anhydrase IX, a hypoxia-induced catalytic component of the pH regulating machinery in tumors.* Front Physiol, 2014. **4**: p. 400.
7. Mancino, A., et al., *Divergent effects of hypoxia on dendritic cell functions.* Blood, 2008. **112**(9): p. 3723-34.
8. Doedens, A.L., et al., *Macrophage expression of hypoxia-inducible factor-1 alpha suppresses T-cell function and promotes tumor progression.* Cancer Res, 2010. **70**(19): p. 7465-75.
9. Facciabene, A., et al., *Tumour hypoxia promotes tolerance and angiogenesis via CCL28 and T(reg) cells.* Nature, 2011. **475**(7355): p. 226-30.
10. Pinato, D.J., et al., *Programmed cell death ligands expression in phaeochromocytomas and paragangliomas: Relationship with the hypoxic response, immune evasion and malignant behavior.* Oncoimmunology, 2017. **6**(11): p. e1358332.
11. Pastorekova, S. and R.J. Gillies, *The role of carbonic anhydrase IX in cancer development: links to hypoxia, acidosis, and beyond.* Cancer Metastasis Rev, 2019. **38**(1-2): p. 65-77.
12. Nordfors, K., et al., *The tumour-associated carbonic anhydrases CA II, CA IX and CA XII in a group of medulloblastomas and supratentorial primitive neuroectodermal tumours: an association of CA IX with poor prognosis.* BMC Cancer, 2010. **10**: p. 148.

13. Proescholdt, M.A., et al., *Function of carbonic anhydrase IX in glioblastoma multiforme.* Neuro Oncol, 2012. **14**(11): p. 1357-66.
14. van Kuijk, S.J., et al., *Prognostic Significance of Carbonic Anhydrase IX Expression in Cancer Patients: A Meta-Analysis.* Front Oncol, 2016. **6**: p. 69.
15. Okuno, K., et al., *Carbonic anhydrase IX enhances tumor cell proliferation and tumor progression in osteosarcoma.* Onco Targets Ther, 2018. **11**: p. 6879-6886.
16. Ameis, H.M., et al., *Carbonic anhydrase IX correlates with survival and is a potential therapeutic target for neuroblastoma*. J Enzyme Inhib Med Chem, 2016. **31**(3): p. 404-9.
17. Dungwa, J.V., L.P. Hunt, and P. Ramani, *Carbonic anhydrase IX up-regulation is associated with adverse clinicopathologic and biologic factors in neuroblastomas.* Hum Pathol, 2012. **43**(10): p. 1651-60.
18. Cetin, B., et al., *Carbonic anhydrase IX is a prognostic biomarker in glioblastoma multiforme.* Neuropathology, 2018. **38**(5): p. 457-462.
19. Damgaci, S., et al., *Hypoxia and acidosis: immune suppressors and therapeutic targets.* Immunology, 2018. **154**(3): p. 354-362.
20. Chafe, S.C., et al., *Targeting Hypoxia-Induced Carbonic Anhydrase IX Enhances Immune-Checkpoint Blockade Locally and Systemically.* Cancer Immunol Res, 2019. **7**(7): p. 1064-1078.
21. McDonald, P.C., et al., *A Phase 1 Study of SLC-0111, a Novel Inhibitor of Carbonic Anhydrase IX, in Patients With Advanced Solid Tumors.* Am J Clin Oncol, 2020. **43**(7): p. 484-490.
22. Mboge, M.Y., R. McKenna, and S.C. Frost, *Advances in Anti-Cancer Drug Development Targeting Carbonic Anhydrase IX and XII.* Top Anticancer Res, 2015. **5**: p. 3-42.
23. Dudutienė, V., et al., *Discovery and characterization of novel selective inhibitors of carbonic anhydrase IX*. J Med Chem, 2014. **57**(22): p. 9435-46.
24. Janoniene, A., et al., *Inhibition of Carbonic Anhydrase IX Suppresses Breast Cancer Cell Motility at the Single-Cell Level.* Int J Mol Sci, 2021. **22**(21).
25. Kazokaitė, J., et al., *Fluorinated benzenesulfonamide anticancer inhibitors of carbonic anhydrase IX exhibit lower toxic effects on zebrafish embryonic development than ethoxzolamide*. Drug Chem Toxicol, 2017. **40**(3): p. 309-319.

26. Kazokaitė, J., et al., *Novel fluorinated carbonic anhydrase IX inhibitors reduce hypoxia-induced acidification and clonogenic survival of cancer cells.* Oncotarget, 2018. **9**(42): p. 26800-26816.
27. Chen, K.T. and Y. Seimbille, *New Developments in Carbonic Anhydrase IX-Targeted Fluorescence and Nuclear Imaging Agents.* Int J Mol Sci, 2022. **23**(11).
28. Matulienė, J., et al., *Picomolar fluorescent probes for compound affinity determination to carbonic anhydrase IX expressed in live cancer cells.* Sci Rep, 2022. **12**(1): p. 17644.
29. Yoshimura, T., *The chemokine MCP-1 (CCL2) in the host interaction with cancer: a foe or ally?* Cell Mol Immunol, 2018. **15**(4): p. 335-345.
30. Xu, M., et al., *Role of the CCL2-CCR2 signalling axis in cancer: Mechanisms and therapeutic targeting.* Cell Prolif, 2021. **54**(10): p. e13115.
31. Fei, L., et al., *Targeting the CCL2/CCR2 Axis in Cancer Immunotherapy: One Stone, Three Birds?* Front Immunol, 2021. **12**: p. 771210.
32. Jin, J., et al., *CCL2: An Important Mediator Between Tumor Cells and Host Cells in Tumor Microenvironment.* Front Oncol, 2021. **11**: p. 722916.
33. Korbecki, J., et al., *Hypoxia Alters the Expression of CC Chemokines and CC Chemokine Receptors in a Tumor-A Literature Review.* Int J Mol Sci, 2020. **21**(16).
34. Mojsilovic-Petrovic, J., et al., *Hypoxia-inducible factor-1 (HIF-1) is involved in the regulation of hypoxia-stimulated expression of monocyte chemoattractant protein-1 (MCP-1/CCL2) and MCP-5 (Ccl12) in astrocytes.* J Neuroinflammation, 2007. **4**: p. 12.
35. Sceneay, J., et al., *Primary tumor hypoxia recruits CD11b+/Ly6Cmed/Ly6G+ immune suppressor cells and compromises NK cell cytotoxicity in the premetastatic niche.* Cancer Res, 2012. **72**(16): p. 3906-11.
36. Noel, M., et al., *Phase 1b study of a small molecule antagonist of human chemokine (C-C motif) receptor 2 (PF-04136309) in combination with nab-paclitaxel/gemcitabine in first-line treatment of metastatic pancreatic ductal adenocarcinoma.* Invest New Drugs, 2020. **38**(3): p. 800-811.
37. Pienta, K.J., et al., *Phase 2 study of carlumab (CNTO 888), a human monoclonal antibody against CC-chemokine ligand 2 (CCL2), in*

metastatic castration-resistant prostate cancer. Invest New Drugs, 2013. **31**(3): p. 760-8.

38. Mirzadegan, T., et al., *Identification of the binding site for a novel class of CCR2b chemokine receptor antagonists: binding to a common chemokine receptor motif within the helical bundle.* J Biol Chem, 2000. **275**(33): p. 25562-71.
39. McNamee, E.N., et al., *Hypoxia and hypoxia-inducible factors as regulators of T cell development, differentiation, and function.* Immunol Res, 2013. **55**(1-3): p. 58-70.
40. McKeown, S.R., *Defining normoxia, physoxia and hypoxia in tumours-implications for treatment response.* Br J Radiol, 2014. **87**(1035): p. 20130676.
41. Keeley, T.P. and G.E. Mann, *Defining Physiological Normoxia for Improved Translation of Cell Physiology to Animal Models and Humans.* Physiol Rev, 2019. **99**(1): p. 161-234.
42. Stamati, K., V. Mudera, and U. Cheema, *Evolution of oxygen utilization in multicellular organisms and implications for cell signalling in tissue engineering.* J Tissue Eng, 2011. **2**(1): p. 2041731411432365.
43. Jiang, B.H., et al., *Hypoxia-inducible factor 1 levels vary exponentially over a physiologically relevant range of O2 tension.* Am J Physiol, 1996. **271**(4 Pt 1): p. C1172-80.
44. Xia, L., et al., *The cancer metabolic reprogramming and immune response*. Mol Cancer, 2021. **20**(1): p. 28.
45. Prabhakar, N.R. and G.L. Semenza, *Adaptive and maladaptive cardiorespiratory responses to continuous and intermittent hypoxia mediated by hypoxia-inducible factors 1 and 2.* Physiol Rev, 2012. **92**(3): p. 967-1003.
46. Infantino, V., et al., *Cancer Cell Metabolism in Hypoxia: Role of HIF-1 as Key Regulator and Therapeutic Target.* Int J Mol Sci, 2021. **22**(11).
47. Semenza, G.L., et al., *Hypoxia-inducible nuclear factors bind to an enhancer element located 3' to the human erythropoietin gene.* Proc Natl Acad Sci U S A, 1991. **88**(13): p. 5680-4.
48. Masoud, G.N. and W. Li, *HIF-1α pathway: role, regulation and intervention for cancer therapy.* Acta Pharm Sin B, 2015. **5**(5): p. 378-89.

49. Kaluz, S., et al., *Transcriptional control of the tumor- and hypoxia-marker carbonic anhydrase 9: A one transcription factor (HIF-1) show?* Biochim Biophys Acta, 2009. **1795**(2): p. 162-72.
50. Shi, Y. and D.M. Gilkes, *HIF-1 and HIF-2 in cancer: structure, regulation, and therapeutic prospects.* Cell Mol Life Sci, 2025. **82**(1): p. 44.
51. Stiehl, D.P., et al., *Normoxic induction of the hypoxia-inducible factor 1alpha by insulin and interleukin-1beta involves the phosphatidylinositol 3-kinase pathway.* FEBS Lett, 2002. **512**(1-3): p. 157-62.
52. Vander Heiden, M.G., L.C. Cantley, and C.B. Thompson, *Understanding the Warburg effect: the metabolic requirements of cell proliferation.* Science, 2009. **324**(5930): p. 1029-33.
53. Weidemann, A. and R.S. Johnson, *Biology of HIF-1alpha.* Cell Death Differ, 2008. **15**(4): p. 621-7.
54. Hourani, T., et al., *Tumor Associated Macrophages: Origin, Recruitment, Phenotypic Diversity, and Targeting.* Front Oncol, 2021. **11**: p. 788365.
55. Han, Z.J., et al., *Roles of the CXCL8-CXCR1/2 Axis in the Tumor Microenvironment and Immunotherapy.* Molecules, 2021. **27**(1).
56. Chen, B., et al., *HIF1A expression correlates with increased tumor immune and stromal signatures and aggressive phenotypes in human cancers.* Cell Oncol (Dordr), 2020. **43**(5): p. 877-888.
57. Abou Khouzam, R., et al., *Tumor Hypoxia Regulates Immune Escape/Invasion: Influence on Angiogenesis and Potential Impact of Hypoxic Biomarkers on Cancer Therapies.* Front Immunol, 2020. **11**: p. 613114.
58. Hughes, C.E. and R.J.B. Nibbs, *A guide to chemokines and their receptors.* FEBS J, 2018. **285**(16): p. 2944-2971.
59. Deshmane, S.L., et al., *Monocyte chemoattractant protein-1 (MCP-1): an overview.* J Interferon Cytokine Res, 2009. **29**(6): p. 313-26.
60. Raman, D., et al., *Role of chemokines in tumor growth.* Cancer Lett, 2007. **256**(2): p. 137-65.
61. Korbecki, J., et al., *CC Chemokines in a Tumor: A Review of Pro-Cancer and Anti-Cancer Properties of Receptors CCR5, CCR6, CCR7, CCR8, CCR9, and CCR10 Ligands.* Int J Mol Sci, 2020. **21**(20).

62. Korbecki, J., et al., *CC Chemokines in a Tumor: A Review of Pro-Cancer and Anti-Cancer Properties of the Ligands of Receptors CCR1, CCR2, CCR3, and CCR4.* Int J Mol Sci, 2020. **21**(21).
63. Korbecki, J., et al., *The Effect of Hypoxia on the Expression of CXC Chemokines and CXC Chemokine Receptors-A Review of Literature.* Int J Mol Sci, 2021. **22**(2).
64. Blengio, F., et al., *The hypoxic environment reprograms the cytokine/chemokine expression profile of human mature dendritic cells.* Immunobiology, 2013. **218**(1): p. 76-89.
65. Araya, P., et al., *HMGB1 decreases CCR-2 expression and migration of M2 macrophages under hypoxia.* Inflamm Res, 2019. **68**(8): p. 639-642.
66. Ouyang, P., et al., *Microarray analysis of differentially expressed genes in L929 mouse fibroblast cells exposed to leptin and hypoxia.* Mol Med Rep, 2017. **16**(1): p. 181-191.
67. Bosco, M.C., et al., *Hypoxia modifies the transcriptome of primary human monocytes: modulation of novel immune-related genes and identification of CC-chemokine ligand 20 as a new hypoxia-inducible gene.* J Immunol, 2006. **177**(3): p. 1941-55.
68. Zhou, J., et al., *Intermittent Hypoxia Enhances THP-1 Monocyte Adhesion and Chemotaxis and Promotes M1 Macrophage Polarization via RAGE.* Biomed Res Int, 2018. **2018**: p. 1650456.
69. Fousek, K., L.A. Horn, and C. Palena, *Interleukin-8: A chemokine at the intersection of cancer plasticity, angiogenesis, and immune suppression.* Pharmacol Ther, 2021. **219**: p. 107692.
70. David, J.M., et al., *The IL-8/IL-8R Axis: A Double Agent in Tumor Immune Resistance.* Vaccines (Basel), 2016. **4**(3).
71. Masucci, M.T., et al., *The Emerging Role of Neutrophil Extracellular Traps (NETs) in Tumor Progression and Metastasis.* Front Immunol, 2020. **11**: p. 1749.
72. Zhang, M., et al., *Interferon gamma inhibits CXCL8-CXCR2 axis mediated tumor-associated macrophages tumor trafficking and enhances anti-PD1 efficacy in pancreatic cancer.* J Immunother Cancer, 2020. **8**(1).
73. Du, L., et al., *CXCR1/Akt signaling activation induced by mesenchymal stem cell-derived IL-8 promotes osteosarcoma cell anoikis resistance and pulmonary metastasis.* Cell Death Dis, 2018. **9**(7): p. 714.

74. Han, X.G., et al., *CXCR1 knockdown improves the sensitivity of osteosarcoma to cisplatin.* Cancer Lett, 2015. **369**(2): p. 405-15.
75. Olbryt, M., et al., *Global gene expression profiling in three tumor cell lines subjected to experimental cycling and chronic hypoxia.* PLoS One, 2014. **9**(8): p. e105104.
76. Fang, H.Y., et al., *Hypoxia-inducible factors 1 and 2 are important transcriptional effectors in primary macrophages experiencing hypoxia.* Blood, 2009. **114**(4): p. 844-59.
77. Delprat, V., et al., *Cycling hypoxia promotes a pro-inflammatory phenotype in macrophages via JNK/p65 signaling pathway.* Sci Rep, 2020. **10**(1): p. 882.
78. Schalper, K.A., et al., *Elevated serum interleukin-8 is associated with enhanced intratumor neutrophils and reduced clinical benefit of immune-checkpoint inhibitors.* Nat Med, 2020. **26**(5): p. 688-692.
79. Yuen, K.C., et al., *High systemic and tumor-associated IL-8 correlates with reduced clinical benefit of PD-L1 blockade.* Nat Med, 2020. **26**(5): p. 693-698.
80. Armstrong, A.J., et al., *CXCR2 antagonist navarixin in combination with pembrolizumab in select advanced solid tumors: a phase 2 randomized trial.* Invest New Drugs, 2024. **42**(1): p. 145-159.
81. Chouaib, S., et al., *Hypoxic stress: obstacles and opportunities for innovative immunotherapy of cancer.* Oncogene, 2017. **36**(4): p. 439-445.
82. Calcinotto, A., et al., *Modulation of microenvironment acidity reverses anergy in human and murine tumor-infiltrating T lymphocytes.* Cancer Res, 2012. **72**(11): p. 2746-56.
83. Figarella, K., et al., *Hypoxia-adenosine axis as therapeutic targets for acute respiratory distress syndrome.* Front Immunol, 2024. **15**: p. 1328565.
84. Vaupel, P. and A. Mayer, *Hypoxia-Driven Adenosine Accumulation: A Crucial Microenvironmental Factor Promoting Tumor Progression.* Adv Exp Med Biol, 2016. **876**: p. 177-183.
85. Di Virgilio, F., *Purines, purinergic receptors, and cancer.* Cancer Res, 2012. **72**(21): p. 5441-7.
86. Hoskin, D.W., et al., *Inhibition of T cell and natural killer cell function by adenosine and its contribution to immune evasion by tumor cells (Review).* Int J Oncol, 2008. **32**(3): p. 527-35.

87. Molon, B., et al., *Chemokine nitration prevents intratumoral infiltration of antigen-specific T cells.* J Exp Med, 2011. **208**(10): p. 1949-62.
88. Palazón, A., et al., *The HIF-1α hypoxia response in tumor-infiltrating T lymphocytes induces functional CD137 (4-1BB) for immunotherapy*. Cancer Discov, 2012. **2**(7): p. 608-23.
89. Sethumadhavan, S., et al., *Hypoxia and hypoxia-inducible factor (HIF) downregulate antigen-presenting MHC class I molecules limiting tumor cell recognition by T cells.* PLoS One, 2017. **12**(11): p. e0187314.
90. Juhász, P., et al., *Carbonic Anhydrase IX (CAIX) Expressing Hypoxic Micro-environment Hampers CD8+ Immune Cell Infiltrate in Breast Carcinoma.* Appl Immunohistochem Mol Morphol, 2023. **31**(1): p. 26-32.
91. Ben-Shoshan, J., et al., *Hypoxia controls CD4+CD25+ regulatory T-cell homeostasis via hypoxia-inducible factor-1alpha.* Eur J Immunol, 2008. **38**(9): p. 2412-8.
92. Clambey, E.T., et al., *Hypoxia-inducible factor-1 alpha-dependent induction of FoxP3 drives regulatory T-cell abundance and function during inflammatory hypoxia of the mucosa.* Proc Natl Acad Sci U S A, 2012. **109**(41): p. E2784-93.
93. Ugel, S., et al., *Tumor-induced myeloid deviation: when myeloid-derived suppressor cells meet tumor-associated macrophages.* J Clin Invest, 2015. **125**(9): p. 3365-76.
94. Laviron, M. and A. Boissonnas, *Ontogeny of Tumor-Associated Macrophages.* Front Immunol, 2019. **10**: p. 1799.
95. Bronte, V., et al., *Recommendations for myeloid-derived suppressor cell nomenclature and characterization standards.* Nat Commun, 2016. **7**: p. 12150.
96. Davidov, V., et al., *Analyzing One Cell at a TIME: Analysis of Myeloid Cell Contributions in the Tumor Immune Microenvironment.* Front Immunol, 2020. **11**: p. 1842.
97. Pan, Y., et al., *Tumor-Associated Macrophages in Tumor Immunity*. Front Immunol, 2020. **11**: p. 583084.
98. Noy, R. and J.W. Pollard, *Tumor-associated macrophages: from mechanisms to therapy.* Immunity, 2014. **41**(1): p. 49-61.
99. Jayasingam, S.D., et al., *Evaluating the Polarization of Tumor-Associated Macrophages Into M1 and M2 Phenotypes in Human*

Cancer Tissue: Technicalities and Challenges in Routine Clinical Practice. Front Oncol, 2019. **9**: p. 1512.
100. Yang, Y., et al., *Myeloid-Derived Suppressor Cells in Tumors: From Mechanisms to Antigen Specificity and Microenvironmental Regulation.* Front Immunol, 2020. **11**: p. 1371.
101. Henze, A.T. and M. Mazzone, *The impact of hypoxia on tumor-associated macrophages.* J Clin Invest, 2016. **126**(10): p. 3672-3679.
102. Murdoch, C. and C.E. Lewis, *Macrophage migration and gene expression in response to tumor hypoxia.* Int J Cancer, 2005. **117**(5): p. 701-8.
103. Colegio, O.R., et al., *Functional polarization of tumour-associated macrophages by tumour-derived lactic acid.* Nature, 2014. **513**(7519): p. 559-63.
104. Zhang, H., et al., *HIF-1 regulates CD47 expression in breast cancer cells to promote evasion of phagocytosis and maintenance of cancer stem cells.* Proc Natl Acad Sci U S A, 2015. **112**(45): p. E6215-23.
105. Chiu, D.K., et al., *Hypoxia inducible factor HIF-1 promotes myeloid-derived suppressor cells accumulation through ENTPD2/CD39L1 in hepatocellular carcinoma.* Nat Commun, 2017. **8**(1): p. 517.
106. Noman, M.Z., et al., *PD-L1 is a novel direct target of HIF-1α, and its blockade under hypoxia enhanced MDSC-mediated T cell activation.* J Exp Med, 2014. **211**(5): p. 781-90.
107. Jantsch, J., et al., *Hypoxia and hypoxia-inducible factor-1 alpha modulate lipopolysaccharide-induced dendritic cell activation and function.* J Immunol, 2008. **180**(7): p. 4697-705.
108. Bosco, M.C. and L. Varesio, *Dendritic cell reprogramming by the hypoxic environment.* Immunobiology, 2012. **217**(12): p. 1241-9.
109. Wang, Y., et al., *Carbonic anhydrase IX has chaperone-like functions and is an immunoadjuvant.* Mol Cancer Ther, 2008. **7**(12): p. 3867-77.
110. Husain, Z., et al., *Tumor-derived lactate modifies antitumor immune response: effect on myeloid-derived suppressor cells and NK cells.* J Immunol, 2013. **191**(3): p. 1486-95.
111. Fink, T., et al., *Natural killer cell-mediated basal and interferon-enhanced cytotoxicity against liver cancer cells is significantly impaired under in vivo oxygen conditions.* Scand J Immunol, 2003. **58**(6): p. 607-12.
112. Estrella, V., et al., *Acidity generated by the tumor microenvironment drives local invasion.* Cancer Res, 2013. **73**(5): p. 1524-35.

113. Fukumura, D., et al., *Hypoxia and acidosis independently up-regulate vascular endothelial growth factor transcription in brain tumors in vivo.* Cancer Res, 2001. **61**(16): p. 6020-4.
114. Lardner, A., *The effects of extracellular pH on immune function.* J Leukoc Biol, 2001. **69**(4): p. 522-30.
115. Kareva, I. and P. Hahnfeldt, *The emerging "hallmarks" of metabolic reprogramming and immune evasion: distinct or linked?* Cancer Res, 2013. **73**(9): p. 2737-42.
116. Bragado, P., et al., *Microenvironments dictating tumor cell dormancy.* Recent Results Cancer Res, 2012. **195**: p. 25-39.
117. Hatfield, S.M., et al., *Immunological mechanisms of the antitumor effects of supplemental oxygenation.* Sci Transl Med, 2015. **7**(277): p. 277ra30.
118. Hatfield, S.M. and M. Sitkovsky, *Oxygenation to improve cancer vaccines, adoptive cell transfer and blockade of immunological negative regulators.* Oncoimmunology, 2015. **4**(12): p. e1052934.
119. Scharping, N.E., et al., *Efficacy of PD-1 Blockade Is Potentiated by Metformin-Induced Reduction of Tumor Hypoxia.* Cancer Immunol Res, 2017. **5**(1): p. 9-16.
120. Ashton, T.M., et al., *The anti-malarial atovaquone increases radiosensitivity by alleviating tumour hypoxia.* Nat Commun, 2016. **7**: p. 12308.
121. Skwarski, M., et al., *Mitochondrial Inhibitor Atovaquone Increases Tumor Oxygenation and Inhibits Hypoxic Gene Expression in Patients with Non-Small Cell Lung Cancer.* Clin Cancer Res, 2021. **27**(9): p. 2459-2469.
122. Fu, Z., et al., *Tumour Hypoxia-Mediated Immunosuppression: Mechanisms and Therapeutic Approaches to Improve Cancer Immunotherapy.* Cells, 2021. **10**(5).
123. Strowd, R., et al., *Activity of a first-in-class oral HIF2-alpha inhibitor, PT2385, in patients with first recurrence of glioblastoma.* J Neurooncol, 2023. **165**(1): p. 101-112.
124. Kheshtchin, N., et al., *Inhibition of HIF-1α enhances anti-tumor effects of dendritic cell-based vaccination in a mouse model of breast cancer.* Cancer Immunol Immunother, 2016. **65**(10): p. 1159-67.
125. Robey, I.F., et al., *Bicarbonate increases tumor pH and inhibits spontaneous metastases.* Cancer Res, 2009. **69**(6): p. 2260-8.
126. Ibrahim Hashim, A., et al., *Reduction of metastasis using a non-volatile buffer.* Clin Exp Metastasis, 2011. **28**(8): p. 841-9.

127. Tian, B., et al., *Production and characterization of a camelid single domain antibody-urease enzyme conjugate for the treatment of cancer.* Bioconjug Chem, 2015. **26**(6): p. 1144-55.
128. Ronca, R. and C.T. Supuran, *Carbonic anhydrase IX: An atypical target for innovative therapies in cancer.* Biochim Biophys Acta Rev Cancer, 2024. **1879**(4): p. 189120.
129. Barathova, M., et al., *Alternative splicing variant of the hypoxia marker carbonic anhydrase IX expressed independently of hypoxia and tumour phenotype.* Br J Cancer, 2008. **98**(1): p. 129-36.
130. Ames, S., et al., *CAIX forms a transport metabolon with monocarboxylate transporters in human breast cancer cells.* Oncogene, 2020. **39**(8): p. 1710-1723.
131. Swietach, P., et al., *Tumor-associated carbonic anhydrase 9 spatially coordinates intracellular pH in three-dimensional multicellular growths.* J Biol Chem, 2008. **283**(29): p. 20473-83.
132. Svastova, E., et al., *Carbonic anhydrase IX interacts with bicarbonate transporters in lamellipodia and increases cell migration via its catalytic domain.* J Biol Chem, 2012. **287**(5): p. 3392-402.
133. Zandberg, D.P., et al., *Tumor hypoxia is associated with resistance to PD-1 blockade in squamous cell carcinoma of the head and neck.* J Immunother Cancer, 2021. **9**(5).
134. McDonald, P.C., et al., *Recent developments in targeting carbonic anhydrase IX for cancer therapeutics.* Oncotarget, 2012. **3**(1): p. 84-97.
135. Aggarwal, M., B. Kondeti, and R. McKenna, *Insights towards sulfonamide drug specificity in α-carbonic anhydrases.* Bioorg Med Chem, 2013. **21**(6): p. 1526-33.
136. Pinard, M.A., B. Mahon, and R. McKenna, *Probing the surface of human carbonic anhydrase for clues towards the design of isoform specific inhibitors.* Biomed Res Int, 2015. **2015**: p. 453543.
137. Tafreshi, N.K., et al., *Carbonic anhydrase IX as an imaging and therapeutic target for tumors and metastases.* Subcell Biochem, 2014. **75**: p. 221-54.
138. Stillebroer, A.B., et al., *Dosimetric analysis of 177Lu-cG250 radioimmunotherapy in renal cell carcinoma patients: correlation with myelotoxicity and pretherapeutic absorbed dose predictions based on 111In-cG250 imaging.* J Nucl Med, 2012. **53**(1): p. 82-9.
139. Doss, M., et al., *Biodistribution and radiation dosimetry of the carbonic anhydrase IX imaging agent [(18) F]VM4-037 determined*

from PET/CT scans in healthy volunteers. Mol Imaging Biol, 2014. **16**(5): p. 739-46.
140. Kulterer, O.C., et al., *A Microdosing Study with.* J Nucl Med, 2021. **62**(3): p. 360-365.
141. Zhu, W., et al., *Preclinical and pilot clinical evaluation of a small-molecule carbonic anhydrase IX targeting PET tracer in clear cell renal cell carcinoma.* Eur J Nucl Med Mol Imaging, 2023. **50**(10): p. 3116-3125.
142. Tu, M.M., et al., *Inhibition of the CCL2 receptor, CCR2, enhances tumor response to immune checkpoint therapy.* Commun Biol, 2020. **3**(1): p. 720.
143. Arifin, W.N. and W.M. Zahiruddin, *Sample Size Calculation in Animal Studies Using Resource Equation Approach.* Malays J Med Sci, 2017. **24**(5): p. 101-105.
144. Carbonell, W.S., et al., *β1 integrin targeting potentiates antiangiogenic therapy and inhibits the growth of bevacizumab-resistant glioblastoma.* Cancer Res, 2013. **73**(10): p. 3145-54.
145. Oda, S., et al., *An in vitro coculture system of human peripheral blood mononuclear cells with hepatocellular carcinoma-derived cells for predicting drug-induced liver injury.* Arch Toxicol, 2021. **95**(1): p. 149-168.
146. Rasouli, M. and F. Safari, *Principles of Indirect Co-culture Method Using Transwell.* Methods Mol Biol, 2024.
147. Bogdanowicz, D.R. and H.H. Lu, *Multifunction co-culture model for evaluating cell-cell interactions.* Methods Mol Biol, 2014. **1202**: p. 29-36.
148. Meltzer, P.S. and L.J. Helman, *New Horizons in the Treatment of Osteosarcoma.* N Engl J Med, 2021. **385**(22): p. 2066-2076.
149. Perut, F., et al., *Carbonic anhydrase IX inhibition is an effective strategy for osteosarcoma treatment.* Expert Opin Ther Targets, 2015. **19**(12): p. 1593-605.
150. Uluçkan, Ö., et al., *Preclinical mouse models of osteosarcoma.* Bonekey Rep, 2015. **4**: p. 670.
151. Tome, Y., et al., *Use of αv Integrin Linked to Green Fluorescent Protein in Osteosarcoma Cells and Confocal Microscopy to Image Molecular Dynamics During Lung Metastasis in Nude Mice.* Anticancer Res, 2016. **36**(8): p. 3811-6.

152. Garcia, J., et al., *Bevacizumab (Avastin®) in cancer treatment: A review of 15 years of clinical experience and future outlook.* Cancer Treat Rev, 2020. **86**: p. 102017.
153. Zhang, C., et al., *The role of vascular endothelial growth factor as a prognostic and clinicopathological marker in osteosarcoma: a systematic review and meta-analysis.* J Orthop Surg Res, 2021. **16**(1): p. 738.
154. McIntyre, A., et al., *Carbonic anhydrase IX promotes tumor growth and necrosis in vivo and inhibition enhances anti-VEGF therapy.* Clin Cancer Res, 2012. **18**(11): p. 3100-11.
155. Gocher, A.M., C.J. Workman, and D.A.A. Vignali, *Interferon-γ: teammate or opponent in the tumour microenvironment?* Nat Rev Immunol, 2022. **22**(3): p. 158-172.
156. Chuang, L.P., et al., *Increased C-C chemokine receptor 2 gene expression in monocytes of severe obstructive sleep apnea patients and under intermittent hypoxia.* PLoS One, 2014. **9**(11): p. e113304.
157. Hassn Mesrati, M., et al., *CD44: A Multifunctional Mediator of Cancer Progression.* Biomolecules, 2021. **11**(12).
158. Chang, Y.H., et al., *Chemokine Ligand 2 Promotes Migration in Osteosarcoma by Regulating the miR-3659/MMP-3 Axis.* Biomedicines, 2023. **11**(10).
159. Kaya, M., et al., *Vascular endothelial growth factor expression in untreated osteosarcoma is predictive of pulmonary metastasis and poor prognosis.* Clin Cancer Res, 2000. **6**(2): p. 572-7.
160. Gross, A.C., et al., *IL-6 and CXCL8 mediate osteosarcoma-lung interactions critical to metastasis.* JCI Insight, 2018. **3**(16).
161. Jiang, H., et al., *CXCL8 promotes the invasion of human osteosarcoma cells by regulation of PI3K/Akt signaling pathway.* APMIS, 2017. **125**(9): p. 773-780.
162. Liu, Q., et al., *The CXCL8-CXCR1/2 pathways in cancer.* Cytokine Growth Factor Rev, 2016. **31**: p. 61-71.
163. Campanile, C., et al., *Characterization of Different Osteosarcoma Phenotypes by PET Imaging in Preclinical Animal Models.* Journal of Nuclear Medicine, 2013. **54**(8): p. 1362-1368.
164. McDonald, P. and S. Dedhar, *Carbonic Anhydrase IX (CAIX) as a Mediator of Hypoxia-Induced Stress Response in Cancer Cells*, in *CARBONIC ANHYDRASE: MECHANISM, REGULATION, LINKS TO DISEASE, AND INDUSTRIAL APPLICATIONS*. 2014. p. 255-269.

165. Kong, L., et al., *Knockdown of CD44 inhibits proliferation, migration and invasion of osteosarcoma cells accompanied by downregulation of cathepsin S.* J Orthop Surg Res, 2022. **17**(1): p. 154.
166. Ji, H., et al., *CD44 expression is correlated with osteosarcoma cell progression and immune infiltration and affects the Wnt/β-catenin signaling pathway*. J Bone Oncol, 2023. **41**: p. 100487.
167. Chen, Y., et al., *Significant difference between sirolimus and paclitaxel nanoparticles in anti-proliferation effect in normoxia and hypoxia: The basis of better selection of atherosclerosis treatment.* Bioact Mater, 2021. **6**(3): p. 880-889.
168. Johnsen, J.I., C. Dyberg, and M. Wickström, *Neuroblastoma-A Neural Crest Derived Embryonal Malignancy.* Front Mol Neurosci, 2019. **12**: p. 9.
169. Qiu, B. and K.K. Matthay, *Advancing therapy for neuroblastoma.* Nat Rev Clin Oncol, 2022. **19**(8): p. 515-533.
170. Påhlman, S. and S. Mohlin, *Hypoxia and hypoxia-inducible factors in neuroblastoma.* Cell Tissue Res, 2018. **372**(2): p. 269-275.
171. Applebaum, M.A., et al., *Integrative genomics reveals hypoxia inducible genes that are associated with a poor prognosis in neuroblastoma patients.* Oncotarget, 2016. **7**(47): p. 76816-76826.
172. Fardin, P., et al., *A biology-driven approach identifies the hypoxia gene signature as a predictor of the outcome of neuroblastoma patients.* Mol Cancer, 2010. **9**: p. 185.
173. Bhaskara, V.K., et al., *Intermittent hypoxia regulates stem-like characteristics and differentiation of neuroblastoma cells.* PLoS One, 2012. **7**(2): p. e30905.
174. Huertas-Castaño, C., et al., *Hypoxia in the Initiation and Progression of Neuroblastoma Tumours.* Int J Mol Sci, 2019. **21**(1).
175. Kacher, J., et al., *Impaired Antitumor Immune Response in.* Cancer Res Commun, 2022. **2**(7): p. 577-589.
176. Nakata, R., et al., *Contribution of neuroblastoma-derived exosomes to the production of pro-tumorigenic signals by bone marrow mesenchymal stromal cells.* J Extracell Vesicles, 2017. **6**(1): p. 1332941.
177. Ferrer, F.A., et al., *Angiogenesis and neuroblastomas: interleukin-8 and interleukin-8 receptor expression in human neuroblastoma.* J Urol, 2000. **164**(3 Pt 2): p. 1016-20.
178. Xiong, X., et al., *CXCL8 in Tumor Biology and Its Implications for Clinical Translation.* Front Mol Biosci, 2022. **9**: p. 723846.

179. Metelitsa, L.S., et al., *Natural killer T cells infiltrate neuroblastomas expressing the chemokine CCL2.* J Exp Med, 2004. **199**(9): p. 1213-21.
180. Liu, H., et al., *Neutralizing IL-8 potentiates immune checkpoint blockade efficacy for glioma.* Cancer Cell, 2023. **41**(4): p. 693-710.e8.
181. Gomes, A., et al., *Oxygen Partial Pressure Is a Rate-Limiting Parameter for Cell Proliferation in 3D Spheroids Grown in Physioxic Culture Condition.* PLoS One, 2016. **11**(8): p. e0161239.
182. Bai, J.W., S.Q. Qiu, and G.J. Zhang, *Molecular and functional imaging in cancer-targeted therapy: current applications and future directions.* Signal Transduct Target Ther, 2023. **8**(1): p. 89.
183. Sun, J., et al., *Imaging-guided targeted radionuclide tumor therapy: From concept to clinical translation.* Adv Drug Deliv Rev, 2022. **190**: p. 114538.
184. Bergers, G. and D. Hanahan, *Modes of resistance to anti-angiogenic therapy.* Nat Rev Cancer, 2008. **8**(8): p. 592-603.
185. Li, G., et al., *Carbonic Anhydrase XII is a Clinically Significant, Molecular Tumor-Subtype Specific Therapeutic Target in Glioma with the Potential to Combat Invasion of Brain Tumor Cells.* Onco Targets Ther, 2021. **14**: p. 1707-1718.
186. Chiche, J., et al., *Hypoxia-inducible carbonic anhydrase IX and XII promote tumor cell growth by counteracting acidosis through the regulation of the intracellular pH.* Cancer Res, 2009. **69**(1): p. 358-68.
187. Qi, W.Q., Q. Zhang, and J.B. Wang, *CXCL8 is a potential biomarker for predicting disease progression in gastric carcinoma.* Transl Cancer Res, 2020. **9**(2): p. 1053-1062.
188. Hosono, M., et al., *CXCL8 derived from tumor-associated macrophages and esophageal squamous cell carcinomas contributes to tumor progression by promoting migration and invasion of cancer cells.* Oncotarget, 2017. **8**(62): p. 106071-106088.
189. Fang, Q.I., et al., *Increased.* Anticancer Res, 2017. **37**(9): p. 4845-4852.
190. Yang, S., et al., *Up-regulation of CXCL8 expression is associated with a poor prognosis and enhances tumor cell malignant behaviors in liver cancer.* Biosci Rep, 2020. **40**(8).
191. Pennel, K.A., et al., *CXCL8 expression is associated with advanced stage, right sidedness, and distinct histological features of colorectal cancer.* J Pathol Clin Res, 2022. **8**(6): p. 509-520.

192. Gross, N., K. Balmas, and C.B. Brognara, *Absence of functional CD44 hyaluronan receptor on human NMYC-amplified neuroblastoma cells.* Cancer Res, 1997. **57**(7): p. 1387-93.
193. Valentiner, U., F.U. Valentiner, and U. Schumacher, *Expression of CD44 is associated with a metastatic pattern of human neuroblastoma cells in a SCID mouse xenograft model.* Tumour Biol, 2008. **29**(3): p. 152-60.
194. Vega, F.M., et al., *CD44-high neural crest stem-like cells are associated with tumour aggressiveness and poor survival in neuroblastoma tumours.* EBioMedicine, 2019. **49**: p. 82-95.
195. Lim, T.S., et al., *CD80 and CD86 differentially regulate mechanical interactions of T-cells with antigen-presenting dendritic cells and B-cells.* PLoS One, 2012. **7**(9): p. e45185.
196. Orecchioni, M., et al., *Macrophage Polarization: Different Gene Signatures in M1(LPS+) vs. Classically and M2(LPS-) vs. Alternatively Activated Macrophages.* Front Immunol, 2019. **10**: p. 1084.
197. Gálvez, B.G., et al., *Membrane type 1-matrix metalloproteinase is regulated by chemokines monocyte-chemoattractant protein-1/ccl2 and interleukin-8/CXCL8 in endothelial cells during angiogenesis.* J Biol Chem, 2005. **280**(2): p. 1292-8.
198. Pausch, T.M., et al., *Metastasis-associated fibroblasts promote angiogenesis in metastasized pancreatic cancer via the CXCL8 and the CCL2 axes.* Sci Rep, 2020. **10**(1): p. 5420.
199. Gao, Y., et al., *CD44 is a direct target of miR-199a-3p and contributes to aggressive progression in osteosarcoma.* Sci Rep, 2015. **5**: p. 11365.
200. Brahmer, J.R., et al., *Safety and activity of anti-PD-L1 antibody in patients with advanced cancer.* N Engl J Med, 2012. **366**(26): p. 2455-65.
201. Cendrowicz, E., et al., *The Role of Macrophages in Cancer Development and Therapy.* Cancers (Basel), 2021. **13**(8).

SUMMARY/ SANTRAUKA

SANTRUMPOS

β-ME – 2-merkaptoetanolis
CAs – karboanhidrazės
CAIX – karboanhidrazė IX
CAF – su vėžiu susiję fibroblastai
CCL2 – C-C motyvo chemokino ligandas 2
CCR2 – 2 tipo C-C chemokino receptorius
CNS – centrinė nervų sistema
DMEM – Dulbeko modifikuota Eagle terpė
DNR – deoksiribonukleorūgštys
ELISA – imunofermentinės analizės metodas
epH – ekstraląstelinis pH
eNKT – natūralios žudikės T ląstelės
FBS – išaktyvintas fetalinio veršiuko serumas
FGFs – fibroblastų augimo faktorius
FFPE – formaline fiksuoti ir parafine įlieti blokai
HIF – hipoksijos indukuojamas faktorius
HRE – hipoksinio atsako elementas
ICB – imuninės sinapsės slopinimas
IFN-γ – interferonas gama
IHC – imunohistochemija
IL – interleukinas
i.p. – intraperitonealiai
i.v. – intraveniškai
LDS – ličio dodecilo sulfatas
MDSC – mieloidinės kilmės supresinės ląstelės
MMP – matrikso metaloproteinazės
MFI – vidutinis fluorescencijos intensyvumas
NBL – neuroblastoma
NIR – artimasis infraraudonųjų spindulių ruožas
PBS – fosfatinis buferis tirpalas su fiziologine druskų koncentracija
PBMC – periferinio kraujo vienbranduolės ląstelės
PD-L1 – programuotos ląstelių žūties baltymo ligandas 1
PD-1 – programuotos ląstelių žūties baltymas 1
PEG – polietilenglikolis
PMSF – fenilmetilsulfonilfluoridas

RIPA – radioimunoprecipitacijos reakcijos buferis
TAM – su naviku susiję makrofagai
TBST – Tris buferinis tirpalas su fiziologine druskų konc. ir 0.1% Tween® 20 detergentu
TGF-β – transformuojantis augimo faktorius beta
TNF-α – naviko nekrozės faktorius alpha
Treg – reguliaciniai T limfocitai
VEGF – kraujagyslių endotelio augimo faktorius
VEGFR – kraujagyslių endotelio augimo faktoriaus receptorius

ĮVADAS

Vaikų, sergančių pažengusios stadijos arba recidyvuojančiais standžiaisiais navikais, išgyvenamumas išlieka prastas net ir taikant naujausius gydymo metodus, įskaitant imunoterapiją [1]. Todėl, norint vystyti naujus priešvėžinius vaistus, reikia geriau suprasti vaikų vėžio biologiją. Vaikų standieji navikai skiriasi nuo suaugusiųjų. Jie turi labai mažą naviko deoksiribonukleorūgščių **(**DNR) mutacijų skaičių, todėl yra mažiau imunogeniški [2]. Vaikų navikuose randamas mažesnis naviką infiltruojančių limfocitų skaičius, taip pat maža imuninės sinapsės baltymų, tokių kaip programuotos ląstelių žūties baltymo ligando-1 (PD-L1) ir programuotos ląstelių žūties baltymo-1 (PD-1), raiška. Šiuose navikuose gausu mieloidinės kilmės supresinių ląstelių (MDSC), su naviku susijusių makrofagų (TAM), su vėžiu susijusių fibroblastų (CAF) ir reguliacinių T limfocitų (Treg), kurie sukuria imunosupresinę aplinką [2]. Tačiau suaugusiųjų ir vaikų navikai turi bendrą bruožą, kuris yra su naviku susijusi hipoksija, ir ji siejama su naviko agresyvumu ir progresavimu.

Naviko augimas ir progresavimas yra susiję su jo prisitaikymu prie hipoksijos. Naviko hipoksija koreliuoja su prasta vėžiu sergančių pacientų prognoze ir atsparumu įprastiniam gydymui [2]. Hipoksija skatina imunosupresinių metabolitų gamybą naviko mikroaplinkoje, o tai, savo ruožtu, turi imunosupresinį poveikį [3, 4]. Sumažėjęs deguonies kiekis stimuliuoja ląstelių procesų pokyčius, kuriuos reguliuoja transkripcijos faktorius – hipoksijos indukuojamas faktorius (HIF). Baltymai, aktyvuojami hipoksijos metu, yra svarbūs naviko progresavimui. Hipoksijos metu ląstelėse vykstantys metaboliniai pokyčiai sukelia rūgštinių medžiagų apykaitos produktų kaupimąsi. Siekdamos išvengti ilgalaikio užrūgštėjimo, ląstelės įjungia papildomus pH reguliavimo mechanizmus. Ląstelėse vyksta intensyvus laktato ir protonų išskyrimas į išorę, o bikarbonato jonai įnešami

vidun. [5]. Tai, savo ruožtu, rūgština užląstelinę terpę auglio mikroaplinkoje, o, tuo pačiu, slopina imuninį atsaką, sukelia uždegimą, skatina angiogenezę ir invaziją, lemia atsparumą chemoterapijai ir radioterapijai [5]. Hipoksijos sukeltas imuninės sistemos slopinimas veikia visų tipų imuninių ląstelių funkciją: nuo dendritinių ląstelių aktyvacijos slopinimo iki TAM brendimo [6] ir M2 poliarizacijos, lemiančios T ląstelių funkcijos slopinimą [7] ir Treg įdarbinimą [8]. Hipoksija taip pat padidina programuotos ląstelių žūties baltymo ligando (PD-L1) raišką navikinėse ląstelėse, todėl atsiranda atsparumas citotoksinių T limfocitų sukeliamai vėžinių ląstelių žūčiai [9]. Vertinant tokį ženklų hipoksijos poveikį naviko imuniniam atsakui, tikslinga ieškoti su hipoksine naviko aplinka susijusių taikinių, kuriuos slopinant galėtų būtų stiprinamas imunoterapinis poveikis.

Karboanhidrazė IX (CAIX) yra fermentas, kurio raiška stipriai aktyvuojama hipoksijos [5]. Jis efektyviai katalizuoja anglies dioksido pavertimą į bikarbonato jonus ir protonus. Tai viena iš penkiolikos žmoguje randamų α-karboanhidrazių šeimos izoformų, kurios reguliuoja jonų transportavimą ir pH homeostazę žmogaus organizme. CAIX palaiko fiziologinį vėžio ląstelių pH taip skatindama šių ląstelių išlikimą ir progresavimą [10]. Tai savo ruožtu sukelia užląstelinės aplinkos užrūgštėjimą. Padidėjusi CAIX raiška yra susijusi su blogesne įvairių vėžio formų prognoze, tarp jų centrinės nervų sistemos (CNS) navikiniai susirgimai [11, 12] osteosarkoma [13], krūties vėžys [14], neuroblastoma (NBL) [15, 16].

Padidėjęs rūgštingumas navike slopina naviko imuninį atsaką ir užtikrina atsparumą gydymui [10, 17]. CAIX fermento slopinimas galėtų pakeisti TME rūgštingumą ir leisti imunoterapijai veikti. Šiuo metu CAIX slopinimo, susieto su imunoterapija, veiksmingumas yra ribotas ir pademonstruotas tik pelių melanomos modelyje [18]. CAIX tikslinės terapijos vystymas link klinikinių tyrimų žmoguje yra komplikuotas. I fazės klinikinių tyrimų rezultatai su mažos molekulinės masės CAIX fermento slopikliu SLC-0111 buvo paskelbti 2016 m., tačiau tolesnės pažangos nepastebėta [19]. Tikslinga naujų, veiksmingesnių CAIX fermento slopiklių paieška. Didelis aminorūgščių sekos panašumas tarp CA izofermentų apsunkina CAIX specifinių slopiklių kūrimą [20]. Mano kolegos Vilniaus universiteto, Gyvybės mokslų centro, Biotechnologijos institute benzeno sulfonamidų pagrindu sukūrė aukšto afiniškumo ir selektyvumo mažos molekulinės masės CAIX fermento slopiklį VD11-4-2, kuris parodė daug žadantį *in vitro* aktyvumą [21-23]. Šis slopiklis buvo toliau modifikuotas į slopiklį AZ19-3-2, kuriame yra dvi VD11-4-2 galvos sujungtos per polietilenglikolio (PEG) jungiamąją grandinę. Lyginant su VD11-4-2, jis pasižymi didesniu afiniškumu ir selektyvumu CAIX

fermento atžvilgiu bei pikomoline jungimosi konstanta. Šiame darbe buvo naudojamas šis slopiklis. Pastebėjus, kad CAIX baltymas išreikštas standžiuosisuose navikuose, jis tapo patraukliu taikiniu vėžio radionuklidų diagnostikos platformai [24]. Mano kolegos Vilniaus universiteto Gyvybės mokslų centro Biotechnologijos institute taip pat susintetino CAIX atpažįstančius junginius, pažymėtus artimojo infraraudonųjų spindulių (NIR) zondu [25]. Šiame darbe išbandytas šių junginių veiksmingumas *in vivo* pelės modelyje.

Hipoksinė auglio niša perprogramuoja chemokinų sekreciją auglyje bei ląstelių tinklą. Vėžyje vyraujančių chemokinų slopinimas kartu su CAIX fermento slopinimu galėtų būti patrauklia gydymo strategija. C-C motyvo chemokino ligando 2 (CCL2) bei 2 tipo C-C chemokino receptoriaus (CCR2) signalinis kelias yra būtinas vėžio progresavimui, nes jis yra aktyvus naviko hipoksijoje, neoangiogenezėje, imunosupresinių ląstelių įdarbinime ir metastazavime [26, 27]. Be vėžinių ląstelių, CCR2 taip pat yra sintetinamas gausybėje ląstelių, tokių kaip monocitai/makrofagai, taip pat T reguliacinėse ląstelėse, CD4+, CD8+ T ląstelėse, natūralios žudikės T ląstelės (eNKT), endotelio ląstelėse ir fibroblastuose [28]. Todėl šis kelias svarbus vėžinių ir imuninių ląstelių komunikacijai. Nors CCR2 turi ir kitus ligandus, tokius kaip CCL8, CCL12 ir kt., CCL2 turi didžiausią afiniškumą [27]. CCL2 yra vienas stipriausių chemoatraktantų, dalyvaujančių makrofagų pritraukime į naviką [29]. CCL2-CCR2 signalinio kelio reguliavimas ir vaidmuo naviko hipoksijoje nėra gerai ištirti. CCL2 turi hipoksijos atsako elementą (HRE), todėl CCL2 raiška gali būti kontroliuojama HIF-1 [30]. Šio chemokino raiška hipoksijoje yra kompleksiška ir priklauso nuo ląstelių tipo ir aplinkos. Lėtinė hipoksija sumažina CCL2 chemokino kiekį monocituose / makrofaguose ir kai kuriose vėžio ląstelių linijose, tačiau ciklišką hipoksija (labiau būdinga navikams) padidina CCL2 chemokino sekreciją ir padidina CCR2 receptorių reguliavimą makrofaguose [30, 31]. Hipoksijoje, navikų išskiriamas CCL2 skatina granuliocitų CD11b+/Ly6Cmed/Ly6G+ mieloidinių ląstelių kaupimąsi pelių pieno liaukos navikuose, kurie padeda sukurti prieš metastazinę nišą. Savo ruožtu CCL2 neutralizavimas šiame modelyje sumažino auglių metastazavimą [32]. Tokiu būdu CCL2-CCR2 signalinis kelias išlieka patraukliu priešvėžinės terapijos taikiniu.

Tyrimo tikslas

Ištirti, ar su hipoksija susijusių baltymų, tokių kaip CAIX, ir (arba) CCL2-CCR2 signalinio kelio slopinimas yra veiksmingas pasirinktuose ikiklinikiniuose standžiųjų navikų modeliuose bei ištirti naujų CAIX fermentą

atpažįstančių junginių, pažymėtų artimųjų infraraudonųjų spindulių ruožo (NIR) fluorescencine žyme pritaikymą auglių *in vivo* vaizdinimui.

Tyrimo uždaviniai:

1. Ištirti CAIX slopiklio poveikį neuroblastomos SK-N-AS bei osteosarkomos 143B ląstelėse *in vitro* bei auglių augimui *in vivo* kaip monoterapiją ir derinyje su pasirinktais vaistais.
2. Apibūdinti CAIX slopinimo poveikį imuninių ląstelių ir neuroblastomos SK-N-AS navikinių ląstelių sąveikai *in vitro*.
3. Apibūdinti CCL2-CCR2 signalinio kelio slopinimo poveikį imuninių ląstelių ir osteosarkomos 143B navikinių ląstelių sąveikai *in vitro*.
4. Apibūdinti CCL2-CCR2 signalinio kelio slopinimo poveikį osteosarkomos 143B ląstelių naviko modelyje *in vivo*.
5. Ištirti naujų CAIX fermentą atpažįstančių ir su NIR fluorescencine žyme konjuguotų junginių AZ21-6 ir GZ22-4 tinkamumą *in vivo* auglių vaizdinimui pelėje.
6. Sukurti vėžinių ląstelių ir sveikų donorų periferinio kraujo vienbranduolių ląstelių (PBMC) bendros kultūros metodą, skirtą vėžinių ląstelių ir imuninių ląstelių sąveikai tirti.

Mokslinis naujumas

Mūsų tyrimas pateikia naujus mokslinius duomenis apie kompensacinius mechanizmus, kurie iššaukiami navike slopinant CAIX fermentą arba CCL2-CCR2 signalinį kelią. Ištyrėme CCR2 antagonisto poveikį eksperimentiniame osteosarkomos modelyje. Taip pat šiame darbe pabrėžiamas daugialypis CAIX vaidmuo naviko ir stromos komunikacijoje. Tai pirmasis tyrimas, kuriame buvo ištirta CAIX slopinimo su CCR2 antagonistu efektas neuroblastomos ksenografto modelyje. Galiausiai buvo išbandytas CAIX atpažįstančių ir NIR fluorescencine žyme pažymėtų junginių pritaikymas žmogaus vėžinių ląstelių ksenograftiniuose augliuose pelėje.

Ginamieji teiginiai:

1. CAIX slopinimas kaip vieno agento terapija turi minimalų veiksmingumą osteosarkomos ikiklinikiniame vėžio modelyje.
2. CAIX slopiklių efektyvumas-yra ženklus juos naudojant kartu su CCR2 antagonistu žmogaus neuroblastomos ląstelių SK-N-AS ksenografto modelyje pelėje.

3. CAIX fermento slopinimas keičia chemokinų CCL2 ir CXCL8 sekreciją sveikų donorų PBMC ir neuroblastomos SK-N-AS ląstelių ko-kultūroje *in vitro.*
4. CCL2-CCR2 signalinio kelio slopinimas osteosarkomos 143B ląstelėse turi skirtingą atsaką skirtingose deguonies aplinkose.
5. Pelių, ekspresuojančių CAIX baltymą navikuose, vaizdinimas *in vivo* yra galimas naudojant CAIX fermentą atpažįstančius ir fluorescencine NIR žyme pažymėtus junginius AZ21-6 ir GZ22-4 .

METODAI

Ląstelių kultūros

SK-N-AS, žmogaus neuroblastomos ląstelių linija gauta iš Prof. A.Y. Huang, Case Western Reserve universitetas, JAV. SK-N-BE, be2c, SH-SY5Y, LA1-55n, HeLa linijas maloniai parūpino prof. Kanopka ir dr. E. Kriukienė. 143B ląstelių linija buvo įsigyta iš ATCC. HeLaCAIX^{KO} liniją išvedė dr. J. Matulienė [25].

Visos linijos buvo kultivuotos naudojant Dulbeko modifikuotą Eagle terpę (DMEM), papildytą 10 % išaktyvinto fetalinio veršiuko serumo (FBS) bei 1 % penicillino/streptomicino (P/S, 100 U/ml/100 μg/ml). Ląstelės buvo auginamos inkubatoriuje palaikant 21 % O_2 ir 5% CO_2 esant 37 °C. Hipoksinės sąlygos buvo pasiektos naudojant hipoksinę kamerą (MACS VA500 mikroaerofilinė darbo stotis, Don Whitley Scientific, JK) su 1 % O_2, 5 % CO_2 ir likutiniu N_2. Ląstelės buvo laikomos hipoksijoje nuo 48 val iki 11 dienų priklausomai nuo eksperimento sąlygų.

Bandomųjų gyvūnų priežiūra

Tyrimui buvo naudojamos 5–6 savaičių Nude pelių patelės (CR ATH HO kodas 24106216) gautos iš Charles River Laboratories. Gyvūnai buvo laikomi, veisiami ir prižiūrimi Vilniaus universiteto Gyvybės mokslų centro Gyvūnų modelių skyriuje. Gyvūnai buvo laikomi Allentown 48 Cage NexGen Mouse IVC Cage & Rack narveliuose su individualia ventiliacija, sterilizuotais narvais ir lizdais. Viename narve buvo laikomos 5 pelės, naudojant 12 valandų šviesos ir tamsos ciklą, esant 21–23 °C temperatūrai ir 40–60 % drėgmei. Gyvūnams buvo taikoma sterilizuota ir apšvitinta dieta skirta transgeninėms pelėms (Altromin, #1414) ir sterilizuotas vanduo ad libitum. Gyvūnai, skirti vaizdinimo eksperimentams, buvo šeriami sterilizuota, apšvitinta bei be chlorofilo dieta (Altromin, #C1086194). Visos eksperimentinės procedūros atitiko ES Direktyvos 2010/63/ES reikalavimus ir buvo patvirtintos Lietuvos valstybinės maisto ir veterinarijos tarnybos

(patvirtinimo Nr. G2-233, 2023-01-18, Nr. G2-194, 2021-11-09). Pelės buvo stebimos kiekvieną darbo dieną ir sveriamos kartą per savaitę.

Neuroblastomos vėžinės linijos SK-N-AS auglių pelėje tyrimas

10-12 savaičių Nude pelių patelėms į dešinio šono paodį buvo suleista 5×10^6 žmogaus neuroblastomos vėžinės linijos SK-N-AS ląstelių. Kai navikai pasiekė vidutinį 35 mm^2 dydį, pelės buvo paskirstytos į grupes pagal naviko dydžius, kad būtų užtikrintas vienodas naviko dydžio pasiskirstymas grupėje (n = 7 vienai grupei). Randomizacijos dieną buvo pradėtas gydymas AZ19-3-2 junginiu po 10 mg/ kg/ doze į pilvaplėvės ertmę (i. p.) kas parą arba kontrolinis nešiklis. CCR2 antagonistas RS504393 (#300816-15-3, TOCRIS) 2 mg/ kg/ doze i. p. per parą buvo pradėtas 5 dieną po randomizacijos, kad AZ19-3-2 junginys būtų prisotintas ir dėl to galimai sumažėtų naviko tarpląstelinės aplinkos rūgštingumas. Naviko dydis buvo matuojamas slankmačiu kas antrą dieną. Naviko tūris buvo apskaičiuojamas pagal formulę: tūris = (D*dΛ2*π)/6, kur D reiškia didžiausią skersmenį, o d – mažesnį skersmenį. Visos pelės buvo nugaišintos, kai bent vienas auglys pasiekė 1500 mm^3 tūrį. Eksperimento pabaigoje gyvūnai buvo nugaišinami naudojant CO_2 dujas 8,0 L/min (Elme Messer Lit, Vilnius, Lietuva) bei cervikalinių slankstelių dislokaciją. Iš pelės išimti navikai buvo analizuojami taikant tėkmės citometrijos metodą.

Osteosarkomos vežinės linijos 143B auglių pelėje eksperimentas

Į 8-12 savaičių Nude pelių patelių dešinius šlaunikaulius buvo suleista $0,5\times10^6$ osteosarkomos 143B ląstelių/ 20 µL fosfato buferio tirpale (PBS). Operacijos metu anestezijai buvo naudojamas isofluranas. Kai navikai pasiekė apčiuopiamą dydį, 16 dieną po naviko inokuliacijos, pelės buvo paskirstytos į tiriamas grupes pagal naviko dydį. Vienai grupei buvo leidžiama CCR2 antagonistas RS504393 (#2517, TOCRIS) 2 mg/ kg dozė i.p (n=10). Antrai kontrolinei grupei buvo leidžiamas nešiklis. Naviko dydis buvo apskaičiuotas taip: tūris = (D*dΛ2*π)/6, D reiškia didžiausią skersmenį, o d – mažesnį skersmenį. Visos pelės buvo nugaišintos, kai bent vienas auglys pasiekė 1500 mm^3 tūrį. Eksperimento pabaigoje gyvūnai buvo nugaišinami naudojant CO_2 dujas 8,0 L/min (Elme Messer Lit, Vilnius, Lietuva) bei cervikalinių slankstelių dislokaciją. Iš pelės išimti navikai buvo analizuojami taikant tėkmės citometrijos metodą.

Gimdos kaklelio vėžio linijos HeLa auglių eksperimentas su vaizdinimu

8-12 savaičių Nude pelių patelėms buvo suleista 3×10^6 HeLaCAIX^{WT} ląstelelių/100 µL PBS į dešinįjį pelių šoną, ir tiek pat HeLaCAIX^{KO} ląstelių buvo suleista į kairįjį tos pačios pelės šoną. Kai navikai pasiekė vaizdavimui tinkamą dydį, GZ22-4 arba AZ21-6 junginiai buvo suleidžiami vienkartinai intraveniškai (i.v.) naudojant 2 mg/ kg/ dozę. Pelės buvo vaizdinamos kas 24 valandas po injekcijos su Alliance^{TM}Q9 Imager sistema pasitelkiant izoflurano anesteziją. Vaizdai buvo kiekybiškai įvertinti naudojant UVIBAND MAX analizės programinės įrangos sistemą. Eksperimento pabaigoje gyvūnai buvo nugaišinami naudojant CO_2 dujas 8,0 L/min (Elme Messer Lit, Vilnius, Lietuva) bei cervikalinių slankstelių dislokaciją.

Ląstelių gyvybingumo įvertinimas (LDH ir XTT tyrimai)

Ląstelės buvo išsėjamos į sterilią 96 šulinėlių plokštelę. Po 24 valandų inkubacijos 1 % O_2, pašalinama ląstelių augimo terpė ir įdedama titruotos dozės CAIX slopiklių ADMEM terpėje. Tada ląstelės inkubuojamos 1 % O_2 48 valandas. LDX ir XTT tyrimai atliekami pagal gamintojo protokolus, naudodami citotoksiškumo aptikimo rinkinį (LDH) (#11644793001, Roche) ir CyQUANT^{TM} XTT ląstelių gyvybingumo rinkinį (#X6493, Invitrogen). Kontrolinės ląstelės gavo nešiklį. Vertės buvo apskaičiuotos kaip kontrolinės grupės % dalis. Duomenys apima 2 atskirus eksperimentus po 3 pakartojimus.

epH matavimas

epH matavimams užsėta $0{,}15\times10^6$ SK-N-AS arba $0{,}075\times10^6$ 143B ląstelių į 12 šulinėlių plokštelę/1 ml terpe su nešikliu arba AZ19-3-2 atitinkamomis koncentracijomis. Ląstelės buvo inkubuojamos 48 val normoksijos ir hipoksijos sąlygomis. pH matavimai buvo atlikti naudojant Mettler Toledo SevenCompact™ pH matuoklį S210. Duomenys apima 9 pakartojimus kiekvienai sąlygai.

Vėžinių ląstelių ir PBMC tėkmės citometrija

PBMC, SK-N-AS ir 143B ląstelės buvo surinktos į citometrinius mėgintuvėlius, centrifuguotos 5 min. 300 g greičiu. Nuplovus surinktas ląsteles, jų paviršiaus receptoriai FcγRIII (CD16) ir FcγRII (CD32) buvo blokuoti Fc bloko (anti-žmogaus CD16/32) tirpalu (1:100). Nuplovus kartotinai, PBMC, SK-N-AS ir 143B ląstelės buvo nudažytos šiais antikūnais atpažįstančiais žmogaus baltymus: anti-hCD3 AF488 (#300320, BioLegend), anti-h/mCD11b FITC (#101206, BioLegend), anti-hCD86 AF488 (#53-0869-42, Invitrogen), anti-hCD274 APC (#17-5983-42, Invitrogen), anti-hCD8

PE/Cy7 (#344712, BioLegend), anti-hCAIX AF488 (#FAB2188G, R&D), anti-hCD45 PE/Cy7 (#304016, BioLegend), anti-hCD80 PE/Cy. 7 (#305218, BioLegend), anti-hVEGFR PE/Cy7 (# 393008, BioLegend), anti-hPD1 PE (#621608, BioLegend), anti-hCCR2 PE (#357206, BioLegend), anti-hCD4 AF647 (#51-0049-42, eBioscience), anti-hCD206 APC (#17-2069-42, Invitrogen) ir anti-hF4/80 APC (#123116, BioLegend). Taip pat dažoma su atitinkamomis izotipinėmis kontrolėmis. 7aad dažas (#00-6993-50, eBioscience) buvo naudojama gyvoms ląstelėms atskirti nuo mirusiųjų. Tėkmės citometrija atlikta naudojnt Partec CyFlow® Space citometrą.

Pelių navikų tėkmės citometrija.

Iš pelių išimti navikai buvo susmulkinti 100 mm Petri lėkštelėje. Tuomet jie aižomiužpilant Kolagenazės D (#1108885, Roche) 1 mg/ml ir DNAzės (#52779120, Roche) 0,05 mg/ ml į 2 ml HBSS ir inkubuojant 15 min 37 °C. Suskaldyti navikai buvo perleidžiami per 70 µm porų filtrą. Ląstelės centrifuguojamos ir eritrocitai lizuojami 2 ml eritriocitų lizavimo (ACK)buferiu 1 minutę. Centrifuguojama ir plaunama FACS buferiniu tirpalu. TruStainFcX (#422302, BioLegend) buvo naudojamas nespecifinei receptorių blokadai. Siekiant išanalizuoti naviko frakciją žmogaus ląstelių ksenograftuose, buvo naudojami šie antikūnai: anti-hCD274 APC (#17-5983-42, Invitrogen), anti-hCA9 AF488 (#FAB2188G, R&D), anti-hVEGFR PE/Cy7 (#393008, BioLegend), anti-hCCR2 PE (#357206, BioLegend), anti-hCD44 APC (#559942, BD PharmingenTM) su atitinkamomis izotipinėmis kontrolėmis. Siekiant išanalizuoti imuninę frakciją ksenografiniuose navikuose, buvo naudojami antikūnai prieš pelės antigenus. Antikūnų Fc receptorių blokavimui buvo naudojamas antikūnų prieš šiuos receptorius mišinys TruStainFcX (#101320, BioLegend). Naudoti antikūnai buvo anti-mCD206 APC (#141708, BioLegend), anti-mCD86 PE (#105008, BioLegend), anti-mPD-L1 PE (#155404, BioLegend), anti-mCCR2 PE (#150610, BioLegend). 7aad dažas (#00-6993-50, eBioscience) buvo naudojamas gyvoms ląstelėms atskirti nuo žuvusių. Tėkmės citometrija atliekama naudojant "Partec CyFlow® Space" arba BD FACS Symphony A1 citometrus. Duomenys buvo analizuojami naudojant "FlowJo" programą.

Imunohistochemija

143B, SK-N-AS ir HeLa navikų imunohistocheminis dažymas (IHC) buvo atliktas Nacionaliniame patologijos centre, Vilniuje. Formaline fiksuoti ir parafine įlieti audiniai (FFPE) buvo supjaustyti 3 mikronų storiu. Dažyta CCR2 antikūnu (Roche klonas SN707, 1:400) arba CAIX antikūnu (Cell

Marque klonas EP161; 1:50). Vaizdinimui naudojamas universalus DAB aptikimo rinkinys (# (92) 760-500, Roche).

Imunoblotingas

SK-N-AS ir 143B ląstelės buvo surinktos po 72 val inkubacijos normoksijoje arba hipoksijoje, du kartus plaunamos PBS ir lizuojamos naudojant radioimunoprecipitacijos reakcijos buferinį tirpalą (RIPA) (#89900, ThermoFisher), kuriame pridėta proteazės ir fosfatazės slopiklių (ThermoFisher Halt Phosphatazės™ slopiklių kokteilis (#78428), Halt proteazės slopiklių kokteilis (#78425) ir fenilmetilsulfonilfluorido (PMSF) proteazės slopiklis (#36978)). Lizatas centrifuguotas 16000× g 15 min 4 °C temperatūroje. Bendras baltymų lizatas buvo kiekybiškai įvertintas Bradfordo metodu (53). Lizatas buvo redukuojamas 4X ličio dodecilo sulfato (LDS) mėginio buferiniame tirpale su β-ME, inkubuojant 10 min. 95 °C temperatūroje. Lizatas frakcionuotas SDS-PAGE elektroforezės būdu, naudojant Bolt 4-12 % Bis-Tris Plus gelius (Thermo Scientific™) ir perkeltas ant 0,2 µm nitroceliuliozės membranų (Thermo Scientific™). Blokavimas vykdytas su 2 % pieno miltelių 1X Tris-Buferio tirpale su 0.1 % Tween® 20 detergentu (TBST) 1 valandą. Inkubuota per naktį 4 °C temperatūroje su pirminiais antikūnais anti-hCAIX M75 (#00414, Abs Ab) 2 % pieno/TBST tirpale. Kontrolei naudoti antikūnai prieš β-aktin (#MA5-15739, ThermoFisher). Po inkubacijos membranos buvo tris kartus plaunamos po 5 min TBST. Po plovimų inkubuojama su atitinkamu antriniu antikūniu 1:1000. Po plovimų, membranos ryškinamos naudojant Novex ECL chemiliuminescencinio substrato reagentų rinkinio substratą (#WP20005). Vaizdinama naudojant Alliance Q9 Advanced (UVITEC) sistemą.

SK-N-AS sferoidų augimo eksperimentas

Maždaug $0{,}2\times10^6$ SK-N-AS ląstelių/2 ml DMEM terpės užsėta į 6 šulinėlių plokštelę. Kitą dieną buvo pridėta NanoShuttleTM 70 µL (#B22073BP, Greiner). Po 24 valandų inkubacijos ląstelės buvo persėtos į 96 šulinėkių plokšteles su F-dugnu (# 655976, Greiner) (400 ląstelių vienoje duobutėje 150 µL DMEMterpėje). Kad sferoidai pradėtų formuotis, išsėtos ląstelės 30 min laikytos ant 96 šulinėlių plokštelėms pritaikyto magnetinio disko (#655837, Greiner). Plokštelės buvo perkeltos į inkubatorius su 1 % O_2 ir 21 % O_2 sąlygomis. Po 48 val. inkubacijos į atitinkamus šulinėlius pridėta junginių: AZ19-3-2 200 nM (n=10, normoksijoje (n=7)) ir nešiklis (n=10). Sferoidai buvo fotografuojami kasdien nuo pirmosios junginio uždėjimo dienos naudojant fluorescencijos vaizdinimo sistemą *EVOS FL Auto Imaging*

System (Life Technologies). Nuotraukoms taikytas 4X padidinimas. Terpė su junginiais buvo reguliariai keičiama kas 48 valandas. Sferoido dydis buvo kiekybiškai įvertintas naudojant "ImageJ" programą.

Vėžinių ląstelių – PBMC ko-kultūros eskperimentas

Vėžinių ląstelių ir sveiko donoro PBMC ko-kultūros metodas yra taikomas vėžio tyrimuose, nes geriau atspindi *in vivo* ląstelių elgesį [33, 34]. Mūsų modelis neleido tiesioginio kontakto tarp ląstelių ir buvo orientuotas į parakrininį signalą ir atsaką į tirpius signalinius baltymus [34].

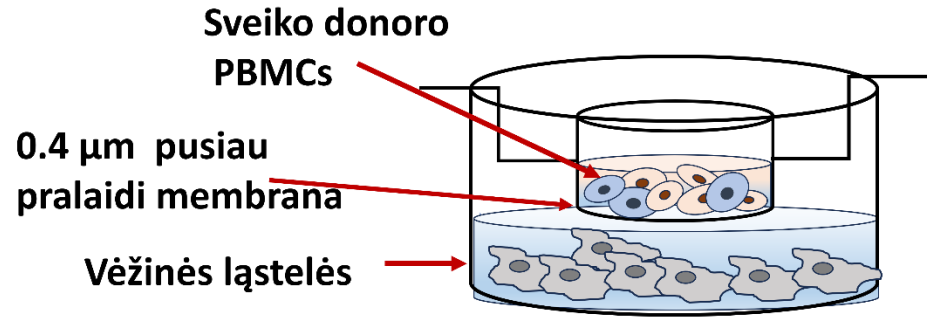

1 paveikslas. Vėžinių ląstelių - PBMC ko-kultūros tyrimo schema.

1 paveiksle pavaizduota ko-kultūtos tyrimo sąranka. Šiam tyrimui mes naudojome Thermo Scientific, Nunc™ polikarbonato ląstelių kultūros intarpus 12 šulinėlių plokštelėse, 0.4 µm (#140652). Pirmiausia, $0{,}15\times10^6$ SK-N-AS ląstelių 2ml ADMEM (#12491-015, Gibco) terpės buvo išsėta į 12 šulinėlių plokštelę ir inkubuota 1 % O_2. Po 24 valandų buvo pridėta 0,2 µM AZ19-3-2 bei kontrolei naudojamas nešiklis. Ląstelės buvo inkubuojamos 1 % O_2 dar 24 valandas.

Sveiko žmogaus donoro kraujas buvo renkamas laikantis Vilniaus regioninio biomedicininių tyrimų komiteto patvirtinto bioetikos protokolo (2020 03 31 Nr.2020/3-1209-694). PBMC buvo izoliuoti naudojant "Ficoll-PaqueTM PREMIUM" (#17-5442-02) "GE Healthcare" pagal gamintojo protokolą. Ląstelės buvo suskaičiuotos ir išsėtos 1 x 10^6 /šulinėliui su ADMEM + 5% FBS. Po 48 valandų inkubacijos 1% O_2 iš viršutinės arba apatinės plokštelių surinktos ląstelės buvo centrifuguojamos ir ruošiamos imunofermentinės analizės metodo (ELISA) bei tėkmės citometrijos tyrimui. Duomenys apima 6 nepriklausomus eksperimentus.

143B eksperimentui buvo užsėjama $0{,}15\times10^6$ 143B ląstelių į šulinėlį ir 24 valandoms auginama 1 % O_2 ADMEM su 3 % FBS. Sekančią dieną buvo

įdedama 0,5 μM RS504393 (#2517, TOCRIS) junginio arba nešiklio kontrolė ir ląstelės inkubuojamos 21 % arba 1 % O_2. Po 24 valandų sveiko donoro kraujas buvo užsėjamas 1×10^6/šulinėliui su ADMEM + 5 % FBS. Po 48 valandų inkubacijos 1 % arba 21 % O_2 iš viršutinės arba apatinės plokštelių surinktos ląstelės buvo centrifuguojamos ir ruošiamos ELISA analizei bei tėkmės citometrijos tyrimui. Duomenys apima 6 skirtingus eksperimentus.

Duomenys buvo analizuojami naudojant "FlowJo" programą. Izotipo kontrolė buvo naudojama teigiamų ląstelių slenksčiui pavaizduoti. Buvo apskaičiuota ir tolesnei analizei panaudota gyvų SK-N-AS arba 143B ląstelių procentinė dalis. PBMC atveju analizei buvo atrinktos gyvos CD45+ ląstelės. T ląstelių žymenys CD4, CD8 arba programuotos ląstelių žūties baltymas (PD-1) buvo apskaičiuoti CD3+ populiacijoje kaip teigiamų ląstelių dalis. PD-L1+, CCR2+, CD86+, CD206+ ir CD86+CD206+ procentinė dalis buvo apskaičiuota iš bendros CD11b+ ląstelių populiacijos. Siekiant išvengti duomenų skirtumų tarp kraujo donorų, imuninių ląstelių duomenys buvo normalizuoti ir naudojami tolesnei analizei. Kiekvieno žymenų rinkinio teigiamų ląstelių procentas (PD-L1+, CCR2+, CD86+, CD206+ ir CD86+CD206+) buvo padalintas iš vidutinės visų gydymo būdų teigiamų ląstelių vertės vienam donorui. Normalizuoti duomenys grafikuose buvo pateikti kaip santykinis tam tikrų žymenų teigiamų ląstelių procentas.

Citokinų ir chemokinų kiekybinis nustatymas ELISA metodu

Citokinų ir chemokinų kiekybiniam nustatymui ląstelių kultūros supernatantuose buvo naudojami šie ELISA rinkiniai: IL-6, IL-10, TNF-α, CCL2, CXCL8 (#88-7066, #88-7106, #88-7346, #88-7399, #88-8086 Invitrogen, Thermo Fisher Scientific, JAV), interferono gama (IFN-γ), IL-4 (#900-T27, #900-T14, PeproTech), VEGF (#DY293B-05, R&D sistemos). Citokinų nustatymas atliktas pagal gamintojo protokolą. Citokinų koncentracija apskaičiuota iš kalibracinės kreivės.

Statistinė analizė

Duomenys buvo analizuojami naudojant Graph Pad Prism programinę įrangą (10.0.2 versija). Duomenų grafikai pateikiami naudojant Matplotlib 3.9.0 arba Graph Pad Prism programinę įrangą (10.0.2 versija). Nepriklausomi eksperimentai, vadinami n, reiškia nepriklausomų ląstelių kultūros preparatų arba gyvūnų skaičių. Buvo tikrinama, ar duomenys atitinka Gauso skirstinį. Jei taip, ANOVA palyginimas buvo atliekamas naudojant Bonfferoni arba Tukey testus. Ko-kultūros tyrimuose, tiriant skirtumus tarp gydytų ir negydytų kohortų, buvo taikomas studento t testas. Jei duomenys nebuvo išsibarstę

pagal normalųjį skirstinį, buvo atliekamas palyginimas Kruskal-Wallis metodu kartu su Dunn's post hoc testu. Jei p vertės buvo mažesnėms už 0.05, buvo laikoma statistiškai reikšmingu skirtumu ir nurodoma taip: *p < .05, **p< 0.01, ***p < 0.001, ****p < 0.0001.

REZULTATAI

Norėdami įvertinti hipoksinių naviko žymenų vaidmenį imuninio naviko mikroaplinkoje, ištyrėme CAIX slopinimo veiksmingumą osteosarkomos 143B ksenografto modelyje bei neuroblastomos SK-N-AS ksenografto modelyje. Be to, ištyrėme CCL2-CCR2 signalinio kelio slopinimo veiksmingumą tuose pačiuose modeliuose. Galiausiai įvertinome CAIX atpažįstančių ir NIR fluorescencine žyme pažymėtų junginių pasisavinimą pelės gimdos kaklelio vėžio HeLa linijos ksenografte *in vivo.*

CAIX slopinimo veiksmingumas osteosarkomos 143B vėžinės linijos modelyje

Osteosarkoma yra agresyvus kaulų vėžys [35]. CAIX baltymo raiška osteosarkomoje yra susijusi su blogesne prognoze [36]. Tokiu būdu CAIX slopinimas gali būti patraukli strategija šio tipo vėžiui, pagrįsta anksčiau paskelbtais tyrimais *in vitro* [36]. Šiame tyrime išbandėme CAIX slopinimo veiksmingumą 143B ląstelių linijos ksenografte [37]. Tai patrauklus modelis metastazuojančios ligos tyrimui [38]. Tyrimuose naudojome mūsų laboratorijoje naujai sukurtą CAIX slopiklį AZ19-3-2.

Imunoblotingo rezultatai patvirtino CAIX raišką 143B ląstelių linijoje hipoksijoje (2A pav.). Ištyrėme CAIX baltymų slopinimo poveikį šiame naviko modelyje *in vivo.* Kadangi CAIX slopinimas pats savaime neparodė veiksmingumo, bandėme taikyti kombinuotą gydymo metodą. Siekdami galimos sinergijos, pasirinkome kraujagyslių endotelio augimo faktoriaus receptoriaus (VEGFR) blokavimą, naudodami į kraujagyslių endotelio augimo faktorių (VEGF-A) nukreiptą monokloninį antikūną Bevacizumabą (Avastin) [38] . Duomenys rodo, kad CAIX slopinimas sustiprina anti-VEGF gydymą kitų standžiųjų navikų atveju [39]. Anestezuotoms 6–12 savaičių amžiaus Nude pelėms buvo sušvirkšta po 0.5 mln. 143B ląstelių intratibialiai. Kai augliai tapo apčiuopiami, pelės buvo suskirstytos į gydomąsias grupes pagal naviko dydį. AZ19-3-2 junginys buvo skiriamas 10mg/kg/dozė i.p. kasdien. Avastinas buvo skiriamas 10 mg/kg/doze i.p. du kartus kas savaitę. Pelės buvo nugaišintos 27 eksperimento dieną, nes augliai pasiekė 1500 mm^3 dydį. Iš jų 2 pelės buvo nugaišintos anksčiau dėl blogos išvaizdos.

Eksperimento pabaigoje buvo stebimas tik minimalus naviko dydžio sumažėjimas kombinuoto gydymo grupėje (2B pav.).

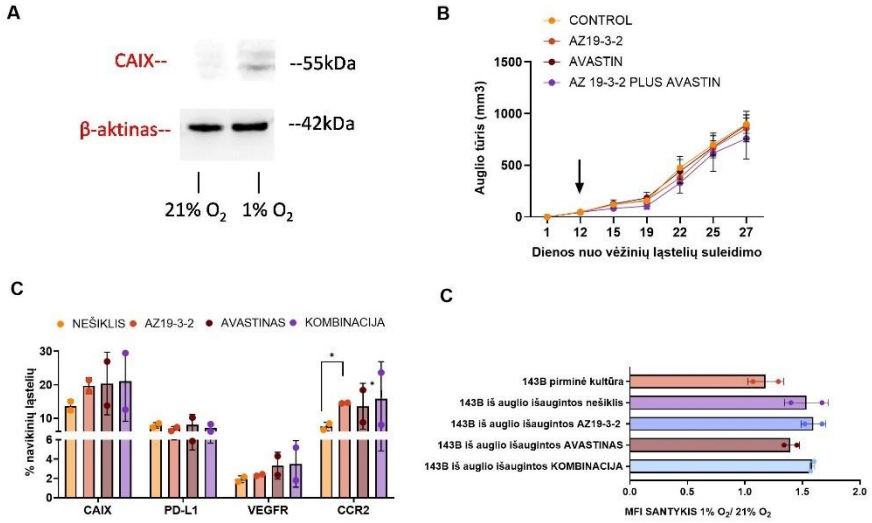

2 paveikslas. CAIX slopininimas 143B osteosarkomos modelyje. A) Imunobloto analizė, vaizduojanti CAIX baltymo raiškos padidėjimą 1 % O_2, palyginti su 21 % O_2. B) Intratibialiai implantuotų 143B ląstelių augimo kinetika taikant skirtingus junginius: AZ19-3-3 junginys (raudona linija ir apskritimai), Avastinas (ruda linija ir apskritimai), kombinacija (violetinė linija ir apskritimai) bei nešiklio kontrolė (oranžinė linija ir apskritimai). C) CAIX, PD-L1, VEGFR, CCR2 paviršiaus baltymų ekspresijos procentiniai pokyčiai 143B navikuose, surinktuose iš pelių po gydymo. C) CAIX vidutinio fluorescencijos intensyvumo (MFI) santykio (1 % O_2 / 21 % O_2) palyginimas išaugintose ląstelėse iš AZ19-3-2 gydytų navikų (mėlyna juosta), nešiklio kontrolės (violetinė juosta), Avastino grupės - ruda juosta, kombinacijos - šviesiai mėlyna juosta) jas lyginant su pradine 143B ląstelių kultūra (oranžinės juostos) ląstelių linija.

Eksperimento pabaigoje surinkti navikai buvo analizuojami tėkmės citometrijos būdu, kuris parodė nežymų CAIX ir CCR2 baltymų procentinės raiškos padidėjimą AZ19-3-2 gydytoje grupėje (CCR2 baltymo procentinė raiška išaugo nuo 7,5±1,3 % nešiklio grupėje iki 14,6±0,1 % AZ19-3-2 junginio grupėje) (2C pav.). Taip pat išauginome surinktas naviko ląsteles ląstelių kultūroje. Kai ląstelių priaugo, mes jas paveikėme 1 % O_2 ir palyginome CAIX ekspresiją apskaičiuodami vidutinio fluorescencijos intensyvumo santykį (1 % O_2/ 21 % O_2). Iš auglio išaugintose ląstelėse MFI

(1 % O_2/ 21 % O_2) santykis buvo didesnis palyginus su pradinėmis kultivuotomis ląstelėmis (1,18±0,1 pradinėse ląstelėse ir 1,4±0,2 iš auglio išaugintose ląstelėse) (2D pav.). Tikėtina, kad tai susiję su dar ryškesne šių navikų hipoksija *in vivo*.

Apibendrinant galima pasakyti, kad bandymas derinti CAIX slopinimą su Avastinu nebuvo sėkmingas. Tačiau šis tyrimas paskatino mus ištirti CCL2-CCR2 signalinio kelio slopinimą 143B osteosarkomos modelyje.

Hipoksija keičia CCR2 antagonistų veiksmingumą 143B modelyje.

Toliau siekėme ištirti CCL2-CCR2 signalinio kelio blokavimo veiksmingumo skirtumus hipoksijoje ir normoksijoje žmogaus osteosarkomos ląstelių linijos 143B modelyje. Siekėme išsiaiškinti sąveikos mechanizmus tarp osteosarkomos ląstelių ir imuninių ląstelių hipoksijoje ir normoksijoje bei kompensacinius mechanizmus, susijusius su CCR2 slopinimu, pasitelkiant vėžinių ląstelių ir sveiko donoro PBMC ko-kultūros metodą [33, 34]. CCL2-CCR2 kelio slopinimui pasirinkome mažą organinę molekulę RS504393 (spiropiperidiną) – selektyvų CCR2 receptoriaus antagonistą [40]. Šis junginys blokuoja CCR2 receptorių, užimdamas CCL2 surišimo vietą, nepaveikdamas CXCR1, CCR1 ar CCR3 receptorių [40]. RS504393 parodė daug žadantį aktyvumą, kai buvo naudojamas kartu su imuninės sinapsės blokada standžiųjų navikų ikiklinikiniuose tyrimuose [41]. Mes ištyrėme CCR2 antagonisto poveikį 143B ląstelių gebėjimui sekretuoti chemokinus CXCL8, CCL2 ir VEGF. Visi šie angiogeniniai ir priešuždegiminiai chemokinai vaidina svarbų vaidmenį osteosarkomos progresavime. Be to, ištyrėme paviršiaus baltymų CAIX, VEGFR bei PD-L1 raiškos pokyčius 143B ląstelėse. Mes taip pat ištyrėme CD44 baltymo raišką, nes šis glikoproteinas svarbus ląstelių adhezijoje ir yra laikomas vėžio kamieninių ląstelių žymeniu [42].

143B ląstelės sekretuoja nedidelį kiekį CCL2 chemokino, kuris ženkliai, 5-8 kartus, išauga paveikus ląsteles IFN-γ (3A pav). CCR2 receptoriaus raiška 143B ląstelėse *in vitro* nėra tokia žymi. Visgi CCR2 receptoriaus procentinė raiška ant CD11b+ ląstelių, lyginant su normoksija, padidėja esant hipoksijai ir tampa dar ryškesne, kai CD11b+ ląstelėse ko-kultūroje su 143B ląstelėmis (0,71 % normoksijoje monokultūroje, 1±0,03 % hipoksiioje monokultūroje, 1.7±0.2 % hipoksijoje ko-kultūroje) (3B pav.).

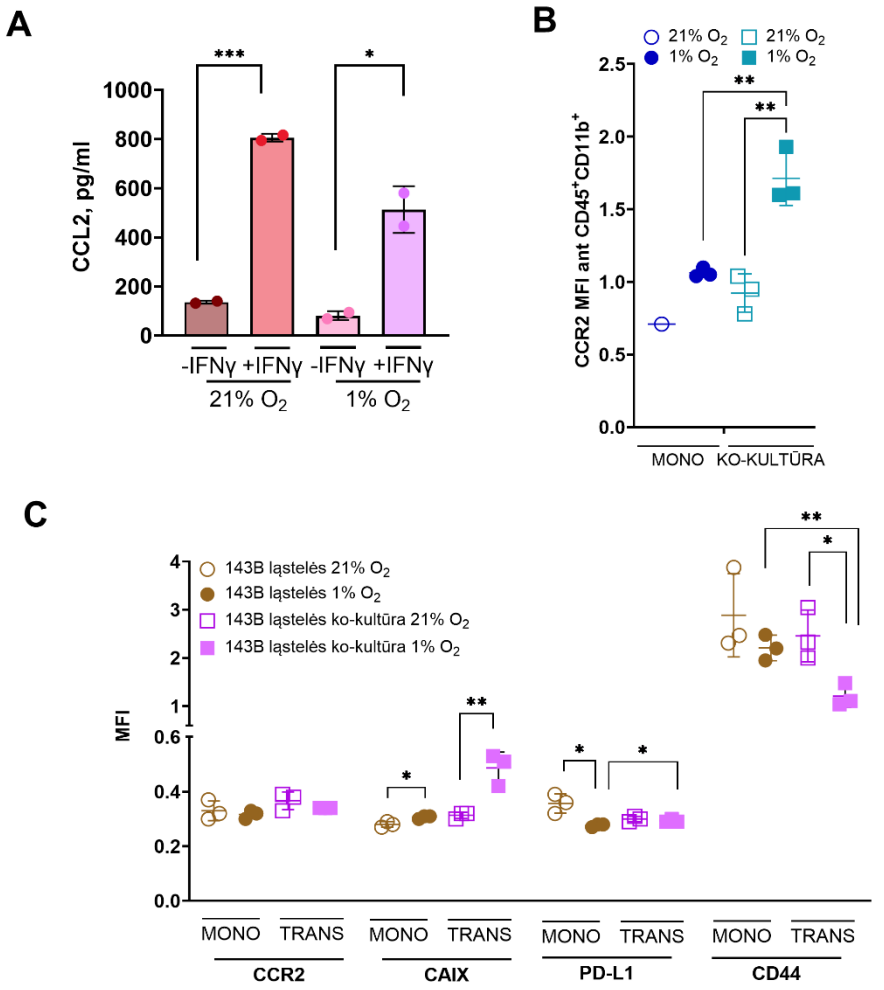

3 paveikslas. 143B ląstelių fenotipas monokultūroje ir kartu su imuninėmis ląstelėmis. A) 143B ląstelių, išaugintų normoksijos ar hipoksijos metu, CCL2 sekrecijos skirtumai -/+ IFNγ atlikus ELISA tyrimą. B) CCR2 ekspresijos skirtumai ant CD11b ląstelių, kai PBMC auginamos monokultūroje (apskritimai) ir ko-kultūroje (kvadratai) normoksijoje (tuščios formos) arba hipoksijoje (užpildytos formos). C) Paviršiaus baltymų ekspresijos pokyčiai vertinant šių žymenų MFI: CCR2, CAIX, VEGFR ir PD-L1, kai 143B ląstelės buvo auginamos monokultūroje (rudi apskritimai), arba ko- kutūroje (violetiniai kvadratai) normoksijos (tuščios formos) arba hipoksijos (užpildytos formos) sąlygomis.

143B ląstelių ko-kultūra su sveiko donoro PBMC sukelia CAIX baltymo raiškos pokyčius. Kaip ir tikėtasi, 143B ląstelėse hipoksijoje CAIX baltymo

raiška vertinant MFI padidėjo lyginant su normoksija (nuo 0,28±0,01 normoksijoje iki 0,3±0,01 hipoksijoje). Įdomu tai, kad CAIX baltymo MFI raiška dar labiau padidėjo kai ląstelės buvo inkubuotos ko-kultūroje su PBMC (nuo 0,3±0,01 normoksijoje iki 0,49±0,06 hipoksijoje). Lyginant su normoksija, PD-L1 baltymo raiška ląstelių paviršiuje vertinant MFI pakito atvirkščiai – sumažėjo hipoksijoje tiek 143B ląstelių monokultūroje, tiek ir ko-kultūroje (nuo 0,35±0,04 monokultūroje normoksijoje iki 0,28±0,01 monokultūroje hipoksijoje bei 0,3±0,01 ko-kultūroje hipoksijoje) (3C pav.). Panašiai, CD44 baltymo MFI 143B ląstelėse sumažėjo nuo 2,9±0,9 monokultūroje normoksijoje iki 2,2 ± 0,3 ląstelėse monokultūroje hipoksijoje ir ko-kultūroje, abiem deguonies sąlygomis (2,5±0,5 21 % O_2 ir 1,2%±0,2 1 % O_2).

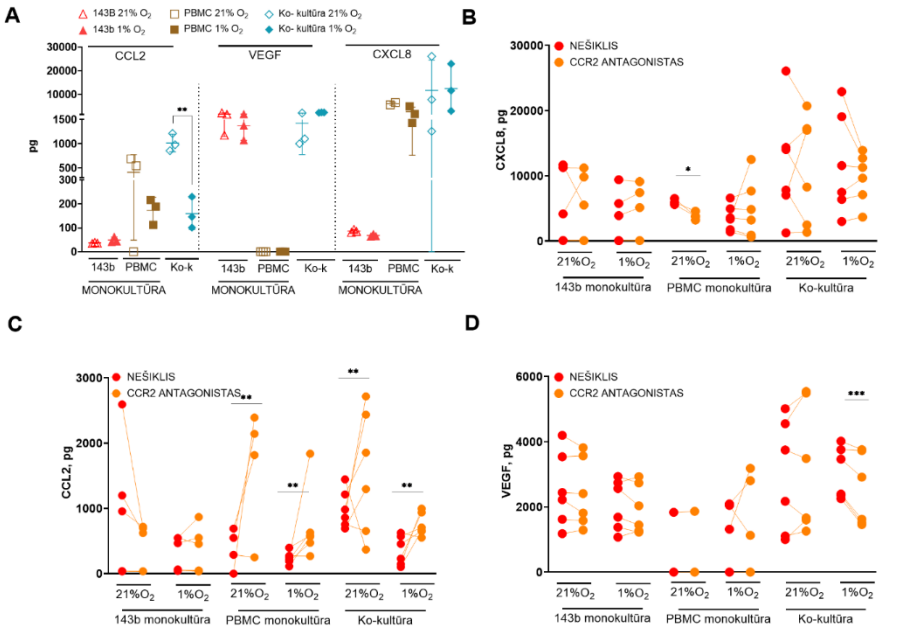

4 paveikslas. 143B ląstelių sekrecijos skirtumai monokultūroje lyginant su ko-kultūra. A) CCL2, VEGF, CXCL8 sekrecijos pokyčiai 143B ląstelėse, PBMC bei ko- kultūroje normoksijoje ir hipoksijoje. B) CXCL8, C) CCL2, D) VEGF sekrecijos pokyčiai143B, PBMC arba ko- kultūroje normoksijoje ir hipoksijoje paveikus ląsteles nešikliu arba CCR2 antagonistu. Raudoni apskritimai – nešiklis, oranžiniai apskritimai – CCR2 antagonistas. *P < 0,05; **P < 0,01, ***P < 0,001, statistinis reikšmingumas buvo nustatytas naudojant Studento t-testą, n=5 eksperimentinėje grupėje.

Atlikta supernatantų iš monokultūros ir ko-kultūros analizė ELISA metodu parodė, kad tiek 143B ląstelės, tiek PBMC sekretuoja CCL2 tiek normoksijoje, tiek hipoksijoje. Nors CCL2 sekrecija padidėjo ko-kultūroje normoksijoje, ji ženkliai sumažėjo esant hipoksijai (nuo 1018 ± 180 pg ko-kultūroje normoksijoje iki 160 ± 65 pg hipoksijoje) (3A pav.). VEGF sekrecija buvo stipresnė 143B ląstelėse, bet ne PBMC (4A pav.) ir nepasikeitė ko-kultūroje. CXCL8 baltymą, atvirkščiai, daugiausia išskyrė PBMC (6070 ± 665 pg 21 % O_2 ir 27212 ± 1950 pg 1 % O_2) ir jis toliau didėjo, kai ląstelės buvo auginamos ko-kultūroje, ypač hipoksijos sąlygomis (11720 ± 12861 pg 21 % O_2 ir 12500±9985 pg 1 % O_2) (4A pav.).

Toliau ištyrėme citokinų ir chemokinų sekrecijos pokyčius po CCR2 antagonisto pridėjimo. Pastebėjome PBMC CXCL8 sekrecijos sumažėjimą monokultūroje nuo 6070 ± 665 pg nešiklio įtakoje iki 3599 ± 323 pg po CCR2 antagonisto esant normoksijai (3B pav). Tačiau CXCL8 sekrecija ko-kultūroje nepakito (4B pav.). CCR2 antagonistas sumažino VEGF sekreciją ko-kultūroje hipoksinėmis sąlygomis (nuo 2336±74 pg po nešiklio iki 1533±84 pg po CCR2 antagonisto) (4C pav.), bet ne 143B ląstelėse monokultūroje. CCR2 slopinimas padidino CCL2 sekreciją PBMC monokultūroje bei ko-kultūroje esant tiek hipoksijai, tiek normoksijai (4D pav.).

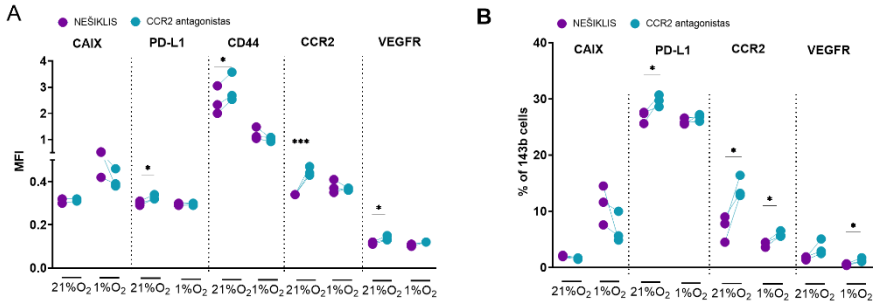

5 paveikslas. Auglio ląstelių žymenų ekspresijos pokyčiai po CCR2 slopinimo hipoksija ir normoksija. CAIX, PD-L1, CD44, CCR2 ir VEGFR paviršiaus ekspresijos pokyčiai 143B ląstelėse vertinant MFI (A) ir pagal gyvų ląstelių (B) procentinę dalį bendroje kultūroje, kai ląstelės buvo iš anksto apdorotos arba neapdorotos 500 nM CCR2 antagonisto hipoksinėmis ar normoksinėmis sąlygomis. * P < 0,05; ** P < 0,01, *** P < 0,001, statistinis reikšmingumas buvo nustatytas naudojant Studento t-testą, n=5 eksperimentinėje grupėje.

Norėdami įvertinti navikinių ląstelių fenotipo pokyčius po CCR2 slopinimo, mes ištyrėme gautus vėžio žymenų raiškos pokyčius 143B ląstelėse, kai jos buvo auginamos monokultūroje arba ko-kultūroje. Lygindami paviršiaus baltymų raišką 143B ląstelėse jų ko-kultūroje su PBMC normoksijos ir hipoksijos sąlygomis pastebėjome, kad CCR2 slopinimas padidino CD44 (nuo 2,5±0 nešiklio kontrolėje iki 2,9±0,5 po CCR2 antagonisto) ir PD-L1 (nuo 0,3±0,01 po nešiklio iki 0,32±0,01 po CCR2 antagonisto) baltymų MFI raišką 143B ląstelėse tik normoksijoje. VEGFR baltymo procentinė paviršiaus raiška pakito tiek normoksijoje (nuo 1,6±0,3 % po nešiklio ir 3,5±1,3 % po CCR2 antagonisto), tiek ir hipoksijoje (nuo 0,5±0,2 % po nešiklio iki 1,3±0,4 % po CCR2 antagonisto) (5A, B pav.). Buvo pastebimas CAIX baltymo procentinės raiškos sumažėjimo hipoksijoje po CCR2 antagonisto pridėjimo (nuo 11,2±3,5 % nešiklio grupėje iki 6,8±2,8 % pridėjus CCR2 antagonisto) (5A, B pav.).

Šie duomenys patvirtina, kad ko-kultūros metodas atskleidžia fiziologiškai reikšmingesnį biologinį poveikį ląstelėms, palyginti su monokultūra. Matome reikšmingus paviršiaus baltymų ekspresijos pokyčius, taip pat padidėjusią chemokinų gamybą vėžio ląstelėse, kai jos yra veikiamos parakrininių faktorių, išskiriamų iš PBMC, palyginti su monokultūra. Taip pat mūsų duomenys rodo, kad CCR2 receptoriaus antagonisto poveikis hipoksijos atveju matomas tik VEGF-VEGFR ašyje, kur matome VEGFR baltymo padidėjimą 143B ląstelėse, bet sumažintą VEGF citokino sekreciją ko-kultūroje. Akivaizdu, kad CCR2 receptoriaus antagonisto poveikis ryškesnis normoksijoje (padidėjusi PD-L1 ir CD44 baltymų paviršiaus ekspresija 143B ląstelėse ir sumažėjusi CXCL8 chemokino sekrecija ko-kultūroje). PD-L1 baltymo raiškos padidėjimas gydant CCR2 antagonistu yra labai įdomus, nes naujausiose publikacijose teigiama, kad gydymas CCR2 receptorių antagonistu sustiprina naviko atsaką į imuninės sinapsės slopiklius [144].

Gydymas CCR2 antagonistu *in vivo* neturi įtakos naviko augimui 143B ksenografto modelyje.

Siekiant įvertinti CCR2 antagonisto efektyvumą 143B naviko modelyje *in vivo* suleidome 143B ląsteles į Nude pelių blauzdikaulį. Kai navikai pasiekė apčiuopiamą dydį, juos suskirstėme į dvi gydymo grupes (n = 10 grupėje). Viena grupė gavo CCR2 antagonistą RS504393 2 mg/ kg dozę i.p. kartą per parą, kita - nešiklį. CCR2 slopinimas nesumažino auglių augimo (6A pav.). Eksperimento pabaigoje navikai buvo surinkti iš pelių ir išanalizuoti taikant tėkmės citometrijos metodą, siekiant įvertinti paviršiaus žymenų raišką naviko

ląstelėse ir pelių monocituose/makrofaguose, nes augliai buvo auginami Nude pelėse su sutrikusiomiaT ląstelelių veikla

Silpnas atsakas į CCR2 antagonistą *in vivo* gali būti susijęs su naviko hipoksija. Hipoksija yra ryškus 143B navikų bruožas [43]. Mūsų eksperimento 143B navikai turėjo ryškią aktyvaus CAIX baltymo raišką hipoksijoje pagal tėkmės citometrijos duomenis (6C pav.) [44]. Mes taip pat įvertinome CD44 baltymo raišką. Įdomu tai, kad mes stebėjome dvi naviko ląstelių populiacijas, turinčias skirtingas CD44 išraiškas: $CD44^{\text{nežymi raiška}}$ ir $CD44^{\text{žymi raiška}}$ (6D pav.). Šių populiacijų santykis pasikeitė po gydymo CCR2 antagonistu. CCR2 slopinimas išlygino ląstelių procentą kiekvienoje populiacijoje, padidindamas $CD44^{\text{žymi raiška}}$ ląstelių skaičių ($CD44^{\text{nežymi raiška}}$ ląstelių procentas sumažėjo nuo 57±14 % nešiklio grupėje iki 52,9±16,6 % CCR2 antagonistų grupėje, o $CD44^{\text{žymi raiška}}$ ląstelių procentas padidėjo nuo 40±14 % nešiklio grupėje iki 47±16 % CCR2 antagonisto grupėje) (6D pav.). Analizuodami naviko ląstelių frakciją tėkmės citometrijos būdu, nepastebėjome jokių CCR2 ar PD-L1 raiškos ląstelės paviršiuje pokyčių pelių, gavusių CCR2 antagonistus, naviko ląstelėse (6B pav.). Tačiau VEGFR signalas vertinant MFI vidutiniškai sumažėjo 1.34 karto esant CCR2 slopinimui (6B pav.). Tirdami monocitų/makrofagų ląstelių populiaciją, pastebėjome padidėjusią CD11b+CD86+ ląstelių infiltraciją į naviką (nuo 4,6±1,6 % nešiklio grupėje iki 8,3±4,7 % CCR2 antagonistų grupėje) (6E pav.). Tačiau CD11b+CCR2+ ląstelių frakcijos pokyčio neaptikome (6F pav.).

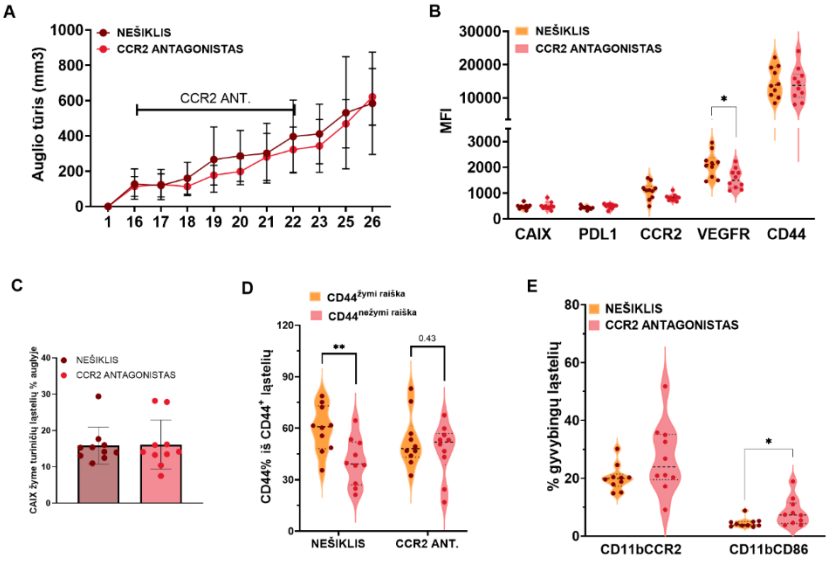

6 paveikslas. Gydymas CCR2 antagonistu *in vivo* neturėjo įtakos naviko augimui, bet pakeitė paviršiaus receptorių raišką naviko ląstelėse ir infiltruojančiuose monocituose/ makrofaguose. A) 143B naviko augimo dinamika Nude pelėse, kai joms buvo skiriamas CCR2 antagonistas (raudoni apskritimai), palyginus su nešiklio kontrole (rudi apskritimai). (Duomenys rodomi kaip vidurkiai +/- SD, n=10 eksperimentinėje grupėje). B) CAIX, PD-L1, CCR2, VEGFR ir CD44 paviršiaus baltymų MFI pelių gavusių nešiklį augliuose (rausva su raudonais apskritimais) arba CCR2 antagonistą (geltona su rudais apskritimais), naviko ląstelių. C) CAIX+ ląstelių procentinė dalis pagal tėkmės citometrijos duomenis augliuose pelių, gavusių nešiklį lyginant su CCR2 antagonistu. D) CD44 raiškos skirtumai naviko ląstelėse. E) CD11bCCR2 ir CD11bCD86 monocitų/makrofagų paviršiaus žymenų raiškos skirtumai tarp pelių, gydytų CCR2 antagonistu (geltona su rudais apskritimais), ir gavusių nešiklį (rausva su raudonais apskritimais). Kiekvienas duomenų taškas rodo atskirą naviko mėginį iš pelių, n=10 kiekvienai eksperimentinei grupei. * P < 0,05; ** P < 0,01, *** P < 0,001, statistinis reikšmingumas buvo nustatytas naudojant Studento t testą.

Šie rezultatai atskleidžia CCR2 receptoriaus antagonisto poveikį VEGF-VEGFR citokinų ašiai, nes matome VEGR baltymo sumažėjimą augliuose (panašų poveikį matėme ir ko-kultūros eksperimente).

143B ląstelių pasirinktų onkogeninių baltymų limituota proteomikos analizė

Nepakankamas atsakas į CCR2 antagonistų gydymą *in vivo* mus paskatino grįžti prie ko-kultūros eksperimentų tam, kad išsiaiškintume mechanizmus nulemiančius silpną atsaką. Tam, ko-kultūroje bei monokultūroje skirtingomis deguonies sąlygomis užaugintas 143B ląsteles išanalizavome naudodami proteomikos rinkinį "Human XL Oncology Array Kit". Pirma, įvertinome 143B ląstelių baltymų pokytį ko-kultūroje lyginant su monokultūra. Pastebėjome ženkliai pakitusias baltymų raiškas ko-kultūroje lyginant su monokultūra (7A pav). Dar svarbiau, kad gydymas CCR2 antagonistu 143B ląstelėse ko-kultūroje atskleidė skirtingą įvairių baltymų raišką normoksijoje palyginus su hipoksija (7B pav).

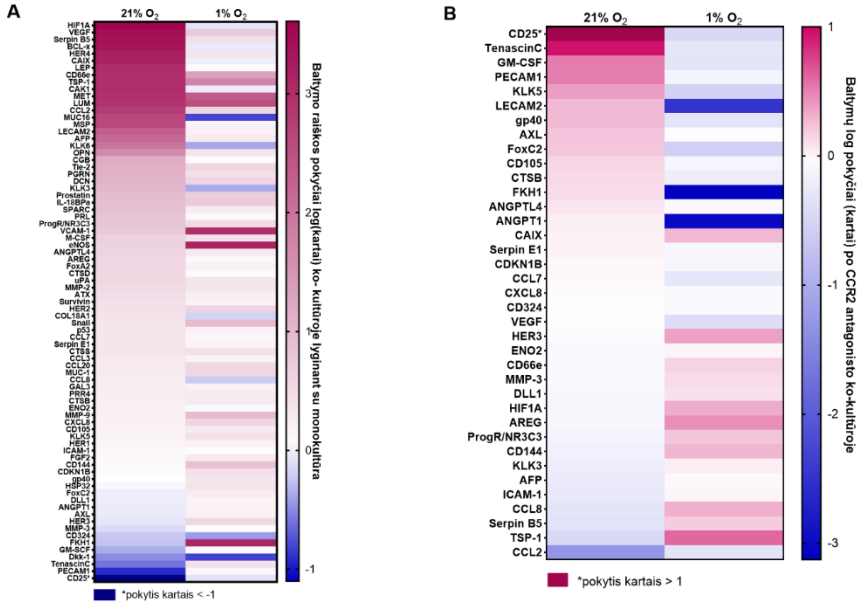

7 paveikslas. Žmogaus su vėžiu susijusių baltymų analizė 143B ląstelėse, užaugintose monokultūroje ir ko-kultūroje normoksijoje ir hipoksijoje bei paveiktose arba ne CCR2 antagonistu. A) Baltymų karštųjų taškų žemėlapis, vaizduojantis diferencinius baltymų raiškos pokyčius lyginant ko-kultūroje užaugintas ląsteles su monokultūra hipoksijos ir normoksijos sąlygomis. B) Baltymų karštųjų taškų žemėlapis, vaizduojantis skirtingus baltymų raiškos pokyčius, ląsteles paveikus CCR2 antagonistu arba nešikliu hipoksijos ir normoksijos sąlygomis.

Šio eksperimento rezultatai patvirtina, kad vėžinių ląstelių ir sveiko donoro PBMC ko-kultūros metodas geriau atspindi ląstelių elgesį *in vivo* lyginant su ląstelių monokultūra. Matomas daugumos su vėžiu susijusių baltymų raiškos sustiprėjimas ant vėžinių ląstelių iš ko-kultūros lyginant su monokultūra. Be to, vėžinėse ląstelėse, augintose ko-kultūroje, mes matome priešingą CCR2 receptoriaus antagonisto poveikį daliems baltymų raiškai esant normoksijai, palyginti su hipoksija. Skirtingas atsakas į vaistus esant normoksijai ir hipoksijai sulaukia vis didesnio susidomėjimo [45]. Tikimasi, kad šie rezultatai paskatins skirti daugiau dėmesio priešvėžinių vaistų poveikio skirtumams skirtingose deguonies aplinkose.

CAIX slopinimo veiksmingumas neuroblastomos SK-N-AS ksenografto modelyje.

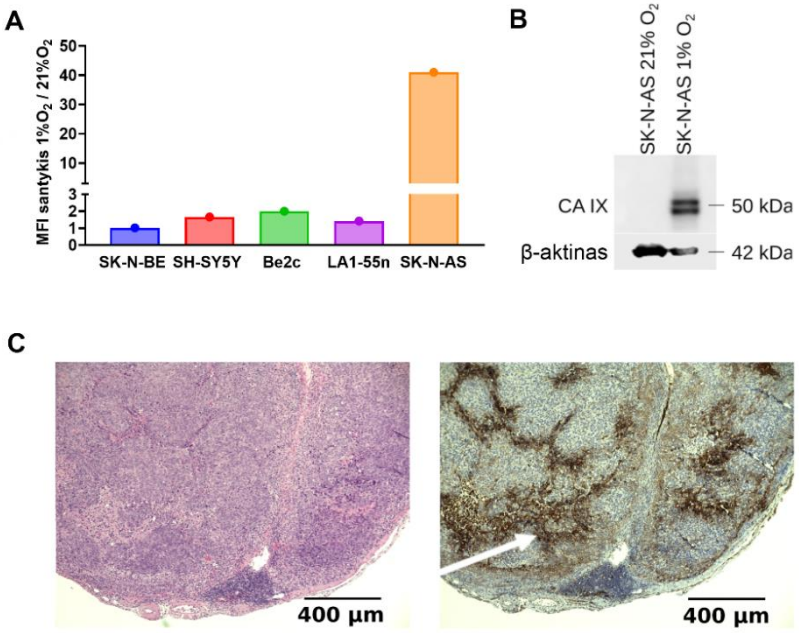

8 paveikslas. CAIX baltymo raiška SK-N-AS ląstelių linijoje. A) CAIX baltymo raiška įvairiose žmogaus neuroblastomos ląstelių linijose (SK-N-BE, SH-SY5Y, Be2C, LA1-55n, SK-N-AS), apskaičiuojant MFI santykį 1 % O_2 ir 21 % O_2 sąlygomis. B) CAIX baltymo raiškos įvertinimas imunoblotu SK-N-AS ląstelių linijoje normoksijoje ir hipoksijoje. C) Imunohistologine analize įvertinta CAIX raiška SK-N-AS ksenograftiniame naviko modelyje, kairėje naviko pjūvis, nudažytas hematoskilinu ir eozinu, dešinėje - naviko pjūvis nudažytas CAIX atpažįstančiu antikūniu (balta rodyklė nurodo ruda spalva nusidažiusias CAIX baltymą ekspresuojančias sritis).

Pirmiausiai ištyrėme CAIX baltymo raišką tėkmės citometrijos metodu keliose žmogaus NBL ląstelių linijose (SK-N-BE, Be2C, SH-SY5Y, LA1-55n, SK-N-AS). SK-N-AS ląstelių linija turėjo stipriausią CAIX raišką hipoksinėmis sąlygomis (8A pav.). Imunobloto analizė patvirtino stiprią CAIX baltymo raišką SK-N-AS linijoje hipoksijoje palyginus su normoksija (8B pav.). Be to, patvirtinome CAIX raišką, atlikdami imunohistologinę analizę ant SK-N-AS navikų iš Nude pelių (8C pav.). Visi rezultatai patvirtino, kad SK-N-AS naviko modelis yra patrauklus CAIX slopinančių junginių tyrimams.

Toksiškumo tyrimai parodė, kad AZ19-3-2 junginys yra netoksiškas SK-N-AS ląstelėms, nes XTT ir LDH rezultatai rodo reikšmingus verčių pokyčius tik esant didelėms, neselektyvioms dozėms, pradedant nuo 2 µM (9A pav.). Taip pat atlikome epH matavimus su skirtingomis AZ 19-3-2 dozėmis ir įvertinome pH pokyčius. AZ19-3-2 junginys parodė terpės rūgštinimo slopinimą mažomis 200 nM dozėmis hipoksijos sąlygomis (9B pav.).

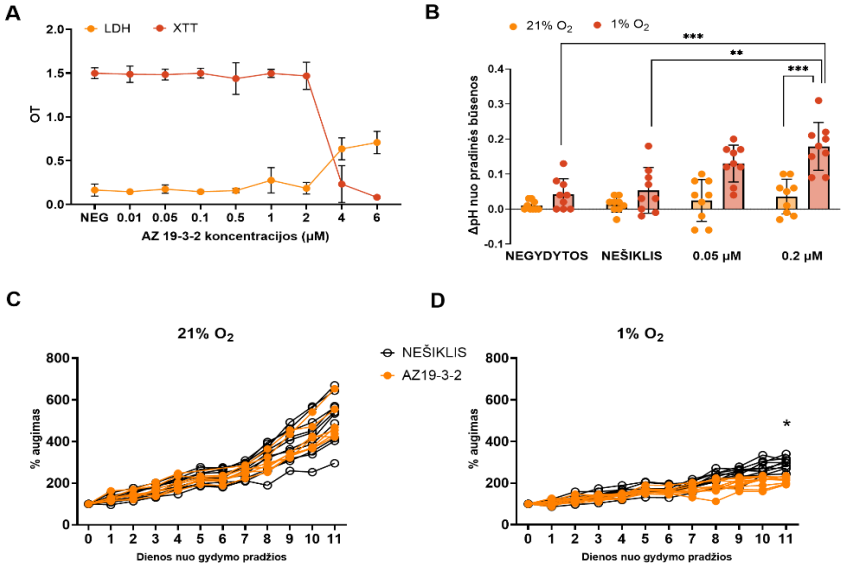

9 paveikslas. CAIX slopiklio poveikio SK-N-AS ląstelių linijoje vertinimas. A) XTT (raudoni apskritimai) ir LDH (oranžiniai apskritimai) 72 val po po AZ19-3-2 junginio pridėjimo į SK-N-AS ląstelių terpę. B) SK-N-AS terpės epH matavimai normoksijoje ir hipoksijoje 96 val. po AZ19-3-2 pridėjimo 50 ir 200 nM junginio dozėmis. Buvo lyginama 21 % O_2 (oranžiniai apskritimai) būklė ir 1 % O_2 (raudoni apskritimai). C) SK-N-AS sferoidų augimas (santykinis dydis) laikui bėgant normoksijoje, kai jis veikiamas AZ19-3-2 (n = 7) arba nešiklio kontrole (n = 10). D) SK-N-AS sferoidų augimas (santykinis dydis) hipoksijoje, kai jie veikiami AZ19-3-2 arba nešiklio kontrole (n = 10 vienai grupei).

AZ19-3-2 junginio veiksmingumas *in vitro* taip pat buvo tiriamas SK-N-AS ląstelių linijos 3D ląstelių kultūroje. Praėjus 48 valandoms po užsėjimo, susidarę sferoidai kas 48 val 11 dienų buvo veikiami AZ19-3-2 arba tirpiklio kontrole. Kaip pavaizduota 9C ir 9D pav., pastebėjome, kad sferoidų augimas hipoksijos metu, matuojant procentinį augimą, sumažėjo perpus, palyginti su normoksija (294±28 % nešiklio grupėje esant normoksijai ir 512±114 % nešiklio grupėje hipoksijoje pagal paskutinės dienos matavimus). Taip pat pastebėjome reikšmingą sferoidų augimo slopinimą AZ19-3-2 poveikyje hipoksijoje lyginant su nešiklio kontrole (294±28 % nešiklio grupėje ir 215±14 % AZ19-3-2 gydytoje grupėje) (9D pav.). Svarbu pažymėti tai, kad toks AZ19-3-2 efektas nebuvo stebimas normoksijos sąlygomis (512±114 % nešiklio grupėje ir 487±86 % AZ19-3-2 gydytoje grupėje) (9C pav.). Tai parodo specifinį CAIX slopinimo veiksmingumą tik hipoksinėmis sąlygomis, kai yra stebima padidėjusi CAIX baltymo raiška.

Navikai yra nevienalytės sudėties, susidedančios ne tik iš naviko ląstelių, bet ir iš imuninių ląstelių, endotelio ląstelių, fibroblastų, užląstelinės terpės ir kt. Kryžminis pokalbis tarp visų šių ląstelių perprogramuoja naviko ląsteles ir keičia jų paviršiaus baltymų raišką. Todėl mes įvertinome tokios kryžminės sąveikos pokyčius hipoksijoje. Tam pritaikėme SK-N-AS ir sveiko donoro PBMC ko-kultūros modelį, aprašytą šiame darbe anksčiau tyrimų skyrelyje su 143B ląstelėmis. Mes atradome, kad CAIX ir PD-L1 baltymų paviršiaus procentinė raiška žymiai padidėjo naviko ląstelėse, kai jos auginamos ko-kultūros sąlygomis (CAIX baltymą ekspresuojančių ląstelių padidėjo nuo 44±12 % monokultūroje iki 85±5 % ko-kultūroje, bei, atitinkamai, PD-L1 baltymą ekspresuojančių ląstelių procentas padidėjo nuo 5±3 % iki 36±6 %) (10A pav.). Tikėtina, kad tai susiję su papildomais PBMC aktyvinančiais veiksniais, kurie skatina šių žymenų raišką ir greičiausiai atspindi realius auglio mikroaplinkos pokyčius. CCR2 receptorių lygis SK-N-AS paviršiuje taip pat neženkliai didėjo (10A pav.).

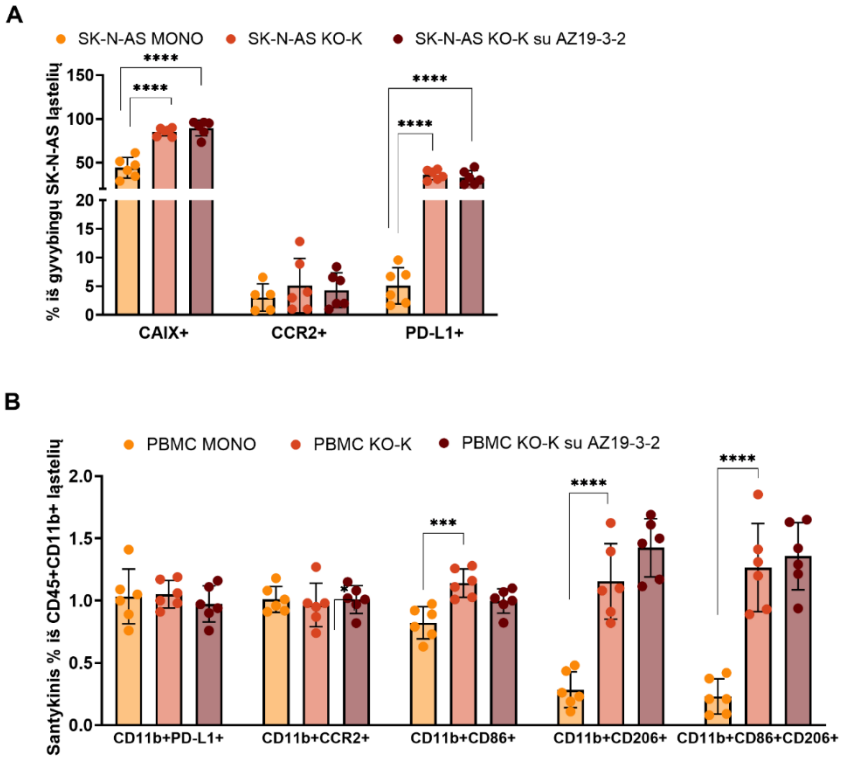

10 paveikslas. **Paviršiaus žymenų raiškos pokyčiai SK-N-AS ir PBMC ląstelėse, auginant monokultūroje ir ko-kultūroje bei esant AZ 19-3-2 poveikiui**. A) CAIX, CCR2 ir PD-L1 raiškos pokyčiai vėžinėse ląstelėse. Oranžiniai stulpeliai – vėžinės ląstelės be PBMC, raudoni – vėžinės ląstelės, paveiktos PBMC, ruda – vėžinės ląstelės, paveiktos PBMC, ir 200 nM AZ19-3-2 (n = 6 vienai grupei). B) PD-L1, CCR2, CD86, CD206 ir CD86+CD206+ raiška CD11b ląstelių paviršiuje PBMC monokultūroje, ko-kultūroje bei 200 nM AZ19-3-2 poveikyje. Raiška vaizduojama kaip santykinė CD11b+ ląstelių frakcija (n = 6 vienai grupei). Statistiškai reikšmingi pokyčiai buvo nustatyti taikant ANOVA (Tukey daugybinio palyginimo) metodą. * $p < 0,05$; ** $p < 0,01$, *** $p< 0,001$, **** $p< 0.0001$.

Vertinant PBMC aktyvinimo žymens paviršiaus raiškos pokyčius, nenustatėme CD4, CD8 ar PD-1 raiškos skirtumų T-ląstelėse. Taip pat nebuvo CCR2 ar PD-L1 raiškos pokyčių (10B pav.). Tačiau ko-kultūroje ženkliai padidėjo ko-stimuliuojančių molekulių CD86 ir CD206 raiška CD11b ląstelių paviršiuje lyginant su monokultūra (CD86 % padidėjo nuo 0,8±0,1 % iki 1,1±0,1 %, o CD206 % - nuo 0,3±0,1 % iki 1,2±0,3 %) (10B pav.). CAIX

slopinimas SK-N-AS ląstelėse mažino CD86 procentinę raišką CD11b ląstelėse nuo 1,1±0,1 % iki 1±0,1 %, tuo tarpu CD206 baltymų procentinė paviršiaus raiška padidėjo nuo 1,2±0,3 % iki 1,4±0,2 % (10B pav).

Taip pat ištyrėme PBMC ir SK-N-AS citokinų/chemokino sekrecijos profilio pokyčius ko- kultūroje. Naviko nekrozės faktoriaus-alfa (TNF-α), IL-6, IFN-γ, IL-4, IL-10, transformuojančio augimo faktorius beta (TGF-β) vertės buvo žemesnės nei naudoto nustatymo rinkinio aptikimo riba. Tačiau buvo nustatyti VEGF, CCL2 ir CXCL8 sekrecijos pokyčiai. Pirmiausia nustatėme reikšmingą VEGF, CCL2 ir CXCL8 sekrecijos padidėjimą ko-kultūroje lyginant su ląstelių monokultūromis (11A,B,C pav.). CAIX slopiklio AZ19-3-2 pridėjimas žymiai padidino VEGF sekreciją PBMC monokultūroje (nuo neaptinkamo lygmens iki 187±57 pg), bet ne ko-kultūroje (nuo 2469±1345 pg iki 2165±1500 pg) (11A pav). AZ19-3-2 žymiai susilpnino CCL2 (nuo 1525±1014 pg iki 831±372 pg) ir CXCL8 (nuo 52487±30315 pg iki 28966±15457 pg) baltymų sekreciją ko-kultūroje, bet ne monokultūroje (11B, C pav.).

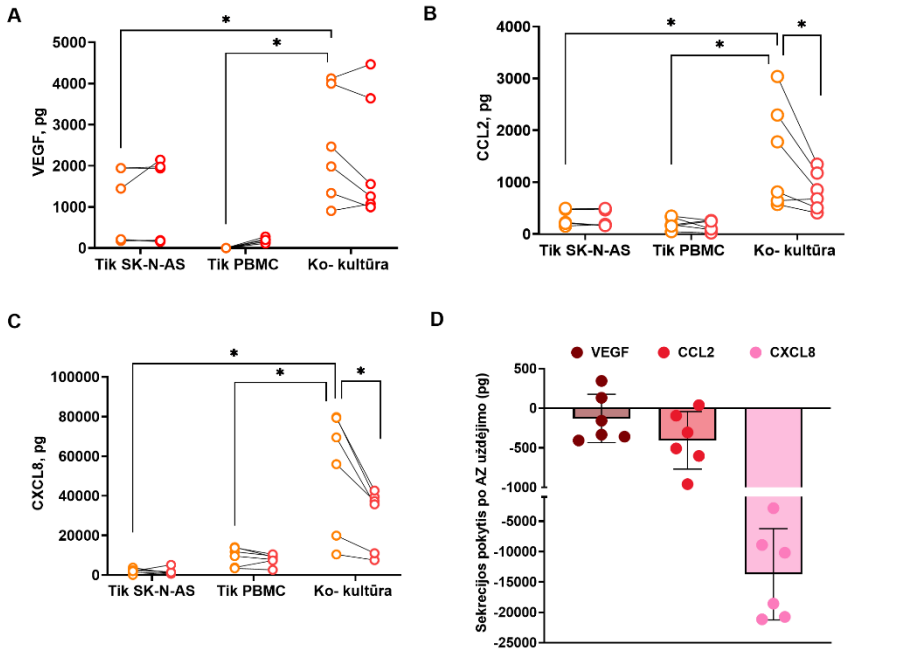

11 paveikslas. Chemokinų/citokinų sekrecijos pokyčiai hipoksijoje SK-N-AS-PBMC ląstelių ko-kultūroje lyginant su monokultūra. (A) VEGF, (B) CCL2 ir (C) CXCL8 sekrecija SK-N-AS ląstelių monokultūroje, PBMC monokultūroje ir ko-kultūroje, veikiant AZ19-3-2 (raudoni apskritimai) arba nešiklio kontrole (oranžiniai apskritimai) (n = 6 vienai grupei). D) VEGF,

CCL2 ir CXCL8 chemokinų lygių skirtumai ko-kultūroje paveikus 200 nM AZ19-3-2. Skirtumas parodomas kaip bendro citokinų sekrecijos lygio pokytis lyginant gydytą su negydyta būkle (NETO vertės, n = 6 vienai grupei). Duomenys pateikiami kaip vidurkis ± SD. Reikšmingumas buvo nustatytas naudojant Kruskall-Wallis testą, siekiant nustatyti skirtumus tarp monokultūros ir ko-kultūros verčių, o skirtumams tarp gydytų ir ne buvo taikomas porinis Studento t testas. * p < 0,05; ** p < 0,01, *** p< 0,001.

Šie rezultatai rodo, kad vėžinių ląstelių poveikis imuninėms ląstelėms hipoksijos metu keičia ląstelių paviršiaus žymenų raišką, žymiai padidindamas CAIX ir PD-L1 raišką vėžinėse ląstelėse. Jis taip pat mažina CD86 reguliavimą ir skatina CD206 raišką CD45+CD11b+ ląstelėse. Be to, CAIX slopinimas mažina CCL2 ir CXCL8 sekreciją ko-kultūroje.

AZ19-3-2 kartu su CCR2 antagonistiniu poveikis SK-N-AS ksenografte *in vivo*.

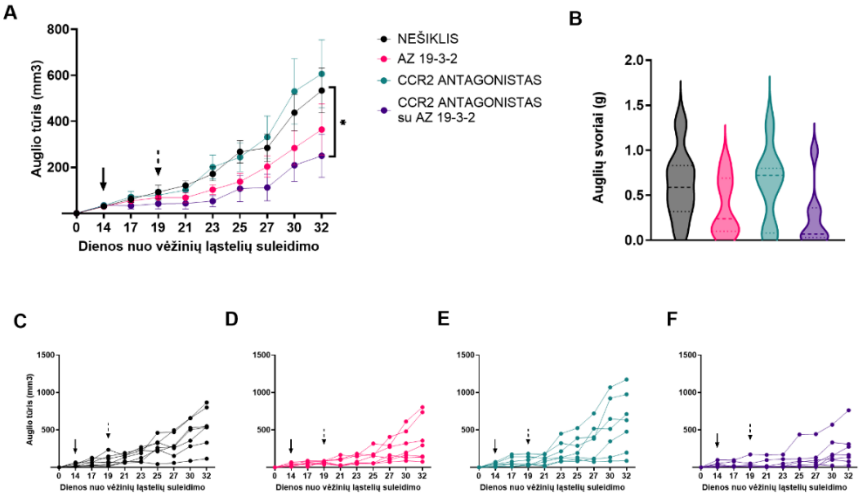

12 paveikslas. AZ19-3-2 kartu su CCR2 antagonistu mažina SK-N-AS navikų augimą. A) Po oda implantuotų SK-N-AS navikų, kuriems buvo taikomas AZ19-3-3 gydymas (rožiniai apskritimai), CCR2 antagonistas (žalieji apskritimai), derinys (purpuriniai apskritimai) arba kontrolė (juodi apskritimai), augimo kinetika (n = 7 vienai grupei). B) galutinė nugaišintų gyvūnų naviko masė eksperimento pabaigoje gydant AZ19-3-2 (rausvos kolonėlės), CCR2 antagonistu (žalios kolonėlės), kombinacija (purpurinė kolonėlė) arba nešikliu (juoda kolona). C) Naviko augimo kinetika atskiriems kiekvienos grupės gyvūnams. Kiekvienas duomenų taškas rodo atskirą pelių naviko mėginį (n = 7 vienai grupei). Statistiškai reikšmingi skirtumai buvo

nustatyti naudojant ANOVA (Tukey's) testą. * $p < 0,05$; ** $p < 0,01$, *** $p< 0,001$.

Nustatę CAIX slopiklio AZ19-3-2 aktyvumą *in vitro*, išbandėme jo veiksmingumą *in vivo*, atlikdami pelių SK-N-AS ksenografto tyrimą. SK-N-AS ląstelės buvo inokuliuojamos po oda į dešinįjį Nude pelių šoną. Kai navikai pasiekė apčiuopiamą dydį, juos suskirstėme į keturias gydymo būdų grupes pagal auglių dydžius (n = 7 vienai grupei). AZ19-3-2 junginys buvo leidžiamas i.p. kasdien 10 mg/ kg/ dozė. CCR2 antagonistas buvo leidžiamas i.p. 2 mg / kg/ doze pradedant 5 diena nuo CAIX slopinimo pradžios. Naviko augimas buvo lėčiausias pelių grupėje, kuriai buvo taikomas kombinuotas gydymas (vidutinis naviko tūris eksperimento pabaigoje buvo 533±258 mm^3 nešiklio grupėje ir 250±247 mm^3 kombinacijos grupėje) (12A, C-F pav.). Tačiau statistiškai reikšmingi naviko svorio skirtumai tarp nešiklio kontrolės ir kombinuoto gydymo nebuvo nustatyti (vidutinis auglio svoris eksperimento pabaigoje buvo 0,6 ± 0,4 g nešiklio grupėje ir 0,3 ± 0,3 g kombinacijos grupėje) (12B pav.).

Eksperimento pabaigoje buvo atlikta navikų analizė taikant tėkmės citometrijos metodą. Išanalizavome naviko ląsteles ir pelių monocitus/makrofagus, nes šie ksenografai buvo auginami Nude pelėse su sutrikusia T ląstelių funkcija. Nenustatėme reikšmingų analizuojamų žymenų pokyčių navike ar stromos ląstelėse, surinktose iš pelių, gavusių AZ19-3-2 junginį. Gydymas CCR2 antagonistu parodė ryškesnę CCR2 procentinę raišką navikuose (6±3,6 % nešiklio grupėje, 16±8 % CCR2 antagonistų grupėje ir 20±6 % derinio grupėje). Manome, kad tai kompensacinis poveikis. Pelėse, gavusiose AZ19-3-2 derinį su CCR2 antagonistu, VEGFR+ ląstelių procentas buvo žymiai didesnis palyginus su kitomis grupėmis (0,9±0,2 % nešiklio grupėje ir 6,9±5,2 % kombinacijos grupėje) (13A pav.). VEGFR yra dar vienas stiprus hipoksijos signalas, kuris gali būti aktyvuotas kaip kompensacinis mechanizmas, kai slopikliai veikia CCR2 ir CAIX baltymus. Taip pat, CAIX procentinė raiška žymiai padidėjo auglio ląstelėse iš pelių gavusių kombinaciją (23,7±7 % nešiklio grupėje ir 52±11 % kombinacijos grupėje) (13A pav.). Kamieninių ląstelių žymens CD44 procentinė raiška ląstelių paviršiuje sumažėjo (nors ir nežymiai) navikuose, gydytuose AZ19-3-2 ir CCR2 deriniu (21,6±4,2 % nešiklio grupėje ir 16,3±3,2% derinio grupėje) (13A pav.).

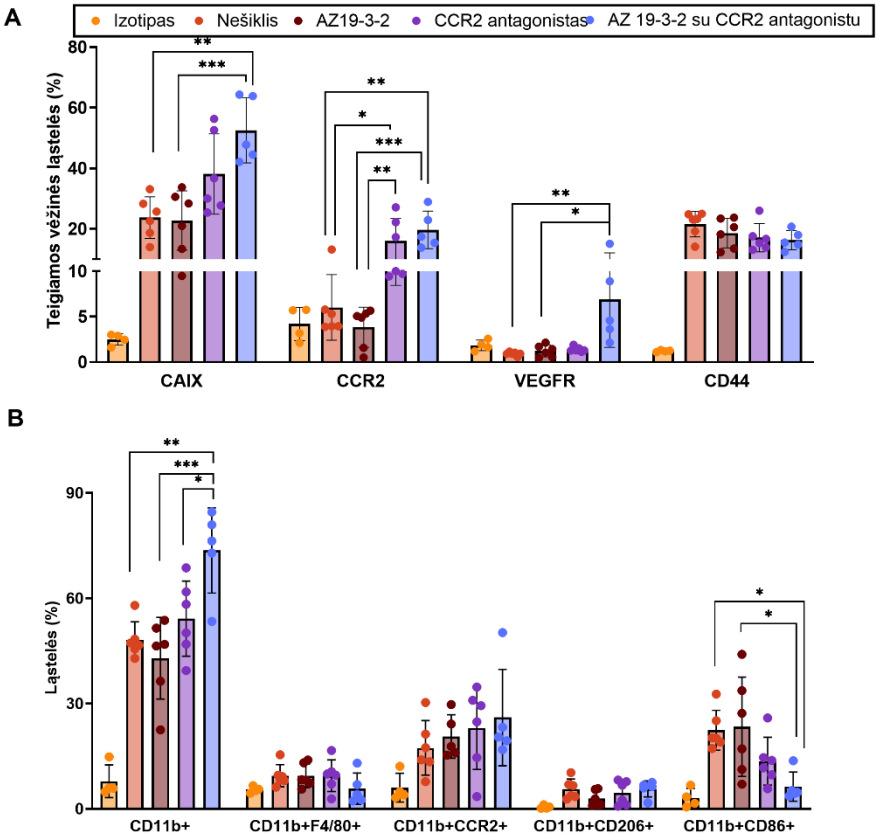

13 paveikslas. SK-N-AS naviko tėkmės citometrija. A) CAIX+, CCR2+, CD44+, VEGFR+ ląstelių procentinė dalis navikinių ląstelių populiacijoje. B) CD11b+, CD11b+ F4/80+, CD11b+ CCR2+, CD11b+ CD206+ ir CD11b+CD86+ ląstelių procentinė dalis tarp pelių naviko stromos ląstelių. (n=7 kiekvienoje grupėje). Statistinis reikšmingumas buvo nustatytas naudojant Studento t-testą.* $p < 0,05$; ** $p < 0,01$, *** $p< 0,001$.

Vertindami pelių monocitų/makrofagų ląstelių CCR2 paviršiaus raišką, nustatėme panašų padidėjimo poveikį pelėms, gydytoms CCR2 antagonistu ar kombinacija. CD11b+F4/80+ populiacija sumažėjo pelėse, gydytose AZ19-3-2 ir CCR2 kombinacija (13B pav.). Tačiau CD11b+CCR2+, CD11b+CD206+ ar CD11b+PD-L1+ pokyčių ląstelių populiacijose nenustatyta. CD11b+CD86+ ląstelių procentas žymiai sumažėjo navikuose, gydytuose AZ19-3-2 ir CCR2 antagonistu (3±2,7 % nešiklio grupėje iki 9,4±4,5 % derinio grupėje) (13B pav.). Įdomu tai, kad kombinuotas gydymas žymiai padidino monocitų/makrofagų ląstelių frakciją (CD11b+ populiacijos)

navikuose (nuo 7,8±4,6 % nešiklio grupėje iki 54±10,7 % derinio grupėje) (13B pav.).

Nors sinergistinio efekto tarp CAIX slopiklio ir CCR2 antagonisto nepastebėta, šie rezultatai rodo, kad CAIX fermento slopinimą galima derinti su CCR2-CCR2 ašies slopinimu. Reikia atlikti tolesnius tyrimus, siekiant įvertinti, ar pakeitus CCR2 antagonisto vartojimo laiką, rezultatai galėtų pagerėti. Taip pat, būtų naudinga pritaikyti šią kombinaciją skirtingų navikų modeliuose.

Naviko vaizdinimo platformos sukūrimas CAIX baltymo raiškos pagrindu

Radiofarmacinių preparatų kūrimas vėžio diagnostikai ir gydymui išlieka aktualus [46]. Taikininės radionuklidų terapijos preparatų vystymas yra įvairiose klinikinių tyrimų stadijose [47]. Iki šiol mažų molekulių junginių pagrindu sukurti CAIX atpažįstantys konjugatai yra nespecifiniai, nes jie remiasi acetazolamido pagrindu [48]. Todėl yra tikslingas jautresnių, tikslesnių CAIX atpažinimui skirtų preparatų kūrimas. Pirmasis žingsnis kuriant tokius preparatus turėtų apimti labai specifinių CAIX atpažįstančių junginių projektavimą ir sintezę. Mūsų laboratorija sukūrė keletą CAIX atpažįstančių junginių kandidatų. Šiam tyrimui pasirinkome perspektyviausius CAIX atpažįstančius junginius pagal *in vitro* duomenis ir pažymėjome juos NIR fluorescencine žyme (CAIX specifinis-NIR konjuguotas junginys). Ištyrėme šių junginių efektyvumą *in vivo* pelės gimdos kaklelio vėžio HeLa ksenografto modelyje.

Anksčiau mūsų laboratorijoje buvo sukurta HeLaCAIX^{KO} ląstelių linija, neturinti CAIX raiškos vertinant pagal tėkmės citometrijos ir imunobloto duomenis (14A, B pav). Jos raiškos nebuvimas, lyginant su HeLaCAIX^{WT}, buvo nustatytas ir imunohistocheminės analizės metodu naviko mėginiuose (14C pav.).

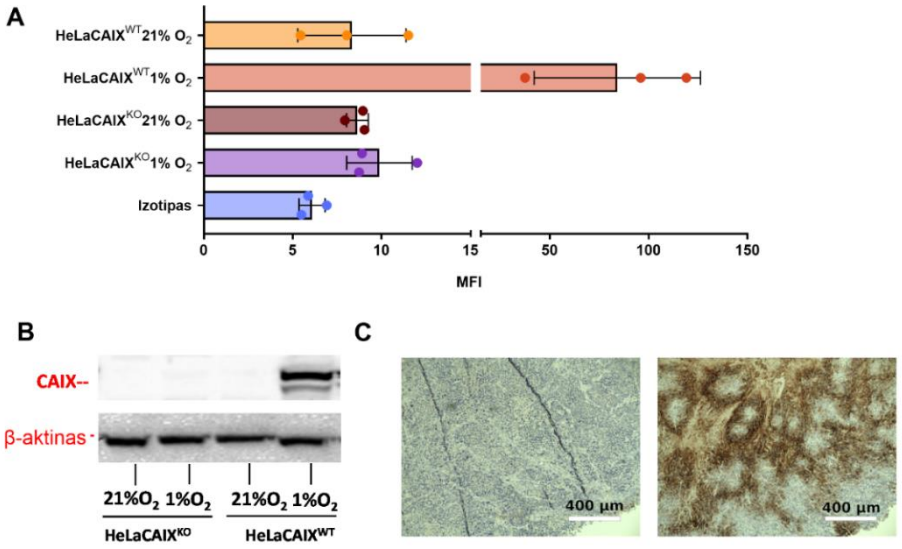

14 paveikslas. CAIX baltymo raiškos vertinimas HeLaCAIX^{WT} ir Hela CAIX^{KO} linijose. A) CAIX fluorescencijos skirtumai atliekant tėkmės citometrijos analizę. B) Imunoblotingas, rodantis CAIX baltymo kiekį HeLaCAIX^{WT} ir Hela CAIX^{KO} linijų ląstelėse normoksijoje ir hipoksijoje. C) CAIX baltymo raiška pagal naviko imunohistocheminę analizę: HeLaCAIX^{WT} dešinėje, HelaCAIX^{KO} kairėje. Skalė 400 µm.

CAIX specifiniams-NIR konjuguotiems junginiams analizuoti buvo pasirinkti du junginiai: AZ21-6 ir GZ22-4. Jie pasižymėjo geriausiomis tirpumo savybėmis ir geriausiu *in vitro* prisijungimu prie ląstelių. Suleidome HeLaCAIX^{WT} ląsteles ir HeLaCAIX^{KO} ląsteles į priešingus Nude pelių šonus. Kai navikai pasiekė apčiuopiamą dydį, atlikome vaizdinimą naudodami Alliance^{TM}Q9 Imager sistemą. Vaizdai buvo gaunami kas 24 valandas po i.v. konjugatų injekcijos į pelės uodegos veną. Naudojant abu junginius buvo nustatytas skirtingas junginio susikaupimas HeLaCAIX^{WT} ir HeLaCAIX^{KO} navikuose (15 ir 16 pav.).

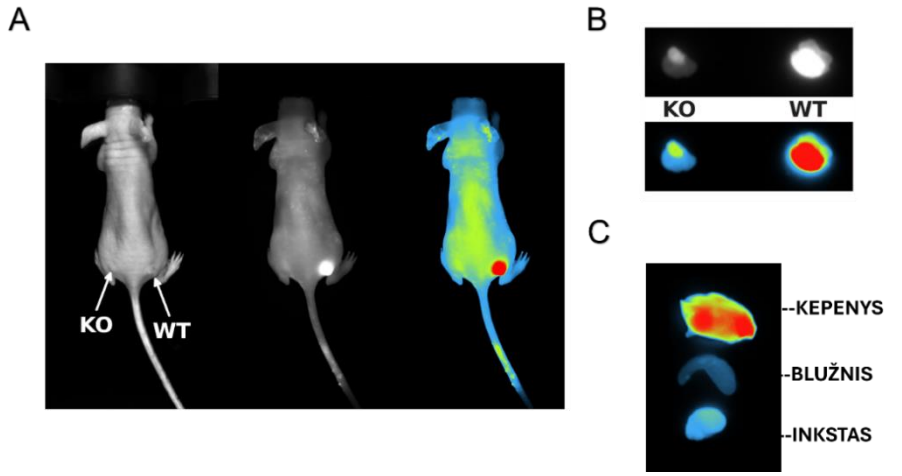

15 paveikslas. GZ22-4 junginio susikaupimas Nude pelėse. A) GZ22-4 junginio susikaupimas Nude pelėse su HeLaCAIX^{WT} naviku dešinėje palyginti su HeLaCAIX^{KO} naviku kairėje praėjus 3 dienoms po junginio injekcijos. Rodomi trys tos pačios pelės vaizdai su trimis vaizdavimo būdais: kairėje- tiesoginės šviesos nuotrauka, viduryje- vienspalvis fluorescencinis vaizdas, dešinėje pusėje- spalvotas fluorescencinis vaizdas. B) Įsotinimo GZ22-4 junginiu intensyvumas HeLaCAIX^{WT}navike (dešinėje) lyginant su su HeLaCAIX^{KO} naviku (kairėje) *ex vivo*. C) GZ22-4 junginio įsisavinimo intensyvumas tirtos pelės kepenyse, blužnyje ir inkste *ex vivo*. Vaizdai, gauti praėjus 3 dienoms po junginio injekcijos į veną.

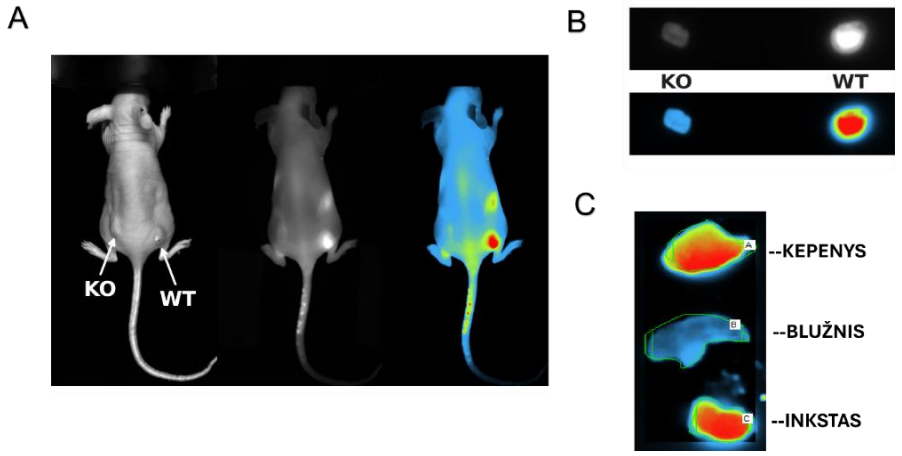

16 paveikslas. AZ21-6 junginio susikaupimas Nude pelėse. A) AZ21-6 junginio susikaupimas Nude pelėse su HeLaCAIX^{WT} naviku dešinėje palyginti su HeLaCAIX^{KO} naviku kairėje praėjus 7 dienoms po junginio

injekcijos. Rodomi trys tos pačios pelės vaizdai su trimis vaizdavimo būdais: kairėje- tiesoginės šviesos nuotrauka, viduryje- vienspalvis fluorescencinis vaizdas, dešinėje pusėje- spalvotas fluorescencinis vaizdas. B) Įsotinimo AZ21-6 junginiu intensyvumas HeLaCAIX^{WT}navike (dešinėje) lyginant su su HeLaCAIX^{KO} naviku (kairėje) *ex vivo*. C) AZ21-6 junginio įsisavinimo intensyvumas tirtos pelės kepenyse, blužnyje ir inkste *ex vivo*. Vaizdai, gauti praėjus 7 dienoms po junginio injekcijos į veną.

Nors CAIX specifiniai-NIR konjuguoti junginiai parodė didelį selektyvumą HeLaCAIX^{WT} navikams lyginant su HeLaCAIX^{KO} navikais, šis tyrimas išryškino keletą problemų. Mes pastebėjome ilgalaikį abiejų junginių kaupimąsi kepenyse, kas yra nepageidautinas efektas (Pav.15C ir 16C). Todėl reikia toliau tobulinti šių junginių dizainą.

DISKUSIJA

Nepaisant naujų imunoterapijos metodų, nemaža vaikų, sergančių standžiaisiais navikais, tokiais kaip osteosarkoma ir neuroblastoma, vis dar yra nepagydomi. Naviko hipoksija yra varomoji jėga, lemianti naviko progresavimą ir atsparumą gydymui. CAIX yra vienas iš ryškiausių hipoksijos žymenų įvairiuose navikuose. Dešimtmečius buvo bandoma sukurti selektyvius CAIX slopiklius priešvėžinei terapijai be didelės sėkmės. Panašiai, ir įvairiuose navikuose aktyvuoto CCL2-CCR2 signalinio kelio slopinimas nėra pakankamai efektyvus, kad būtų galima veiksmingai gydyti vėžį. Tokios gydymo nesėkmės gali būti siejamos su plastišku vėžio atsaku į gydymą bei aktyvia hipoksijos signalų sąveika. Gydymo metu navikuose išsivysto atsparumas, kai yra aktyvuojami alternatyvūs signaliniai keliai, palaikantys naviko augimą, nepaisant pirminio taikinio slopinimo. Pavyzdžiui, gydymo angiogenezę slopinančiu antikūnu prieš VEGF metu atsiranda navikų, turinčių alternatyvius angiogeninius signalinius kelius, tokius kaip fibroblastų augimo faktorius (FGF) [49].

Mūsų tyrimuose su 143B ksenografto modeliu nustatėme atsparumo mechanizmus, kai buvo slopinama CAIX fermentas *in vivo*. Taip pat nustatėme CCR2 baltymo raiškos padidėjimą gydytuose navikuose. Bandymas derinti CAIX slopinimą su Avastinu *in vivo* taip pat nebuvo sėkmingas. CAIX fermento slopinimo nulemti atsparumo mechanizmai yra mažai ištirti, tačiau tikėtina, kad vyksta kitų karboanhidrazių, kaip CAXII, išaugimas [50]. Kita CAIX fermento slopiklių neveiksmingumo priežastis gali būti susijusi su sunkumais kuriant specifinius slopiklius. Dauguma kliniškai

naudojamų karboanhidrazės slopiklių nėra selektyvūs, nes tarp CA izofermentų yra didelė homologinė aminorūgščių seka [20]. CA katalizinio domeno sekos tapatumas yra didesnis nei 30 % [51, 52].

Skirtingai nuo 143B ląstelių linijos, neuroblastomos ląstelių linija SK-N-AS turi ženkliai didesnę CAIX baltymo raišką esant hipoksijos sąlygoms. Todėl tyrėme CAIX fermento slopinimą ir šiame modelyje. Naudojome vėžinių ląstelių ir PBMC ko-kultūros modelį, kuriame nėra tiesioginio ląstelių kontakto, bet vyksta parakrininė sąveika. Siekėme ištirti CAIX fermento slopinimo poveikį, esant naviko ir imuninių ląstelių sąveikai. PBMC buvimas ko-kultūroje padidino hipoksijos atsaką vėžinėse ląstelėse. Nustatėme padidėjusią CAIX, CCR2, PD-L1 baltymų raišką vėžinių ląstelių paviršiuje bei padidėjusią VEGF citokino ir CXCL8, CCL2 chemokinų sekreciją. Mechanizmai nėra aiškūs, bet tikėtina, kad tai vyksta per įvairius sekrecinius signalus. Įdomu tai, kad nenustatėme uždegiminių (TNF-α, IL-6, IFN-γ) ir priešuždegiminių citokinų (IL-4, IL-10, TGF-β) sekrecijos. Svarbu tai, kad gydymas AZ19-3-2 susilpnino chemokinų CXCL8 ir CCL2 sekreciją, bet ne kitus hipoksijos žymenis.

CAIX slopiklio ir CCR2 receptoriaus antagonisto derinys SK-N-AS ksenografto modelyje parodė lėtesnį naviko augimą kombinacijos grupėje lyginant su monoterapija. Navikų tėkmės citometrijos analizė parodė reikšmingą CD44 baltymo raiškos sumažėjimą pelių, gydytų kombinacija, navikuose. Tikėtina, kad tai gydymo efektas, o ne adaptyvus atsparumas. CD44 baltymas priklauso heterogeninei paviršinių glikoproteinų grupei, dalyvaujančiai ląstelių-ląstelių ir ląstelių-užląstelinės terpės sąveikoje. NBL atveju CD44 baltymo raiška ir funkcinis aktyvumas yra ryškesni MYCN transkripcijos faktoriaus raiškos nevykdančiuose navikuose ir ląstelių linijose [53], nes MYCN transkripcijos faktorius slopina CD44 baltymo raišką. Neseniai paskelbti tyrimų duomenys parodė, kad CD44 baltymo raiška, nepaisant MYCN statuso, nulemia blogesnę prognozę pacientams, turintiems MYCN raiškos nevykdančius NBL navikus[54].

CD11b+ ląstelių analizė navike parodė reikšmingą CD86+ raiškos sumažėjimą ląstelių paviršiuje navikuose, gautuose iš pelių, gydytų CAIX slopiklio ir CCR2 antagonisto kombinacija, palyginus su kitomis grupėmis. CD11b yra mieloidinių-monocitinių ląstelių diferenciacijos žymuo [55]. CD86 baltymas yra vienas iš I tipo transmembraninių baltymų, CD28 ligandas, susijęs su imuninės sistemos T ląstelių aktyvacija [56]. Todėl CD86+ ląstelių sumažėjimas gali būti nepageidaujamas naviko atsparumo mechanizmas, nes CD11b+CD86+ ląstelės yra svarbios aktyvuojant adaptyvų imuninį atsaką.

Mes taip pat bandėme įvertinti CCR2-CCL2 signalinio kelio slopinimo poveikį 143B osteosarkomos modelyje. Pirmiausia ištyrėme CCR2 antagonisto poveikį 143B ląstelių linijos gebėjimui išskirti chemokinus CXCL8, CCL2 ir VEGF. Visi šie chemokinai yra angiogeniniai ir susiję su vėžio metastazėmis [57, 58]. Yra nustatyta, jog CXCL8 chemokino ir VEGF citokino koncentracija yra padidėjusi osteosarkoma sergančių pacientų kraujo serume [59]. Toliau palyginome šių baltymų sekrecijos skirtumus vėžinių ląstelių ir PBMC ko-kultūros modelyje. Lyginant su 143B monokultūra, nustatėme CXCL8 chemokino sekrecijos padidėjimą ko-kultūroje. Įdomu tai, kad CCR2 antagonistas veiksmingai sumažino PBMC CXCL8 baltymo sekreciją tik normoksijos atveju. CCL2 chemokino sekrecija buvo ryškesnė PBMC, bet ne 143B ląstelėse. Nors CCL2 baltymo lygis padidėjo ko-kultūroje normoksijos metu, jis ženkliai sumažėjo hipoksijoje. Tokio CCL2 baltymo sekrecijos reguliavimo mechanizmas hipoksijos atveju yra neaiškus. Gydymas CCR2 antagonistu dramatiškai padidino CCL2 gamybą eksperimentinėmis sąlygomis. Manome, kad tai yra kompensacinis CCR2 receptorių blokavimo poveikis, kai siekiama kompensuoti neaktyvų/užblokuotą receptorių, padidinant jo raišką.

VEGF-VEGFR signalinis kelias yra susijęs su naviko angiogeneze ir yra prognostinis žymuo osteosarkoma sergantiems pacientams [60]. Pažymėtina, kad VEGF citokino sekrecijos pobūdis skyrėsi nuo CCL2 ir CXCL8 chemokinų sekrecijos, nes šį citokiną daugiausia gamino 143B ląstelės, o ne PBMC monokultūrose. Bendroje kultūroje nustatėme, kad padidėjusi VEGF baltymo sekrecija buvo ryškesnė hipoksijoje nei normoksijoje. Savo ruožtu CCR2 antagonistas veiksmingiau mažino VEGF baltymo sekreciją esant hipoksijai ko-kultūroje. Apibendrinant, nustatėme skirtingą CCR2 antagonisto poveikį CXCL8 ir VEGF baltymų sekrecijai normoksijoje ir hipoksijoje.

Mūsų tyrimas taip pat atskleidė PD-L1, CD44, CAIX ir CCR2 baltymo raiškos pokyčius 143B ląstelių paviršiuje ko-kultūros modelyje, palyginti su ląstelių monokultūra. CD44 yra transmembraninis glikoproteinas, hialurono rūgšties receptorius, kuris vaidina svarbų vaidmenį ląstelių tarpusavio sąveikoje per osteopontiną,kolagenus irmatrikso metaloproteinazes (MMP) kurios yra susijęs su naviko progresavimu ir metastazėmis ikiklinikiniuose osteosarkomos tyrimuose [42]. Tai, taip pat, susiję su blogesniu osteosarkoma sergančių pacientų išgyvenamumu [61]. Padidėjusi CD44 baltymo raiška skatina osteosarkomos ląstelių migraciją ir proliferaciją bei teigiamai koreliuoja su osteosarkomos imuninės patikros taško baltymais, tokiais kaip PD-L1 [62, 63]. Remdamiesi šia samprata, nustatėme, kad 143B ląstelės turi

didelę abiejų žymenų, PD-L1 ir CD44, raišką, o hipoksija sukelia mažesnį šių žymenų raiškos reguliavimą. Mūsų tyrime CCR2 antagonisto pridėjimas padidino PD-L1 ir CD44 baltymų raišką normoksijoje, bet neturėjo poveikio esant hipoksijai.

Toliau nustatėme reikšmingą CAIX baltymo raiškos padidėjimą 143B ląstelių paviršiuje hipoksijos metu, o dar labiau ko-kultūroje su PBMC. CCR2 antagonistas sumažino CAIX baltymo raišką 143B ląstelėse esant hipoksijai, nors šis pokytis nebuvo statistiškai reikšmingas. Reikia toliau nagrinėti galimą CCR2-CCL2 signalinio kelio ir CAIX fermento ryšio mechanizmą. Mūsų tyrime CCR2 baltymo raiška šiek tiek sumažėjo 143B ląstelėse esant hipoksijai. Priešingai, esant hipoksijai, CD45+CD11b+ ląstelėse žymiai padidėjo CCR2 baltymo paviršiaus raiška, o tai rodo, kad šis ląstelių pogrupis gali būti jautresnis hipoksijai. Gydymas CCR2 antagonistu padidino CCR2 paviršiaus raišką 143B ląstelėse ko-kultūroje esant skirtingoms deguonies sąlygoms, ir tikėtina, kad tai buvo kompensacinis poveikis. Nors ankstesni tyrimai parodė apie sumažėjusią CCR2 baltymo raišką M2 makrofaguose esant hipoksijai [64], nustatėme priešingą poveikį. Nors CCL2-CCR2 signalinio kelio slopinimas osteosarkomoje tebėra patrauklus imunoterapinis gydymas, šiandien daugybė įrodymų rodo, kad CCR2 receptoriaus slopinimas kaip monoterapija neveikia [28]. Sutikdami su šiais pastebėjimais, mūsų tyrime pelių gydymas CCR2 antagonistu *in vivo* nesulėtino naviko augimo lyginant su nešiklio kontrole. Greičiausiai tai yra dėl įvairių deguonies koncentracijų navike. Jos galimai turi įtakos gydymo atsakui, kaip matėme ko-kultūros eksperimentuose. Pelių, gydytų CCR2 antagonistu, navikų tėkmės citometrijos analizė parodė naviko CD44, VEGFR ir PD-L1 baltymo raiškos pokyčius. CCR2 antagonisto poveikis padidino VEGFR+ ir PD-L1+ naviko ląstelių frakciją, o tai gali būti atsparumo mechanizmai, kai aktyvuojami pro-angiogeniniai/imunosupresinis signaliniai keliai.

CCR2 antagonisto poveikis modifikavo CD44+ ląstelių frakciją. Taip pat įdomu tai, kad aptikome dvi naviko ląstelių populiacijas, turinčias skirtingą CD44 raišką: $CD44^{\text{nežymi raiška}}$ ir $CD44^{\text{žymi raiška}}$. CCR2 receptoriaus slopinimas išlygino ląstelių procentą kiekvienoje populiacijoje, padidindamas santykinį $CD44^{\text{žymi raiška}}$ ląstelių skaičių.

Atlikdami naviko stromos analizę, nustatėme CD11b+CD86+ ląstelių populiacijos padidėjimą po CCR2 slopinimo. CD86 yra kostimuliacinė molekulė, kurią CD11b+ ląstelės gamina kaip atsaką į uždegimą skatinančius signalus [56]. TAM, ekspresuojantys CD86, gali atlikti tiek pro-tumorigenines, tiek anti-tumorogenines funkcijas, priklausomai nuo jų

aktyvacijos būsenos [65]. Todėl šių ląstelių pogrupių skaičiaus padidėjimas gali būti pageidaujamas su CCR2 blokavimu susijusio gydymo poveikis.

Kadangi CCR2 antagonisto neveiksmingumas *in vivo* gali būti susijęs su hipoksine naviko mikroaplinka, atlikome išsamią su vėžiu susijusių taikinių proteominę analizę naviko ląstelėse, pakartodami ko-kultūros eksperimentą. Proteominė analizė atskleidė diferencinius raiškos modelius naviko ląstelėse. Su hipoksija susiję baltymai, tokie kaip CAIX ir HIF1A, dar labiau sustiprėja hipoksijoje veikiant CCR2 antagonistui. Įdomu tai, kad remiantis proteomikos duomenimis, VEGF sekrecija sumažėjo ko-kultūroje veikiant CCR2 antagonistui. Nustatėme tą pačią pelių navikų VEGFR raiškos mažėjimo tendenciją pelėse gavusiose CCR2 antagonistą.

Galiausiai bandėme ištirti naviko CAIX aptikimo *in vivo* galimybes gimdos kaklelio vėžio HeLa ksenografto modelyje. *In vivo* tyrimai su CAIX specifiniais-NIR konjuguotais junginiais parodė žymiai ryškesnę jų lokalizaciją HeLaCAIX^{WT} navikuose lyginant su HeLaCAIX^{KO} navikais. Su NIR fluorescencine žyme konjuguotas GZ22-4 junginys buvo jautresnis CAIX atžvilgiu ir turėjo greitesnį pasišalinimą lyginant su AZ21-6 junginiu *in vivo*. Šie tyrimai reikšmingi toliau plėtojant vėžio vaizdinimo technologijas, nukreiptas į CAIX baltymo atpažinimą.

IŠVADOS

Nepaisant imunoterapijos sukelto proveržio vėžio gydyme, navikai išlieka viena iš pagrindinių vaikų mirties priežasčių visame pasaulyje [1]. Priešvėžinio gydymo metu navikuose yra pajungiami įvairūs kompensaciniai mechanizmai, padedantys apeiti vaistų poveikį. Naviko hipoksija ir su ja susijęs tarpląstelinės terpės užrūgštėjimas reikšmingai prisideda prie vėžio progresavimo ir atsparumo gydymui. CAIX, hipoksijos indukuotas fermentas, padeda vėžinėms ląstelėms išgyventi hipoksijos sąlygomis. CCL2-CCR2 signalinis kelias yra svarbus navikų imunosupresinės nišos formavime. Tiek CAIX fermentas, tiek CCL2-CCR2 signalinis kelias yra patrauklūs taikiniai priešvėžinei terapijai. Mūsų darbas nagrinėjo šių taikinių slopinimo galimybes vaikų standžiųjų navikų osteosarkomos ir neuroblastomos modeliuose.

Mes atskleidėme daugialypį CAIX vaidmenį naviko ir monocitų/makrofagų komunikacijoje. Tai yra pirmasis tyrimas, kuriame bandoma pritaikyti CAIX slopinimo ir CCR2 antagonisto derinį neuroblastomos ksenografte *in vivo.* Mūsų tyrimas atskleidžia galimus adaptyvaus atsparumo mechanizmus naudojant šiuos junginius.

Mes, taip pat, parodėme, kad hipoksinės sąlygos keičia skirtingų ląstelių žymenų ekspresiją ir pablogina CCR2 antagonistinį poveikį eksperimentiniame osteosarkomos modelyje. CCR2 slopinimas 143B ląstelių modelyje turi skirtingą poveikį baltymų paviršiaus raiškai ir citokinų sekrecijai, priklausomai nuo deguonies kiekio. CCR2-CCL2 signalinio kelio blokavimas naudojant CCR2 antagonistą nestabdo 143B naviko augimo, bet keičia auglio mikroaplinką dėl sumažėjusios VEGFR raiškos ir CD44 ekspresuojančių ląstelių populiacijos padidėjimo.

143B ląstelių ko-kultūros proteomo tyrimai atskleidė įvairių baltymų, dalyvaujančių angiogenezėje, hipoksijoje, adhezijoje diferencinius pokyčius esant skirtingoms deguonies koncentracijoms. Mūsų duomenys rodo CCL2-CCR2 signalinio kelio blokavimo galimybes deriniuose su VEGFR, HIF arba CAIX slopikliais. Mūsų darbas parodė galimą vėžinių ląstelių ir PBMC ko-kultūros modelio pritaikymą siekiant atskleisti naviko ląstelių fenotipą tiksliau, labiau atitinkant gyvo auglio aplinką. Galiausiai mes parodėme galimą CAIX fermentui specifinių, su NIR žyme sujungtų, junginių pritaikymą gyvame organizme. Visi šie tyrimai gali prisidėti prie ateities vėžio gydymo ir diagnostikos nukreiptos į hipoksinę naviko nišą.

Išvados:

1. CAIX slopiklis AZ19-3-2 nebuvo veiksmingas osteosarkomos 143B ksenografto modelyje pelėje nei kaip vienas agentas nei kombinacijoje su Avastinu.
2. Lyginant su nešiklio kontrole, 200 nM CAIX slopiklio AZ19-3-2 slopino neuroblastomos SK-N-AS ląstelių sferoidų augimą 1.38 karto hipoksijoje, bet ne normoksijoje.
3. CAIX slopiklio AZ19-3-2 ir CCR2 antagonisto kombinacija dvigubai sumažino naviko augimą neuroblastomos SK-N-AS ksenografto modelyje pelėje.
4. CAIX slopinimas naudojant AZ19-3-2 1.8 karto sumažino CXCL8 ir 2.19 karto sumažino CCL2 baltymų sekreciją SK-N-AS- PBMC ko-kultūros tyrime.
5. CCR2 antagonistas nebuvo veiksmingas žmogaus osteosarkomos 143B ksenografto modelyje pelėje.
6. CAIX specifiniai ir su NIR fluorescencine žyme konjuguoti junginiai AZ21-6 ir GZ22-4 gebėjo atskirti CAIX baltymo raiška pasižyminčius navikus nuo CAIX baltymo raiškos neturinčių navikų pelėje.
7. Hipoksijoje, CAIX baltymo procentinė raiška ant osteosarkomos 143B ir neuroblastomos SK-N-AS vėžinių ląstelių paviršiaus

padidėjo atitinkamai 3.6 bei 1.9 karto kai jos buvo auginamos kokultūroje su PBMC lyginant su monokultūra.

Ateities tyrimų kryptys galimai apims: 1) su hipoksija susijusių naviko atsparumo gydymui mechanizmų iššifravimą, 2) skirtingų gydymo derinių, įtraukiančių CCR2 antagonistą bei CAIX slopiklius, ištyrimą, 3) CAIX atpažinimu pagrįstos vėžio diagnostikos vystymą.

LITERATŪROS ŠALTINIAI

1. Sherif, S., et al., *The immune landscape of solid pediatric tumors.* J Exp Clin Cancer Res, 2022. **41**(1): p. 199.
2. McDonald, P.C., S.C. Chafe, and S. Dedhar, *Overcoming Hypoxia-Mediated Tumor Progression: Combinatorial Approaches Targeting pH Regulation, Angiogenesis and Immune Dysfunction.* Front Cell Dev Biol, 2016. **4**: p. 27.
3. Barsoum, I.B., et al., *A mechanism of hypoxia-mediated escape from adaptive immunity in cancer cells.* Cancer Res, 2014. **74**(3): p. 665-74.
4. Noman, M.Z., et al., *Hypoxia: a key player in antitumor immune response. A Review in the Theme: Cellular Responses to Hypoxia.* Am J Physiol Cell Physiol, 2015. **309**(9): p. C569-79.
5. Sedlakova, O., et al., *Carbonic anhydrase IX, a hypoxia-induced catalytic component of the pH regulating machinery in tumors.* Front Physiol, 2014. **4**: p. 400.
6. Mancino, A., et al., *Divergent effects of hypoxia on dendritic cell functions.* Blood, 2008. **112**(9): p. 3723-34.
7. Doedens, A.L., et al., *Macrophage expression of hypoxia-inducible factor-1 alpha suppresses T-cell function and promotes tumor progression.* Cancer Res, 2010. **70**(19): p. 7465-75.
8. Facciabene, A., et al., *Tumour hypoxia promotes tolerance and angiogenesis via CCL28 and T(reg) cells.* Nature, 2011. **475**(7355): p. 226-30.
9. Pinato, D.J., et al., *Programmed cell death ligands expression in phaeochromocytomas and paragangliomas: Relationship with the hypoxic response, immune evasion and malignant behavior.* Oncoimmunology, 2017. **6**(11): p. e1358332.
10. Pastorekova, S. and R.J. Gillies, *The role of carbonic anhydrase IX in cancer development: links to hypoxia, acidosis, and beyond.* Cancer Metastasis Rev, 2019. **38**(1-2): p. 65-77.

11. Nordfors, K., et al., *The tumour-associated carbonic anhydrases CA II, CA IX and CA XII in a group of medulloblastomas and supratentorial primitive neuroectodermal tumours: an association of CA IX with poor prognosis.* BMC Cancer, 2010. **10**: p. 148.
12. Proescholdt, M.A., et al., *Function of carbonic anhydrase IX in glioblastoma multiforme.* Neuro Oncol, 2012. **14**(11): p. 1357-66.
13. Okuno, K., et al., *Carbonic anhydrase IX enhances tumor cell proliferation and tumor progression in osteosarcoma.* Onco Targets Ther, 2018. **11**: p. 6879-6886.
14. Hedlund, E.E., et al., *Harnessing Induced Essentiality: Targeting Carbonic Anhydrase IX and Angiogenesis Reduces Lung Metastasis of Triple Negative Breast Cancer Xenografts.* Cancers (Basel), 2019. **11**(7).
15. Dungwa, J.V., L.P. Hunt, and P. Ramani, *Carbonic anhydrase IX up-regulation is associated with adverse clinicopathologic and biologic factors in neuroblastomas.* Hum Pathol, 2012. **43**(10): p. 1651-60.
16. Cetin, B., et al., *Carbonic anhydrase IX is a prognostic biomarker in glioblastoma multiforme.* Neuropathology, 2018. **38**(5): p. 457-462.
17. Damgaci, S., et al., *Hypoxia and acidosis: immune suppressors and therapeutic targets.* Immunology, 2018. **154**(3): p. 354-362.
18. Chafe, S.C., et al., *Targeting Hypoxia-Induced Carbonic Anhydrase IX Enhances Immune-Checkpoint Blockade Locally and Systemically.* Cancer Immunol Res, 2019. **7**(7): p. 1064-1078.
19. McDonald, P.C., et al., *A Phase 1 Study of SLC-0111, a Novel Inhibitor of Carbonic Anhydrase IX, in Patients With Advanced Solid Tumors.* Am J Clin Oncol, 2020. **43**(7): p. 484-490.
20. Mboge, M.Y., R. McKenna, and S.C. Frost, *Advances in Anti-Cancer Drug Development Targeting Carbonic Anhydrase IX and XII.* Top Anticancer Res, 2015. **5**: p. 3-42.
21. Dudutienė, V., et al., *Discovery and characterization of novel selective inhibitors of carbonic anhydrase IX.* J Med Chem, 2014. **57**(22): p. 9435-46.
22. Janoniene, A., et al., *Inhibition of Carbonic Anhydrase IX Suppresses Breast Cancer Cell Motility at the Single-Cell Level.* Int J Mol Sci, 2021. **22**(21).
23. Kazokaitė, J., et al., *Novel fluorinated carbonic anhydrase IX inhibitors reduce hypoxia-induced acidification and clonogenic survival of cancer cells.* Oncotarget, 2018. **9**(42): p. 26800-26816.

24. Chen, K.T. and Y. Seimbille, *New Developments in Carbonic Anhydrase IX-Targeted Fluorescence and Nuclear Imaging Agents.* Int J Mol Sci, 2022. **23**(11).
25. Matulienė, J., et al., *Picomolar fluorescent probes for compound affinity determination to carbonic anhydrase IX expressed in live cancer cells.* Sci Rep, 2022. **12**(1): p. 17644.
26. Yoshimura, T., *The chemokine MCP-1 (CCL2) in the host interaction with cancer: a foe or ally?* Cell Mol Immunol, 2018. **15**(4): p. 335-345.
27. Xu, M., et al., *Role of the CCL2-CCR2 signalling axis in cancer: Mechanisms and therapeutic targeting.* Cell Prolif, 2021. **54**(10): p. e13115.
28. Fei, L., et al., *Targeting the CCL2/CCR2 Axis in Cancer Immunotherapy: One Stone, Three Birds?* Front Immunol, 2021. **12**: p. 771210.
29. Jin, J., et al., *CCL2: An Important Mediator Between Tumor Cells and Host Cells in Tumor Microenvironment.* Front Oncol, 2021. **11**: p. 722916.
30. Korbecki, J., et al., *CC Chemokines in a Tumor: A Review of Pro-Cancer and Anti-Cancer Properties of the Ligands of Receptors CCR1, CCR2, CCR3, and CCR4.* Int J Mol Sci, 2020. **21**(21).
31. Mojsilovic-Petrovic, J., et al., *Hypoxia-inducible factor-1 (HIF-1) is involved in the regulation of hypoxia-stimulated expression of monocyte chemoattractant protein-1 (MCP-1/CCL2) and MCP-5 (Ccl12) in astrocytes.* J Neuroinflammation, 2007. **4**: p. 12.
32. Sceneay, J., et al., *Primary tumor hypoxia recruits CD11b+/Ly6Cmed/Ly6G+ immune suppressor cells and compromises NK cell cytotoxicity in the premetastatic niche.* Cancer Res, 2012. **72**(16): p. 3906-11.
33. Oda, S., et al., *An in vitro coculture system of human peripheral blood mononuclear cells with hepatocellular carcinoma-derived cells for predicting drug-induced liver injury.* Arch Toxicol, 2021. **95**(1): p. 149-168.
34. Rasouli, M. and F. Safari, *Principles of Indirect Co-culture Method Using Transwell.* Methods Mol Biol, 2024.
35. Meltzer, P.S. and L.J. Helman, *New Horizons in the Treatment of Osteosarcoma.* N Engl J Med, 2021. **385**(22): p. 2066-2076.

36. Perut, F., et al., *Carbonic anhydrase IX inhibition is an effective strategy for osteosarcoma treatment.* Expert Opin Ther Targets, 2015. **19**(12): p. 1593-605.
37. Uluçkan, Ö., et al., *Preclinical mouse models of osteosarcoma.* Bonekey Rep, 2015. **4**: p. 670.
38. Tome, Y., et al., *Use of αv Integrin Linked to Green Fluorescent Protein in Osteosarcoma Cells and Confocal Microscopy to Image Molecular Dynamics During Lung Metastasis in Nude Mice.* Anticancer Res, 2016. **36**(8): p. 3811-6.
39. McIntyre, A., et al., *Carbonic anhydrase IX promotes tumor growth and necrosis in vivo and inhibition enhances anti-VEGF therapy.* Clin Cancer Res, 2012. **18**(11): p. 3100-11.
40. Mirzadegan, T., et al., *Identification of the binding site for a novel class of CCR2b chemokine receptor antagonists: binding to a common chemokine receptor motif within the helical bundle.* J Biol Chem, 2000. **275**(33): p. 25562-71.
41. Tu, M.M., et al., *Inhibition of the CCL2 receptor, CCR2, enhances tumor response to immune checkpoint therapy.* Commun Biol, 2020. **3**(1): p. 720.
42. Gvozdenovic, A., et al., *CD44 enhances tumor formation and lung metastasis in experimental osteosarcoma and is an additional predictor for poor patient outcome.* J Bone Miner Res, 2013. **28**(4): p. 838-47.
43. Campanile, C., et al., *Characterization of Different Osteosarcoma Phenotypes by PET Imaging in Preclinical Animal Models.* Journal of Nuclear Medicine, 2013. **54**(8): p. 1362-1368.
44. McDonald, P. and S. Dedhar, *Carbonic Anhydrase IX (CAIX) as a Mediator of Hypoxia-Induced Stress Response in Cancer Cells*, in *CARBONIC ANHYDRASE: MECHANISM, REGULATION, LINKS TO DISEASE, AND INDUSTRIAL APPLICATIONS*. 2014. p. 255-269.
45. Chen, Y., et al., *Significant difference between sirolimus and paclitaxel nanoparticles in anti-proliferation effect in normoxia and hypoxia: The basis of better selection of atherosclerosis treatment.* Bioact Mater, 2021. **6**(3): p. 880-889.
46. Bai, J.W., S.Q. Qiu, and G.J. Zhang, *Molecular and functional imaging in cancer-targeted therapy: current applications and future directions.* Signal Transduct Target Ther, 2023. **8**(1): p. 89.

47. Sun, J., et al., *Imaging-guided targeted radionuclide tumor therapy: From concept to clinical translation.* Adv Drug Deliv Rev, 2022. **190**: p. 114538.
48. Doss, M., et al., *Biodistribution and radiation dosimetry of the carbonic anhydrase IX imaging agent [(18) F]VM4-037 determined from PET/CT scans in healthy volunteers.* Mol Imaging Biol, 2014. **16**(5): p. 739-46.
49. Bergers, G. and D. Hanahan, *Modes of resistance to anti-angiogenic therapy.* Nat Rev Cancer, 2008. **8**(8): p. 592-603.
50. Li, G., et al., *Carbonic Anhydrase XII is a Clinically Significant, Molecular Tumor-Subtype Specific Therapeutic Target in Glioma with the Potential to Combat Invasion of Brain Tumor Cells.* Onco Targets Ther, 2021. **14**: p. 1707-1718.
51. Aggarwal, M., B. Kondeti, and R. McKenna, *Insights towards sulfonamide drug specificity in α-carbonic anhydrases.* Bioorg Med Chem, 2013. **21**(6): p. 1526-33.
52. Pinard, M.A., B. Mahon, and R. McKenna, *Probing the surface of human carbonic anhydrase for clues towards the design of isoform specific inhibitors.* Biomed Res Int, 2015. **2015**: p. 453543.
53. Gross, N., K. Balmas, and C.B. Brognara, *Absence of functional CD44 hyaluronan receptor on human NMYC-amplified neuroblastoma cells.* Cancer Res, 1997. **57**(7): p. 1387-93.
54. Valentiner, U., F.U. Valentiner, and U. Schumacher, *Expression of CD44 is associated with a metastatic pattern of human neuroblastoma cells in a SCID mouse xenograft model.* Tumour Biol, 2008. **29**(3): p. 152-60.
55. Lim, T.S., et al., *CD80 and CD86 differentially regulate mechanical interactions of T-cells with antigen-presenting dendritic cells and B-cells.* PLoS One, 2012. **7**(9): p. e45185.
56. Orecchioni, M., et al., *Macrophage Polarization: Different Gene Signatures in M1(LPS+) vs. Classically and M2(LPS-) vs. Alternatively Activated Macrophages.* Front Immunol, 2019. **10**: p. 1084.
57. Gálvez, B.G., et al., *Membrane type 1-matrix metalloproteinase is regulated by chemokines monocyte-chemoattractant protein-1/ccl2 and interleukin-8/CXCL8 in endothelial cells during angiogenesis.* J Biol Chem, 2005. **280**(2): p. 1292-8.

58. Pausch, T.M., et al., *Metastasis-associated fibroblasts promote angiogenesis in metastasized pancreatic cancer via the CXCL8 and the CCL2 axes.* Sci Rep, 2020. **10**(1): p. 5420.
59. Jiang, H., et al., *CXCL8 promotes the invasion of human osteosarcoma cells by regulation of PI3K/Akt signaling pathway.* APMIS, 2017. **125**(9): p. 773-780.
60. Zhang, C., et al., *The role of vascular endothelial growth factor as a prognostic and clinicopathological marker in osteosarcoma: a systematic review and meta-analysis.* J Orthop Surg Res, 2021. **16**(1): p. 738.
61. Gao, Y., et al., *CD44 is a direct target of miR-199a-3p and contributes to aggressive progression in osteosarcoma.* Sci Rep, 2015. **5**: p. 11365.
62. Brahmer, J.R., et al., *Safety and activity of anti-PD-L1 antibody in patients with advanced cancer.* N Engl J Med, 2012. **366**(26): p. 2455-65.
63. Ji, H., et al., *CD44 expression is correlated with osteosarcoma cell progression and immune infiltration and affects the Wnt/β-catenin signaling pathway.* J Bone Oncol, 2023. **41**: p. 100487.
64. Araya, P., et al., *HMGB1 decreases CCR-2 expression and migration of M2 macrophages under hypoxia.* Inflamm Res, 2019. **68**(8): p. 639-642.
65. Cendrowicz, E., et al., *The Role of Macrophages in Cancer Development and Therapy.* Cancers (Basel), 2021. **13**(8).

ACKNOWLEDGEMENTS

"No one is useless in this world who lightens the burdens of another." Ch. Dickens.

I would like to thank Prof. Daumantas Matulis and Dr. Jurgita Matulienė for their mentorship, guidance, and support. In addition, I would like to thank Prof. Matulis's laboratory members Dr. Vytautas Petrauskas, Audrius Zakšauskas, Dr. Asta Zubrienė, Dr. Lina Baranauskienė, Dr. Joana Smirnovienė, Aurelija Mickevičiūtė, Marius Gedgaudas, Vaida Juozapatienė, Gediminas Žvinys, Agnė Kvietkauskaitė, Dr. Edita Čapkauskaitė and Dr. Švitrigailė Grincevičienė.

I am grateful for the hard work of my current and former students Marta Tamošiūnaitė, Justina Musvicaitė, Sasha Arnold, and Melissa Maria Misar.

My special gratitude goes to Dr. Asta Lučiūnaitė, a true comrade, who kept me going throughout these 5 years.

I would also like to thank Prof. A. Žvirblienė and Prof. Sonata Jarmalaitė for their helpful and timely advice. In addition, I am very grateful to Dr. Virginija Bukelskienė and Alvilė Ščerbavičienė for their help with animal studies.

I want to thank my former mentor, Prof. Alex Y. Huang, for instilling a love for science, and my clinical mentor, late Prof. Yousif H. Matloub, for helping me mature as a clinician.

I wish to express my heartfelt gratitude to all my former patients. They sustain my desire to make a change so that no family would lose their loved one to cancer.

Finally, I want to thank my family, especially my sons, Lukas, Simonas, and Paulius, for their love and support. I love them to the billion stars and back.

LIST OF PUBLICATIONS

PUBLICATIONS INCLUDED IN THE DISSERTATION

Petrosiute A, Zakšauskas A, Lučiūnaitė A, Petrauskas V, Baranauskienė L, Kvietkauskaitė A, Ščerbavičienė A, Tamošiūnaitė M, Musvicaitė J, Jankūnaitė A, Žvinys G, Stančaitis L, Čapkauskaitė E, Mickevičiūtė A, Juozapaitienė V, Dudutienė V, Zubrienė A, Grincevičienė Š, Bukelskienė V, Schiöth HB, Matulienė J, Matulis D. Carbonic anhydrase IX inhibition as a path to treat neuroblastoma. Br J Pharmacol. 2025 Jan 7. doi: 10.1111/bph.17429. Epub ahead of print. PMID: 39776083.

Petrosiute A, Musvicaitė J, Petroška D, Ščerbavičienė A, Arnold S, Matulienė J, Žvirblienė A, Matulis D, Lučiūnaitė A. CCL2-CCR2 Axis Inhibition in Osteosarcoma Cell Model: The Impact of Oxygen Level on Cell Phenotype. J Cell Physiol. 2024 Nov 25. doi: 10.1002/jcp.31489. Epub ahead of print. PMID: 39587819.

Grincevičienė Š, Vaitkienė D, Kanopienė D, Vansevičiūtė R, Tykvart J, Sukovas A, Celiešiūtė J, Ivanauskaitė Didžiokienė E, Čižauskas A, Laurinavičienė A, Král V, Hlavačková A, Zemanová J, Stravinskienė D, Sližienė A, Petrošiūtė A, Petrauskas V, Balsytė R, Grincevičius J, Navratil V, Jahn U, Konvalinka J, Žvirblienė A, Matulis D, Matulienė J. Factors, associated with elevated concentration of soluble carbonic anhydrase IX in plasma of women with cervical dysplasia. Sci Rep. 2022 Sep 13;12(1):15397. doi: 10.1038/s41598-022-19492-y. PMID: 36100684; PMCID: PMC9470728.

PUBLICATIONS NOT INCLUDED IN THE DISSERTATION

Matulienė J, Žvinys G, Petrauskas V, Kvietkauskaitė A, Zakšauskas A, Shubin K, Zubrienė A, Baranauskienė L, Kačenauskaitė L, Kopanchuk S, Veiksina S, Paketurytė-Latvė V, Smirnovienė J, Juozapaitienė V, Mickevičiūtė A, Michailovienė V, Jachno J, Stravinskienė D, Sližienė A, Petrošiūtė A, Becker HM, Kazokaitė-Adomaitienė J, Yaromina A, Čapkauskaitė E, Rinken A, Dudutienė V, Dubois LJ, Matulis D. Picomolar fluorescent probes for compound affinity determination to carbonic anhydrase IX expressed in live cancer cells. Sci Rep. 2022 Oct 21;12(1):17644. doi: 10.1038/s41598-022-22436-1. PMID: 36271018; PMCID: PMC9586938.

Žvinys G, Petrosiute A, Zakšauskas A, Zubrienė A, Ščerbavičienė A, Kalnina Z, Čapkauskaitė E, Juozapaitienė V, Mickevičiutė A, Shubin K, Grincevičienė Š, Raišys S, Tars K, Matulienė J, Matulis D. High-Affinity NIR-Fluorescent Inhibitors for Tumor Imaging via Carbonic Anhydrase IX. Bioconjug Chem. 2024 Jun 19;35(6):790-803. doi: 10.1021/acs.bioconjchem.4c00144. Epub 2024 May 15. PMID: 38750635; PMCID: PMC11191402.

LIST OF CONFERENCES

Oral presentations:

"Tumor Imaging in Tissues and Mice". Carbonic Anhydrase Workshop December 1, 2022, Vilnius.

"Development of CAIX-targeted therapeutics and diagnostics in murine cancer model". LSC Retreat Conference April 3-4, 2023, Dubingiai.

Poster presentations:

Petrosiute A., Luciunaite A., Musvicaite A., Zaksauskas A., Baranauskiene L., Matuliene J., Matulis D. „Interplay of CAIX and CCL2-CCR2 axis in neuroblastoma xenograft model". CRI-ENCI-AACR Seventh International Cancer Immunotherapy Conference: Translating Science Into Survival September 20-23, 2023 Milano, Italy

Arnold S., Musvicaitė J., Zakšauskas A., Čapkauskaitė E., Lučiūnaitė A., **Petrosiute A** "Assessing the Impact of CAIX Inhibitor EA2-3 on the Medulloblastoma Cell Line UW228". The COINS 2024, April 15-18, 2024, Vilnius, Lithuania.

G. Žvinys, **A. Petrosiute**, A. Zakšauskas, A. Zubrienė, E. Čapkauskaitė, V. Juozapaitienė, A. Mickevičiūtė, Š. Grincevičienė, J. Matulienė, A. Ščerbavičienė, S. Raišys, Z. Kalnina, K. Tars, K. Shubin, D. Matulis. "High-affinity infrared-fluorescent probes for cancer imaging via CAIX ". Baltic Organic Syntheticum July 7-10, 2024, Riga.

Gediminas Žvinys, **Agne Petrosiute**, Audrius Zakšauskas, Asta Zubrienė, Edita Čapkauskaitė, Jurgita Matulienė, Daumantas Matulis. High-Affinity NIR-Fluorescent Probes for Cancer Imaging via Carbonic Anhydrase IX. 48th FEBS congress. June 26-July 3, 2024, Milan.

CURRICULUM VITAE

Name: Agne Petrosiute, M.D.

Education: 09/ 1996- 06/ 2002 Doctor of Medicine, Kaunas University of Medicine, Kaunas, Lithuania

Postgraduate training:

10/ 2019- to date	PhD candidate, Institute of Biotechnology, Vilnius University, Lithuania
08/ 2008- 08/ 2011	Fellow, Pediatric Hematology/ Oncology, University Hospitals of Cleveland, Rainbow Babies and Children's Hospital, Cleveland, USA
07/ 2005- 07/ 2008	Resident, Pediatrics, MetroHealth Medical Center, Case Western Reserve University, Cleveland, USA.
08/ 2003- 06/ 2005	Resident, Family Medicine, Santariskiu Clinics of Vilnius, University Hospitals, Vilnius, Lithuania
07/ 2002- 07/ 2003	Internship, Jonava Hospital, Lithuania

Professional appointments

09/ 2024- to date	Biologist, Department of Biothermodynamics and Drug Design, Institute of Biotechnology, Life Sciences Center, Vilnius University.
10/ 2019- 09/ 2024	Junior Researcher, Department of Biothermodynamics and Drug, Design, Institute of Biotechnology, Life Sciences Center, Vilnius University.
07/ 2014- 10/ 2019	Assistant Professor, Department of Pediatrics, CWRU, Cleveland, OH
09/ 2011- 07/ 2014	Instructor, Department of Pediatrics CWRU, Cleveland, OH.

Licensure and board certification:

State Medical Board of Ohio; No. 92373
Board Certified, American Board of Pediatrics, 2008- ongoing
Board Certified, Pediatric Hematology-Oncology, 2013- ongoing

Professional service:

Grant Reviewer

St. Baldrick's Foundation Scientific Review (2016, 2017, 2018, 2019)

Teaching activities:

2008 – 2019	Weekly Pediatric Hematology-Oncology Fellows Conference.
2012 – 2014	Pediatric Boards Review Course, "Pediatric Oncology Boards Review", Rainbow Babies & Children's Hospital. Contact hours: 3 hours per year (Organizer: Pediatric Chief Residents).
2011- 2019	Weekly Pediatric Hematology- Oncology clinic preceptor: 400 hours.

Research support:

Grant support from 2019 to date:

1) Young researchers' grant 2024, Lithuania. *Correlation of CAIX expression in pediatric CNS tumors with the immune markers*. 05/ 2024- 12/ 31/ 2025. Role: PI.
2) Healthy aging P-SEN-20-28, Lithuania. *Development of visualization systems for tumor and metastases detection in cancer diagnostics and optically-guided surgery using CA IX biomarker*. 02/ 03/ 2020- 12/ 31/ 2021. Role: Investigator.
3) Scholar Award St. Baldrick Foundation. *Cdk5 confers Host Immune Resistance by PD-L1 upregulation in Medulloblastoma.* 7/ 1/ 2015- 6/ 30/ 2020. Role: PI.

My co-authored publications:

1. **Petrosiute, A**, Auletta, J.J., Lazarus, H.M. Achieving graft-versus-tumor effect in brain tumor patients: from autologous progenitor cell transplant to active immunotherapy. ***Immunotherapy.*** 2012; 4(11): 1139-51. PMID: 23194364.
2. Huang, A.Y., Haining, W.N., Barkauskas, D.S., Myers, J.T., **Petrosiute, A**., Garrett, A.P., Singh, K., Cooke, K.R., Kean, L.S.

Viewing transplantation immunology through today's lens: new models, new imaging, and new insights. ***Biol. Blood Marrow Transplantation*** 2013; 19(1 Suppl): S44-51. PMID: 23092813.

3. Barkauskas, D.S., Evans, T.A., Myers, J., **Petrosiute, A.**, Silver, J., Huang, A.Y. Extravascular $CX3CR1^+$ cells extend intravascular dendritic processes into intact central nervous system vessel Lumen. ***Micros. Microanal.*** 2013, 19(4): 778-90. PMID: 23652852.
4. Bobanga, I.D., **Petrosiute, A.*,** Huang, A.Y.* Chemokines as Cancer Vaccine Adjuvants. ***Vaccines***, 2013; 1(4): 444-462. PMC4067044.
5. Myers, J.T., **Petrosiute, A.,** Huang, A.Y. Utilization of multiphoton imaging for real-time fate determination of mesenchymal stem cells in an immunocompetent mouse model. ***J. Stem Cell Res Ther*** 2014; 4(7): 217. PMC4218747.
6. Dorand, R.D., Barkauskas, D.S., Evans, T.A., **Petrosiute, A.**, Huang, A.Y. Comparison of intravital thinned skull and cranial window approaches to study CNS immunobiology in the mouse cortex. ***IntraVital.*** 2014; 3:e29728. PMC4283137.
7. Owusu-Ansah, A., Choi, S.H., **Petrosiute, A.,** Letterio, J.J., Huang, A.Y. Triterpenoid inducers of Nrf2 signaling as a potential therapeutic agents in sickle Cell disease - a review. ***Frontiers of Medicine.*** 2015; 9(1): 46-56. PMID: 25511620.
8. Dorand, R.D., Nthale, J., Myers, J.T., Barkauskas, D.S., Avril, S., Chirieleison, S.M., Pareek, T., Abbott, D.W., Stearns, D.S., Letterio, J.J., Huang, A.Y.*, **Petrosiute, A***. Cdk5 Disruption attenuates tumor PD-L1 response to IFNγ leading to $CD4^+$ T-cell mediated rejection. ***Science*** 2016; 353:399-403 (*co-senior authors). PMC5051664.
9. Vatsayan, A., Fenner, J., **Petrosiute, A**. Stomatocytosis and spherocytosis in a patient with novel heterozygous novel mutation in the erythrocyte protein 4.2 gene and parenteral nutrition-associated liver disease. ***Clin Res Trials***, 2017 doi: 0.15761/CRT.1000188
10. Dorand, R.D., **Petrosiute, A.**, Huang, A.Y. Multifactorial regulators of tumor PD-L1 response. ***Trans. Cancer Research*** **2017;** Doi: 10.21037/tcr.2017.11.08.
11. Dorand, R.D., Benson, B.L., **Petrosiute, A.,** Huang, A.Y. Insights from Dynamic Neuro-Immune Imaging on Tissue Immune Responses in the CNS. ***Frontiers in Neuroscience*** 2019 Jul 17;13:737. PMID: 31379488.
12. Grincevičienė Š, Vaitkienė D, Kanopienė D, Vansevičiūtė R, Tykvart J, Sukovas A, Celiešiūtė J, Ivanauskaitė Didžiokienė E, Čižauskas A,

Laurinavičienė A, Král V, Hlavačková A, Zemanová J, Stravinskienė D, Sližienė A**, Petrošiūtė A**, Petrauskas V, Balsytė R, Grincevičius J, Navratil V, Jahn U, Konvalinka J, Žvirblienė A, Matulis D, Matulienė J. Factors, associated with elevated concentration of soluble carbonic anhydrase IX in plasma of women with cervical dysplasia. ***Sci Rep.*** 2022 Sep 13;12(1):15397. doi: 10.1038/s41598-022-19492-y. PMID: 36100684;

13. Matulienė J, Žvinys G, Petrauskas V, Kvietkauskaitė A, Zakšauskas A, Shubin K, Zubrienė A, Baranauskienė L, Kačenauskaitė L, Kopanchuk S, Veiksina S, Paketurytė-Latvė V, Smirnovienė J, Juozapaitienė V, Mickevičiūtė A, Michailovienė V, Jachno J, Stravinskienė D, Sližienė A, **Petrošiūtė A**, Becker HM, Kazokaitė-Adomaitienė J, Yaromina A, Čapkauskaitė E, Rinken A, Dudutienė V, Dubois LJ, Matulis D. Picomolar fluorescent probes for compound affinity determination to carbonic anhydrase IX expressed in live cancer cells. ***Sci Rep.*** 2022 Oct 21;12(1):17644. doi: 10.1038/s41598-022-22436-1. PMID: 36271018;
14. Žvinys G, **Petrosiute A**, Zakšauskas A, Zubrienė A, Ščerbavičienė A, Kalnina Z, Čapkauskaitė E, Juozapaitienė V, Mickevičiutė A, Shubin K, Grincevičienė Š, Raišys S, Tars K, Matulienė J, Matulis D. High-Affinity NIR-Fluorescent Inhibitors for Tumor Imaging via Carbonic Anhydrase IX. **Bioconjug Chem.** 2024 Jun 19;35(6):790-803. doi: 10.1021/acs.bioconjchem.4c00144. Epub 2024 May 15. PMID: 38750635; PMCID: PMC11191402.
15. **Petrosiute A**, Musvicaitė J, Petroška D, Ščerbavičienė A, Arnold S, Matulienė J, Žvirblienė A, Matulis D, Lučiūnaitė A. CCL2-CCR2 Axis Inhibition in Osteosarcoma Cell Model: The Impact of Oxygen Level on Cell Phenotype. **J Cell Physiol.** 2024 Nov 25. doi: 10.1002/jcp.31489. Epub ahead of print. PMID: 39587819.
16. **Petrosiute A**, Zakšauskas A, Lučiūnaitė A, Petrauskas V, Baranauskienė L, Kvietkauskaitė A, Ščerbavičienė A, Tamošiūnaitė M, Musvicaitė J, Jankūnaitė A, Žvinys G, Stančaitis L, Čapkauskaitė E, Mickevičiūtė A, Juozapaitienė V, Dudutienė V, Zubrienė A, Grincevičienė Š, Bukelskienė V, Schiöth HB, Matulienė J, Matulis D. Carbonic anhydrase IX inhibition as a path to treat neuroblastoma. **Br J Pharmacol**. 2025 Jan 7. doi: 10.1111/bph.17429. Epub ahead of print. PMID: 39776083.

Book Chapter:

1. Letterio J., Ahuja S.P., **Petrosiute A.** Care of the High-Risk Neonate. Hematology problems. Edited by Fanaroff A. and Fanaroff J.M. Elsevier, 6th edition, 2012.
2. Letterio J., Ahuja S.P., Pateva I., **Petrosiute A.** Chapter 79: Hematologic and Oncologic Problems in the Fetus and Neonate. Fanaroff & Martin's Neonatal-Perinatal Medicine. Elsevier, 11th edition, 2019.

Invention Disclosure:

CWRU 2016-3059: "Inhibition of Cdk5 can sensitize tumors to Immunotherapy by Modulating IRF2BP2 Phosphorylation resulting in Suppression of Immune Checkpoint, PD-L1." (Co-Inventor)

Selected abstracts since 2019:

1. Miller Ch., Gupta A., Silver E., Notarenegelo L., Dalal J., Dallas M., **Petrosiute A.** Treatment of phenotypic STAT1 gain-of-function presenting as IPEX-like syndrome and CAEBV. 32nd Annual Meeting of the American Society of Pediatric Hematology/Oncology, May 1-4, 2019, New Orleans, LA.
2. **Petrosiute A.,** Luciunaite A., Musvicaite A., Zaksauskas A., Baranauskiene L., Matuliene J., Matulis D. „Interplay of CAIX and CCR2-CCL2 axis in neuroblastoma xenograft model". CRI-ENCI-AACR Seventh International Cancer Immunotherapy Conference: Translating Science Into Survival September 20-23, 2023 Milano, Italy**.**
3. Arnold S., Musvicaitė J**.**, Zakšauskas A., Čapkauskaitė E., Lučiūnaitė A., **Petrosiute A.** "Assessing the Impact of CAIX Inhibitor EA2-3 on the Medulloblastoma Cell Line UW228". The COINS 2024, April 15-18, 2024, Vilnius, Lithuania.
4. G. Žvinys, **A. Petrosiute**, A. Zakšauskas, A. Zubrienė, E. Čapkauskaitė, V. Juozapaitienė, A. Mickevičiūtė, Š. Grincevičienė, J. Matulienė, A. Ščerbavičienė, S. Raišys, Z. Kalnina, K. Tars, K. Shubin, D. Matulis. "High-affinity infrared-fluorescent probes for cancer imaging via CAIX ". Baltic Organic Syntheticum July 7-10, 2024, Riga.
5. Gediminas Žvinys, **Agne Petrosiute**, Audrius Zakšauskas, Asta Zubrienė, Edita Čapkauskaitė, Jurgita Matulienė, Daumantas Matulis. High-Affinity NIR-Fluorescent Probes for Cancer Imaging via Carbonic Anhydrase IX. 48th FEBS congress. June 26-July 3, 2024, Milan.

Meeting attendance (since 2019):

1. 4th Satellite *Meeting* on *Carbonic Anhydrases*. Parma, Italy. November 14-17, *2019.*
2. Life Sciences Center Conference 2023.Vilnius, Lithuania. April 03, 2023.
3. CRI-ENCI-AACR Seventh International Cancer Immunotherapy Conference: Translating Science Into Survival. September 20-23, 2023 Milano, Italy**.**

Vilniaus universiteto leidykla
Saulėtekio al. 9, III rūmai, LT-10222 Vilnius
El. p. info@leidykla.vu.lt, www.leidykla.vu.lt
bookshop.vu.lt, journals.vu.lt
Tiražas 15 egz.